

Thermal Stability of Hydrocarbon Radicals

Wing Tsang
National Institute of Standards and Technology
Gaithersburg, MD 20899

ABSTRACT

This paper reviews the present state of knowledge regarding the stability of hydrocarbon radicals. We will begin with some definitions regarding thermodynamic and kinetic stability and general comments justifying our interest. A number of the important issues dealing with the accurate determination of these properties will be discussed. This will be followed by a survey of some of the problems and controversies regarding correct values. Finally, thermodynamic and kinetic data bearing on the stability of the radicals will be summarized.

BACKGROUND

The reactions of hydrocarbons in the gas phase and non-polar media frequently proceed through free radical mechanisms. Quantitative understanding of the temporal behavior of such processes depends on knowledge of the thermodynamic and kinetic properties of the radicals. The thermodynamic stability of any compound can most conveniently be expressed in a quantitative sense in terms of its free energy or equilibrium constant of formation. This can be expressed as,

$$\Delta F = \Delta H - T\Delta S = -RT \ln K_p \quad [1]$$

$$K_p = k_f/k_r(RT)^n \quad [2]$$

where the reference state is for the elements at 1 bar and 298 K, k_f and k_r are the rate constants in the two directions and n represent the order of the reaction. Thermodynamic properties serve as limits for kinetics and the basis for the estimation and evaluation of kinetic information. A particularly important application is its use for the calculation of the rate constant in one direction if that for the reverse reaction is known. Alternatively, when the rates in both directions have been measured, the reproduction of the equilibrium property serves as an important check of the validity of the data. Thermodynamic properties of radicals are not only important for their own sake but can be used to infer the chemical stability and reactivity of the compounds formed by any two radicals. This is largely due to the fact that radical combination rate constants do not vary greatly.

Enthalpy and entropy define the properties of a molecule in terms of energetics and structure (1). Traditionally, they form the basis for estimation (2). Modern day computational packages (3) permit their direct calculation from ab initio quantum mechanics. Such methods work quite well for small radicals and are in general more reliable with respect to structural or entropic factors than the energies. In time, these methods will play an ever more important role in defining the properties of radicals. In the meantime dependence must remain with experimental determinations. A key role for accurate measurements is as a means of validating calculations. A combination of group additivity and small molecule calculational results should in principal give all the information necessary for the determination of the thermodynamic properties of larger entities.

As suggested above, the thermodynamic properties of radicals can be determined through the measurement of the equilibrium constant (1). From measurements at one temperature enthalpies can be determined if entropies can be estimated. This is usually known as the 3rd law method. Alternatively, from determinations of the equilibrium constant as a function of temperature, the enthalpy of the process can be determined from the slope or

$$d[\ln K_p]/d(1/T) = -\Delta H/R. \quad [3]$$

This is known as the second law method. Substituting back into Eq 1 then leads to a determination of the entropy. In order to determine the property of a radical the thermodynamic properties of the other compounds for the reaction must be known and if reactions are carried out at temperatures different than 298 K heat capacity corrections must be made.

Much effort has been devoted to determining the enthalpies of free radicals (4,5). They are directly related to the bond dissociation energies of the molecular entity from which the radicals are formed and is a convenient marker for molecular stability or reactivity. Many measurement methods lead only to the determination of the energies. If one applies the second

law method, then a slope can be determined without the need for an absolute value of the equilibrium constant, if the calibration factor does not vary over the temperature range used and assumptions can be made about the reverse process. Complete quantitative description in the context of molecular stability will also require knowledge of the entropy. Our knowledge and understanding of radical structure and vibrational frequencies are such that for the less complex radicals, measurements exist or they can be estimated with considerable accuracy. There remains uncertainties for larger species. This is particularly the case for the molecular motions associated with low frequency vibrations. Unfortunately, these are also the largest contributors to the entropies. In the case of simple hydrocarbon radicals, the important issues are the frequency of the umbrella motion at the radical site. It is in fact uncertain as to whether they can be represented in the simple harmonic oscillator approximation. Another issue is the barrier to internal rotation of rotors at the radical site.

Kinetic stability(6) can most readily be defined in terms of the rate expressions for decomposition of radicals or the parent hydrocarbon,

$$k = A_{\infty} T^n \exp(-E_{\infty}/RT) s^{-1} \quad [4]$$

where we have chosen to write the rate expression in the modified Arrhenius form. Over short ranges, data can be written in the regular Arrhenius form where $n=0$. The infinities are given to define the results in terms of the rate constant in the limiting high pressure region. This means the results are for a system where the distribution function for the molecule is Boltzmann. High pressure rate expression for decomposition is a fundamental property of a molecule and is given in this form in order to differentiate it from the more general case where the distribution function are perturbed when the chemical lifetimes become shorter than energy transfer times, leading to a distorting of the Boltzmann distribution. The high pressure rate expressions are one of the fundamental inputs for the understanding of many complex reaction systems. They define the non-reactive lifetimes of the radicals and play a key role in the evolution of such systems. Even for the cases where energy transfer is important, the high pressure rate expression is the basis upon which estimates for energy transfer effects are made. As suggested earlier, these rate expressions can be used to derive or be derived from the thermodynamics.

EXPERIMENTAL METHODS

All experimental procedures for determining the thermodynamic and kinetic stability of radicals involve quantitative measurement of some property associated with their generation or destruction. Kinetic measurements in both directions is a prime method for determining equilibrium constants of formation. The reliable values that are now available owe much to the understanding of how to carry out accurate kinetic measurements. The first prerequisite is to find systems that are mechanistically unambiguous. This requirement is aided by the sensitivity of modern detection methods. It is thus possible to work under conditions where there are no ambiguity regarding the process being studied. Table 1 summarizes a variety of kinetic methods that have made significant contributions to the determination of the thermodynamic properties of hydrocarbon radicals. In general, the thermal decomposition reactions are carried out at the highest temperatures, the radical decompositions at intermediate temperatures while the metathesis and ion-molecule reactions are at the lowest or ambient temperatures. The choice of a technique is highly dependent on the availability of a suitable precursor. This is particularly true at the lower temperatures. At the higher temperatures more channels are opened up. However this can lead to mechanistic complications.

An alternative approach is to subject a molecule to some form of physical excitation such as a photon or electron which leads to the formation of the radical in question and then observing their formation and deducing the energetics on the basis of an energy balance. Since molecules have a distribution of energies an important issue has always been the proper selection of reaction thresholds. As with the kinetic methods, the availability of an appropriate precursor is an important determinant of what can be measured. Since this is a physical method, the most reliable numbers are for the smaller species. Furthermore, as with kinetic methods, earlier workers were much too optimistic regarding measurement accuracy. The tendency has been to reproduce the kinetic results that are now known to be in error. Here again improvements in understanding and techniques are leading to more accurate determinations.

RESULTS

A: Thermodynamic Stability: Table 2 contains a summary of data on bond dissociation energies that can be derived from heats of formation data. These have largely been derived from the methods summarized in Table 1. Also included in Table 2 are the recommendations of

Table 1: Kinetic procedures and methods used in determining the thermodynamic properties of organic radicals.(8,9)

Process	Method	Reaction Type (example)
Thermal Decomposition	Single Pulse Shock Tube Flow and Static systems. Detection of stable products	$R_1-R_2 \rightleftharpoons R_1+R_2$ $((tC_4H_9)_2 \rightleftharpoons 2 tC_4H_9)$
Radical Combination	Photolytic generation of Radicals and spectroscopic Detection	
Radical Decomposition	Photolytic and thermal generation of radicals. Detection of stable products or decay of radicals	$R \rightleftharpoons H/CH_3 + \text{olefin}$ $nC_3H_7 \rightleftharpoons C_2H_4 + CH_3$
Radical Addition	Decay of photolytically generated small radicals	
Metathesis of halogenated organics	Photolytic generation of radicals Followed by their decay	$X + RH \rightleftharpoons R + HX$ $Br + tC_4H_9$
Ion-molecule equilibria	Metathesis reaction involving ions in flow system. Mass spectrometric detection of reactants and products	$C_3H_6 + CH_3O \rightleftharpoons$ $C_3H_5 + CH_3OH$

McMillen and Golden(4) published in 1982 which are based largely on iodination results. It can be seen that in all cases except for methyl, for which the best results are from physical approaches, there have been significant increases in the heats of formation. This is surprising to those who are not intimately acquainted with the field. Since much of chemistry is involved in the breaking or forming of bonds, there is a natural attempt to interpret experimental observations in terms of bond dissociation energies. Unfortunately, it is now clear that earlier investigators were much too optimistic regarding the accuracy of their estimates.

The following contains a brief historical sketch of the sequence of studies of which the data in Table 2 represent hopefully the final correct values. The first systematic investigation of the thermodynamic properties of hydrocarbon radicals were the studies of Butler et al (9) where the kinetics of the decomposition of the alkyl iodides was interpreted in terms of the breaking of the carbon-iodine bond. Subsequent analysis revealed that the decomposition reaction is in fact a radical chain process with the additional possibility of a molecular decomposition channel. A few years later, Szwarc and coworkers (10) studied inhibited decomposition of simple hydrocarbons in flow systems. Radical processes were suppressed by the addition of the radical inhibitor, toluene. It is now clear that the conditions in the flow reactor were very poorly defined. The consequence was that the rate expressions are all now known to be characterized by low A-factors and activation energies. Several years later Benson and coworkers(1) used iodination kinetics to determine bond energies. The specific reactions used in their work were largely those involving the bimolecular attack of iodine atom on alkyl iodide to form the hydrocarbon radical and the iodine molecule or the reverse. A number of major errors were corrected leading once again to large increases in the measured heats of formation.

These results which first appeared in the early 1960s were summarized in a 1982 article in Annual Reviews of Physical Chemistry (4) and for many years represented the generally accepted values. However beginning with the single pulse shock tube work in the late 1960s(11) it became increasingly difficult to fit experimental results with such heats of formation. Some of the consequences are summarized in Table 2 and represent a further increase of 10-20 kJ/mol. The correctness of these numbers is attested by the large volume of experimental data that can now reproduce the thermodynamic properties of the radicals. Indeed, if errors are substantially larger than the estimated uncertainties, this will call into question much that is believed to be understood about experimental gas phase kinetics. Actually, of all the numbers given in Table 2, only that for t-butyl radical is still subject to any controversy. It should also be noted that there may also be uncertainties of the order of several kJ/mol in the heats of formation of the larger alkanes (12). This will of course be directly reflected in the errors of the radicals.

The ultimate importance of data such as summarized in Table 2 is as a basis for estimation. It is of interest to consider the consequences of errors in such values. If they are directly reflected in the rate or equilibrium constants, then an error of 5.5 kJ/mol will lead to an

Table 2: Heats of formation for some hydrocarbon radicals and their corresponding bond dissociation energies. (7,8) Heats of formation in italics are from McMillen and Golden (4)

R1/R2 (kJ/mol)	(Ref 4)	H	CH ₃ 147 ± 1	C ₂ H ₅ 119 ± 2	i-C ₃ H ₇ 90 ± 2	t-C ₄ H ₉ 48 ± 3
CH ₃ (147 ± 1)	<i>(147±1)</i>	440	378	370	370	360
C ₂ H ₅ (119 ± 2)	<i>(108±4)</i>	422	370	364	362	352
n-C ₃ H ₇ (100 ± 2)	<i>(88±4)</i>	422	373	365	362	353
i-C ₃ H ₇ (90 ± 2)	<i>(76±4)</i>	412	372	364	361	343
s-C ₄ H ₉ (69 ± 2)	<i>(54±8)</i>	413	370	362	356	336
i-C ₄ H ₉ (70 ± 2)		422	371	363	360	341
t-C ₄ H ₉ (48 ± 3)	<i>(39±4)</i>	400	360	352	341	321
t-C ₅ H ₁₁ (28 ± 3)		402	361	354	334	314
C ₃ H ₅ (allyl)(171 ± 3)	<i>(164±6)</i>	368	318	311	309	302
C ₃ H ₅ (propenyl)(267 ± 3)		465	421	414		
C ₄ H ₇ (isobutenyl)(138 ± 3)		373				
C ₄ H ₇ (methylallyl)(158 ± 3)		375				
C ₃ H ₃ (propargyl)(351 ± 2)		384	333	326	322	
C ₄ H ₅ (methylpropargyl)(313 ± 2)		385				
C ₆ H ₅ (phenyl)(341 ± 4)		475	436	428	423	408
C ₆ H ₅ CH ₂ (benzyl)(207 ± 4)	<i>(200± 6)</i>	375	324	318	317	309

error of a factor of 10 in these quantities at room temperature and a factor of 2 at 1000 K. Correspondingly an error of 21 kJ/mol will lead to an error of 4 orders of magnitude at room temperature and a factor of 10 at 1000 K. This is a direct reflection of the logarithmic dependence of the rate and equilibrium constants on the thermodynamic functions. It is clear that the accuracy that are now attainable is probably sufficient for higher temperature applications but is still somewhat unsatisfactory for room temperature use.

B: Kinetic Stability: The kinetic stability of hydrocarbon molecules and radicals that are consistent with the thermodynamics are summarized in Tables 3-4. Table 3 contains experimental data on the decomposition of a number of simple alkanes and alkynes and are the results of single pulse shock tube studies. They have been a major factor in the development of the results given in Table 2. Some noteworthy factors are the following: (a) It can be seen that at the high temperature end of the experimental studies, for a particular type of reaction the A-factors do not vary greatly except for the influence of reaction path degeneracy and differences in rate constants are largely due to activation energy changes. (b) It is possible to discern a difference in the A-factors for the cases where alkyl radicals are formed as opposed to the formation of a resonance stabilized radical. This difference is explicable in terms of the stiffer structure of the latter. (c) Over the entire temperature range, for the bond breaking reaction of alkanes there is a negative curvature of the Arrhenius plot. This is much larger for the most highly substituted hydrocarbon. Actually, the lowest temperature results are derived from the conversion of the combination rate constants to the dissociation values through the equilibrium

Table 3: Summary of rate expressions for the decomposition of some alkanes and alkynes

Reaction	Rate Expressions
Alkanes 1000-1200K	
k(iC ₃ H ₇ -tC ₄ H ₉) => iC ₃ H ₇ + tC ₄ H ₉	2.5x10 ¹⁶ exp(-36800/T)s ⁻¹
k(iCH ₃ -tC ₄ H ₉) => CH ₃ + tC ₄ H ₉	1x10 ¹⁷ exp(-41100/T)s ⁻¹
k(C ₂ H ₅ tC ₅ H ₁₁) => C ₂ H ₅ + tC ₅ H ₁₁	6x10 ¹⁶ exp(-38800/T)s ⁻¹
k(iC ₃ H ₇ -tC ₅ H ₁₁) => iC ₃ H ₇ + tC ₅ H ₁₁	2.3x10 ¹⁶ exp(-35900/T)s ⁻¹
k(sC ₄ H ₉ -tC ₄ H ₉) => sC ₄ H ₉ + tC ₄ H ₉	3x10 ¹⁶ exp(-36400/T)s ⁻¹
k(sC ₄ H ₉ -sC ₄ H ₉) => sC ₄ H ₉ + sC ₄ H ₉	3.5x10 ¹⁶ exp(-37900/T)s ⁻¹
k(C ₆ H ₁₁ -tC ₄ H ₉) => C ₆ H ₁₁ + tC ₄ H ₉	3x10 ¹⁶ exp(-37400/T)s ⁻¹
k(tC ₄ H ₉ -tC ₄ H ₉) => tC ₄ H ₉ + tC ₄ H ₉	3x10 ¹⁶ exp(-34500/T)s ⁻¹
Alkynes 1000-1200 K	
k(HCCCH ₂ -nC ₃ H ₇) => HCCCH ₂ + nC ₃ H ₇	8x10 ¹⁵ exp(-36300/T) s ⁻¹
k(HCCCH ₂ -iC ₄ H ₉) => HCCCH ₂ + iC ₄ H ₉	1.2x10 ¹⁶ exp(-36700/T) s ⁻¹
k(CH ₃ CCCH ₂ -nC ₃ H ₇) => CH ₃ CCCH ₂ + nC ₃ H ₇	1.5x10 ¹⁶ exp(-36800/T) s ⁻¹
k(HCCCH ₂ -sC ₄ H ₉) => HCCCH ₂ + sC ₄ H ₉	8x10 ¹⁵ exp(-35000/T) s ⁻¹
k(HCCCH ₂ -iC ₃ H ₇) => HCCCH ₂ + iC ₃ H ₇	5x10 ¹⁵ exp(-34800/T) s ⁻¹
Alkanes 300 - 1200 K	
k(C ₂ H ₅ -C ₂ H ₅) => 2 C ₂ H ₅	4.4x10 ²⁵ (1/T) ^{2.7} exp(-44441/T)s ⁻¹
k(iC ₃ H ₇ -iC ₃ H ₇) => 2 iC ₃ H ₇	1.6x10 ³¹ (1/T) ^{4.2} exp(-43897/T)s ⁻¹
k(tC ₄ H ₉ -tC ₄ H ₉) => 2tC ₄ H ₉	5.5x10 ³⁸ (1/T) ^{6.45} exp(-41065/T)s ⁻¹

Table 4: Derived rate expressions for radical decomposition, based on thermodynamics and rate constant for addition 300–900 K

Reaction	Rate Expressions s ⁻¹	Rate Constants at 750 K s ⁻¹
nC ₃ H ₇ = C ₂ H ₄ + CH ₃	1.2x10 ¹³ exp(-15260/T)	1.8x10 ³
sC ₄ H ₉ = C ₃ H ₆ + CH ₃	9x10 ¹² exp(-14770/T)	2.5x10 ⁴
iC ₃ H ₇ = C ₃ H ₆ + H	2.6x10 ¹³ exp(-18730/T)	3.7x10 ²
sC ₄ H ₉ = 1-C ₄ H ₈ + H	1.3x10 ¹³ exp(-18320/T)	3.2x10 ²
sC ₄ H ₉ = c-C ₄ H ₈ + H	4.2x10 ¹² exp(-17500/T)	3.1x10 ²
sC ₄ H ₉ = t-C ₄ H ₈ + H	4.7x10 ¹² exp(-17100/T)	5.8 x10 ²
tC ₄ H ₉ = C ₄ H ₈ + H	8.5x10 ¹³ exp(-18900/T)	9.7 x10 ²

constant. Rate constants are in fact so small that they are not measurable and thus physically meaningful. The relative invariance of the A-factor at the higher temperatures is in contrast to the situation at the lower temperatures. The consequence is that with the existing data base on thermodynamics and decomposition kinetics it should be fairly straightforward to predict rate constants for decomposition of simple hydrocarbons.

Table 4 contains rate expressions for the decomposition of a number of alkyl radicals(12). The experimental data set of rate expressions for the decomposition of the larger alkyl radicals are unsatisfactory. Even for the same system rate expressions can be widely divergent. The situation is much better regarding rate constants. For such studies radicals must be generated in situ. Furthermore it is likely that many of the studies are in the region where energy transfer effects make significant contributions. However at somewhat lower temperatures there exist very good data on radical addition to olefins or the reverse of the decomposition reaction. Combination of this data with the equilibrium constants leads to rate expressions for decomposition. A check is offered through a match of the rate constants for decomposition at the experimental decomposition temperature. The results on H-bond cleavage is indicative of the effect of methyl substitution. Reaction pathway degeneracy must also be considered. We have also found that the effect of methyl substitution on C-C bond cleavage is very similar to that for the stable compounds (13).

CONCLUSION

Experimental studies have now led to highly accurate values for the thermodynamic and kinetic stability of a large number of hydrocarbon radicals. The techniques that have been employed are extensible to other systems. There is the need for such measurements for many of the larger highly unsaturated radicals with or without resonance stabilization. The increased accuracy requirements under ambient conditions mean that there is still a need to reduce uncertainty limits in all cases. In combination with rapidly developing theory, the expectation is for increasingly accurate predictions of the properties of reactive hydrocarbon systems.

REFERENCES

- O'Neal, H. E., Benson, S. W., "Thermochemistry of Free Radicals" in "Free Radicals" (Kochi, J., ed.) John Wiley and Sons, New York, 1973
- Benson, S. W., "Thermochemical Kinetics", John Wiley and Sons, New York, 1974
- Frisch, M. J.; Trucks, G. W.; Head-Gordon, M.; Gill, P. M. W.; Wong, M. W.; Foresman, J. B.; Johnson, B. G.; Schlegel, H. B.; Robb, M. A.; Replogle, E.S.; Gomperts, R.; Andres, J. L.; Raghavachari, K.; Binkley, J. S.; Gonzalez, C.; Martin, R. L.; Fox, D. J.; Defrees, D. J.; Baker, J.; Stewart, J. J. P.; Pople, J. A. Gaussian 92, revision F.4; Gaussian, Inc.: Pittsburgh, PA, 1992.
- McMillen, D. E. and Golden, D. M., (1982), *Annu. Rev. Phys. Chem.*, 33, 493-532
- Berkowitz, J., Ellison, G. B., and Gutman, D., *J. Phys. Chem.*, 98, 2744, 1995
- Tsang, W. and Kiefer, J. H., "Unimolecular Reactions over Extended Pressure and Temperature Ranges" in *Dynamics and Kinetics of Small Radicals*, ed. K. Liu and A. Wagner. World Scientific Company, Singapore, 1995, 59.
- Tsang, W., "Heats of Formation of Organic Free Radicals by Kinetic Methods" in "Energetics of Free Radicals" (A. Greenberg and J. Liebman, ed.) Blackie Academic and Professional, 1996, 22
- Ellison G. B., Davico, G. E., Bierbaum, V., and DePuy, C., *Int. J. Mass Spec.* 1996, 156, 109
- Butler, E. T., Mandel, E. and Polanyi, M., *Trans. Faraday Soc.*, 41, 298, 1945
- Szwarc, M., *Chem. Rev.*, 47, 1675, 1950
- Stull, D. R., Westrum, E. F., and Sinke, G. R., (1969) "The Chemical Thermodynamics of Organic Compounds", John Wiley and Sons, New York, NY
- Tsang, W., *J. Amer. Chem. Soc.*, 107, 2872, 1985
- Tsang, W., unpublished results

CLIMBING MOUNT PSI: THE LEVEL OF THEORY NEEDED TO OBTAIN 1 KCAL/MOL
ACCURACY IN THERMOCHEMICAL PROPERTIES

David Feller
Environmental Molecular Sciences Laboratory,
Pacific Northwest National Laboratory, MS K1-96
P.O. Box 999, Richland, Washington 99352

ABSTRACT

A variety of molecular properties, including atomization energies, bond lengths and harmonic vibrational frequencies were computed for more than 80 experimentally well-characterized molecules, many of which were taken from the Gaussian-2 and G2/97 collections. This body of data was stored in the Environmental Molecular Sciences Laboratory Computational Results Database and was subsequently analyzed to determine the sensitivity of each property towards the electron correlation treatment and the quality of the underlying Gaussian basis set. In light of the importance of the basis set in limiting the ultimate accuracy of the theoretical predictions, a wide range of correlation consistent basis sets (including, in some cases, up through aug-cc-pV6Z) was used. These were combined with five popular levels of theory, ranging from simple Hartree-Fock theory up through coupled cluster theory. The importance of core/valence, scalar relativistic, atomic spin-orbital effects and more extensive correlation recovery were also examined in terms of their impact on agreement with experiment. All of these effects can contribute on the order of 1 - 2 kcal/mol or more to quantities such as a heat of formation.

I. INTRODUCTION

The accuracy of five widely-used electronic structure methods in reproducing experimental atomization energies (ΣD_e), electron affinities, proton affinities, ionization potentials, vibrational frequencies and geometries were recently examined by Feller and Peterson.¹ Methods included Hartree-Fock (HF) theory, second- and fourth-order Møller-Plesset perturbation theory (MP2 and MP4), coupled cluster theory with single and double excitations (CCSD) and coupled cluster theory with a quasiperturbative treatment of triples (CCSD(T)). In addition to the raw errors resulting from each specific (method/ basis set) pair, an attempt was made to assess a given method's *intrinsic* error, i.e. the deviation with respect to experiment in the limit of a complete 1-particle basis set.

Throughout the development of quantum chemistry, up until the early 1990s, the primary sources of error in most electronic structure calculations were more-or-less evenly attributable to relatively poor quality basis sets and an inadequate treatment of the electron correlation problem. However, following the development of the correlation consistent basis sets²⁻⁵ it became possible to exploit the regularity of these basis sets to perform an effective extrapolation to the complete basis set (CBS) limit. This was accomplished by fitting results obtained from successively larger and larger basis sets with one of a number of simple functional forms. Feller and Peterson examined three extrapolations. The first of these is the empirically motivated exponential form, given for total energies by the expression:

$$E(x) = E_{\text{CBS}} + b e^{-cx} \quad (1)$$

where x is an index associated with each basis set, $x=2$ (DZ), 3(TZ), 4(QZ), etc.⁶⁻¹⁰ The second is a combined Gaussian/exponential function:^{11,12}

$$E(x) = E_{\text{CBS}} + b e^{-(x-1)} + c e^{-(x-1)**2} \quad (2)$$

And, the final expression is:

$$E(\ell_{\text{max}}) = E_{\text{CBS}} + b/(\ell_{\text{max}} + 1)^4 \quad (2)$$

where ℓ_{max} is the maximum angular momentum present in the basis set.¹³ For second and third row correlation consistent basis sets, x (eq. 1) = ℓ_{max} (eq. 2).

II. PROCEDURE

Most geometries were optimized with a gradient convergence criterion of $1.5 \times 10^{-5} E_h/a_0$, corresponding to the "tight" criterion defined in Gaussian-94,¹⁴ using the same level of theory as was used in evaluating the desired property. For example, CCSD(T) thermochemical properties were evaluated at the optimal CCSD(T) geometries. A looser convergence criterion of $1.0 \times 10^{-4} E_h/a_0$ was necessary for the largest basis set CCSD(T) optimizations.

Unless otherwise noted, open shell energies were based on unrestricted Hartree-Fock (UHF) zeroth order wavefunctions and were performed with the Gaussian-94 program.¹⁴ Orbital symmetry and equivalence restrictions were not imposed in atomic calculations. Closed shell CCSD(T) calculations were performed with MOLPRO-97¹⁵ and Gaussian-94. CCSDT calculations were obtained from ACES II.¹⁶ All calculations were performed on a 16 processor Silicon Graphics, Inc. PowerChallenge, a 32 processor SGI Origin 2000 or an SGI/Cray J90 at D.O.E.'s National Energy Research Supercomputing Center. The largest CCSD(T) calculation reported in this study included 734 functions. As in the previous study, results were stored and analyzed using the Environmental Molecular Sciences Laboratory (EMSL) Computational Results Database,¹⁷ which currently contains over 32,000 entries.

Atomization energies were corrected for the effects of core/valence (CV) correlation (which is not included in normal frozen core calculations run with programs like Gaussian) by performing all electron calculations with the cc-pCVQZ basis sets, which are specially designed for this purpose. The 1s pairs of electrons for third period elements was treated as frozen cores.

Atomic spin-orbit and molecular/atomic scalar relativistic corrections were also appended to our nonrelativistic atomization energies and are denoted ΔE_{SO} and ΔE_{SR} , respectively. The former account

for the improper description of the atomic asymptotes, since atomic energies determined by our calculations correspond to an average over the possible spin multiplets. In some cases, such as the 2Π states of molecules like CH and OH, there is an additional *molecular* spin-orbit correction due to the splitting of the $2\Pi_1$ and $2\Pi_2$ states. Spin-orbit corrections were taken from the atomic and molecular values reported by Dunning and coworkers,^{10,12} which are based on the experimental values of Herzberg¹⁸ and Moore.¹⁹ Scalar relativistic corrections were obtained from configuration interaction wavefunctions including single and double excitations (CISD) using the cc-pVTZ basis set. The CISD(FC) wavefunction was used to evaluate the dominant 1-electron Darwin and mass-velocity terms in the Breit-Pauli Hamiltonian.

Our results will be compared to experimental atomization energies extrapolated to 0 K, both with and without zero point energies (ZPEs), i.e. $\Sigma D_0(0K)$ and $\Sigma D_e(0K)$, respectively. A majority of the experimental data used in this report was taken from the NIST-JANAF Tables (4th. Edition)²⁰ and Huber and Herberg.²¹ Our zero point energies were based on harmonic CCSD(T) frequencies.

III. RESULTS

Table 1 contains representative comparisons between CCSD(T) values of ΣD_0 and the corresponding, best available experimental values. The three right-most columns contain the differences with respect to experiment for the three CBS estimates, eqs. 1 - 3. For most of the 80 molecules the convergence in the frozen core binding energies is slow enough that fairly large basis sets are required. Of all the methods tested, only CCSD(T) shows continuous improvement in the level of agreement with experiment as the basis set size increases. If a double zeta basis set is largest that can be afforded, MP2 actually gives better statistical agreement with experiment.

In general, the errors arising from the use of $ZPE = 1\Sigma\omega$, where ω are harmonic frequencies obtained from CCSD(T) calculations, is relatively small. The mean absolute deviation with respect to experiment, ϵ_{MAD} , for frozen core CCSD(T) is ~ 1.5 kcal/mol, with worse case errors as large as 4.5 kcal/mol. This value includes adjustments for atomic spin-orbit effects. Core/valence corrections range from essentially zero to as much as 7.1 kcal/mol, and can be of either sign. By including core/valence corrections ϵ_{MAD} drops into the 0.7 - 0.8 kcal/mol range. Relativistic corrections produce no *overall* change in ϵ_{MAD} , but did reduce the maximum errors. Although scalar relativistic corrections tend to decrease the binding energy, they can be of either sign and vary from near zero to 2.4 kcal/mol.

A correction should also be applied for the difference between CCSD(T) and full CI. Very little is known about this difference because CCSD(T) recovers such a large percentage of the correlation energy that determining energies with even greater accuracy is a very difficult task. We recently examined the impact of higher order correlation effects on the dissociation energies of HF, N₂ and CO. Among the higher order methods examined were two variations of coupled cluster theory (CCSDT and CCSDT(Q)) and two approximations to full configuration interaction. Again, basis sets were chosen from the correlation consistent family of basis sets, with the largest being the aug-cc-pVQZ set. Polarized valence double zeta quality basis sets were found to yield corrections that differed substantially from larger basis set results. At the double zeta level, higher order corrections increased the binding energies, whereas calculations with triple and quadruple zeta basis sets gave the opposite effect. Although the absolute magnitude of the higher order corrections was small for these diatomics, they were nonetheless significant in light of a target accuracy of ± 1 kcal/mol. Among molecules composed of first-through-third period elements, such as those in the G2 and G2/97 collections, the contribution to ΣD_0 from higher order correlation effects could easily exceed 1 kcal/mol. CCSD(TQ) often overestimated the higher order correction, sometimes exceeding the estimated full configuration interaction result by a factor of three.

Normally, because CCSD(T) is based on only a single reference configuration, it would not be expected to describe transition states very well. However, for some transition states, where the Hartree-Fock configuration still constitutes a significant component in the transition state wavefunction, CCSD(T) may perform as well as explicit multireference methods like configuration interaction (CI). The transition state for the reaction $H_2CO \rightarrow H_2 + CO$ has been obtained with a wide assortment of theoretical methods. Compared to complete active space CI, CCSD(T) does a good job of predicting the barrier height and is far less costly.

VII. CONCLUSIONS

CCSD(T) atomization energies were computed for a set of 80 molecules with reliable experimental data. Basis sets were taken from the augmented correlation consistent family and represent some of the largest Gaussian basis sets currently available. By using any of the three complete basis set extrapolations (eqns. 1 - 3), it is possible to enter a regime where core/valence, scalar relativistic, atomic spin-orbit, anharmonic ZPE effects or higher order correlation effects can become as important as the remaining error due to the use of finite basis set. Failure to account for any one of these effects can lead to errors on the order of several kcal/mol or more in particularly troublesome cases. On the other hand, in fortunate cases some of these corrections can nearly cancel. The overall mean absolute deviation is below 1 kcal/mol.

Although CCSD(T) suffers from some of the same limitations as other single-reference methods, it is currently the most accurate *ab initio* electronic structure technique that can be applied with large basis sets to small molecules. Coupled cluster theory *without* the inclusion of triple excitations was found to be frequently less accurate for atomization energies than second order perturbation theory. CCSD(T) is not capable of describing large regions of most potential energy surfaces, but nonetheless it may do quite well for certain transition states.

ACKNOWLEDGMENTS

This research was supported by the U. S. Department of Energy under Contract No. DE-AC06-76RLO 1830. The Pacific Northwest National Laboratory is a multiprogram national laboratory operated by Battelle Memorial Institute.

REFERENCES

- (1) Feller, D.; Peterson, K. A. *J. Chem. Phys.* **1998**, *108*, 154.
- (2) Dunning, T. H., Jr. *J. Chem. Phys.* **1989**, *90*, 1007.
- (3) Woon, D. E.; Peterson, K. A.; Dunning, T. H., Jr. **to be published**.
- (4) Wilson, A. K.; Mourik, T. v.; Dunning, T. H., Jr. *J. Mol. Struct. (Theochem)* **1996**, *388*, 339.
- (5) van Mourik, T.; Dunning, T. H., Jr. *Theor. Chem. Acc.* **to be published**.
- (6) Feller, D. *J. Chem. Phys.* **1992**, *96*, 6104.
- (7) Xantheas, S. S.; Dunning, T. H., Jr. *J. Phys. Chem.* **1993**, *97*, 18.
- (8) Feller, D. *J. Chem. Phys.* **1993**, *98*, 7059.
- (9) Woon, D. E.; Dunning, T. H., Jr. *J. Chem. Phys.* **1993**, *99*, 1914.
- (10) Peterson, K. A.; Kendall, R. A.; Dunning, T. H., Jr. *J. Chem. Phys.* **1993**, *99*, 1930.
- (11) Peterson, K. A.; Woon, D. E.; Dunning, T. H., Jr. *J. Chem. Phys.* **1994**, *100*, 7410.
- (12) Woon, D. E.; Dunning, T. H., Jr. *J. Chem. Phys.* **1994**, *101*, 8877.
- (13) Martin, J. M. L. *Chem. Phys. Lett.* **1996**, *259*, 679.
- (14) Frisch, M. J.; Trucks, G. W.; Schlegel, H. B.; Gill, P. M. W.; Johnson, B. G.; Robb, M. A.; Cheeseman, J. R.; Keith, T. A.; Petersson, G. A.; Montgomery, J. A.; Raghavachari, K.; Al-Laham, M. A.; Zakrzewski, V. G.; Ortiz, J. V.; Foresman, J. B.; Cioslowski, J.; Stefanov, B. B.; Nanayakkara, A.; Challacombe, M.; Peng, C. Y.; Ayala, P. Y.; Chen, W.; Wong, M. W.; Andreas, J. L.; Replogle, E. S.; Gomperts, R.; Martin, R. L.; Fox, D. J.; Binkley, J. S.; Defrees, D. J.; Baker, J.; Stewart, J. J. P.; Head-Gordon, M.; Gonzalez, C.; Pople, J. A. Gaussian 94, E.3, Gaussian, Inc. Pittsburg PA, 1996.
- (15) Werner, H. J.; Knowles, P. J.; Almlöf, J.; Amos, R. D.; Berning, A.; Cooper, D. L.; Deegan, M. J. O.; Dobbyn, A. J.; Eckert, F.; Elbert, S. T.; Hampel, C.; Lindh, R.; Lloyd, A. W.; Meyer, W.; Nicklass, A.; Peterson, K. A.; Pitzer, R. M.; Stone, A. J.; Taylor, P. R.; Mura, M. E.; Pulay, P.; Schütz, M.; Stoll, H.; Thorsteinsson, T. MOLPRO, Universität Stüttgart, Stüttgart, Germany, University of Sussex, Falmer, Brighton, England, 1997.
- (16) Stanton, J. F.; Gauss, J.; Watts, J. D.; Nooijen, M.; Oliphant, N.; Perera, S. A.; Szalay, P. G.; Lauderdale, W. J.; Gwaltney, S. R.; Beck, S.; Balkova, A.; Bernholdt, D. E.; Baeck, K.-K.; Rozyczko, P.; Sekino, H.; Hober, C.; Bartlett, R. J.; Almlöf, J.; Taylor, P. R.; Helgaker, T.; Jensen, H. J. A.; Jørgensen, P.; Olsen, J. ACES II, University of Florida, 1998.
- (17) Feller, D. *J. Comp. Chem.* **1996**, *17*, 1571.
- (18) Herzberg, G. *Molecular Spectra and Molecular Structure I. Spectra of Diatomic Molecules*; Van Nostrand Reinhold Co., Inc.: New York, 1950.
- (19) Moore, C. E. *Atomic Energy Levels* Washington, D.C., 1949; Vol. U.S. National Bureau of Standards Circular 467, NBS.
- (20) Chase, M. W., Jr. *NIST-JANAF Tables (4th Edition)*, *J. Phys. Chem. Ref. Data*, **1998**, *Mono. 9*, Suppl. 1.
- (21) Huber, K. P.; Herzberg, G. *Molecular Spectra and Molecular Structure: Constants of Diatomic Molecules*; Van Nostrand Reinhold Co. Inc.: New York, 1979; Vol. 4.

Table 1. Contributions to CCSD(T) Atomization Energies (kcal/mol) for a Selected Subset of the G2 Molecules.^a

Molecule	ΣD_e	ZPE Expt.			Atom. Expt. ΣD_0			Erro r	w.r.t. Mixed Exp.	Expt. ℓ_{\max}
		$1\Sigma_{01}$	ZPE	ΔE_{CV}	ΔE_{SR}	ΔE_{SO}	(0K)			
CH ₄ (¹ A ₁)	418.9	27.8	27.6	1.3	-0.2	-0.1	392.5 ± 0.1	-0.4	-0.4	-0.3
H ₂ O (¹ A ₁)	232.5	13.5	13.3	0.5	-0.3	-0.2	219.35 ± 0.01	-0.4	-0.6	-0.4
HF (¹ Σ^+)	141.4	5.9	5.9	0.2	-0.2	-0.4	135.2 ± 0.2	-0.1	-0.1	-0.1
SiH ₂ (¹ A ₁)	153.6	7.3	7.3	0.0	-0.2	-0.4	144.4 ± 0.7	1.3	1.3	1.5
HCl (¹ Σ^+)	107.0	4.3	4.2	0.3	-0.2	-0.8	102.24 ± 0.5	-0.2	0.0	0.1
CO (¹ Σ^+)	258.2	3.1	3.1	0.9	-0.2	-0.3	256.2 ± 0.2	-0.7	-0.7	-0.5
N ₂ (¹ Σ_g^+)	226.1	3.4	3.4	1.0	-0.1	0.0	225.1 ± 0.4	-1.5	-1.1	-0.8
SO ₂ (¹ A ₁)	257.6	3.9	4.4	1.0	-0.9	-1.0	254.0 ± 0.2	-1.2	-0.3	0.4
Cl ₂ (¹ Σ_g^+)	58.8	0.8	0.8	0.2	+0.7	-1.7	57.18 ± 0.01	0.0	0.4	0.7

^aThe atomic asymptotes were described with the UCCSD(T) method. The column labeled " ΣD_e " contains complete basis set estimates based on aug-cc-pVTZ through aug-cc-pV6Z basis sets. Theoretical zero point energies were obtained from CCSD(T) calculations. Errors for the exponential, mixed and $1/\ell_{\max}$ CBS atomization energies (ΣD_0), which appear in the three right-most columns, were computed as the difference between the theoretical value, defined as: $E[\text{CCSD(T)}(\text{FC})/\text{CBS}] - 1\Sigma_{01} + \text{CV} + \text{scalar relativistic} + \text{atomic/molecular S.O.}$ and the bolded experimental value. For diatomics with a nonzero molecular spin-orbit contribution, e.g. OH (² $\tilde{\text{I}}$), the sum of the atomic and molecular contributions is included in ΔE_{SO} .

REVERSE RADICAL DISPROPORTIONATION: A MECHANISTIC STUDY

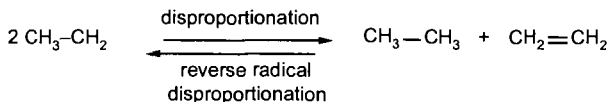
Christoph Rüchardt

Institut für Organische Chemie und Biochemie, Universität Freiburg
Albertstr. 21, D-79104 Freiburg, Germany
E-Mail: ruechardt@oca.chemie.uni-freiburg.de

Keywords: Retro-disproportionation, hydrogen transfer, thermochemistry, free radicals

INTRODUCTION

Radical disproportionations are well known radical destroying processes. The reverse reaction, accordingly, generates free radicals e.g. from an alkene and a hydrocarbon:



Despite a few early references (1) the scope and the mechanistic details of reverse radical disproportionations (retrodisproportionations) have been investigated only recently. In this context it was suggested that reverse disproportionations are important components to the complex network of reactions which are responsible for coal liquefaction processes (2) but also to synthetic dehydrogenations by quinones (3) or nitro compounds (4). In addition there is evidence which supports the assumption that NAD(P)H-reductions in the cell are initiated by reverse disproportionation (1,3).

EXPERIMENTAL

The methodology and the materials were described previously in detail (5).

RESULTS AND DISCUSSION

The mechanistic study which was performed in our laboratory concentrated in the beginning on the reactions of 9,10-dihydroanthracene (DHA), xanthene, acridane and N-methylacridane and a series of similarly structured hydrocarbons with weak C-H-bonds and α -methylstyrene as hydrogen acceptor. Then, in addition, a series of substituted styrene, cyclic dienes and aromatic hydrocarbons like azulene or polyacenes were included. These reactions are performed generally in the temperature range from 200 – 350° C. The reactions lead usually to quantitative transformations of starting materials. From this investigation, which will be reviewed briefly in this preprint, the three-step non chain radical mechanism of Scheme 1 was suggested

If the radicals formed from the donor in step 1 cannot disproportionate, alternative termination reactions are observed, frequently by participation of the solvent. In the case of styrene as an acceptor the DHA-derived radicals do add to another styrene molecule and a formal addition product of DHA to styrene is isolated (an-reaction) (6).

The following results support the suggested mechanism:

1. When the H-donors are varied, $\log k$ decreases proportionally with the increasing C-H-bond strength (Polanyi-relationship)
2. The activation enthalpies ΔH^\ddagger are a few kcal smaller than the reaction enthalpies of the rate determining retrodisproportionation step and they correlate linearly with each other (thermochemical kinetics) (7).
3. Solvent effects are small (<factor 10) and they do not correlate with solvent polarity.
4. Polar substituents in the acceptor (subst. α -methylstyrenes) or donor (xanthene or acridane vs. DHA or substituted DHA) are also small (< factor 10).
5. When deuterated donors are used no deuterium incorporation into the starting acceptor is found in most examples proving that step 1 is irreversible. The kinetic isotope effects

in these experiments $k(H)/k(D)$ are close to the maximal expected values at a given temperature.

6. The observation of an *isokinetic relationship* over a wide range of reactivity supports the assumption that no change of mechanism is occurring within this series.
7. The existence of free radical intermediates and their structures are shown by epr, by spin trapping, by radical clock experiments and by the observation of other radical rearrangements e.g. the azulene - naphthalene rearrangement (8).

A phenomenon which may be of importance in coal liquefaction processes is the observation that the H-transfer reaction of e.g. DHA to α -methylstyrene is strongly enhanced by the addition of a hydrocarbon with a weaker C-H bond (e.g. 7H-benz(de)anthracene) which is not used up during the overall reaction. This reaction, therefore, can be performed at temperatures as low as 200 – 230° C instead of 300° C when a „catalyst“ of this type is added (9). Fullerenes like C_{60} or C_{70} are transfer hydrogenated with DHA in a specific way to the partially hydrogenated products $C_{60}H_{16}$, $C_{60}H_{36}$ and $C_{70}H_{36}$ (10). The mechanistic criteria discussed above apply also to quinone oxidations of acridanes or N-subst.-nicotinamides. This suggests, that biochemicals NAD(P)H-reductions are also initiated by retrodisproportionation.

CONCLUSIONS

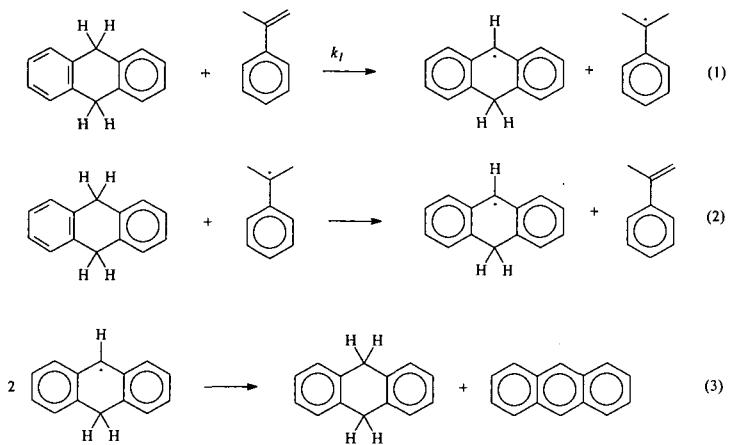
Retrodisproportionations are a class of important free radical reactions which have been unduly neglected for a long time. They are responsible in particular for high temperature hydrogen transfer reactions e.g. in coal liquefaction processes and their mechanisms are well understood now. The quantitative kinetic investigations should allow predictions for simulations of complex high temperature radical reactions of hydrocarbons.

ACKNOWLEDGEMENT

The contributions of a large group of coworkers, whose names are mentioned in the references, are gratefully acknowledged. The research reported in this paper was generously supported by the State of Baden - Württemberg, Deutsche Forschungsgemeinschaft and the Fonds der Chemischen Industrie.

REFERENCES

- (1) For a recent review and for references see C. Rüchardt, M. Gerst, J. Ebenhoch, *Angew. Chem. Int. Ed. Engl.* **1997**, 36, 1406 - 1430.
- (2) see e.g. M. L. Poutsma, *Energy and Fuel*, **1990**, 4, 113 - 131.
- (3) C. Hoefler, C. Rüchardt, *Liebigs Ann.* **1996**, 183 - 188.
- (4) M. Coellen, C. Rüchardt, *Chem. Eur. J.* **1995**, 1, 564 - 571.
- (5) see ref. and literature quoted there.
- (6) J. O. Metzger, F. Bangert, *Chem. Ber.* **1994**, 127, 673 - 675.
J.O.Metzger in Houben-Weyl, *Methoden der Organischen Chemie*, 4th. Edition, (M. Regitz, B. Giese Ed.), Vol E 19a/part1, p. 60.
- (7) S. W. Benson, *Thermochemical Kinetics*, 2nd. ed., Wiley, New York, 1976.
- (8) F. Keller, H.-D. Beckhaus, C. Rüchardt, *Liebigs Ann.* **1997**, 2055 - 2063.
- (9) M. Gerst, J. Morgenthaler, C. Rüchardt, *Chem. Ber.* **1994**, 127, 1039 - 1045.
J.Morgenthaler, C.Rüchardt, *Eur.J.Org.Chem.* **1999**, (in print).
- (10) R. Bini, J. Ebenhoch, M. Fantì, P. W. Fowler, S. Leach, G. Orlandi, C. Rüchardt, J. P. B. Sandall, F. Zerbetto, *Chem. Phys.* **1998**, 232, 75 - 84, and references given there.



Scheme 1. Mechanism Proposed for Transfer Hydrogenation with DHA.

HYDROGEN ATOM ABSTRACTION BY TRANSITION METAL COMPLEXES

James M. Mayer, Justine P. Roth, Mark A. Lockwood, Kun Wang
Department of Chemistry
University of Washington, Box 351700
Seattle, Washington 98195

ABSTRACT

A key step in many oxidation reactions is hydrogen atom abstraction by a metal-containing reactive site. We have examined oxidations of alkanes and alkylaromatic compounds by metal-oxo compounds and metal coordination complexes, including chromyl chloride (CrO_2Cl_2), permanganate, manganese μ -oxo dimers, copper(III) compounds, and iron(II)-diimine complexes. The data indicate that many of the reactions proceed by initial hydrogen atom abstraction to give the hydrocarbyl radical. Addition of $\text{H}\cdot$ to the metal complex occurs with protonation of a ligand and one-electron reduction of the metal center. For example, $\{(\text{phen})_2\text{Mn}(\mu\text{-O})_2\text{Mn}(\text{phen})_2\}^{3+}$ is reduced first to $\{(\text{phen})_2\text{Mn}(\mu\text{-O})(\mu\text{-OH})\text{Mn}(\text{phen})_2\}^{3+}$ with protonation of a bridging oxo group. The rates at which these reagents abstract $\text{H}\cdot$ are quantitatively related to their thermodynamic affinity for $\text{H}\cdot$ (in other words, the strength of the O-H or N-H bond they form). On this basis, there are strong analogies to well-known organic radical chemistry, even though the oxidants may not have any radical character. In efforts toward a more detailed understanding of H-atom transfer, studies are ongoing of hydrogen-atom self exchange rates.

INTRODUCTION

The oxidation of hydrocarbons often involves initial abstraction of a hydrogen atom to form a carbon radical (eq 1). This occurs in combustion reactions and in a range of industrial partial oxidation processes, many of which are done on an enormous scale. Hydrogen atom abstraction is also implicated in a variety of biochemical processes and is increasingly valuable in organic synthesis. The abstracting agent in H-atom transfer reactions is typically a reactive main group radical, a species with at least one unpaired electron spin. For this reason, H-atom transfer is classified as a "radical reaction."



The current understanding of rates of hydrogen abstraction by radicals is based not on radical character but on the enthalpy of reaction.¹ This was first enunciated by Evans and Polanyi in the 1930s. The enthalpy change (ΔH) for reaction 1 is simply the difference between the strength of the R-H bond being cleaved and the strength of the H-X bond formed. Activation energies E_a (and rate constants $\log k$) correlate closely with ΔH when comparing similar radicals. This is reminiscent of the Marcus-Hush theory of electron transfer, in which rates correlate with driving force as long as reagents of similar intrinsic barriers are compared. Different classes of radicals fall on different correlation lines. The standard explanation for this is termed polar effects, a result of the overlap of the half-occupied frontier orbital of the radical with the HOMO and LUMO of the C-H bond.

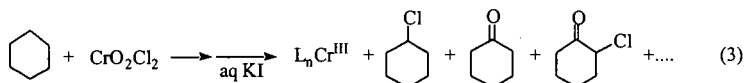
We have been exploring hydrocarbon oxidations by transition metal complexes, many of which proceed by $\text{H}\cdot$ transfer to a ligand on the transition metal (eq 2). The presence or absence



of unpaired electrons in such complexes does not correlate with reactivity and therefore cannot be used to understand $\text{H}\cdot$ transfer. So instead of looking at the spin state of the metal complex $\text{M}(\text{X})\text{L}_n$, it has often been assumed that there is a requirement for radical character at the ligand that accepts the H (X in eq 2). We find that the metal reactions are predominantly influenced by the ground state thermodynamics (the ΔH) rather than by radical character. Similar conclusions have recently been reached for hydrogen atom transfer between alkanes and alkenes (and related reactions).² We are now beginning to explore what is meant by the phrase *similar radicals* when the abstractor is not a radical. [An experimental section is not included here; the reader is referred to the original, peer-reviewed literature for such information.^{5,7,8}]

RESULTS AND DISCUSSION

The oxidation of alkanes by chromyl chloride, CrO_2Cl_2 (e.g., eq 3), is known as the Étard reaction and dates from the nineteenth century. In the 1960s, Wiberg and co-workers argued convincingly for organic radical intermediates (though other mechanisms have been discussed).³ Organic radicals have also been implicated in the oxidations of alkylaromatic compounds by permanganate.⁴ Detailed mechanistic studies in our labs⁵ have indicated that both types of reactions occur by initial hydrogen atom transfer (e.g., eq 4).



Hydrogen atom abstraction by CrO_2Cl_2 and permanganate was at first surprising because these are d^0 , closed-shell species, with no unpaired spin density. Their reactions are better explained on the basis of the strength of the bond they can make to $\text{H}\cdot$, which can be calculated by a thermochemical cycle (Scheme 1).^{5,6} For permanganate, the value derived is 80 kcal/mol. As shown in Figure 1, the rate constant for hydrogen abstraction from toluene for permanganate is close to what would be predicted based on the Polanyi correlation of rates with driving force.

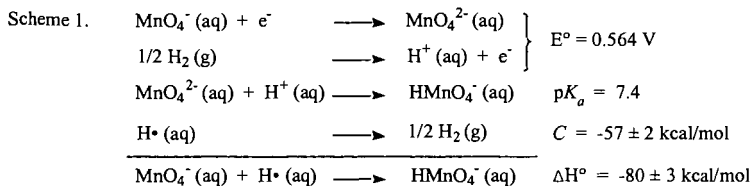
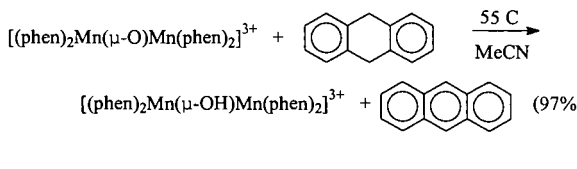
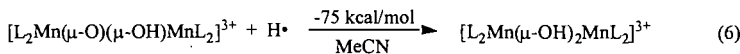
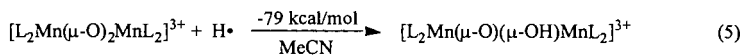


Figure 1 $\log k$ vs. O-H bond strength for reactions of toluene with ${}^n\text{Bu}_4\text{NMnO}_4$ and $\text{RO}\cdot$.

In principle, any active site with affinity for $\text{H}\cdot$ (that is, an affinity for both an electron and a proton) should be able to abstract hydrogen atoms from a substrate. And the rate constant for H-atom transfer should be roughly predictable from the Polanyi correlation illustrated in Figure 1. Our first efforts in this direction involved the dimanganese di- μ -oxo complex $[\text{Mn}_2(\mu\text{-O})_2(\text{phen})_4]^{3+}$.⁷ Redox potential and pK_a measurements yielded the O-H bond strengths in eqs 5 and 6 (using a variant of Scheme 1). As predicted from this bond strength, $[\text{Mn}_2(\mu\text{-O})_2(\text{phen})_4]^{3+}$ oxidizes dihydroanthracene (DHA) to anthracene in high yield over 11 h at 55 °C (eq 7; traces of anthrone and anthraquinone are also formed). Kinetic and mechanistic studies⁷ indicate a pathway of initial hydrogen atom abstraction from the weak C-H bond, with a deuterium isotope effect $k_{\text{DHA}}/k_{d_{12}\text{-DHA}}$ of 4.2 ± 0.3 at 55 °C and formation of bifluorenyl and 9-fluorenone from fluorene.



Hydrogen atom abstraction has also been observed for an iron(III) complex,⁸ as shown in equation 8. Complex 1 has an affinity for an electron, because the Fe³⁺ center is oxidizing, and an affinity for a proton, because one of the biimidazole ligands is deprotonated. The measured *E* and p*K*_a values translate into an affinity for H• of 76 ± 2 kcal/mol. H-atom abstraction reactivity is perhaps surprising in this case because the proton accepting site is three bonds removed from the redox active iron.

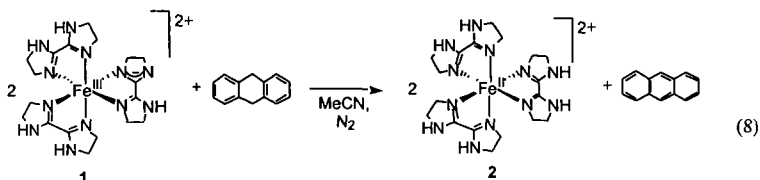


Figure 2 plots the rate constants for hydrogen abstraction from DHA versus the strength of the O–H or N–H bond formed for oxygen radicals, permanganate, the manganese μ -oxo dimers, and the iron complex 1. Remarkably, the rate constants for the metal complexes are within a factor of 10² of the values predicted by linear extrapolation of the values for ^tBuO• and ^{sec}BuOO• (Figure 2). This is a one-parameter fit of the rate constants, based only on the ground state affinity of the oxidant for H•. While it is not yet known how general a result this will be, it seems clear that analyzing a hydrogen transfer reaction should start with the relevant bond strengths.

Figure 2. log*k* vs. X–H bond strength for H-atom abstraction from dihydroanthracene.

Viewed from another perspective, the rough success of the correlation in Figure 2 indicates that ^tBuO•, ^{sec}BuO₂•, and the four metal complexes behave as “similar radicals.” We are now trying to understand what makes these oxidants are similar. A frontier orbital/polar effect argument is difficult to make, as the orbital patterns of the metal complexes are varied and quite different from that of the oxygen radicals. A polar effect rationale would also incorrectly predict that the iron complex would not correlate with the others, because it has a nitrogen rather than an oxygen as the atom that receives the hydrogen. An alternative possibility, following Marcus theory, is that these reagents are similar because they have similar intrinsic barriers. To explore this view, we have been studying the possible hydrogen atom self-exchange reaction between iron complexes 1 and 2. The oral presentation will describe recent results, and discuss the possibility that intrinsic barriers and polar effects are both needed to understand H-atom transfer reactions.

ACKNOWLEDGMENTS.

We want to thank those who have been involved in this effort in addition to the authors: Dr. Jerry Cook, Dr. Kim Gardner, Teresa Blubaugh, Andrea Collier, and Linda Kuehnert. We are also grateful the National Institutes of Health for the primary funding for this work, with early support from the donors of the Petroleum Research Fund, administered by the American Chemical Society, the National Science Foundation, Union Carbide, Chevron Research, BP America, DuPont, and the Exxon Education Foundation.

REFERENCES

- (1) Ingold, K. U. Chapter 2, pp. 69ff and Russell, G. A. Chapter 7, pp. 283-293 in *Free Radicals* Kochi, J. K., Ed.; Wiley: New York, 1973. Tedder, J. M. *Angew. Chem., Int. Ed. Engl.* **1982**, *21*, 401.
- (2) Richardt, C.; Gerst, M.; Ebenhoch, J. *Angew. Chem., Int. Ed.* **1997**, *36*, 1406-1430.
- (3) Wiberg, K. B. in *Oxidation in Organic Chemistry Part A*: K. B. Wiberg, Ed., Academic, New York, 1965, pp. 69-184. Freeman, F. in *Organic Syntheses by Oxidation with Metal Compounds* W. J. Mijs, C. R. H. I. de Jonge, Eds., Plenum, New York, 1986, Chapter 2. Nenitzescu, C. D. *Bull. Soc. Chim. Fr.* **1968**, *4*, 1349. Rappé, A. K.; Goddard, W. A., III *J. Am. Chem. Soc.* **1982**, *104*, 3287.
- (4) Waters, W. A. *Quart. Rev. (London)* **1958**, *277*. Stewart, R. *Oxidation Mechanisms*; Benjamin: New York, 1964. Fatiadi, A. J. *Synthesis (Stuttgart)* **1987**, 85.
- (5) Cook, G. K.; Mayer, J. M. *J. Am. Chem. Soc.* **1994**, *116*, 1855. Cook, G. K.; Mayer, J. M. *ibid* **1995**, *117*, 7139. Wang, K.; Mayer, J. M. *J. Org. Chem.* **1997**, *62*, 4248. Gardner, K. A.; Kuehnert, L. L.; Mayer, J. M. *Inorg. Chem.* **1997**, *36*, 2069. Mayer, J. M. *Acc. Chem. Res.* **1998**, *31*, 441-50.
- (6) Leading references: Bordwell, F. G. *et al. J. Am. Chem. Soc.* **1991**, *113*, 9790; **1996**, *118*, 8777. Parker, V. D. *ibid.* **1992**, *114*, 7458 & **1993**, *115*, 1201. Tilset, M.; Parker, V. D. *ibid.* **1989**, *111*, 6711 & *ibid.* **1990**, *112*, 2843. Parker, V. D.; Handoo, K. L.; Roness, F.; Tilset, M. *ibid.* **1991**, *113*, 7493. Wayne, D. D. M.; Luszytky, E.; Page, D.; Ingold, K. U.; Mulder, P.; Laarhoven, L. J. J.; Aldrich, H. S. *ibid.* **1995**, *117*, 8737.
- (7) Wang, K.; Mayer, J. M. *J. Am. Chem. Soc.* **1997**, *119*, 1470.
- (8) Roth, J. P.; Mayer, J. M. *Inorg. Chem.*, in press.

THERMODYNAMIC AND KINETIC STUDIES OF REACTIONS OF THIOLS, DISULFIDES,
SULFUR, AND HYDROGEN SULFIDE

Carl D. Hoff
Department of Chemistry,
University of Miami
Coral Gables, Florida 33124

ABSTRACT

A range of SAT [sulfur atom transfer] enthalpies have been determined for reactions involving both main group and transition metal compounds. These include sulfur atom transfer reactions to phosphine, arsine and stibine¹, carbene², and stannylene³ compounds as well as insertion of sulfur into metal-hydrogen⁴ and metal-metal bonds⁵. Kinetic and thermodynamic studies of reactions of thiols⁶, disulfides⁷, hydrogen sulfide⁸, and sulfur⁹ with complexes of chromium, molybdenum, and tungsten, have also been performed. The choice of mechanism appears to depend primarily on the strength of the sulfur-sulfur or sulfur-hydrogen bond that is broken, but also can be changed by ligand donor ability of the sulfur compound.

I. INTRODUCTION

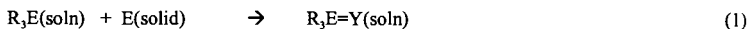
The chemistry of transition metal sulfur complexes is important to a number of industrial and biochemical processes.¹⁰ Oxidative addition of the sulfur-sulfur and sulfur hydrogen bond to metals play a fundamental role in these reactions. Thermochemical data for these reactions are rare in spite of their importance. In addition, there are relatively few mechanistic studies of reactions with transition metal complexes in solution of the simple sulfur reactants H₂S and S₈.¹¹ The mechanisms and energetics of these reactions may lend some insight into possible heterogeneous reactions of the same substrates.

II. PROCEDURE

Enthalpies of reaction have been measured by reaction calorimetry using either a Setaram Calvet Calorimeter or Guild Solution Calorimeter using techniques described in detail elsewhere.¹ Kinetic studies were performed using a flow through FT-IR microscope/reactor system that has also been described in the literature¹². Reagents, solvents, and gases were all carefully purified using standard techniques.

III. RESULTS

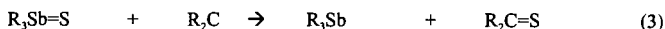
The enthalpies of reaction with chalcogen donors [Y = S, Se, Te] have been measured for a range of R₃E complexes [E = P, As, Sb] according to eqn. (1) in toluene solution at room temperature:



For 1/8 S₈ these data span over 32 kcal/mole depending on R and E. The heavier donor atoms As and Sb are labile enough to measure directly sulfur atom transfers such as those shown in eqn.(2):

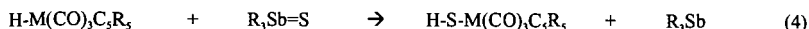


These data provide additional checks on the thermochemical data. They also provide a basis for direct measure of single S atom transfer reactions using R3Sb=S or R3As=S which in some cases are more selective than sulfur, as discovered by Jason¹³. The organostannylene complexes LSn [L = Me₃taa = octamethylidibenzotetraaza[14]annulene] prepared by Kuchta and Parkin¹⁴ also react directly with chalcogens and chalcogen atom transfer reagents to form the LSn=Y complexes. Enthalpies of addition to and subtraction from chalcogens at the Sn(II) center are in the expected order Se < S. The stable carbenes prepared by Arduengo and coworkers¹⁵ also undergo clean S atom transfer:

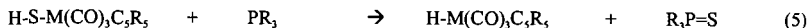


The enthalpies of S atom transfer to the carbene carbon are more exothermic than to the stannylene tin. The crystal structures of two of the R₂C=S complexes have been determined. There is a correlation between the structures, the enthalpies of sulfurization, and also the enthalpies of binding to metals of the carbene and stannylene ligands.

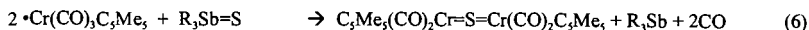
The enthalpies of insertion of a single sulfur atom into the metal-hydrogen bonds have been determined as shown in eqn. (4):



These data allow estimation of the M-SH bond strength which follows the order Cr < Mo < W. Desulfurization by phosphines of the metal sulphydryl complexes occurs in some cases as shown in eqn.(5), in keeping with thermochemical predictions:



Reaction (6) between two moles of the 17 electron stable chromium centered radical and triphenyl antimony sulfide occurs cleanly as shown:

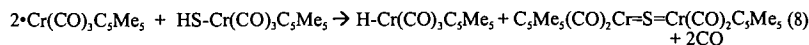


The enthalpy of reaction (6) has been measured and used to estimate the energy of "embedding" a single S atom in the multiply bonded bridging sulfido complex.

The stable transition metal radical $\bullet\text{Cr}[\bullet\text{Cr} = \bullet\text{Cr}(\text{CO})_3\text{C}_3\text{Me}_5]$ provides a good area for study of the mechanisms of reaction of a transition metal radical fragment with organosulfur substrates. Earlier work has shown a variety of mechanisms for reactions of thiols⁶ and disulfides⁷. This work has been extended to include H_2S and S_8 . Reaction of hydrogen sulfide with the radical species is much faster than analogous reactions of thiols. Initial oxidative addition of one sulfur-hydrogen bond occurs as shown in eqn. (7):



The metal sulphydryl complex formed in the first step can be further attacked by two moles of radical:

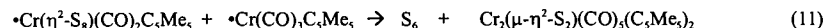


The mechanism of reaction (7) follows two pathways. Under pressure of carbon monoxide a third order rate law is obeyed [first order in hydrogen sulfide and second order in metal radical]. At low pressures of carbon monoxide, at higher temperatures, or under argon atmosphere, a second order rate law is obeyed [first order in hydrogen sulfide and first order in metal radical]. Rate and activation parameters as well as CO dependence are all consistent with rate determining ligand substitution to form the hydrogen sulfide substituted radical complex shown in eqn. (9):



In spite of the fact that the equilibrium in eqn. (9) lies to the left, the hydrogen sulfide substituted radical complex once formed can undergo rapid attack by a second mole of metal radical. Under appropriate conditions the rate of oxidative addition occurs at the rate of ligand substitution itself. The small size of hydrogen sulfide probably accounts for its increased ability, relative to thiols, to compete with carbon monoxide as a ligand.

In a similar way, S_8 also shows a complex reactivity pattern with the chromium radical and depends on carbon monoxide pressure. Kinetic evidence supports a pathway under argon atmosphere involving steps shown in eqn.(10) and (11):



Formation of $\text{Cr}_2(\mu\text{-}\eta^2\text{-S}_2)(\text{CO})_3(\text{C}_3\text{Me}_5)_2$ is clean under appropriate conditions and its enthalpy of formation as well as desulfurization to $\text{Cr}_2(\mu\text{-S})(\text{CO})_4(\text{C}_3\text{Me}_5)_2$ have been measured.

VII. CONCLUSIONS

Some insight into factors determining the enthalpies of sulfur atom transfer and insertion as well as the rates and mechanisms of related reactions have been determined. Considerable additional work is needed before the understanding of inorganic sulfur reactions achieves the level of understanding currently present in organic sulfur chemistry.

ACKNOWLEDGMENT

This research was supported by the Petroleum Research Fund administered by the American Chemical Society as well as the National Science Foundation.

REFERENCES

- (1) Capps, K. B.; Wixmerten, B.; Bauer, A.; Hoff, C. D. *Inorg. Chem.* **1998**, *37*, 2861.
- (2) Huang, J.; Schanz, H. J.; Nolan, S. P.; Bauer, A.; Capps, K. B.; Hoff, C. D.; **to be published.**
- (3) Parkin, G.; Kuchta, M. C.; Capps, K. B.; Wixmerten, B.; Bauer, A.; Hoff, C. D. **to be published.**
- (4) Bauer, A.; Capps, K. B.; Wixmerten, B.; Abboud, K. A.; Hoff, C. D. *Inorg. Chem.* **1999**, *38*, 2136.
- (5) Capps, K. B.; Bauer, A.; Hoff, C. D.; **to be published.**
- (6) Ju, T. D.; Capps, Lang, R. F.; Roper, G. C.; Hoff, C. D. *J. Am. Chem. Soc.* **1996**, *118*, 5328.
- (7) Ju, T. D.; Capps, K. B.; Lang, R. F.; Roper, G. C.; Hoff, C. D.; *Inorg. Chem.* **1997**, *36*, 614.
- (8) Capps, K. B.; Bauer, A.; Hoff, C. D.; *Inorg. Chem.* **submitted for publication.**
- (9) Capps, K. B.; Bauer, A.; Hoff, C. D.; **to be published.**
- (10) Transition Metal-Sulfur Chemistry. *ACS Symp. Ser.* **1996**, *653*.
- (11) James, B. R. *Pure and Appl. Chem.* **1997**, *69*, 2213.
- (12) Ju, T. D.; Capps, K. B.; Roper, G. C.; Lang, R. F.; Hoff, C. D.; *Inorg. Chim. Acta.* **1998**, *270*, 488.
- (13) Jason, M. E.; *Inorg. Chem.* **1997**, *36*, 241.
- (14) Kuchta, M. C.; Parkin, G.; *J. Amer. Chem. Soc.* **1994**, *116*, 8372.
- (15) Arduengo, A. J. III, Harlow, R. L.; Kline, M.; *J. Am. Chem. Soc.* **1991**, *113*, 361.

HYDROGEN TRANSFER FROM CATALYST INTERMEDIATE PROTOTYPES TO STABILIZED RADICALS

James A. Franz, Douglas S. Kolwaite, John C. Linehan and Jerome C. Birnbaum
Pacific Northwest National Laboratory
Richland, Washington 99352

Edward Rosenberg
University of Montana
Missoula, MT 59812

Keywords: Free Radicals, Organometallic Hydrides, Hydrogen Transfer, Kinetics, Benzyl Radical, Absolute Rates

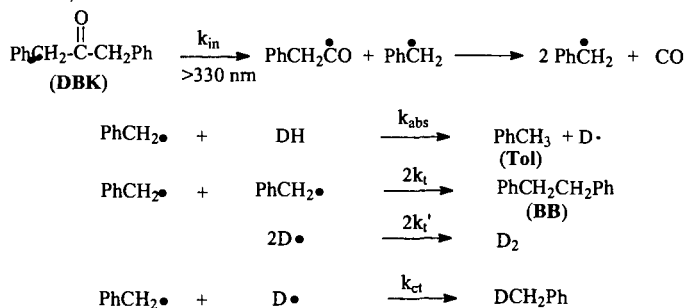
INTRODUCTION

The transfer of hydrogen from metal-hydrogen bonds (M-H) to closed-shell molecules or free radicals, from metal-activated organic structure (MC-H) and from metal-activated heteroatom-hydrogen bonds (MS-H) are primary processes involved in catalytic hydroxypropylolysis of organic structure. The characterization of the reactivity of transition metal hydride μ - and σ -bonds and agostic M-H₂ bonds in fundamental catalysis steps is of wide interest. Whereas a substantial body of data now exists describing the kinetics of reactions of alkyl organic free radicals with main group hydrides (e.g., S-H¹, Se-H², Sn-H and Si-H³), few kinetic studies of the reactions of transition metal hydrides⁴, and particularly hydrides involving novel metal bonding arrangements, exist. Relatively few kinetic studies of the reaction of benzylic radicals with either main group or transition metal hydrides exist. In previous work we have determined families of basis rate expressions for abstraction of hydrogen atom by alkyl and benzylic radicals from a variety of hydrogen donors for use in competition kinetic studies to measure rate constants for homolytic molecular rearrangements related to coal and biomass hydroxypropylolysis.⁵ Recently, we have carried out kinetic studies to determine the homolytic hydrogen transfer properties of hydrogen bonded in novel arrangements in metal clusters and other catalyst related systems. In this paper, we review recent results from application of competition kinetic methods to determination of absolute rates of abstraction of hydrogen atom from M-H, C-H and S-H bonds to the benzyl radical, where M = Mo, Os, Ru, Ir, and Rh.

KINETIC APPROACH

The kinetic method used in studies in this laboratory to determine rates of reaction of stabilized organic free radicals makes use of the competition of self-termination of the radical of interest with abstraction of hydrogen from the donor (DH) of interest. The competition of self-termination of benzyl radical to form bibenzyl (BB) versus hydrogen abstraction to form toluene (Tol) is depicted in Scheme 1. Thus, photolysis of a convenient photoprecursor (DBK) to form benzyl radical under conditions of constant rate of photolysis of DBK is followed by abstraction of hydrogen to form toluene (k_{abs}) versus self-termination ($2k_t$) to form bibenzyl.

Scheme 1



The rate of formation of bibenzyl and toluene are given by the differential equations ($[PhCH_2\bullet] = [B\bullet]$):

$$\frac{d[Tol(t)]}{dt} = k_{abs}[DH(t)][B\bullet] \quad (1)$$

$$\frac{d[BB(t)]}{dt} = k_t[B\bullet]^2 \quad (2)$$

Note that for constant benzyl radical concentration and short extent of consumption of donor, DH, integration of eq 1 and eq 2 yield expressions that are linear in toluene and bibenzyl with time.

Combining eqs 1 and 2, for $DH(t) = DH(0) - Tol(t)$ leads to eqs 3 and 4:

$$\int \left(\frac{d[Tol(t)]}{[DH(0)] - [Tol(t)]} \right) = k_{abs} \sqrt{\frac{1}{k_t} [BB] \Delta t} \quad (3)$$

$$Tol(t) = DH_0 \left(1 - e^{-\frac{k_{abs}(\sqrt{BB} \sqrt{\Delta t})}{\sqrt{k_t}}} \right) \quad (4)$$

Eq. 4 provides the time dependence of formation of toluene in terms of self-termination product, bibenzyl (BB), the elapsed time of the photolysis in seconds (Δt), the initial hydrogen donor concentration, DH_0 , and the rate constants for abstraction, k_{abs} , and self-termination, k_t .

At short extent of conversion of the donor, DH, and DBK, the exponent in eq 4 is small and the expression reduces to:

$$Tol(t) = DH_{av} \left(\frac{k_{abs}}{\sqrt{k_t}} (\sqrt{BB(t)} \sqrt{\Delta t}) \right) \quad (5)$$

or

$$k_{abs} = \frac{[Tol]}{[DH_{av}] \sqrt{BB} \sqrt{\Delta t}} \sqrt{k_t} \quad (6)$$

Short extent of conversion of photoprecursor, DBK, and hydrogen donor DH, results in constant benzyl radical concentration and linear formation of toluene and bibenzyl with duration of photolysis. If DBK is photolyzed at a constant rate of photolysis to short extent of conversion, but the donor DH is appreciably consumed, the time dependence of toluene and bibenzyl production will exhibit curvature described by eq 4. Providing values of k_t are available for a given solvent system, the method is a particularly convenient method for the determination of rate constants for abstraction, k_{abs} , by stabilized radicals from donors.

Experimental rate constants for self-termination of organic free radicals are available from the work of Fischer and coworkers.⁶ Rate constants can be estimated using the empirical method recommended by Fischer using the von Smoluchowski equation (eq 7) with diffusion coefficients derived from the Spornol-Wirtz modification of the Debye-Einstein equation (eq 8), or estimated by measurement of the diffusion coefficient of a model of the radical of interest (e.g., toluene for benzyl radical) in the solvent of interest by the Taylor method.⁷

$$2k_t = (8\pi / 1000) \sigma \rho D_{AB} N \quad (7)$$

$$D_{AB} = kT / 6\pi\eta f \quad (8)$$

In eq 7, N is Avogadro's number, D_{AB} is the diffusion coefficient of the radical A in solvent B, σ is a spin statistical factor describing the percent of singlet radical encounter pairs formed (1/4) and ρ is the diameter of the diffusing radical. Eq. 8 is the Spornol-Wirtz (SW)⁸ modification of the Debye Einstein equation ($f = SW$ microfriction factor, η is the viscosity of the solvent). A number of the assumptions inherent in this semiempirical approximation are subject to challenge. The assumption that 100% of singlet encounter radical pairs react in the solvent cage, and the assumption that the diffusion constants for the parent hydride can be used as a model⁹ for the radical can be challenged. Empirically it has been established by Fischer and coworkers that self-termination rate constants k_t for small carbon-centered radicals in non-associating solvents

can be estimated with errors less than about 20%. For benzyl radical in alkanes and in toluene, the errors in estimation of the rate constant for self termination of benzyl are less than 15%. Details of the procedure for estimation of values of k_t have been presented elsewhere. For self-termination of benzyl radical in benzene, the procedure provides the expression:

$$\ln(2k_t/M^{-1}s^{-1}) = 26.94 - 2733/RT, \text{ RT in calories.} \quad (9)$$

The competition kinetic method is most suitable for rate constants in the range 10^3 - $10^6 \text{ M}^{-1}\text{s}^{-1}$.

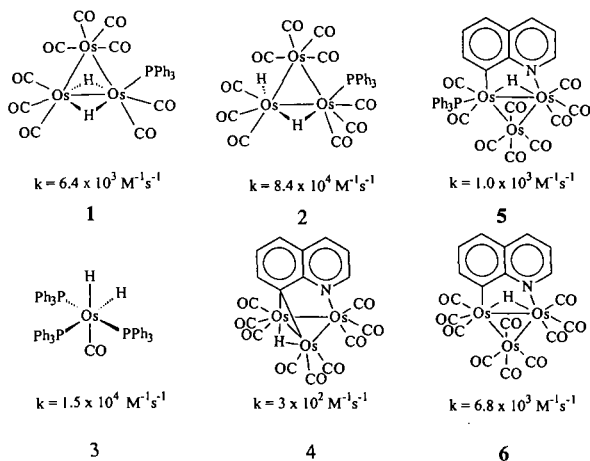
EXPERIMENTAL APPROACH

Samples of dibenzyl ketone (DBK), $\sim 0.01 \text{ M}$, hydrogen donor, 10^{-4} - 10^{-2} M , and internal gas chromatography standard are dissolved in benzene in 5-mm x 6-cm diameter pyrex tubes. The solutions are freeze-thaw degassed in three cycles and sealed on a vacuum line. The samples are temperature-equilibrated in an aluminum block equipped with thermocouples in a temperature-controlled oven equipped with a quartz window to allow photolysis. The samples are photolyzed with the water-filtered light of a 1-kW Hanovia high pressure xenon arc lamp for periods of 0.5 second to typically 30 seconds, to short extent (e.g., < 1-2%) of conversion of DBK and donor. Samples are opened and the yields of toluene and bibenzyl are determined by gas chromatography. Care is taken to ensure that the temperature of the sample remains constant during the photolysis. To verify that equation (6) is appropriate, the time dependence of production of toluene and bibenzyl is measured using constant lamp power levels and carefully reproducible sample positioning. The use of eq 6 is appropriate for linear production of toluene and bibenzyl, as predicted by eqs 1 and 2, where benzyl radical concentration is a constant. For extensive conversion of donor, but constant photolysis rate of the photoprecursor, eq. 4 may be employed. For very fast donors, where significant consumption of donor occurs, very short photolysis times are necessary to operate in the linear range of toluene/bibenzyl concentration. A Uniblitz computer-controlled optical shutter was employed to allow accurate, short photolysis times. Hydrides were synthesized or purchased from Strem Chemical.¹⁰

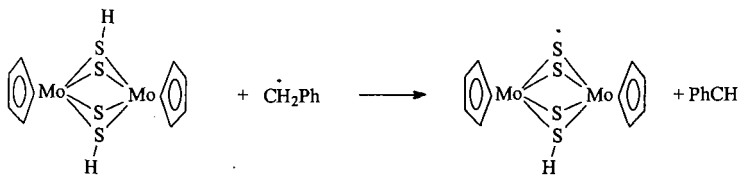
RESULTS AND DISCUSSION

Rate expressions for hydrogen atom abstraction from a selection of osmium mono- and trimetallic clusters were determined, as well as rate constants for ruthenium and rhodium hydrides have been examined. Rate constants for reaction of benzyl radical with metal hydrides in benzene are shown in Figure 1. The immediate observation is that μ -bonding does not render the hydrogen atom inaccessible to abstraction by benzyl radical. Structure 1 is only 2-10 times less reactive than σ dihydride 3, and only a factor of ten slower than mixed σ - and μ -hydride 2.

Figure 1. Hydrogen Abstraction from Mono- and Triosmium hydrides. Rate constants are in benzene at 298K.



The highly congested and electron deficient structure of 4 results in a rate constant an order of magnitude less than 1. This rate constant is near the practical lower limit of the



11

The results illustrate the surprising effects on homolytic reactivity that can be imparted by incorporation of the heteroatom function in the Mo_2S_4 cluster.

CONCLUSIONS

We have presented a preliminary account of characterization of the homolytic kinetic reactivity of a selection of transition metal hydrides, including a selection of trisium clusters that include σ - and μ -bonding of hydrogen to electron-deficient and electron-precise (18-electron) trimetallic clusters, and we have presented new rate constants for reaction of rhodium, ruthenium, iridium and molybdenum hydrides. The results show that μ -bonded hydrogen is reduced only moderately in reactivity compared to σ -bonded hydrides for non-fluorinated systems, in which migration of the hydrogen about the trisium skeleton appears to be slow. The rate constants are sensitive to steric bulk about the cluster, and are sensitive to the degree of electron-deficiency or lack thereof. Work to characterize the reactivity of homolytic intermediates arising from mononuclear and cluster organometallics is underway. Finally, this work has provided quantitative insight into the homolytic reactivity of metal-hydrogen bonding configurations in catalyst intermediates and a view of the enhancement of heteroatom reactivity resulting from incorporation in small clusters.

ACKNOWLEDGEMENT

This work was supported by the Office of Science, Office of Basic Energy Sciences, U.S. Department of Energy, under contract DE-ACO6-76RLO 1830.

REFERENCES

- 1 Franz, J.A.; Bushaw, B.A.; and Alnajjar, M.S. *J. Am. Chem. Soc.* **1989**, *111*, 268
- 2 Newcomb, M.; Choi, S.-Y.; Horner, J. H. *J. Org. Chem.* **1999**, *In press*
- 3 (a) Curran, D. P. *Synthesis* **1988**, *6*, 417-39, (b) Baguley, P. A.; Walton, J. C. *Angew. Chem. Int. Ed.* **1998**, *37*, 3072-3082, (c) Davies, A. G. *Organotin Chemistry*; WILEY-VCH: Weinheim, 1997.
- 4 For examples, see (a) Bakac, A. *Inorg. Chem.* **1998**, *37*, 3548-3552, (b) Ash, E. A.; Hurd, P. W.; Darenbourg, M. Y.; Newcomb, M. J. *J. Am. Chem. Soc.* **1987**, *109*, 3313-3317, (c) Bullock, R. M.; Samsel, E. G. *J. Am. Chem. Soc.* **1990**, *112*, 6886-6898, (d) Eisenberg, D. C.; Lawrie, C. J. C.; Moody, A. E.; Norton, J. R. *J. Am. Chem. Soc.* **1991**, *113*, 4888-4895, (e) Eisenberg, D. C.; Norton, J. R. *Isr. J. Chem.* **1991**, *31*, 55-66, (f) Kinney, R. J.; Jones, W. D.; Bergman, R. G. *J. Am. Chem. Soc.* **1978**, *100*, 7902-7915.
- 5 See, e.g. (a) Alnajjar, M.S. and Franz, J.A. *J. Am. Chem. Soc.* **1992**, *114*, 1052, (b) Autrey, S.T.; Alnajjar, M.S.; Nelson, D.A.; and Franz, J.A. *J. Org. Chem.* **1991**, *56*, 2197.
- 6 (a) Fischer, H.; Paul, H. *Acc. Chem. Res.* **1987**, *20*, 200-266, (b) Lehni, M.; Schuh, H.; Fischer, H. *Int. J. Chem. Kinet.* **1979**, *11*, 705-713. (c) Claridge, R. F. C.; Fischer, H. *J. Phys. Chem.* **1983**, *87*, 1960-1967, (d) Huggenberger, C.; Fischer, H. *Helv. Chim. Acta* **1981**, *64*, 338-353.
- 7 See ref. 5b for a detailed description of the procedure for obtaining von Smoluchowski rate expressions.
- 8 Spemol, A.; Wirtz, K., *Z. Naturforsch.* **1953**, *8a*, 522.
- 9 Polarizable radicals may not be well served by this assumption, but benzyl radical is well-behaved: (a) Okamoto, K.; Hirota, N.; and Terazima, M. *J. Chem. Soc. Far. Trans.* **1998**, *94(2)*, 185 and *J. Phys. Chem. A.* **1997**, *101*, 5269.
- 10 Compounds **1** and **2**: (a) Deeming, A.J.; Hasso, S. J., *J. Organomet. Chem.*, **1975**, *88*, C21. (b) Shaply, J.R., Keister, J.B.; Churchill, M.R., *J. Am. Chem. Soc.*, **1975**, *97*, 4145. (c) Deeming, A.J.; Hasso, S. J., *J. Organomet. Chem.*, **1976**, *114*, 313. Compounds **4,5**, and **6**: Kabir, S.E.; Kolwaite, D.S.; Rosenberg, E.; Hardcastle, K.; Cresswell, W.; Gringstaff, J., *Organometallics*, **1995**, *14*, 3611. Arcia, E.; Kolwaite, D.S.; Rosenberg, E.; Hardcastle, K.; Ciurash, J.; Duque, R.; Osella, D.; Gogetto, R.; Milone, L., *Organometallics*, **1998**, *17*, 415. Compound **3**: Ahmad, N.; Levison, J. J.; Robenson, S. D.; Uttley, M. F.; Parshall, G. W. ed., *Inorganic Synthesis*, **1974**, *15*, 54-56. Compound **7**: Ahmad, N.; Levison, J. J.; Robenson, S. D.; Uttley, M. F.; Parshall, G. W. ed., *Inorganic Synthesis*, **1974**, *15*, 48-50. Compounds **8** and **10** purchased from Strem Chemicals.
- 11 Franz, J.A.; Linehan, J.C.; Birnbaum, J.C.; Hicks, K.S.; and Alnajjar, M.S. *J. Am. Chem. Soc.*, submitted.
- 12 Rakowski DuBois, M.; VanDerveer, M.C.; DuBois, D.L.; Haltiwanger, R.C. and Miller, W.K. *J. Am. Chem. Soc.* **1980**, *102*, 7456.

EXPERIMENTAL APPROACHES TO MEASURE THE CHEMICAL AND PHYSICAL
PROPERTIES OF RADICAL INTERMEDIATES; TIME-RESOLVED PHOTOACOUSTIC
CALORIMETRY WITH THE LAYERED PRISM CELL.

Tom Autrey and Nancy Foster-Mills

Pacific Northwest National Laboratory
Environmental Health Sciences Division
Richland, WA 99352

KEYWORDS

Thermochemistry, kinetics, radical intermediates

ABSTRACT.

Mechanistic kinetic modeling has been successfully used to elucidate the contributions of strong bond scission by various competing hydrogen transfer pathways as a function of the reaction conditions. The success of the MKM approach is limited by the availability and quality of kinetic and thermodynamic data derived from either experimental and/or theoretical methods. New and improved experimental methods to obtain quantitative information regarding the thermochemical and kinetic properties of reactive intermediates in condensed phases will facilitate the development new and improved mechanistic kinetic models. We have used time-resolved photoacoustic calorimetry, employing the Layered Prism Cell (LPC), to measure the chemical and physical properties of short-lived reactive intermediates in solution. The lifetimes and thermochemical properties of reactive radicals in the presence of various hydrogen atom donors will be presented and comparisons will be drawn to the literature.

INTRODUCTION.

Mechanistic Kinetic Modeling (MKM) is a useful experimental approach to quantify and understand the important reaction pathways occurring in a complex reaction scheme. MKM combined with traditional experimental and semi-empirical approaches have been used to investigate high temperature (> 600 K) hydrogen atom transfer pathways between hydroaromatic structures.¹⁻¹⁷ The approach is develop a model inclusive of the important reaction pathways that will "predict" (or fit) experimental observations. However, the quality of the model is limited by inclusion of the important reaction steps and the availability of thermochemical kinetic parameters to provide temperature dependent rate data. The models have evolved with enhanced methods to predict contributing reaction pathways and improvements in measuring or calculating heats of formation of transient radical intermediates. For example, inclusion of the reverse hydrogen transfer step for a thermal neutral hydrogen transfer yields a model that fits the experimental data without the need to invoke the controversial radical hydrogen transfer pathway.⁷ In another example, it was shown that varying the barrier for the initiation step for hydrogen transfer between alkyl pyrenes by less a few kcal/mol resulted in a model that fits the experimental data without the need to invoke the rht pathway.² Even the observed experimental selectivity of bond scission could be explained by a change in reaction pathways (hydrogen atoms and/or molecular assisted homolysis) with a change in solvent composition.¹

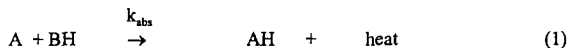
One of the goals of our research is to use experimental and theoretical approaches to measure or calculate the heats of formation of organic free radicals and to measure rate constants of reactions of reactive transient species. In this symposium new methods using time-resolved photoacoustic calorimetry to obtain rate constants for hydrogen atom transfer reactions and determinations of heats of formation of transient species will be presented.

APPROACH.

Time-resolved photoacoustic calorimetry has been used to obtain both chemical and physical properties of photo-generated reactive intermediates. Absorption of electromagnetic energy (hv) by a molecule in solution generates an electronically/vibrational excited meta-stable intermediate. The excess energy can be released from the excited state by a combination of emission, internal conversion (IC) and/or *chemical pathways*. The release of heat by either IC or chemical pathways generates an acoustic pressure pulse that can be detected with an ultrasonic transducer. The mathematical solutions describing the events leading to formation of the acoustic pressure pulse and the subsequent detection with piezoelectric transducers to yield a

photoacoustic signal,¹⁸⁻²⁰ and the methods to analyze the photoacoustic signals to obtain information on the chemical and physical properties of short-lived reactive intermediates have been studied in detail.²¹⁻²⁷

A model is useful to illustrate the time dependent response, $M(t)$, provided by an ultrasonic transducer for a simple scheme involving the reaction of a reactive intermediate A to AH as shown in equation 1. In this example A is a photo-generated reactive intermediate and B is a hydrogen donor. $M(t)$ is adequately described by a convolution (*) of the exponential release of heat $H(t)$ with a model instrument response function, $S(t)$. In our model $S(t)$ is a dampened sine wave, where ν is the resonant frequency, τ_c is the dampening constant of the transducer and K is an instrument constant. Using our model instrument response function we can demonstrate that for τ_A , ($\tau_A = 1/k_{abs}$, rate of abstraction) in $H(t)$, varied between 100 ns and 10 μ s result in a calculated response $M(t)$ that is distinguishable in shape from model instrument response $S(t)$ as shown in Figure 1.



$$M(t) = H(t) * S(t) \quad (2)$$

$$H(t) = \phi_{abs} \exp(-t/\tau_A) \quad (3)$$

$$S(t) \sim K [\exp(-t/\tau_c) \sin(\nu t)] \quad (4)$$

The experimental instrument response $R(t)$ can be obtained with a photoacoustic standard, where $\phi = 1$, and $\tau \ll \nu$. The experimentally observed photoacoustic signal $E(t)$ is therefore the convolution of $H(t)$ with the experimental instrument response $R(t)$ as shown in equation 5.

$$E(t) = H(t) * R(t) \quad (5)$$

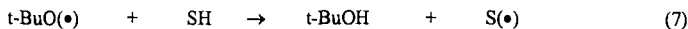
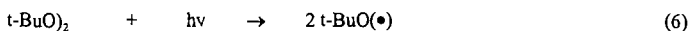
From the *shape* and *amplitude* of the experimental photoacoustic waveform, $E(t)$, we can obtain a description of the events that occurred as a consequence of the absorption of energy to generate radical intermediate A. The exponential release of heat $H(t)$ is comprised of two separable parameters, ϕ_{abs} the fraction of absorbed energy released as heat in the conversion of A \rightarrow AH, and τ_A , the lifetime of reactive intermediate A. This is an important point, the *amplitude* of the photoacoustic waveform is directly proportional to the magnitude of the fraction of absorbed energy released as heat, and the *shape* of the photoacoustic waveform is proportional to the rate of decay of A \rightarrow AH.

Deconvolution of the experimental waveform $E(t)$, with the experimentally measured instrument response, $R(t)$ can provide quantitative information regarding both the quantity of energy released in the transformation of A \rightarrow AH and the rate at which the process occurs. Both ϕ_{abs} and τ_A depend on the concentration and properties of the hydrogen atom donor BH. Importantly, these two parameters can be treated independently. Specifically, sources of heat (or volume changes) contributing to the amplitude of the photoacoustic signal need not be quantitatively discriminated if a kinetic analysis is all that is desired.

In our laboratory we have been developing methods to improve the sensitivity, enhance the time-resolution and increase experimental flexibility.²⁸⁻³¹ We have taken an approach to treat the kinetic and thermodynamic components of the experiment separately when necessary. Using optical transparent (thin) samples the kinetic information (τ) can be obtained from the shape of the waveform, even if the thermodynamic and volumetric components contributing to the amplitude of the signals are still difficult to quantify.

RESULTS.

Pulsed photolysis of di-t-butylperoxide in the uv generates a pair of reactive t-butoxyl radicals. The lifetime of the radicals is solvent dependent. The reaction scheme shown in equations 6-7 can be modeled as a sequential two step reaction pathway.



In previous work²⁸ we demonstrated the capability to obtain the lifetime of the t-butoxyl radical in binary solvent mixtures containing methanol and ethanol. Using the layered PA cell permits the a direct measure of the rate of hydrogen abstraction by measuring the volume change induced by the reaction of the alkoxyl radical with the solvent (even when the thermodynamic properties of the sample and reference solutions are not matched).

To obtain quantitative thermochemical estimates a reasonable understanding of both thermal and volumetric contributions to the PA amplitude must be evaluated. There has been some effort undertaken to separate the enthalpic and volumetric contributions in organic solvents using both photoacoustic and transient grating approaches. Another potential hindrance is thermal changes brought about by changes in heats of solvation. In order to separate the ΔV_{rxn} and $\Delta \Delta H_{\text{soliv}}$ terms from the experimentally measured amplitude a few groups have used correction terms. The approach is to use a standard hydrogen donor, e.g., cyclohexadiene and assume the difference between the gas phase literature value and the experimental PA signal is constant. Then the difference between gas phase values and observed value (a correction term) can be subtracted from experimental value to arrive at an experimental measurement of the BDE. One of the assumptions used in the correction term approach is the equivalency of the solvent quality factors for an organic solvent with and without significant concentrations of peroxide. For unmatched solvents there can be a substantial difference. Additionally correction factors must be determined for each experimental condition, i.e., irradiation in a 30% peroxide solution will yield a different correction term need for a 6% peroxide solution and different corrections are necessary for various excitation wavelengths, i.e., 308 nm will yield a different magnitude correction than 355 nm.

The advantage of the layered prism cell is that a direct measure can be possible because the reaction volume change, due to peroxide bond scission, can be separated from the thermal volume change, due to an exothermic hydrogen atom abstraction, in a time-resolved manner. Unfortunately interpretation of thermochemistry data obtained in the layered cell can suffer from the same difficulties experienced with the traditional cuvette geometry in solvents where the contribution due to enthalpies of solvation of the different species can be significant. An accurate evaluation of the thermochemistry requires equivalent thermoelastic properties ($\beta/\alpha\rho C_p$) for both the sample and reference solution and the ability to separate the ΔV_{rxn} and $\Delta \Delta H_{\text{soliv}}$ from the amplitude of the signal. Results for some of our energy determinations are shown in Table 1. The lower limits determined for the BDE in polar solvents is likely due to the contribution differences in enthalpy of solvation between the alkoxyl radical/donor pair and the t-BuOH/donor radical pair. The benefits and limitations of time-resolved photoacoustic calorimetry with the layered prism cell will be presented.

ACKNOWLEDGMENTS.

This work was supported by the U.S. Department of Energy, Office of Basic Energy Research, Chemical Sciences Division, Process and Techniques Branch. The work was conducted at Pacific Northwest Laboratory, which is operated for the U. S. Department of Energy under Contract DE-ACO6-76RL0 1830. Support for NFM was provided through AWU-NW under grant DE-FG06-89ER-75522 with the U.S. Department of Energy.

REFERENCES.

- (1) Autrey, T.; Albom, E. A.; Franz, J. A.; Camaioni, D. M. *Energy Fuels* 1995, 9, 420-8.
- (2) Autrey, T.; Powers, T.; Albom, E. A.; Camaioni, D. M.; Franz, J. A. *Coal Sci. Technol.* 1995, 24, 1431-4.
- (3) Autrey, T.; Albom-Cleveland, E.; Camaioni, D. M.; Franz, J. A. *Prepr. Pap. - Am. Chem. Soc., Div. Fuel Chem.* 1994, 39, 627-31.
- (4) Autrey, S. T.; Camaioni, D. M.; Ferris, K. F.; Franz, J. A. *Conf. Proc. - Int. Conf. Coal Sci., 7th* 1993, 1, 336-9.
- (5) Autrey, T.; Gleicher, G. J.; Camaioni, D. M.; Ferris, K. F.; Franz, J. A. *Prepr. Pap. - Am. Chem. Soc., Div. Fuel Chem.* 1991, 36, 521-8.
- (6) Autrey, T.; Franz, J. A. *Prepr. Pap. - Am. Chem. Soc., Div. Fuel Chem.* 1990, 35, 381-6.
- (7) Camaioni, D. M.; Autrey, S. T.; Franz, J. A. *J. Phys. Chem.* 1993, 97, 5791-2.
- (8) Camaioni, D. M.; Autrey, S. T.; Franz, J. A. *Prepr. - Am. Chem. Soc., Div. Pet.*

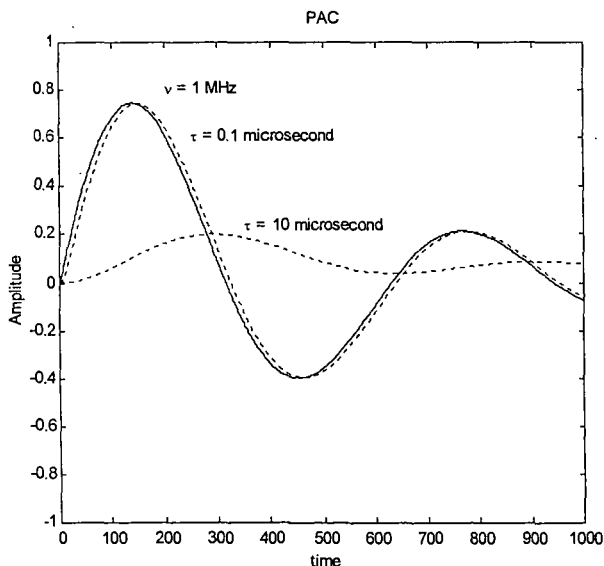
- Chem.* **1994**, *39*, 303-9.
- (9) Camaioni, D. M.; Autrey, S. T.; Salinas, T. B.; Franz, J. A. *J. Am. Chem. Soc.* **1996**, *118*, 2013-22.
 - (10) Savage, P. E. *Energy Fuels* **1995**, *9*, 590-8.
 - (11) McMillen, D. F.; Malhotra, R.; Tse, D. S. *Energy Fuels* **1991**, *5*, 179.
 - (12) McMillen, D. F.; Malhotra, R.; Chang, S.-J.; Fleming, R. H.; Ogier, W. C.; Nigenda, S. E. *Fuel* **1987**, *66*, 1611.
 - (13) Malhotra, R.; McMillen, D. F. *Energy Fuels* **1993**, *1993*, 227.
 - (14) Stein, S. E. *Acc. Chem. Res.* **1991**, *24*, 350.
 - (15) Autrey, T.; Linehan, J. C.; Steams, C. J.; Camaioni, D. M.; Kaune, L.; Franz, J. A. *Prepr. Pap. - Am. Chem. Soc., Div. Fuel Chem.* **1997**, *42*, 66-69.
 - (16) Autrey, T.; Linehan, J. C.; Camaioni, D. M.; Kaune, L. E.; Watrob, H. M.; Franz, J. A. *Catal. Today* **1996**, *31*, 105-111.
 - (17) Autrey, T.; Linehan, J.; Camaioni, D.; Powers, T.; Wartob, H.; Franz, J. *Prepr. Pap. -Am. Chem. Soc., Div., Fuel Chem.* **1995**, *40*, 973.
 - (18) Patel, C. K. N.; Tam, A. C. *Rev. Modern Phys.* **1981**, *53*, 517-549.
 - (19) Lai, H. M.; Young, K. *J. Acoust. Soc. Am.* **1982**, *72*, 2000-2006.
 - (20) Diebold, G. J. *J. Phys. Chem. B* **1998**, *102*, 5404-5408.
 - (21) Rudzki, J. E.; Goodman, J. L.; Peters, K. S. *J. Am. Chem. Soc.* **1985**, *107*, 7849-7854.
 - (22) Braslavsky, S. E.; Heihoff, K. *Photothermal Methods*; Scaiano, J. C., Ed.; CRC Press, 1989; Vol. 1, pp 327-355.
 - (23) Braslavsky, S. E.; Heibel, G. E. *Chemical Reviews* **1992**, *92*, 1381-1410.
 - (24) Melton, L. A.; Ni, T.; Qingzheng, L. *Rev. Sci. Instrum.* **1989**, *60*, 3217-3223.
 - (25) Arnaut, L. G.; Caldwell, R. A.; Elbert, J. E.; Melton, L. A. *Rev. Sci. Instrum.* **1992**, *63*, 5381-5389.
 - (26) Beck, K. M.; Gordon, R. J.; Tardy, D. C. *Adv. Chem. Kinetics and Dynamics* **1995**, *2B*, 299-332.
 - (27) Puchenkov, O. V.; Malkin, S. *Rev. Sci. Instrum.* **1996**, *67*, 672-680.
 - (28) Autrey, T.; Foster-Mills, N.; Klepzig, K. *Photochem. Photbio. A* **1999**. In press
 - (29) Autrey, T.; Foster, N. S.; Klepzig, K.; Amonette, J. E.; Daschbach, J. L. *Rev. Sci. Instrum.* **1998**, *69*, 2246-2258.
 - (30) Foster, N. S.; Amonette, J. E.; Autrey, T. *Applied Spectroscopy* **1999**, *53*(6), in press.
 - (31) Foster, N. S.; Autrey, T.; Amonette, J. E.; Small, J. R.; Small, E. W. *American Laboratory* **1999**, *31*(4), 96.

Table 1. Experimentally measured heats of reaction for hydrogen atom abstraction by t-butoxyl radical from a series of organic hydrogen donor solvents determined by time-resolved photoacoustic calorimetry in the layered prism cell. The calculated BDE's are compared to the literature values.

Donor	ϕ^a	Experimental		Literature BDE
		ΔH_{rxn} (kcal/mol)	BDE ^b	
MeOH	0.28	-9.2±.5	(>89.6) ^c	92-96
EtOH	0.24	-13±.7	(>90.4) ^c	>93
IPA	0.22	-13±1	(>90.7) ^c	>91
THF	0.29	-13.1±.5	(>89.1) ^c	92-95
Cyclohexane	0.31	-5.6±.8	98.6	98.2
Toluene	0.31	-16.6±.9	88.0	88.6

(a) fraction of heat released in hydrogen abstraction step. (b) calculated bond dissociation energy determined from photoacoustic measurement. (c) lower limit, see text.

Figure 1. Model of a photoacoustic signal obtained using a 1 MHz piezoelectric transducer. Comparison of the instrument response $S(t)$ with $M(t)$ with $\tau_A = 100$ ns, and $M(t)$ with $\tau_A = 10$ μ s.



VARIATIONAL TRANSITION STATE THEORY METHODS FOR CALCULATING REACTION RATE CONSTANTS IN GAS AND CONDENSED PHASES

Bruce C. Garrett

Environmental Molecular Sciences Laboratory,
Pacific Northwest National Laboratory,
P.O. Box 999, Richland, WA 99352

1. Introduction

Transition state theory (TST) in its thermodynamic formulation¹ is the most widely used tool for analyzing rate constants of chemical reactions (for example, see Benson²). The dynamical formulation of TST³ provides the best approach to examine the approximations in TST and the basis for systematically improving the conventional theory. Over the past two decades, significant progress has been made in developing methods for quantitative predictions of reaction rate constants based upon the dynamical formulation of TST (see reviews by Truhlar, Hase, and Hynes⁴ and Truhlar, Garrett, and Klippenstein⁵). As an example, quantized variational transition state theory (VTST) with multidimensional, semiclassical tunneling corrections⁶⁻⁸ are capable of accurate predictions of gas-phase rate constants.^{9,10} The accuracy of the potential energy surface is typically the major factor limiting the accuracy of the calculated rate constants. In this paper we briefly review VTST methods and their application to gas-phase reaction. We also briefly outline an approach to extend these methods to treat reactions in solution.

2. VTST for Gas-Phase Reactions

In the dynamical formulation of TST, the classical equilibrium rate constant is derived using a single approximation, the fundamental assumption of TST.^{3,11} A dividing surface is defined so that all reactive trajectories must pass through it. The fundamental dynamical assumption is then defined as follows: a reactive trajectory originating in reactants must cross the dividing surface only once and proceed to products. The TST expression for the rate constant can then be expressed using equilibrium statistical mechanics without the need to calculate classical trajectories. Classical trajectories that recross the dividing surface cause a breakdown of the fundamental assumption. All reactive classical trajectories must cross the dividing surface and these are correctly counted in TST. However, some nonreactive trajectories may also be counted as reactive so that TST provides an upper bound to the exact reactive flux of classical trajectories through the dividing surface. This is the basis of classical variational TST in which the definition of the dividing surface is optimized to minimize the rate constant.¹²⁻¹⁴

In VTST the dividing surface is viewed as a tentative dynamical bottleneck to flux in the product direction, and the best bottleneck (the dividing surface allowing the least flow of flux) is located variationally. A practical approach is to define the dividing surfaces to be orthogonal to the reaction path, where the reaction path is defined as the minimum energy path connecting the saddle point with both the reactant and product regions. The minimum energy path is located by following the path of steepest descents in both directions from the saddle point in a mass-weighted coordinate system such that each degree of freedom has the same effective mass in the kinetic energy expression. The generalized expression for the thermal rate constant for temperature T is given as a function of the location s of the dynamical bottleneck along the reaction coordinate

$$k^{GT}(T, s) = \sigma \frac{k_B T}{h} \frac{Q^{GT}(T, s)}{\Phi^R(T)} \exp(-V_{MEP}(s)/k_B T) \quad (1)$$

where σ is a symmetry factor, k_B is Boltzmann's constant, h is Planck's constant, $Q^{GT}(T, s)$ is the generalized partition function for the bound degrees of freedom orthogonal to the reaction path at s , $\Phi^R(T)$ is the reactant partition function, and $V_{MEP}(s)$ is the value of the potential along the reaction path at s . In conventional TST, the dividing surface is placed at the saddle point, defined by $s=0$

$$k^{TST}(T) = k^{GT}(T, s=0) \quad (2)$$

Conventional transition state theory requires information about the potential energy surface only in the saddle point and reactant regions. In particular, the value of the potential at the saddle point (relative to the reactant value) is required, and if the partition functions are computed using a harmonic approximation, then the matrix of second derivatives of the potential energy with respect to mass-weighted coordinates (Hessian matrix) suffices. In one version of variational transition state theory, the canonical variational theory (CVT),^{15,16} the rate constant expression in eq. (1) is minimized with respect to s

$$k^{CVT}(T) = \min_s k^{GT}(T, s) \quad (3)$$

The improved canonical variational theory (ICVT)¹⁷ also variationally optimizes the location of the transition state dividing surface for a given temperature, but provides an improved treatment of threshold energies by using an ensemble which removes energies below the ground-state adiabatic threshold. To compute the rate constant using either the canonical or improved canonical variational theory, more information about the potential energy surface is required than for a conventional transition state theory calculation; information about the potential in a region around the reaction path is also required. For a harmonic treatment of the partition functions, the Hessian matrix along the minimum energy path will suffice. In this case the potential information needed is the energy and its first and second derivatives along the minimum energy path.

For many reactions of practical interest, particularly those involving hydrogen atom transfer, quantitative accuracy in computed rate constants requires that quantum mechanical effects be included in the theory. However, the fundamental assumption is inherently a classical approximation since it requires knowledge of both the coordinate and momentum (or flux) at the dividing surface. Additional approximations are needed to include quantum mechanical effects into TST. The standard approach is a separable approximation^{1,18} that replaces classical partition functions by quantum mechanical ones and includes a correction factor for quantum mechanical motion along the reaction coordinate (e.g., tunneling). The failure of this approach has been attributed largely to nonseparable effects, particular on quantum mechanical tunneling.^{19,20} The development of multidimensional tunneling correction factors that are consistent with variational transition state theory was greatly facilitated by the realization that the adiabatic theory of reactions is equivalent to one form of variational TST (microcanonical VTST).^{15,16} In this approach, the partition functions in eq. (1) are evaluated quantum mechanically, and quantum mechanical effects on the reaction coordinate motion (e.g., quantum mechanical tunneling) are included by a multiplicative factor – the transmission coefficient.

In VTST, it is consistent to treat tunneling as occurring through the vibrationally-rotationally adiabatic potential

$$V_a(s, \alpha) = V_{\text{MEP}}(s) + \epsilon_{\alpha}^{\text{GT}}(s) \quad (4)$$

where α is a collective index of the quantum numbers for the bound modes and $\epsilon_{\alpha}^{\text{GT}}(s)$ is the bound energy level for state α at the generalized transition state located at s along the reaction path. For thermal rate constants the tunneling is approximated using only the ground-state adiabatic potential curve ($\alpha=0$). The adiabatic approximation is made in a curvilinear coordinate system, and although the potential term is simple, the kinetic energy term is complicated by factors dependent upon the curvature of the reaction path. For systems in which the curvature of the reaction path is not too severe, the small-curvature semiclassical adiabatic ground state method^{21,22} includes the effect of the reaction-path curvature to induce the tunneling path to 'cut the corner' and shorten the tunneling length. The small-curvature tunneling (SCT) probabilities $P^{\text{SCT}}(E)$ are computed for energies below the maximum in the ground-state adiabatic potential curve (denoted V^{AG}) where transmission occurs by tunneling and above V^{AG} where nonclassical reflection can diminish the transmission probability. The SCT transmission coefficient is given by the normalized Boltzmann average of $P^{\text{SCT}}(E)$

$$\kappa^{\text{SCT}}(T) = \beta \exp(\beta V^{\text{AG}}) \int_0^{\infty} dE P^{\text{SCT}}(E) \exp(-\beta E) \quad (5)$$

where $\beta=1/k_B T$. Combining the SCT transmission coefficient with the improved canonical variational theory rate constant yields

$$k^{\text{ICVT/SCT}}(T) = \kappa^{\text{SCT}}(T) k^{\text{ICVT}}(T) \quad (6)$$

To construct the adiabatic potential, the type of potential information required is identical to that needed for the variational transition state theory calculation. For the SCT calculation it is also necessary to know the curvature of the reaction path which can be obtained from second derivatives of the potential along the reaction path. Thus, to provide a consistent and accurate estimate of the tunneling, no new information about the potential energy surface is required.

Accurate quantum rate constants for nearly forty gas-phase bimolecular reactions provide benchmarks to test the accuracy of the VTST calculations. VTST calculations, which include multidimensional tunneling corrections, have been tested against accurate quantal results for about 30 atom-diatom reactions in a collinear world and nearly 10 reactions in three dimensions. Conventional TST was found to be accurate within a factor of 2 for only about 25% of these systems and had errors larger than of 5 in about 25% of the systems. The VTST calculations were generally within 50% of the accurate results with errors less than a factor of two in all cases.

3. VTST for Solution-Phase Reactions

The computational procedures described above to perform VTST calculations require identification of a saddle point and a reaction path connecting the saddle point with reactants and

products. For reactions in solution, there can be many saddle points that are close in energy and that differ significantly only in the configuration of the solvent. The multiple saddle points are a reflection of the large anharmonicity in the solvent that makes the quantum mechanical calculation of the partition functions impractical. Procedures are outlined elsewhere²³ that allow VTST calculations, which are based upon potential energy surfaces and include quantum effects, to be extended to solution-phase reactions. In this approach the system is separated into a cluster model that contains the part of the system undergoing reaction and the solvent that is treated in an approximate manner. The coordinates of the cluster model are treated explicitly, and the effects of the extended solvent are approximately included in an effective Hamiltonian. The constant proximity of solvent molecules around the solute changes the interaction potential within the solute. The resulting mean field potential for the solute is obtained from an equilibrium ensemble average over solvent configurations. Since this mean field potential is obtained from an equilibrium ensemble average at each solute configuration, the equilibrium solvation assumption implies that the solvent molecules instantaneously equilibrate to each new solute configuration. Effects of solvent fluctuation from their equilibrium values upon reaction dynamics are included using a reduced-dimensionality model that introduces a limited number of additional degrees of freedom in the effective Hamiltonian.

This approach for including solvation effects requires explicit treatment of only a limited number of degrees of freedom and information about the effective potential energy surface for these explicit coordinates is needed only in the region of a reaction valley. Explicitly treating only a limited number of coordinates obviates some of the difficulties inherent in quantum mechanical TST calculations on solution-phase reactions (e.g., the multiple saddle point problem) and also allows the quantum mechanical effects to be included by the standard gas-phase procedures outlined above. These procedures are computationally intensive, but given the recent advances in computational hardware and software, these calculations are possible.

Acknowledgments

This work was supported by the Division of Chemical Sciences, Office of Basic Energy Sciences, U.S. Department of Energy. Pacific Northwest National Laboratory is operated for the DOE by Battelle.

References

- (1) Glasstone, S.; Laidler, K. J.; Eyring, H. *The Theory of Rate Processes*; McGraw-Hill: New York, 1941.
- (2) Benson, S. W. *Thermochemical Kinetics*, second ed.; Wiley: New York, 1976.
- (3) Wigner, E. *Trans. Faraday Soc.* **1938**, *34*, 29.
- (4) Truhlar, D. G.; Hase, W. L.; Hynes, J. T. *J. Phys. Chem.* **1983**, *87*, 2664.
- (5) Truhlar, D. G.; Garrett, B. C.; Klippenstein, S. J. *J. Phys. Chem.* **1996**, *100*, 12771.
- (6) Truhlar, D. G.; Garrett, B. C. *Ann. Rev. Phys. Chem.* **1984**, *35*, 159.
- (7) Truhlar, D. G.; Isaacson, A. D.; Garrett, B. C. In *Theory of Chemical Reaction Dynamics*; Baer, M., Ed.; CRC Press: Boca Raton, FL, 1985; Vol. IV; pp 65.
- (8) Steckler, R.; Hu, W.-P.; Liu, Y.-P.; Lynch, G. C.; Garrett, B. C.; Isaacson, A. D.; Melissas, V. S.; Lu, D.-h.; Truong, T. N.; Rai, S. N.; Hancock, G. C.; Lauderdale, J. G.; Joseph, T.; Truhlar, D. G. *Comp. Phys. Comm.* **1995**, *88*, 341.
- (9) Garrett, B. C.; Truhlar, D. G. *J. Chem. Phys.* **1984**, *81*, 309.
- (10) Allison, T. C.; Truhlar, D. G. In *Modern Methods for Multidimensional Dynamics Computations in Chemistry*; Thompson, D. L., Ed.; World Scientific: Singapore, 1998; pp 618.
- (11) Miller, W. H. *J. Chem. Phys.* **1974**, *61*, 1823.
- (12) Wigner, E. *J. Chem. Phys.* **1937**, *5*, 720.
- (13) Horiuti, J. *Bull. Chem. Soc. Japan* **1938**, *13*, 210.
- (14) Keck, J. C. *J. Chem. Phys.* **1960**, *32*, 1035.
- (15) Garrett, B. C.; Truhlar, D. G. *J. Phys. Chem.* **1979**, *83*, 1052.
- (16) Garrett, B. C.; Truhlar, D. G. *J. Phys. Chem.* **1979**, *83*, 1079.
- (17) Garrett, B. C.; Truhlar, D. G.; Grev, R. S.; Magnuson, A. W. *J. Phys. Chem.* **1980**, *84*, 1730.
- (18) Eyring, H. *J. Chem. Phys.* **1935**, *3*, 107.
- (19) Truhlar, D. G.; Kuppermann, A. *Chem. Phys. Lett.* **1971**, *9*, 269.
- (20) Miller, W. H. *Acc. Chem. Res.* **1976**, *9*, 306.
- (21) Skodje, R. T.; Truhlar, D. G.; Garrett, B. C. *J. Phys. Chem.* **1981**, *85*, 3019.
- (22) Skodje, R. T.; Truhlar, D. G.; Garrett, B. C. *J. Chem. Phys.* **1982**, *77*, 5955.
- (23) Garrett, B. C.; Schenter, G. K. *Int. Rev. Phys. Chem.* **1994**, *13*, 263.

THERMOCHEMISTRY, SOLVATION, AND DYNAMICS

Donald G. Truhlar, Yao-Yuan (John) Chuang, E. Laura Coitiño, José C. Corchado, Christopher J. Cramer, Derek Dolney, Joachin Espinosa-Garcia, Patton L. Fast, Gregory D. Hawkins, Yongho Kim, Jiabo Li, Benjamin Lynch, Mala L. Radhakrishnan, Orlando Roberto-Neto, Jocelyn M. Rodgers, Maria Luz Sánchez, Jordi Villà, Paul Winget, and Tianhai (Tony) Zhu,

Department of Chemistry and Supercomputer Institute, University of Minnesota,
Minneapolis, MN 55455-0431

KEYWORDS: Multicoefficient correlation methods, solvation models, variational transition state theory with semiclassical multidimensional tunneling contributions

Abstract. This paper reviews recent advances in computational thermochemistry, solvation modeling, and the calculation of chemical reaction rates in the gas phase and in solution. Recent advances in computational thermochemistry include integrated molecular orbital methods, scaling correlation energy, extrapolation to infinite basis sets, and multi-coefficient correlation methods. Recent advances in solvation modeling include Charge Model 2 (a class IV charge model) and the SM5.42R and SM5.42 solvation models; the solvation models are based on semiempirical molecular orbital theory, the *ab initio* Hartree-Fock method, or density functional calculations in the presence of a reaction field and on atomic surface tensions representing first-solvation-shell effects of water or an organic solvent. Our reaction rate calculations are based on variational transition state theory with multidimensional semiclassical tunneling approximations; in liquid solution we may add either equilibrium or nonequilibrium solvation effects.

INTRODUCTION

Much of our recent work is directed to one or another of two complementary goals: (1) to develop improved practical methods for electronic structure calculations in the gas-phase and in liquid-phase solutions and (2) to develop improved methods for interfacing these electronic structure calculations with dynamical methods for the prediction of chemical reactions rates, especially in systems with hydrogenic motion in the reaction coordinate where it is necessary to take account of quantum effects on the nuclear motion. The present paper provides an overview of some areas where progress has been achieved.

GAS-PHASE ELECTRONIC STRUCTURE

Substituent effects on bond energies are very important for both thermochemistry and kinetics. We have recently shown that integrated molecular orbital methods may be used to calculate accurate substituent effects on bond energies by treating a small capped subsystem at a high level of quantum mechanical electronic structure and the rest of a large system at a much lower level.¹⁻³ We have also developed a method for geometry optimization with such a dual-level scheme^{4,5} In the same spirit one may use molecular mechanics for the low level on the entire system; we have recently applied this

technique to treat an enzyme reaction where the subsystem had 25 atoms and the entire system had 8888 atoms.⁶

Another type of dual-level or multi-level strategy involves applying two or more levels of electronic structure calculation to the entire system. One strategy we have used is to combine the results at the various levels linearly in order to extrapolate to the limit of full configuration interaction (FCI) or an infinite one-electron basis set (IB) or both (full configuration interaction for an infinite basis is denoted complete configuration interaction or CCI). We have developed several variations on this scheme:

SAC	scaling all correlation: combine an uncorrelated and a correlated calculation with a given basis to extrapolate to CCI ^{5,7}
MC-SAC	multicoefficient SAC: combine an uncorrelated and two or more correlated calculations with a single basis to extrapolate to CCI ⁸
IB	combine calculations with two basis sets to extrapolate to the infinite-basis-set limit for a given level of electron correlation ⁹⁻¹¹
MCCM	multicoefficient correlation method: simultaneous application of MC-SAC and IB to extrapolate to CCI. ⁸

We have organized our MC-CM calculations by the shape of a polygon enclosing the methods in the level-basis plane, and we have proposed Colorado, Utah, and New Mexico methods, where the polygons have the shapes of those states.⁸ In addition we have proposed multicoefficient Gaussian-2¹² and multicoefficient Gaussian-3¹³ methods that outperform the original Gaussian-2 and Gaussian-3 methods.

For dynamics calculations we sometimes use a bootstrap technique in which high-level electronic structure calculations are carried out at stationary points, and then the parameters of semi-empirical molecular orbital theory, for example, Austin Model 1 (AM1), are adjusted to reproduce these properties as well as possible; the adjusted parameters are called specific reaction parameters or specific range parameters (SRP), and the modified AM1 is called AM1-SRP.¹⁴⁻²⁰ The advantage is that now the AM1-SRP calculation provides a smooth interpolation of the original high-level calculations between the stationary points. We have also used specific reaction parameters in Becke's 3-parameter hybrid Hartree-Fock-density-functional theory that he derived by adiabatic connection; we call this adiabatic connection-SRP (AC-SRP).²¹

A more powerful version of the AM1-SRP approach is a dual-level scheme in which the energy is given by a linear combination of *ab initio* Hartree-Fock calculations and AM1-SRP calculations. This is called HF||AM1-SRP.²¹ We are currently working on another global interpolation scheme which we hope will accomplish many of the goals of SRP methods but in a more systematic way. The new method is called multiconfiguration molecular mechanics (MCMM), and it involves combining high-level *ab initio* calculations with the valence bond formalism and molecular mechanics calculations.

There are situations in which each of these many strategies may be the best way to achieve an objective. We believe that such multi-level strategies will become increasingly important in the coming years.

Many one-electron basis sets are available for electronic structure calculations, and in essentially all cases they have been developed on the basis of variational energy calculations. But this strategy ignores the fact that many times the molecular energy is not the goal of a calculation. For example, modest basis sets are often used to obtain molecular geometries or reaction paths, at which or along which higher-level calculations are often used to calculate energies. In other applications, modest-sized basis sets are used to calculate partial atomic charges for large molecules for use with

molecular mechanics calculations of the energy. In order to allow more accurate applications of this type, we developed the MIDI! basis set, which is a heteroatom-polarized split valence basis with polarization functions optimized entirely on the basis of geometries and balanced one-electron charge distributions.^{22,23}

Electronically excited states of very large molecules are of great interest but can typically be modeled only by semiempirical molecular orbital theory such as intermediate-neglect-of-differential-overlap for spectroscopy (INDO/S). We have reparameterized this theory for carbonyl compounds leading to a new version called INDO/S2.²⁴

Electronic structure calculations yield not only energies but also molecular properties. We have developed the concept of class IV charges,²⁵ which (like some of our methods for energies) are an attempt to transcend the limitations of truncated CI and finite basis sets at as low a cost as possible. Our second class IV charge model, called Charge Model 2²⁶ (CM2), has been parameterized for ground states with neglect-of-diatomic-differential-overlap (NDDO) semiempirical molecular theory,²⁶ INDO/S and INDO/S2 semiempirical molecular orbital theory,²⁴ *ab initio* Hartree-Fock (HF)^{26,27} theory, density functional theory (DFT),²⁶ and adiabatic-connection hybrid HF-DFT (AC).²⁶ It has been parameterized for electronically excited states with INDO/S and INDO/S2.²⁴ These parameterizations have been shown to yield accurate partial atomic charges. The combination of CM2 with HF/MIDI! is a particularly powerful combination.²⁶

LIQUID-PHASE ELECTRONIC STRUCTURE

Whereas a goal of gas-phase electronic structure calculations is to produce potential energies for atomic motions, the corresponding goal of liquid-phase electronic structure calculations is to produce free energies or potentials of mean force. These can be used to calculate free energies of solvation, partition coefficients, solvatochromic shifts, and solvation effects on reaction rates. We have developed Solvation Model 5 as a fifth-generation approach (following SM1, SM1a, SM2, and SM4—SM3 involved the same approach as SM2) to the calculation of electronic wave functions and free energies in liquids (neat and solutions). SM5 is actually a suite of models, each of which may have more than one parameterization. In general, SM5 models approximate the standard-state free energy of solvation as

$$\Delta G_s^0 = \Delta G_{\text{ENP}} + G_{\text{CDS}}$$

where ΔG_{ENP} is a bulk electrostatic term includes solute electronic (E) and nuclear (N) energies and solvent electric polarization (P) free energy, and G_{CDS} is a semiempirical first-solvation shell term including cavitation (C), dispersion (D), solvent structure (S), and the breakdown of the bulk electrostatic model in the first solvation shell. The models may be applied with gas-phase geometries (in which case we append R to the model name), or geometries may be optimized in liquid solution using analytic gradients (in which case the model name does not end in R). The SM5 models are:

SM5.0R ^{28,29}	SM5 model in which electrostatics are implicit
SM5.2R ³⁰	SM5 model in which electrostatics are based on class II charges
SM5.4 ³¹⁻³⁴	SM5 model in which electrostatics are based on class IV charges calculated by Charge Model 1
SM5.42R, SM5.42 ^{21,35-39}	SM5 models in which electrostatics are based on class IV charges calculated by CM2
SM5CR ⁴⁰	SM5 model in which electrostatics are treated by the Conductor-like Screening Model (COSMO).

All of these models have been parameterized for aqueous solution and for general organic solvents. The parameterizations are based on over 200 free energies of solvation in 91 solvents (and in some cases on additional free energies of transfer as well). The SM5.0R model is designed for use with molecular mechanics calculations. The SM5.2R model is parameterized for AM1, PM3, MNDO, and MNDO/d. The SM5.4 model is parameterized for AM1 and PM3. The SM5.42R model is parameterized for AM1, PM3, HF/MIDI!, HF/MIDI!6D, HF/6-31G*, HF/6-31+G*, HF/cc-pVDZ, BPW91/MIDI!, BPW91/MIDI!6D, BPW91/6-31G*, BPW91/DZVP, B3LYP/MIDI!, INDO/S, and INDO/S2. The SM5.42 model uses the same parameters as SM5.42R. The SM5CR model is parameterized for AM1, PM3, and MNDO/d. In addition to the original papers, some overviews discussing the SM5 models are available.⁴¹⁻⁴⁴

The SM5.42R/HF/6-31G*, SM5.42R/BPW91/MIDI!, and SM5.42R/AM1 all yield excellent results for the free energy of transfer of nucleic acid bases from water to chloroform.⁴⁵

GAS-PHASE DYNAMICS

Variational transition state theory with optimized multidimensional tunneling contributions (VTST/OMT) provides an accurate yet practical method for calculating chemical rate constants.⁴⁶⁻⁴⁸ The optimized multidimensional tunneling calculation allows for corner cutting tunneling paths of two kinds: small-curvature tunneling paths, which are localized in the zero-point-amplitude hypertube enclosing the reaction path, and large-curvature tunneling paths, which are straight lines in isoinertial coordinates. The calculations may be carried out in redundant curvilinear coordinates, which are more physical than rectilinear coordinates.^{49,50}

Our recent emphasis has been on devising algorithms for interfacing VTST/OMT calculations with electronic structure calculations in convenient and efficient ways, and we have especially concentrated on minimizing the amount of electronic structure data required because that would make it more affordable to calculate the required data at high levels.

For example, we have recently shown how the orientation of generalized transition state dividing surfaces may be optimized, and how such optimization allows one to increase the step size used to trace the reaction path or even to use local optimization at nonstationary points to obviate the need for a continuous reaction path. The resulting algorithms are called re-orientation of the dividing surface (RODS)⁵¹⁻⁵³ and variational reaction path (VRP).⁵⁴

Another way to increase the amount of electronic structure data needed is to use sophisticated interpolation schemes. We have developed a method called interpolated variational transition state theory by mapping (IVTST-M) that allows one to greatly reduce the number of energies, gradients, and Hessians required for VTST calculations with small-curvature tunneling contributions.⁵⁵ Another approach is to use two levels, including geometry optimization at both levels but reaction-path following only at the lower level; by interpolating the *difference* between the lower and higher levels one can greatly reduce the amount of data needed at the higher level. This approach, called variational transition state theory with interpolated corrections (VTST-IC), can be used for small-curvature, large-curvature, or optimized multidimensional tunneling contributions.^{5,14,17} We have shown that the VTST-IC method is much more accurate than simply adding single-point energy corrections at geometries optimized by the lower level.⁵⁶ The VTST-IC approach is particularly powerful when the high-level

calculations are used not only as corrections to the lower level but also to optimize SRP parameters for the lower level.

A recent set of applications⁵⁷⁻⁵⁹ of these techniques involved calculating the rate constant for $\text{H} + \text{C}_2\text{H}_4 \rightarrow \text{C}_2\text{H}_5$ and several isotopically substituted versions of these reactions. This reaction involves small-curvature tunneling, and we treated it using a dual-level scheme involving variable scaling of external correlation energy, the RODS algorithm, redundant curvilinear coordinates, and the IVTST-M algorithm. We obtained good agreement with experiment both for absolute rate constants and for kinetic isotope effects.

Other recent applications include $\text{H} + \text{N}_2\text{H}_2 \rightarrow \text{H}_2 + \text{N}_2\text{H}_3$,^{17,49} $\text{OH} + \text{C}_3\text{H}_8 \rightarrow \text{H}_2\text{O} + \text{C}_3\text{H}_7$,¹⁸ $\text{RhCl}(\text{PH}_3)_2(\eta^2\text{-CH}_4) \rightarrow \text{RhCl}(\text{PH}_3)_2(\text{CH}_3)\text{H}$,⁶⁰ $\text{O} + \text{HCl} \rightarrow \text{OH} + \text{Cl}$,⁶¹ $\text{Cl} + \text{CH}_4 \rightarrow \text{HCl} + \text{CH}_3$,¹⁹ $\text{O} + \text{CH}_4 \rightarrow \text{OH} + \text{CH}_3$,²⁰ and $\text{Cl} + \text{H}_2 \rightarrow \text{HCl} + \text{H}$.⁶²

SOLUTION-PHASE DYNAMICS

We have extended the gas-phase variational transition state theory formalism to treat reaction rates in solution, including curvilinear coordinates, small- and large-curvature tunneling, optimized multidimensional tunneling, and equilibrium and nonequilibrium solvation effects. The methods are designed to take full advantage of the advances discussed in all three sections above. We distinguish three general levels of liquid-phase dynamics calculations:

- SES separable equilibrium solvation⁶³
- ESP equilibrium solvation path^{21,63,64}
- NES nonequilibrium solvation^{65,66}

In SES calculations, one calculates stationary point geometries and/or reaction paths in the gas-phase and then adds the free energy of solvation to each point. In ESP calculations one first creates a potential of mean force surface by adding free energies of solvation to the gas-phase potential energy surface; then stationary point geometries and/or reaction paths are computed using the potential of mean force. Tunneling calculations involve a function of the potential mean force called the canonical mean shape potential, which reduces to the potential of mean force in zero order. Nonequilibrium effects may be incorporated via coupling of the solute to collective solvent coordinates.

We have recently demonstrated all three levels of theory for the reaction $\text{H} + \text{CH}_3\text{CH}_2\text{OH} \rightarrow \text{H}_2 + \text{CH}_3\text{CHOH}$ in aqueous solution.^{21,66}

ACKNOWLEDGMENTS

This research is supported by the National Science Foundation under grant no. CHE97-25965 (liquid-phase electronic structure and dynamics research and part of the gas-phase electronic structure research) and by the U.S. Department of Energy, Office of Basic Energy Sciences under grant no. DOE-DE-FG02-85ER13579 (gas-phase kinetics research and part of the gas-phase electronic structure research).

REFERENCES

1. Coitiño, E. L.; Truhlar, D. G.; Morokuma, K. *Chem. Phys. Lett.* **1996**, *259*, 159.
2. Noland, M., Coitiño, E. L., Truhlar, D. G. *J. Phys. Chem. A* **1997**, *101*, 1193.
3. Coitiño, E. L.; Truhlar, D. G. *J. Phys. Chem. A* **1997**, *101*, 4641.
4. Corchado, J. C.; Truhlar, D. G. *J. Phys. Chem. A* **1998**, *102*, 1895.
5. Corchado, J. C.; Truhlar, D. G. *ACS Symp. Ser.* **1998**, *712*, 106.

6. Alhambra, C.; Gao, J.; Corchado, J. C.; Villa, J.; Truhlar, D. G. *J. Amer. Chem. Soc.* **1999**, *121*, 2253.
7. Fast, P. L.; Corchado, J. C.; Sánchez, M. L.; Truhlar, D. G. *J. Phys. Chem. A* **1999**, *103*, 3139.
8. Fast, P. L.; Corchado, J. C.; Sánchez, M. L.; Truhlar, D. G. *J. Phys. Chem. A*, submitted.
9. Truhlar, D. G. *Chem. Phys. Lett.* **1998**, *294*, 45.
10. Chuang, Y.-Y.; Truhlar, D. G. *J. Phys. Chem. A* **1999**, *103*, 651.
11. Fast, P. L.; Sánchez, M. L.; Truhlar, D. G. *J. Chem. Phys.*, in press.
12. Fast, P. L.; Sánchez, M. L.; Corchado, J. C.; Truhlar, D. G. *J. Chem. Phys.*, in press.
13. Fast, P. L.; Sánchez, M. L.; Truhlar, D. G. *Chem. Phys. Lett.*, in press.
14. Hu, W.-P.; Liu, Y.-P.; Truhlar, D. G. *J. Chem. Soc. Faraday Trans.* **1994**, *90*, 1715.
15. Corchado, J. C.; Espinosa-Garcia, J.; Hu, W.-P.; Rossi, I.; Truhlar, D. G. *J. Phys. Chem.* **1995**, *99*, 687.
16. Rossi, I.; Truhlar, D. G. *Chem. Phys. Lett.* **1995**, *233*, 231.
17. Chuang, Y.-Y.; Truhlar, D. G. *J. Phys. Chem. A* **1997**, *101*, 3808. Erratum: **1997**, *101*, 8741 (1997).
18. Hu, W.-P.; Rossi, I.; Corchado, J. C.; Truhlar, D. G. *J. Phys. Chem. A* **1997**, *101*, 6911.
19. Roberto-Neto, O.; Coitiño, E. L.; Truhlar, D. G. *J. Phys. Chem. A* **1998**, *102*, 4568.
20. Corchado, J. C.; Espinosa-Garcia, J.; Roberto-Neto, O.; Chuang, Y.-Y.; Truhlar, D. G. *J. Phys. Chem. A* **1998**, *102*, 4899.
21. Chuang, Y.-Y.; Radhakrishnan, M. L.; Fast, P. L.; Cramer, C. J.; Truhlar, D. G. *J. Phys. Chem. A*, in press.
22. Easton, R. E.; Giesen, D. J.; Welch, A.; Cramer, C. J.; Truhlar, D. G. *Theor. Chim. Acta* **1996**, *93*, 281.
23. Li, J.; Cramer, C. J.; Truhlar, D. G. *Theor. Chem. Acc.* **1998**, *99*, 192.
24. Li, J.; Williams, B.; Cramer, C. J.; Truhlar, D. G. *J. Chem. Phys.* **1999**, *110*, 724.
25. Storer, J. W.; Giesen, D. J.; Cramer, C. J.; Truhlar, D. G. *J. Comput.-Aided Mol. Design* **1995**, *9*, 87.
26. Li, J.; Zhu, T.; Cramer, C. J.; Truhlar, D. G. *J. Phys. Chem. A* **1998**, *102*, 1820.
27. Li, J.; Xing, J.; Cramer, C. J.; Truhlar, D. G. *J. Chem. Phys.*, in press.
28. Hawkins, G. D.; Cramer, C. J.; Truhlar, D. G. *J. Phys. Chem. B* **1997**, *101*, 7147.
29. Hawkins, G. D.; Liotard, D. A.; Cramer, C. J.; Truhlar, D. G. *J. Org. Chem.* **1998**, *63*, 4305.
30. Hawkins, G. D.; Cramer, C. J.; Truhlar, D. G. *J. Phys. Chem. B* **1998**, *102*, 3257.
31. Chambers, C. C.; Hawkins, G. D.; Cramer, C. J.; Truhlar, D. G. *J. Phys. Chem.* **1996**, *100*, 16385.
32. Giesen, D. J.; Gu, M. Z.; Cramer, C. J.; Truhlar, D. G. *J. Org. Chem.* **1996**, *61*, 8720.
33. Giesen, D. J.; Chambers, C. C.; Cramer, C. J.; Truhlar, D. G. *J. Phys. Chem. B* **1997**, *101*, 2061.
34. Giesen, D. J.; Hawkins, G. D.; Liotard, D. A.; Cramer, C. J.; Truhlar, D. G. *Theor. Chem. Acc.* **1997**, *98*, 85. Erratum: **1999**, *101*, 309.
35. Zhu, T.; Li, J.; Hawkins, G. D.; Cramer, C. J.; Truhlar, D. G. *J. Chem. Phys.* **1998**, *109*, 9117.
36. Li, J.; Hawkins, G. D.; Cramer, C. J.; Truhlar, D. G. *Chem. Phys. Lett.* **1998**, *288*, 293.
37. Li, J.; Zhu, T.; Hawkins, G. D.; Winget, P.; Liotard, D. A.; Cramer, C. J.; Truhlar, D. G. *Theor. Chem. Acc.*, in press.
38. Li, J.; Cramer, C. J.; Truhlar, D. G. to be published.
39. Zhu, T.; Li, J.; Liotard, D. A.; Cramer, C. J.; Truhlar, D. G. *J. Chem. Phys.* **1999**, *110*, 5503.

40. Dolney, D.; Hawkins, G. D.; Liotard, D. A.; Cramer, C. J.; Truhlar, D. G. to be published.
41. Giesen, D. J.; Chambers, C. C.; Hawkins, G. D.; Cramer, C. J.; Truhlar, D. G. *ACS Symp. Ser.* **1998**, *677*, 285.
42. Chambers, C. C.; Giesen, D. J.; Hawkins, G. D.; Vaes, W. H. J.; Cramer, C. J.; Truhlar, D. G. *IMA Series Math. Its Applic.* **1999**, *108*, 51.
43. Hawkins, D. G.; Li, J.; Zhu, T.; Chambers, C. C.; Giesen, D. J.; Liotard, D. A.; Cramer, D. J.; Truhlar, D. G. *ACS Symp. Ser.*, in press.
44. Hawkins, G. D.; Zhu, T.; Li, J.; Chambers, C. C.; Giesen, D. J.; Liotard, D. A.; Cramer, C. J.; Truhlar, D. G. *ACS Symp. Ser.* **1999**, *712*, 201.
45. Li, J.; Cramer, C. J.; Truhlar, D. G. *Biophys. Chem.* **1999**, *78*, 147.
46. Truhlar, D. G.; Garrett, B. C.; Klippenstein, S. J. *J. Phys. Chem.* **1996**, *100*, 12771.
47. Garrett, B. C.; Truhlar, D. G. In *Encyclopedia of Computational Chemistry*; Schleyer, P. v. R.; Allinger, N. L.; Clark, T.; Gasteiger, J.; Kollman, P. A.; Schaefer, H. F. III, Eds.; Wiley: Chichester, UK, 1998; Vol. 5, p. 3094.
48. Allison, T. C.; Truhlar, D. G. In *Modern Methods for Multidimensional Dynamics Computations in Chemistry*; Thompson, D. L., Ed.; World Scientific: Singapore, 1998; p. 618.
49. Chuang, Y.-Y.; Truhlar, D. G. *J. Chem. Phys.* **1997**, *107*, 83.
50. Chuang, Y.-Y.; Truhlar, D. G. *J. Phys. Chem. A* **1998**, *102*, 242.
51. Villà, J.; Truhlar, D. G. *Theor. Chem. Acc.* **1997**, *97*, 317.
52. González-Lafont, A.; Villà, J.; Lluch, J. M.; Bertrán, J.; Steckler, R.; Truhlar, D. G. *J. Phys. Chem. A* **1998**, *102*, 3420.
53. Fast, P. L.; Corchado, J. C.; Truhlar, D. G. *J. Chem. Phys.* **1998**, *109*, 6237.
54. Fast, P. L.; Truhlar, D. G. *J. Chem. Phys.* **1998**, *109*, 3721.
55. Corchado, J. C.; Coitiño, E. L.; Chuang, Y.-Y.; Fast, P. L.; Truhlar, D. G. *J. Phys. Chem. A* **1998**, *102*, 2424.
56. Chuang, Y.-Y.; Corchado, J. C.; Truhlar, D. G. *J. Phys. Chem. A* **1999**, *103*, 1140.
57. Villà, J.; González-Lafont, A.; Lluch, J. M.; Truhlar, D. G. *J. Amer. Chem. Soc.* **1998**, *120*, 5559.
58. Villà, J.; Corchado, J. C.; González-Lafont, A.; Lluch, J. M.; Truhlar, D. G. *J. Amer. Chem. Soc.* **1998**, *120*, 12141.
59. Villà, J.; Corchado, J. C.; González-Lafont, A.; Lluch, J. M.; Truhlar, D. G. *J. Phys. Chem.*, submitted.
60. Espinosa-García, J.; Corchado, J. C.; Truhlar, D. G. *J. Amer. Chem. Soc.* **1997**, *119*, 9891.
61. Allison, T. C.; Ramachandran, B.; Senekowitsch, J.; Truhlar, D. G.; Wyatt, R. E. *J. Mol. Struct. Theochem.* **1998**, *454*, 307.
62. Srinivasan, J.; Allison, T. C.; Schwenke, D. W.; Truhlar, D. G. *J. Phys. Chem. A* **1999**, *103*, 1487.
63. Chuang, Y.-Y.; Cramer, C. J.; Truhlar, D. G. *Int. J. Quantum Chem.* **1998**, *70*, 887.
64. Truhlar, D. G.; Liu, Y.-P.; Schenter, G. K.; Garrett, B. C. *J. Phys. Chem.* **1994**, *98*, 8396.
65. Truhlar, D. G.; Schenter, G. K.; Garrett, B. C. *J. Chem. Phys.* **1993**, *98*, 5756.
66. Chuang, Y.-Y.; Truhlar, D. G., to be published.

A Combined Static and Dynamic Density Functional Theory Approach to Elementary Reaction Steps in Homogeneous Catalysis.

Peter Margl, Tom K. Woo, Rochus Schmid, Liqun Deng and Tom Ziegler*

Department of Chemistry, University of Calgary, 2500 University Drive, N.W., Calgary, Alberta, T2N 1N4, CANADA

email: ziegler@ucalgary.ca

Phone: (voice) 403 220-5368 (fax) 403 289-9488

KEYWORDS: molecular modeling, density functional theory, QM/MM, Brookhart catalyst, constrained geometry catalyst, *ab initio* molecular dynamics

ABSTRACT

We describe an approach in which first principle molecular dynamics calculations based on density functional theory (DFT) are used to locate reaction pathways and estimate free energies of activation whereas static DFT calculations were used to obtain stationary points and relative energies as well as reaction paths by the intrinsic reaction coordinate method. The approach has been applied to (a) copolymerization of polar and non-polar monomers by nickel and palladium based catalysts as well as (b) a comparison between rhodium and iridium based catalysts in Monsanto's acetic acid process (c) carbonylation of methane by a rhodium catalyst.

Introduction

Homogenous catalytic systems have often been used to model more complicated heterogeneous systems. However, even seemingly simple homogenous systems pose many challenges for computational chemists. Often times a first principle's calculation involves a stripped down model that only vaguely resembles the true system. If large, bulky ligand systems are involved they are most often neglected in high level calculations with the hope that they do not substantially influence the nature of the reaction mechanisms. Unfortunately, the surrounding ligand system or matrix can often play a crucial mechanistic role. In addressing this issue, the combined quantum mechanical/molecular mechanics (QM/MM) method¹ has recently received significant attention. In this hybrid method part of the molecule, such as the active site, is treated quantum mechanically while the remainder of the system is treated with a molecular mechanics force field. This allows extremely large systems which are out of the reach of pure QM calculations to be studied in an efficient and detailed manner. We have applied the QM/MM method to study the homogenous Brookhart diimine Ni olefin polymerization catalyst.² Since the QM/MM method was originally conceived to more adequately treat larger, more "real life" systems it naturally has applications in the area of heterogeneous catalysts.

Recently, our group has been utilizing Car-Parinello³ flavor *ab initio* molecular dynamics to explore potential energy surfaces and to obtain free energy barriers for catalytic processes. We have determined free energy barriers for several processes at the *ab initio* molecular dynamics level for the Ti mono-Cp constrained geometry olefin polymerization catalysts, (CpSiH₂NH)Ti-R⁺.⁴ The results compare well with similar free energy barriers determined from more traditional "static" electronic structure calculations. We will demonstrate that the *ab initio* molecular dynamics method (i) provides a general way of determining finite temperature free energy barriers which are in good agreement with static methods, (ii) can be used to efficiently explore complicated free energy surfaces and (iii) that the method can be effectively utilized in a synergistic fashion with traditional static methods.

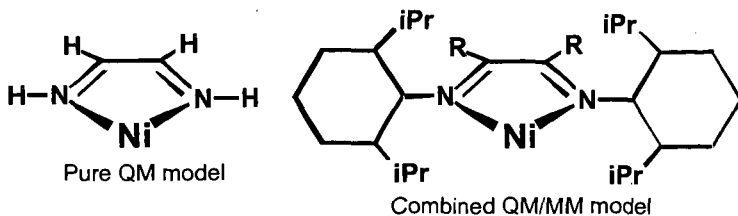
Computational Details

The reported "static" density functional calculations were all carried out by the ADF program system, developed by Baerends and others.⁵ Energy differences were calculated by including the local exchange-correlation potential by Vosko⁶ *et al.* with Becke's⁷ nonlocal exchange corrections and Perdew's⁸ nonlocal correlation correction. For the QM/MM calculations a version of the ADF program system as modified according to Morokuma and co-workers was utilized with the AMBER⁹ force field. For more details of the QM/MM work see reference¹⁰. All reported molecular dynamics simulations were carried out with the Car-Parinello Projector Augmented Wave (CP-PAW) code developed by Blöchl.¹¹ For more details of the molecular dynamics simulations and the constrained geometry work see references¹².

Results and Discussion

Combined QM/MM: Recently, Ni(II) and Pd(II) diimine based single-site catalysts have emerged as promising alternatives to newly developed metallocene catalysts for olefin polymerization.² Brookhart's group has shown that these catalysts are able to convert ethylene into high molecular mass polymers with a controlled level of polymer branching when bulky ligand systems are used.

We have investigated the chain propagation, chain termination and the chain branching processes with a truncated pure quantum mechanical model system where the bulky ligands are neglected and with a combined QM/MM model where the bulky ligands are included via a MM force field. Scheme 2 depicts the two model systems. The QM region of the QM/MM model is the same as the pure QM model.



Scheme 1

Experimentally, it has been determined that the relative magnitude of the barriers are in the order insertion > isomerization > termination. Table 1 shows that the pure QM model does not reproduce this trend. In fact, the results of the pure QM simulation suggest that the catalyst should not produce polymers at all but rather dimers or oligomers.

Table 1.

process	Reaction Barrier, ΔH^\ddagger (kJ/mol)	
	pure QM model	QM/MM model
propagation	71	49
branching	52	64
termination	42	77

However, when bulky ligands are not neglected but rather modeled by molecular mechanics force field, the barriers do follow the experimentally established trends. Moreover, the calculated propagation barrier is in remarkable agreement with the experimental estimate of 40-46 kJ/mol.¹³

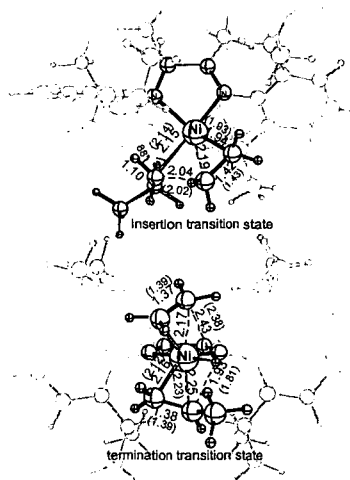


Figure 1. Combined QM/MM transition states for the propagation and termination processes. The parenthetical parameters are those of the equivalent pure QM transition states. The ghosted portions of the molecules represent the pure MM atoms.

Ab Initio Molecular Dynamics: We have examined several chain termination and long chain branching mechanisms with conventional "static" electronic structure calculations and with *ab initio* molecular dynamics in the density functional theory framework. Free energy barriers were computed by both methods and were found to be in excellent agreement with one another. Movies of all molecular dynamics simulations presented here can be found at our research group's world wide web home page <<http://www.chem.ucalgary.ca/groups/ziegler>>.

Table 2. Static and dynamic free energy barriers.

Process	Free Energy Barrier	
	ΔF^\ddagger	
	at 300 K (kJ/mol)	
	MD ^a	static
β -H transfer to monomer ^b	43 \pm 8	40.1
β -H transfer to metal ^c	57 \pm 3	53.9
olefin σ -bond metathesis ^b	87 \pm 5	91.7
alkyl σ -bond metathesis ^b	70 \pm 3	72.3

^a values are the average of the forward and reverse scans. Error bars are half the difference.

^b ethyl group and propyl group used to model growing chain in the static and dynamic simulations, respectively.

^c A propyl group used to model the growing chain.

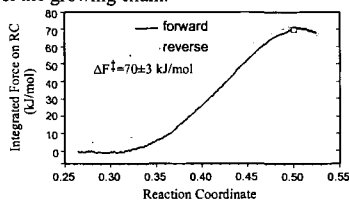


Figure 2. Free energy profile determined from the *ab initio* molecular dynamics simulation of the alkyl σ -bond metathesis process.

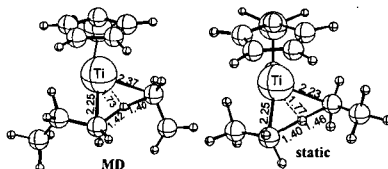


Figure 3. Transition state structures for the alkyl σ -bond metathesis process. The molecular dynamics (MD) structure is a snapshot geometry taken from the transition state region.

Although we have applied the Car-Parinello molecular dynamics method to study homogeneous catalytic reactions on a *ab initio* dynamics level, the method is as well suited to treating periodic systems. Hence the method shows promise for the computational modeling of heterogeneous catalytic processes such as those that take place in zeolite cavities.

Acknowledgment: This investigation was supported by NSERC of Canada, as well as by the donors of the Petroleum Research Fund, administered by the American Chemical Society (ACS-PRF No 31205-AC3).

REFERENCES

- Maseras, F.; Morokuma, K. *J. Comp. Chem.* **1995**, *16*, 1170.
- Johnson, L. K.; Killian, C. M.; Brookhart, M. *J. Am. Chem. Soc.* **1995**, *117*, 6414.
- Car, R.; Parrinello, M. *Phys. Rev. Lett.* **1985**, *55*, 2471.
- Chum, P. S.; Kao, C. I.; Knight, G. W. in *Plastics Engineering*, June 1995; pp. 21.
- Baerends, E. J.; Ellis, D. E.; Ros, P. *Chem. Phys.* **1973**, *2*, 41.
- Vosko, S. H.; Wilk, L.; Nusair, M. *Can. J. Phys.* **1980**, *58*, 1200.
- Becke, A. *Phys. Rev. A* **1988**, *38*, 3098.
- Perdew, J. P. *Phys. Rev. B* **1986**, *33*, 8822.
- Cornell, W. D.; Cieplak, P.; Bayly, C. I.; Gould, I. R., Jr., K. M. M.; Ferguson, D. M.; Spellmeyer, D. C.; Fox, T.; Caldwell, J. W.; Kollman, P. A. *J. Am. Chem. Soc.* **1995**, *117*, 5179.
- Deng, L.; Margl, P. M.; Ziegler, T. *J. Am. Chem. Soc.* **1997**, in press.
- Blöchl, P. E. *Phys. Rev. B* **1994**, *50*, 17953.
- (a) Woo, T. K.; Margl, P. M.; Blöchl, P. E.; Ziegler, T. **1997**, submitted. (b) Woo, T. K.; Margl, P. M.; Lohrenz, J. C. W.; Blöchl, P. E.; Ziegler, T. *J. Am. Chem. Soc.* **1996**, in press.
- Maurice Brookhart - a private communication.

Toward a New Generation of Hydrocarbon Reaction Models

John H. Shinn, Anil N. Patel.
Chevron Research and Technology
100 Chevron Way, Richmond, CA-USA 94802

ABSTRACT

Significant advances in several independent areas are enabling the development of new modeling tools well beyond those capable a short time ago. These significant advances include improvements in experimental kinetics, a priori prediction of molecular energetics and rates, instrumental approaches to the composition of complex mixtures, computational conversion of compositional information to molecular structure determination, and automated generation of reaction networks and modeling software. In this presentation, we will examine the state of development of these tools and their incorporation into online molecular optimization of conversion processes.

INTRODUCTION

The current business environment in the chemical process industry has resulted in an emphasis on improving performance of existing operations to maximize profitability of existing capital equipment. One strategy to achieve this objective is an increase in process monitoring, automation, control and optimization. For process equipment involved in chemical conversion, an essential step in reaching the on-line optimization objective is the creation of detailed reaction models capable of simulating a multitude of simultaneous reactions.

Much work has been done in moving chemical process models from the early linear programming correlative tools to a new generation of models based on actual reaction kinetics. Workers at Mobil introduced models based on molecular structural characteristics of the feed (Quann and Jaffe). This pioneering work demonstrated the practicality of construction of kinetic models for even the most complex feedstocks and processes.

Recent advances in many fields are enabling the construction of ever more detailed chemical reaction models. Although it is still not possible to identify and provide detailed kinetics of every reaction in a mixture as complex as a petroleum vacuum gas oil, significant improvements are now possible which will create a new generation of reaction models capable of controlling processes at the molecular level. This paper will discuss these advances and how they may be incorporated to improve the existing generation of modeling tools.

ADVANCES IN RELATED FIELDS

I. Analytical approaches – identifying the molecules

For years, gas chromatography has been the workhorse of detailed analysis. However, the use of gas chromatography for mixtures boiling above the light distillates range is greatly limited by the presence of a myriad of possible components at similar or equal retention times. Methods such as GCMS and separation-analysis approaches such as employed by Boduzsynski enable identification of some of the overlapping areas, but are too tedious or expensive to apply to online applications.

The use of simulated distillation methods and their extension to high boiling ranges, while not providing molecular detail, significantly expanded the range of chromatographic approaches. Petroleum-derived feeds boiling up to 1200 F and higher could be characterized in terms of the mass of materials boiling in very narrow boiling range fractions, with high precision. Workers began to develop additional methods to allow additional characterization of these narrow fractions, for instance by using chemiluminescence detectors (Chawla). Recent work employing Atomic Emissions Detection has made elemental determination practical for many elements including of carbon, hydrogen, nitrogen, sulfur, nickel, vanadium, and iron (Quimby et al). Use of additional detectors permit other molecular characteristics to be determined for the

narrow fractions such as mass distribution (GC-FIMS, Malhotra et al), and molecular type (using fragmentation MS detection). While still short of the objective of individual component determination, the capability exists for providing far greater detail than was previously available via methods that provided similar information across far wider boiling ranges.

The detailed information on composition of the narrow fractions must now be converted to an accurate quantitative representation of the distribution of molecular species in the sample. The work of Wilcox and Faulon have shown that this may be accomplished through optimization of selection of molecules from a library of possible species representing the possible components in a given boiling range. The development of the Signature algorithm by Faulon permits automated construction of molecular structures from analysis information. Application of Signature with expert knowledge of the molecular types present in petroleum fractions enables the construction of a library of possible molecular species for each boiling range fraction. The process of providing detailed molecular type distributions for a given feed then becomes an optimization problem of choosing the best possible match for the characteristics of each narrow fraction with the available library species. The analytical information is converted to a set of molecules representing in the greatest detail available the distribution of molecular types within the feed. Figure 1 provides an example application of this approach for the prediction of the molecular species in a light gas oil fraction. A high level of accuracy is obtained in comparison to detailed GCMS identification. The remaining degeneracy is between species with similar reaction performance (e.g. paraffin isomers).

II. Kinetics Advances – how do the molecules react?

With information on the distribution of molecular types in the feed, it is necessary to have kinetic information on their behavior in the mixture. Use of model compound reactions continues to be a key in defining the reaction pathways and rules that define the kinetics of specific reaction types (for example the work of Mochida and co-workers on desulfurization, Korre et al in aromatics hydrogenation, Souverijns et al in cycloparaffins isomerization). Additional information is required of the reactions of these species in complex mixtures as 'matrix effects' can cause variations in reactivity beyond those observed in pure feed studies. The analytical methods described above permit the examination of reactivities of individual species within complex mixtures. Recent revealing work by Shin and Mochida has shown the importance of these effects in HDN and HDS reactions.

III. Computation and Modeling advances – building the reaction models.

A central problem in construction of complex kinetic models is known as the 'explosion of species', that is the number of possible molecular species increases dramatically with carbon number. This fundamental problem makes it difficult to represent the possible reactions completely, and renders measurement of the detailed kinetics of each species impossible. One needs a way to reduce the number of species considered and to provide rate information and reaction network information to describe the process performance of the complex mixture. Research developments in computational chemistry and its use to model kinetics are enabling significant advances in this arena.

Approaches to limit the number of species utilize the molecular characteristics of the molecules to form groups that are presumed to behave similarly, a technique known as 'lumping'. Early lumped models grouped all molecules in a single boiling range as equivalent. The advances of Quann et al have moved this approach to the molecular characteristics level. The ultimate lumped model would group molecules on a reaction kinetic behavior basis. This possibility is enhanced by the presence of the advanced analytical information described above.

Another 'explosion' problem results due to the expansion in the possible reactions of species as carbon number increases. Early kinetic models used hand-written reaction networks to describe the essential reactions which connect feed and product species. Advances by Michael Klein and coworkers has created the prospect of computer-generated reaction networks, employing chemically specific reaction rules to limit the explosion of reaction types. Recently, Hou et al have shown that these approaches can be successful in representing the reaction behavior of catalytic hydroprocessing, while producing a model small enough to be solved on a personal-computer platform in solve times of under one minute. The Klein et al approach also employs computational approaches to write the necessary set of differential equations to integrate them to solve

the reaction model and predict the products from a given set of feed molecules and conditions.

Klein has also demonstrated approaches for lumping the reaction behavior of molecular species according to kinetic behavior. The work of Korre et al demonstrated the use of the relationship between linear free energy of formation and reaction rate for similar species to permit the calculation of the kinetics of many similar molecules without measuring the kinetics of each member. This approach has been demonstrated to be very effective even for complex reactions of molecular groups such as polynuclear aromatic hydrocarbons.

Advances in computational chemistry allow rate predictions for groups of molecules from first principles calculations. A first level approach allows computation of the free energies of reactants and intermediates to construct plausible reaction pathways and form the abscissa for the Linear Free Energy-Rate relationships developed by Klein. Perry and Goddard demonstrated the effectiveness of this approach even for catalytic systems by showing that the kinetic performance of catalytic reforming could be predicted using gas-phase molecular energetics with a very limited set of parameters to represent the interactions of various molecular types with the surface catalytic functions. More recent work involves the development of high-level group additivity relationships, based on detailed quantum mechanical calculations, to permit the rapid determination of the energetics of millions of molecules in a mixture. This information also facilitates the grouping of these molecules into species that have similar bonding energetics – a key to lumping based on reaction performance.

CONNECTING THE PIECES

The challenge for the modeler is to utilize the advances collectively to produce more accurate predictive tools based upon detailed reaction chemistry. Figure 2 provides a schematic representation of this approach. Analytical information is passed to the structure generator module providing detailed information on the composition of the feed (or products). The molecular information is passed to model, constructed on the basis of the process information using the automated reaction network generator, reaction-property information, and a model solver. QM calculations provide a basis for reaction rate information for similar molecules. The output molecules are then utilized with additional Quantitative Structure Property Relationship information (made possible by employing the detailed analysis approach on a broad range of products).

An additional critical step involves the use of database technology to sample the performance of pilot plant and commercial operations and determine the relationship between feed composition, controllable process parameters, and product composition. These commercial data sources are essential in validating and adjusting the model performance in a feedback loop that includes the kinetic model reconstruction (adjustments in reaction rules, molecular family kinetics, etc).

The ultimate use of these kinetic models comes in integration with the process itself. The analysis approaches described above are specifically developed for their capability to be utilized on-line. Computational network generation allows adjustment of the model itself as part of the validation process. Combination of the analysis information, 'living' kinetic models, and advanced monitoring and control information will permit a level of sophistication of process tuning we term 'molecular optimization'.

ACKNOWLEDGEMENTS

This work would not be possible without the ingenuity of leading research groups from around the world. Collaborations of this type are essential to create the prospects of significant advances in kinetic models – it is unlikely that any single research organization would have the combined capability to provide these advances. We are greatly indebted to and grateful for the work of Professor William A. Goddard of California Institute of Technology, Professor Michael T. Klein of Rutgers University, Professor Isao Mochida of Kyushu University, Dr. D. Duayne Whitehurst (consultant), Dr. Jason K. Perry of First Principles Inc., Dr. Jean Loup Faulon and R. Wilcox of Sandia National Laboratory, and Chevron colleagues Dr. David A. Grudowski, Dr. Ram Ramamoorthy, and Dr. Michael A. Shippey.

REFERENCES

- Boduszynski M. M.; *Energy & Fuels*, 1998, 2, 597-613
- Chawla B.; *Journal of Chromatographic Science*, 35, 97 - 104, 1997.
- Hou, G., T. I. Mizan and M. T. Klein, "Computer-Assisted Kinetic Modeling of Hydroprocessing," *ACS Div. Pet. Preprints*, 42, pp 670-673, 1997.
- Korre, S. C., M. T. Klein and R. J. Quann, "Hydrocracking of Polynuclear Aromatic Hydrocarbons. Development of Rate Laws Through Inhibition Studies," *I&EC Research*, 36, 2041-2050, 1997.
- Malhotra R., Coggiola M.J., Young S., Hsu C.S., Dechert G.J., Rahimi P.M., and Briker Y.; Symposium on Chemistry of Diesel Fuels, 216th meeting, ACS, Boston, MA, 1998
- Mochida I., Shin S., Sakanishi K., Grudoski D., and Shinn J.; *Hydrotreatment and Hydrocracking of Oil Fractions*, Unpublished
- Quann R. J., and Jaffe S. B.; *Ind. Eng. Chem. Res.* 31, 2483-2497, 1992
- Quimby B., Grudoski D., and Giarroccol V.; *Journal of Chromatographic Science*, 36, 1 - 9, 1998.
- Shin S. and Mochida I., Private communication, January 1999
- Souverijns W., Houvenaghel A., Feijen E.J.P., Martens J.A., Jacobs P.A.; *Journal of Catalysis*, 174, 201-209, 1998
- Whitehurst D.D., T. Isoda, Mochida I.; *Advances in Catalysis*, 42, 345-471, 1998
- Wilcox Robert, Grudoski D., Faulon J. L.; "Measurements to Molecules" Poster presentation at Gordon Research Conference, Ventura CA, January 1999

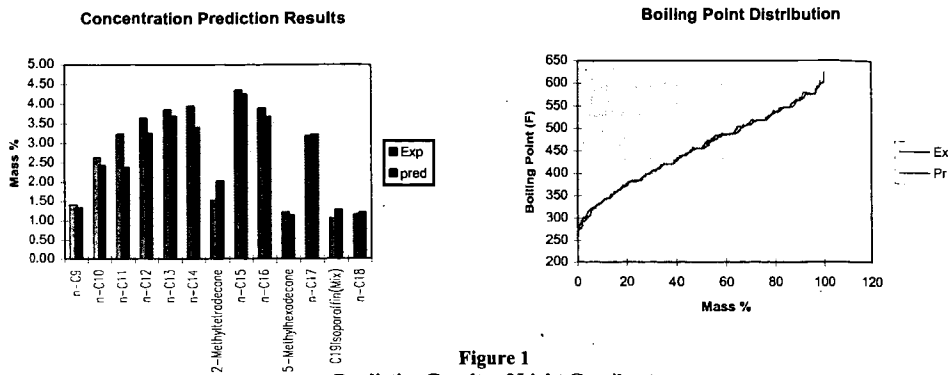


Figure 1
Prediction Results of Light Gasoil cut

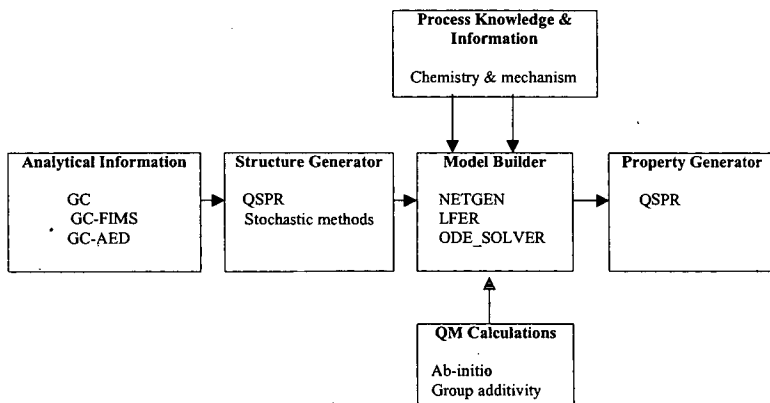


Figure 2
New Generation Models - Connecting the Pieces

Simulation of Chemical Mechanisms Using Computational Methods

Michael J. Manka, *Alchemy Software, Wesley Chapel, FL 33543-5759*

Keywords: Computer simulation, reaction modeling software, chemical mechanisms

Abstract

The use of computational methods for the simulation of chemical mechanisms is discussed. A computer program, *REACT for Windows*, is presented which implements the basic functions for simulating chemical mechanisms. Strategies for modeling experimental data and complex chemical mechanisms are discussed including methods for estimating kinetic rate data.

Introduction

With the proliferation and advancement of powerful desktop computers, the ability to simulate complex chemical mechanisms is readily available to even the most casual users of computational tools. An important factor in simulating chemical mechanisms is the availability of software which performs the necessary integration calculations and provides an easy to use interface for the entry of mechanistic and reaction time data, and contains the ability to present the calculated results in tables and plots for the user to view and print. Until recently software with these features has not been available in a single program running in a Microsoft Windows environment. A computer program, which provides all these features and many more, is now available. This program is called *REACT for Windows* and runs on desktop personal computers with any of the Microsoft Windows operating system. In this paper, I would like to review the important features involved in simulating chemical mechanisms and how they are implemented in a computer program such as *REACT for Windows*.

The three basic features of a functional program which performs computational simulations of chemical mechanisms are the input of mechanistic and reaction time data, the differential equation integration algorithm, and the output of the calculated results in useable formats. We will discuss each of these three areas and how they are implemented in the *REACT for Windows* program. Using specific mechanistic examples, we will also present results calculated using the *REACT* program. We will also suggest strategies for the modeling of experimental data based on a hypothetical mechanism and the simulation of a chemical mechanism where, perhaps, not all the reaction rate coefficients are known. While it may be straightforward to hypothesize individual reactions in a chemical mechanism, it can be a much more difficult matter to provide reasonable kinetic rate data for those reactions if none are available. Thus, methods for the estimation of kinetic rate coefficients will be discussed in some detail.

React for Windows Program

General Description. The *REACT for Windows* program evolved from previous programs^{1,2} developed at the National Institute of Standards and Technology (NIST) and used to solve chemical mechanisms by experimental chemical kineticists. Unlike its predecessors, *REACT* has been written to execute on personal computers (PC) running any of the popular Microsoft Window operating system environments, including Windows 3.1/3.11, Windows 95/98 and Windows NT. The program requires as a minimum an Intel 80486 microprocessor with math coprocessor and a clock speed of 66 MHz or its equivalent. The program also recommends a graphics accelerator card capable of supporting a monitor resolution of 1024 × 768 and 256 colors or better. The program was designed for a 17 inch monitor and this size monitor or larger is recommended for optimal use with the recommended monitor resolution. While a mouse is required, there is an equivalent keystroke combination for most mouse initiated actions. The program supports the printing of reports with tabulated results as well as printing plots of results. The program is composed of three integral parts: the chemical mechanism editor, differential equation integration algorithm, and calculated results tabulation and plotting function. Each of these three parts will now be discussed.

Chemical Mechanism Editor. The chemical mechanism editor facilitates the entry and editing of the mechanistic and reaction time data. This data includes the title of the mechanism and any ancillary information about the mechanism, the chemical reactions in the mechanism and their respective forward and reverse rate coefficients, the initial concentrations of each species involved in the mechanism, and the reaction times where the concentration data and its time derivative are reported for each species. The mechanism title identifies the mechanism under simulation and any additional information, such as the reaction temperature, can be entered as ancillary information and saved with the mechanistic data. The reaction equations are entered into the program with the limitation that each species name cannot exceed twelve characters. There is provision for including the charge of ions and the spectroscopic state of the species

within the species name. Like its predecessor programs, the *REACT* program does not permit the entry of reactions with orders higher than two. If higher order reactions, such as third-order reactions are involved in the mechanism, they can be simulated by using consecutive, second-order reactions. The program does allow the introduction and removal of species using zeroth-order reactions, as well as the more familiar first- and second-order reactions. If the rate coefficients are known, they can be entered directly after the entry of the reaction equation. If they are not known, but kinetic rate parameters for the reaction are available from the literature or a kinetic rate database like the NIST Chemical Kinetics Database⁵, a reaction rate calculator is provided to facilitate the calculation and entry of rate coefficient data. The mechanism editor provides the ability to add a reaction to the mechanism, insert a reaction into the mechanism, reposition a reaction within the mechanism, delete and hide a reaction from the mechanism, and edit a reaction within the mechanism. Once a reaction is added to the mechanism, it appears in the mechanism list of reactions where it can be accessed for editing or deletion. These features provide abundant flexibility in manipulating the reaction mechanism.

The mechanism editor monitors all entries for reasonableness and prevents illegal entries. It also automatically performs all the necessary bookkeeping regarding species in the mechanism as reactions are entered, deleted or edited. The species are arranged alphabetically by length of name in a list of components. Initial concentrations of species having non-zero values are easily entered using this list of components. The initial concentration of all newly added species are initialized to zero and may need to be changed prior to performing a calculation.

There is considerable flexibility available in selecting the reaction times. The reaction times can be any combination of as many as 1000 linearly or geometrically spaced values and any number of other specific values. Once all the pertinent mechanistic data has been entered, the integration algorithm can be called to perform the calculations. The mechanism can have no more than 85 species in the current version of the program, but the number of reactions allowed is quite large (>2000) and is mainly limited by the memory available in the computer. The program uses dynamic memory allocation to accommodate the array size requirements of the mechanism. Mechanistic data are easily saved to memory for future retrieval and use.

Integration Algorithm. The integration calculation simulates homogeneous reactions occurring in a fixed volume at a constant temperature. The differential equation integration algorithm is an implementation of an adaptive step size fifth-order implicit Runge-Kutta method with fourth-order error control^{2,4}. Similar differential equation integration algorithms have been presented previously⁵⁻¹⁰. To perform the integration in a reliable and efficient manner, the integration algorithm uses variable order, variable step methods of the linear multi-value type. This means that the integration algorithm adapts its integration step size, as well as the integration formula order, so as to progress from the initial end of the time range to the other with the least amount of work. The step size selection is completely automatic, including the initial step size. The relative integration error value, which is set by the user, controls the integration step size. A smaller value results in greater overall integration accuracy, at the expense of longer execution time. Solution values at the user's reaction time are rarely exact integration end points. Normally, integration proceeds beyond a reaction time value and then the solution is obtained by an appropriate backward interpolation. The integration method is implicit and requires the use of a Jacobian matrix, which is calculated exactly by the algorithm. The relative integration error value governs the error control mechanism, which in turn controls the step size strategy as previously mentioned. Errors are measured with each individual step. Thus, there is no guarantee that cumulative errors will not be significantly larger, but experience has shown that for stable systems this very rarely occurs. The integration process can be halted and its progress monitored. The integration algorithm automatically reports its status every 5000 integration steps if the final end point of the time range is not achieved or when an error occurs. The results of the integration process include not only concentration data but also the time derivative of the concentration data for each time point including zero time. The latter data are important in the simulation of photon emission in spectroscopic measurements.

Displaying Results. Once the integration has been successfully completed, the program displays the concentration results for all the species in a tabular format. The program provides considerable flexibility in the presentation and viewing of both the concentration data and time derivative of the concentration data of each species. The data for any number of species can be presented in any desired order for an enhanced focus and comparison of pertinent results. Any desired set of results can also be printed in a report format together with optional mechanistic information. Specific sets of data can be exported to an ASCII file for importing into other software applications such as Microsoft Excel for further analysis. Finally, any data set type, concentration or time derivative of concentration data, can be plotted for a graphical summary view of trends in the data for that species. In an effort to limit the complexity of an individual plot, no more than five such data sets can be plotted at one time. A printed copy of the plot can

also be readily obtained using either laser or inkjet type printers. Customized plots intended for presentation or publication can be obtained using graphics programs and data exported as mentioned above. Reports containing calculated results can also be generated. Again, like the ability to display data, any combination of selected data can be included in the report. The amount of mechanistic information included in the report can be controlled as well.

Program Interface. As a Windows compatible program REACT has many features common to Windows programs. The menu bar contains menu items familiar to most users as well as menu items specific to REACT. It contains an extensive online Help function to aid the user in using the program efficiently and answering questions about the program. A tool bar is included to provide access to icons, which activate the most frequently used commands. A status bar at the bottom of the program window provides information about the status of the program and instructions about what to do next. The interface of the program is composed of four tabbed pages which can be selected using the mouse. The first page is titled, Mechanistic Data, and is used to enter and edit all the mechanistic data. The second page is the Reaction Times page and is used to enter and edit the reaction times and adjust the Relative Error Value for the integration process. The command button to begin the integration calculation is also located on this page as well as in the tool bar. The Tabulated Data page, which is used to present the calculated results in a tabular format, is automatically exposed after an integration calculation has been successfully completed. Once exposed, one can view the calculated results and access the display options for selecting data items for display. The Plot of Results page, which is used to display plots of selected results, also becomes accessible after an integration calculation has been successfully completed and is exposed to access the plot options for the selection of data items to be presented in a plot.

Modeling of Experimental Data

The modeling of experimental data provides a straightforward example of the application of the REACT program. Under ideal circumstances, experimental data is obtained under conditions where a single rate coefficient is determined from the rate of appearance or disappearance of a single reaction component. In this case a straightforward mathematical analysis of the data may be sufficient. However, modeling the complete mechanism may reveal insights into discrepancies in the fit of the data due to unanticipated reactions. The strategy used in making experimental measurements of kinetic rate parameters is to reduce the kinetic importance of all reactions except the one under investigation. This is usually done by judiciously adjusting the initial concentrations of the reactants and the reaction temperature. However, by modeling the mechanism in sufficient detail one can obtain a better appreciation for the influence each reaction may have on the one under investigation and anticipate difficulties in making kinetic rate measurements under various reaction conditions, i.e. as the initial component concentrations or reaction temperature are changed. Under simulation, any prior assumptions about reaction species, such as steady-state conditions, are not only not required but are totally unnecessary.

The recommended approach to modeling experimental data is as follows. First, it requires entering the chemical mechanism under investigation in as much detail as possible into the REACT or similar program. Consider the mechanism shown below which is operative for many mechanisms involving fuel-related reactions where radical chemistry is predominant. The mechanism includes thermally initiated bond homolysis, hydrogen transfer and radical recombination and disproportionation reactions. The available rate coefficients for the reactions at the temperature of interest and the initial species concentrations are also entered into the program. Reasonable estimates of the upper or lower limit for some of the rate coefficients may



Fuel-Related Thermal Mechanism

suffice if actual values are not available. The rate coefficient under investigation is then adjusted to provide the best fit with experimental results. Simulated results may be exported for use in a spreadsheet program like Microsoft Excel where statistical analyses of the experimentally measured results and the calculated results can be performed.

Dissociation Reaction. Let us first consider the modeling of experimental data from the measurement of the dissociation reaction of AA. Once the relevant mechanistic information, including available kinetic rate data, and initial species concentrations have been entered into the program, reaction times corresponding to experimental times are entered using the specific reaction times program feature. An initial choice for the value of k_1 can be made based on the first reliable experimental measurement of the disappearance of AA using the following equation.

$$k_1 = \frac{1}{t} \ln \frac{[AA]_0}{[AA]_t}$$

where t is the experimental time at which the measurement of the disappearance of AA was made. The simulation calculation is repeated, while adjusting the value of k_1 in the program mechanism, until an acceptable fit of the experimental data and the calculated results are obtained. Statistical analyses can be applied to obtain the goodness of fit using external programs. A typical plot of the result of modeling k_1 using the above mechanism is shown below in Figure 1. Alternatively, each experimental data point could be fit exactly under simulation and the resultant rate coefficient values would then be averaged. This method is effective when there are only a few data points. The ratio of the rate coefficients for the radical recombination and disproportionation reactions of D• radicals may also be obtained from experimental data if these reactions are operative in the above mechanism. The rate of hydrogen transfer may also be obtained, but more suitable initial reaction conditions will provide more reliable experimental data which we will address next.

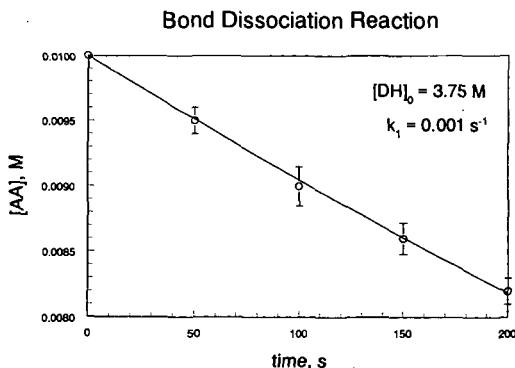


Figure 1. Plot of bond dissociation reaction experimental measurements and its reaction simulation results.

Hydrogen Transfer Reaction. The rate of hydrogen transfer from the hydrogen donor DH to the radical A• is governed by the rate coefficient k_2 in the above mechanism. This rate coefficient can be determined by again experimentally measuring the disappearance of AA and DH and the appearance of AH, but with the relative initial amounts of AA and DH changed. In this reaction the initial reactant concentrations of AA and DH are adjusted so that the rate of recombination of A• becomes competitive with its rate of hydrogen abstraction from DH. An initial choice for k_2 is given by the following equations¹¹.

$$k_2 = \frac{1}{t} \frac{[AH]}{[DH][A^{\bullet}]}$$

where

$$[\text{DH}] = [\text{DH}]_0 - [\text{DD}] - \frac{[\text{AD}]}{2}$$

and

$$[\text{A}^*] = \frac{\sqrt{k_1 [\text{AA}]^2}}{1 + 2 \frac{[\text{DD}]}{[\text{AD}]}}$$

The time average concentration of AA is given by

$$[\overline{\text{AA}}] = \sqrt{(1 - \xi_{\text{AA}}) [\text{AA}]_0^2}$$

where ξ_{AA} is the extent of reaction based on the disappearance of AA. The simulation calculation is repeated, while adjusting the value of k_2 in the program mechanism, until an acceptable fit of the experimental data and the calculated results is obtained. A typical plot of the result of modeling k_2 using the above mechanism is shown in Figure 2. Using additional experimental measurements of the concentrations of AA, DH and the various combination products, the rate coefficients for reactions affecting these species can also be adjusted to improve the overall fit of all the experimental data to the calculated results.

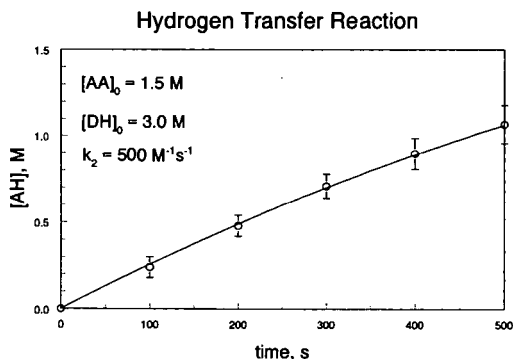


Figure 2. Plot of hydrogen transfer reaction experimental measurements and its reaction simulation results.

The strategy for adjusting any rate coefficient in a mechanism under simulation is to focus on the reactions having the most kinetic importance. This can be accomplished by determining the time derivative of each species concentration at initial reaction times where the reactant concentrations are known. Using estimated rate coefficients if necessary, a crude reaction analysis can be performed to provide an ordering of reaction importance. If the rate coefficient for a reaction is adequately known, it can be removed from the group of reactions with uncertain rate coefficients. If two reactions are contributing prominently to the change in the concentration of the species being measured, the only recourse may be to adjust the reactant concentrations of these reactions in order to discriminate their contributions. Once the final rate coefficients of interest are determined, the agreement between calculated results and experimental data should remain good for a wide range of initial species concentrations.

Simulation of Complex Chemical Mechanisms

The ability to simulate a complex chemical mechanism depends not only on providing a sufficiently complete reaction mechanism, but also requires providing rate coefficients for these reactions with adequate accuracy. As chemists, it should not be particularly difficult to hypothesize the important reactions in a mechanism, but the determination or estimation of

unknown rate coefficients can be quite challenging. The first step in the preparation for the simulation of any mechanism is to obtain as much information about it as possible from the literature. This information should provide the basic framework for developing a model of the mechanism. Once this information has been gathered, the task of assigning forward and reverse rate coefficients to each reaction begins. As information on the mechanism is researched in the literature, information on reaction rates should also be obtained. Kinetic rate parameters found in the literature can be used to calculate rate coefficients appropriate for the reaction temperature used in any simulation, even if the kinetic data must be extended to apply to the reaction conditions of interest. An excellent source for the compilation of gas phase rate data is the NIST Chemical Kinetics Database³ which is available for searching on personal computers. The NIST kinetics database primarily contains kinetic rate measurements of hydrocarbon reactions in the gas phase and provides kinetic rate parameters and references to the literature on these measurements. Some of the references provide critical evaluations of the available rate data for a reaction and these evaluations should be used as part of the evaluation of the kinetic rate parameters for the reactions in the mechanism being modeled. Often, however, an evaluation of the available kinetic rate data is left to the user. While this analysis may not be straightforward, it should provide a set of kinetic rate parameters which can be used to initially calculate rate coefficients. These initial values can be adjusted later to agree with whatever experimental data is available on the process. A similar compilation of gas phase reactions to consider is *Bimolecular and Termolecular Gas Reactions*¹², although these reactions should be included in the NIST database. Another excellent source of kinetic rate data is the *International Journal of Chemical Kinetics* where rate measurements for hydrocarbon reactions occurring in the liquid phase are also reported. *Chemical Abstracts* can also be searched to find additional literature references in other journals like the *Journal of Physical Chemistry* and engineering oriented journals on process chemistry. Despite the availability of these resources, it is often necessary to estimate the rate of a reaction where little or no data exists.

Estimation of Kinetic Rate Data

The ability to calculate kinetic rate data from first principles has made important progress. The calculation of energy barriers for hydrogen transfer reactions involving small hydrocarbon radicals and various hydrocarbons using *ab initio* methods and transition state theory has yielded results in good agreement with reliable experimental data¹³. But before we resort to this type of high-level calculation, let us explore simpler and more straightforward approaches to estimating rate parameters for a reaction. The relationship between kinetics and thermodynamics lies in the equilibrium constant. For a given reaction in the gas phase, the equilibrium constant for the reaction is given by the ratio of the forward and reverse rate coefficients as shown in the following equation.

$$K_{eq}(T) = \frac{k_f(T)}{k_r(T)} \quad (7)$$

where each variable is a function of the temperature T . But the equilibrium constant can be calculated directly from thermodynamic properties of the reactants and products involved in the reaction yielding the Gibbs energy of the reaction, $\Delta G(T)$. This relationship is represented by the following equation.

$$K_{eq}(T) = \exp\left(\frac{-\Delta G(T)}{RT}\right) \quad (8)$$

where R is the universal gas constant and

$$\Delta G(T) = \Delta H(T) - T\Delta S(T)$$

The enthalpy and entropy changes of a reaction, $\Delta H(T)$ and $\Delta S(T)$, respectively, are determined from the individual reactant and product enthalpies and entropies.

$$\Delta H(T) = \sum_{\text{products}} H_p(T) - \sum_{\text{reactants}} H_r(T)$$

and

$$\Delta S(T) = \sum_{\text{products}} S_p(T) - \sum_{\text{reactants}} S_r(T)$$

The problem is now reduced to determining the enthalpy and entropy change of the reaction over the temperature range of interest. This subject has been covered in detail in *Thermochemical Kinetics*¹⁴ by S. Benson. Benson eloquently discusses in his book how thermodynamic data are used to calculate kinetic rate parameters. However, the problem often arises that there are insufficient thermodynamic data to perform the calculation. Benson solves this problem in his book by introducing a group additivity method for calculating the enthalpy and entropy of a species based on group enthalpy and entropy values for molecular fragments of chemical species. Group values have been used to estimate thermodynamic properties of hydrocarbon molecules and radicals for over ten years^{15, 16} and new group values continue to be added although there does not seem to be a common compilation of currently accepted values.

Once the thermodynamic data is assembled and ΔH and ΔS are calculated, we can begin to address the problem of calculating the individual rate coefficients. If one of the rate coefficients is known, the other can be obtained directly using equations 7 and 8. If neither rate coefficient is known then one of them must be calculated. Benson addresses this calculation in his book as well for a number of common reaction types. He relates the above thermodynamic properties with the kinetic rate parameters, Arrhenius A factor and activation energy, E , for the forward and reverse reactions.

$$\frac{A_f}{A_r} = \exp\{T\Delta S\}$$

and

$$E_f - E_r = \Delta H$$

where the subscripts f and r refer to the forward and reverse reactions, respectively. In each of the equations above, one of the rate parameters for the forward or reverse reaction must be known in order to solve for the other parameter,

The rate coefficient for a reaction may also be obtained by analogy with a similar reaction whose rate coefficient is known or can be more easily estimated. Adjustment in the activation energy and A factor may be made to account for differences in the enthalpy and entropy change differences in the two reactions. Since the enthalpy change for a bond dissociation reaction can be equated with the bond dissociation energy, these values can be used directly as the activation energy when calculating these rate coefficients.

As an example, let us consider the initial stages of the pyrolysis mechanism of tetralin (1,2,3,4-tetrahydronaphthalene). Briefly, the mechanism initiation involves the bond homolysis reaction of a carbon-carbon bond in the saturated ring producing a diradical with benzylic and alkyl carbon-centered radicals. The alkyl carbon-centered radical portion in turn abstracts a hydrogen atom from other tetralin molecules forming a resonance stabilized radical, 1-tetralyl and reducing the diradical to a single resonance-stabilized carbon-centered radical, 3-propylbenzyl radical. Hydrogen transfer and structural rearrangements occur to form the major products, 1-methylindan, naphthalene and butylbenzene. The mechanism includes 20 reactions and 20 species. These reactions and their rate coefficients were obtained from the literature¹⁷⁻²⁸ or estimated for a reaction temperature of 478°C. Simulation calculations were performed in an effort to model experimental data. Comparisons of the calculated results and experimental data for the concentrations of tetralin and the major products are shown in Figures 3 and 4. The result of modeling this mechanism provides an affirmation of the important reactions involved and a framework by which evaluate extensions to this mechanism.

In conclusion, it can be stated that the simulation of chemical mechanisms is an important computational tool for understanding and modeling chemical reactions. Hypothetical mechanisms can be tested by comparison with experimental data and once verified predictive calculations can be performed with confidence. The simulation of chemical mechanisms is applicable to all areas of chemistry which involve chemical reactions and with the availability of

powerful desktop computers and suitable software, like *REACT for Windows*, its application is well within the capabilities of most researchers.

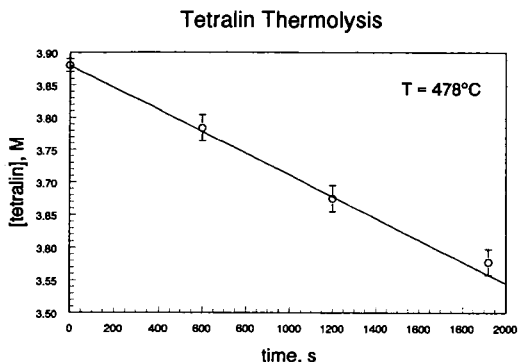


Figure 3. Simulation of tetralin concentration as a function of time during its thermolysis at a temperature of 478°C . Experimental data is indicated by the open circles and associated error bars.

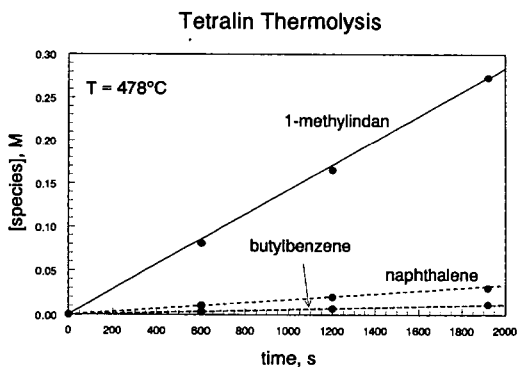


Figure 4. Simulation of species concentrations as a function of time during tetralin thermolysis at a temperature of 478°C . Experimental data is indicated by the closed circles.

References

1. Brown, R. L. *HICHM: A Fortran Code for Homogeneous Isothermal Chemical Kinetics Systems*, NBSIR 81-2281; National Bureau of Standards: Gaithersburg, MD, 1981.
2. Braun, W.; Herron, J. T.; Kahaner, D. K. *Int. J. Chem. Kinet.* **1988**, *20*, 51.
3. Mallard, W. G.; Westley, F.; Herron, J. T.; Hampson, R. F.; Frizzell, D. H. *NIST Chemical Kinetics Database: Version 5.0*; National Institute of Standards and Technology: Gaithersburg, MD, 1993.
4. Boisvert, R. F.; Howe, S. E.; Kahaner, D. K. *The Guide to Available Mathematical Software (GAMS)*, PB 84-17135; National Technical Information Service (NTIS): Springfield, VA 12161, 1984.
5. Gear, C. W. *Numerical Initial Value Problems in Ordinary Differential Equations*; Prentice Hall: Englewood Cliffs, NJ, 1971.
6. Vernier, J. H. *SIAM J. Numer. Anal.* **1978**, *15*.

7. Norris, A. C. *Computational Chemistry: An Introduction to Numerical Methods*; John Wiley & Sons: New York, 1981.
8. Cash, R.; Karp, A. H. *ACM Transactions on Mathematical Software* **1990**, *16*, 201.
9. Press, W. H.; Teulosky, S. A.; Vetterling, W. T.; Flannery, B. F. *Numerical Recipes in C*, 2nd ed.; Cambridge University: Cambridge, UK, 1992.
10. Conway, D. J. *Dr. Dobbs's J.* **1995**, *20*(12), 52.
11. Manka, M. J.; Brown, R. L.; Stein, S. E. *Int. J. Chem. Kinet.* **1987**, *19*, 943.
12. Kerr, J. A.; Moss, S. J. *Bimolecular and Termolecular Gas Reactions*, Vol. 1; CRC Press: Boca Raton, FL, 1981.
13. Litwinowicz, J. A.; Ewing, D. W.; Jurisevic, S.; Manka, M. J. *J. Phys. Chem.* **1995**, *99*, 9709.
14. Benson, S. W. *Thermochemical Kinetics*, 2nd ed.; John Wiley & Sons: New York, 1981.
15. O'Neil, H. E.; Benson, S. W. *Int. J. Chem. Kinet.* **1969**, *1*, 221.
16. McMillen, D. F.; Golden, D. M. *Annu. Rev. Phys. Chem.* **1988**, *33*, 493.
17. Hooper, R. J.; Battaerd, H. A. J.; Evans, D. G. *Fuel*, **1979**, *58*, 132.
18. Benjamin, B. M.; Hagaman, E. W.; Raaen, V. F.; Collins, C. J. *Fuel*, **1979**, *58*, 386.
19. Collins, C. J.; Raaen, V. F.; Benjamin, B. M.; Maupin, P. H.; Raork, W. H. *J. Am. Chem. Soc.* **1979**, *101*, 5009.
20. Franz, J. A.; Camaioni, D. M. *J. Org. Chem.* **1980**, *45*, 5247.
21. Franz, J. A.; Camaioni, D. M. *Fuel* **1980**, *59*, 803.
22. Pennington, J. M. L. *Int. J. Chem. Kinet.* **1982**, *14*, 761.
23. Brower, K. R.; Pajak, J. *J. Org. Chem.* **1984**, *49*, 3970.
24. Franz, J. A.; Barrows, R. D.; Camaioni, D. M. *J. Am. Chem. Soc.* **1984**, *106*, 3964.
25. McPherson, W. P.; Foster, N. R.; Hastings, D. W.; Kalman, J. r.; Gilbert, T. D. *Fuel* **1985**, *64*, 457.
26. King, H.; Stock, L. M. *Fuel* **1981**, *60*, 748.
27. Allen, D. T.; Gavalas, G. R. *Int. J. Chem. Kinet.* **1983**, *15*, 219.
28. Franz, J. A.; Camaioni, D. M.; Beishline, R. R.; Dalling, D. K. *J. Org. Chem.* **1984**, *49*, 3563.

APPLICATION OF COMPUTER GENERATION OF REACTION MECHANISMS USING QUANTITATIVE RATE INFORMATION TO HYDROCARBON PYROLYSIS

Matthew J. De Witt, David J. Dooling and Linda J. Broadbelt
Department of Chemical Engineering
2145 Sheridan Road, Northwestern University
Evanston, IL 60208

ABSTRACT

Novel modifications were made to the core components of the algorithms for rate-based generation of reaction mechanisms¹, including introducing thermodynamic constraints into the estimation of the controlling rate parameters and an alternative approach for determining the species included in the final mechanism. Once implemented, the adapted rate-based building criterion was successfully employed to construct a compact mechanistic model for low-pressure tetradecane pyrolysis. Though thousands of species and reactions were generated, only a small portion of these were deemed necessary and incorporated into the final model. Experimental data were used to determine frequency factors for a subset of the reaction families, while all other kinetic parameters were set based on the literature. The final optimized values for the frequency factors were consistent with literature, and the model was able to accurately fit experimental data from different reaction conditions. With no adjustment to the optimized frequency factors, the mechanistic model for tetradecane pyrolysis was able to accurately predict reactant conversions and product yields for varying reaction conditions. Both relative trends and the actual values were predicted correctly over a wide range of reactant conversions and initial reactant loadings.

I. INTRODUCTION

The advent of tools for computer generation of reaction mechanisms has dramatically reduced the time for the development of complex reaction models and increased the level of detail they may include. One of the challenges in building reaction mechanisms using algorithms for automated model construction, however, is to describe the essential chemistry and enable prediction of experimental data over wide ranges of reaction conditions while maintaining a manageable model size. For example, hydrocarbon pyrolysis is a chemistry in which molecular weight growth reactions may be important, and a mechanism generated automatically would therefore grow to infinite size without the application of external termination criteria. Implementation of a species rank criterion, which restricts those species capable of undergoing reaction based on the order in which they appear in the mechanism, overcame this obstacle². However, this criterion is usually not restrictive enough since insignificant species must also be included to capture the important ones.

This limitation motivated development of an alternative strategy for computer generation of reaction mechanisms that includes important reactions based on quantitative evaluation of reactivity¹. This approach exploits the capability to estimate rate constants as the mechanism is generated, allowing it to be solved at any point. The mechanism is built iteratively, as a growing reaction mechanism is alternatively generated and solved. Quantitative evaluation of the formation rates of all species during the mechanism building process determines the next set of species allowed to undergo reaction. The formation rates are compared to a characteristic rate of the current system, and a weighting factor, ϵ , is used to adjust the characteristic rate to allow more or fewer species to be included in the mechanism.

The work that will be described builds upon the previous work¹ but includes several important improvements. The first implementation of the rate-based approach used the disappearance rate of a single reactant to define a characteristic rate in the system to which all of the other rates were compared, and the conversion of this reactant was used as the marker of the completeness of the mechanism. If the reactant quickly equilibrated, the mechanism building process would not advance. In the new implementation, time is used as the independent variable, and the rates of all of the species in the system are used to determine the overall characteristic rate. Secondly, since the mechanism building process requires on-the-fly kinetic information, a lookup capability was implemented to allow experimental rate information to be incorporated. Finally, equilibrium information was obtained through on-the-fly calculation of heat capacity, enthalpy and entropy values. By marking reversible pairs of reactions, the rate constant for the reverse reaction could be calculated from the forward rate constant and the value of the equilibrium constant. This latter capability represents a substantial advance in our ability to generate complex reaction mechanisms via the computer.

II. PROCEDURE

A mechanism for low pressure tetradecane pyrolysis was generated to determine the effectiveness of the adapted rate-based generation algorithm. This reaction system serves as an adequate test for the rate-based generation criterion since thermolysis of a long chain paraffin can lead to thousands of intermediates and stable products. However, only a small fraction of these is actually kinetically significant. Furthermore, experimental information collected in our laboratory³ was available to test the ability of the model generated to capture the reactant conversion and product selectivities over a wide range of reaction conditions. Low pressure batch pyrolysis reactions were conducted using initial loadings of tetradecane ranging from 0.01 to 0.045 M for times ranging from 10-150 minutes at temperatures of 420 and 450°C.

The reaction mechanism was built by implementing six reaction families deemed important for gas-phase hydrocarbon pyrolysis at moderate temperatures: bond fission, radical recombination, β -scission, radical addition, disproportionation and hydrogen abstraction (intermolecular and intramolecular through 1,4-, 1,5- and 1,6-hydrogen shift reactions). Estimates of the Arrhenius frequency factors and the parameters of an Evans-Polanyi relationship⁴, E_0 and α , for each reaction family were obtained from the literature. The model

was constructed using an initial tetradecane concentration of 0.0322 M and a reaction temperature of 420°C. The weighting factor, ϵ , was varied from 1.0 to 5×10^{-5} . The total number of species, the reactive species, the total number of reactions and the number of reactive reactions were tabulated as a function of the weighting factor. Each individual elementary step is specifically tallied; the numbers of reactions reported are not consolidated according to the known reaction path degeneracies nor are reverse and forward pairs lumped as a single reaction.

III. RESULTS

The model characteristics as a function of weighting factor are summarized in Table 1. As the weighting factor decreased, all quantities reported increased. However, the growth in the total number of species was more dramatic than the moderate growth observed for the number of reactive species. Thus, using rate-based building and the weighting factor as a "tuning" parameter, the size of the mechanism solved was easily controlled. The adequacy of the reaction mechanism was assessed by monitoring two key characteristics: whether all of the major products observed experimentally were included and if secondary reactions of olefins were described. For example, at a weighting factor of 1.0, only C₁-C₇ alkane products were included in the model, while C₁-C₁₃ alkanes were detected experimentally. It was necessary to decrease the weighting factor to 5×10^{-5} before tridecane, the major product observed in the lowest yield, was included in the mechanism as a reactive species.

The mechanism generated employing a weighting factor of 5×10^{-5} was therefore used to capture the experimental behavior. Experimental data from 20 mg pyrolysis reactions of tetradecane conducted at 420°C and 450°C were used to determine controlling rate parameters. There were 27 parameters which could be varied, a frequency factor, an E₀ and an α value for each reaction family. However, only four parameters, A_{bond fission}, A _{β -scission}, A_{H-abstraction by R₁} and A_{1,5-hydrogen shift}, were fit against the experimental data. All other parameters were set constant at values obtained from the literature. Note that only frequency factors were permitted to vary, while all intrinsic barriers and transfer coefficients were fixed.

A parity plot comparing the fitted model yields to the experimentally observed yields for major and minor products is shown in Figure 1. The model did an excellent job of fitting the experimental data from the pyrolysis reactions over several orders of magnitude. Reactant conversions for both temperatures were fit extremely well, even though no activation energies were used as fitting parameters. Gaseous hydrocarbons and liquid α -olefins were also fit very well.

The predictive capabilities of the model were then assessed by solving for the product yields and conversion at other reactant loadings with no further adjustment to any of the model parameters. A comparison of predicted and experimental yields of undecene as a function of reactant conversion and reactant loading is shown as a representative example of the predictive capability of the model in Figure 2. The model was able to predict accurately the trends in the data and the actual values over a wide range of conversions and reactant loadings. Similar predictive capabilities were observed for gaseous hydrocarbons and other long chain α -olefins.

ACKNOWLEDGMENT

The authors are grateful for the financial support from the Department of Energy (DE-FG22-96-PC96204).

REFERENCES

- (1) Susnow, R.G., Green, W.H., Dean, A., Peczak, P.K. and Broadbelt, L.J. "Rate-Based Construction of Kinetic Models for Complex Systems", *J. Phys. Chem. A*, 1997, 101, 3731-3740.
- (2) Broadbelt, L.J., Stark, S.M. and Klein, M.T., "Termination of Computer Generated Reaction Mechanisms: Species Rank-Based Convergence Criterion", *Ind. Eng. Chem. Res.*, 1995, 34(8), 2566-2573.
- (3) De Witt, M.J. and Broadbelt, L.J., "Binary Interactions Between Tetradecane and 4-(1-Naphthylmethyl) Bibenzyl During Low and High Pressure Pyrolysis", *submitted to Energy & Fuels*, 1999.
- (4) Evans, M.G. and Polanyi, M. "Inertia and Driving Force of Chemical Reactions", *Trans. Faraday Soc.*, 1938, 34, 11-29.

Table 1. Summary of model characteristics as a function of the weighting factor used to direct rate-based building.

Weighting factor	Number of total species	Number of reactive species	Number of reactions	Number of reactive reactions
1	1908	103	57116	15605
0.1	2401	107	65866	17633
0.01	3349	120	98286	26116
0.001	4676	130	132450	30436
0.0001	11158	236	319408	63004
0.00005	16269	302	477566	98240

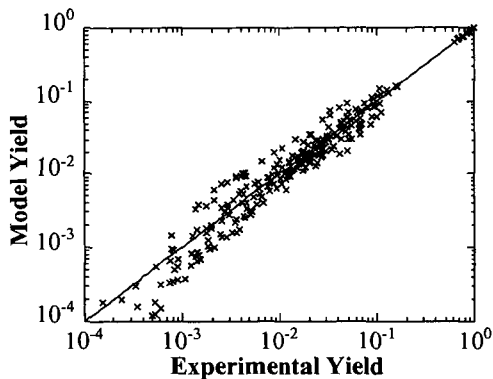


Figure 1. Comparison of fitted model yields and experimentally observed yields for major and minor products of tetradecane pyrolysis.

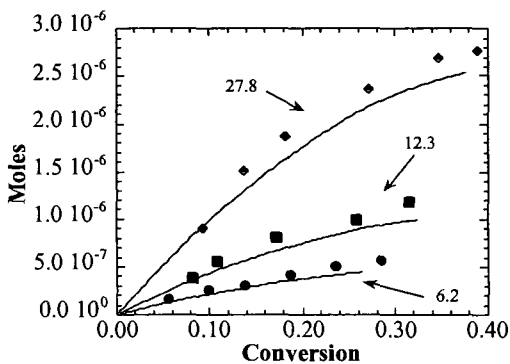


Figure 2. Comparison of the experimental (symbols) and predicted (lines) evolution of undecene for initial tetradecane loadings of 6.2, 12.3 and 27.8 mg.

FIRST PRINCIPLES STUDY OF POISONING BY SULFUR AND DEPOISONING BY CHLORINE OF PALLADIUM BASED HYDROGENATION CATALYSTS: FROM CLUSTERS TO SURFACES

Herve Toulhoat, Peter Gravil, and Gabriele Valerio
Institut Français du Pétrole
1 & 4 Avenue de Bois Preau
92852 Rueil-Malmaison, France

KEYWORDS

DFT Calculations, Thioresistant Catalysts, Palladium

ABSTRACT

From first-principles calculations we find evidence for a direct effect of co-adsorbed chlorine on the adsorption of dihydrogen and ethylene on sulfur-poisoned palladium. On the model (111) surface, chlorine restores molecular and atomic adsorption energies, and decreases the barrier to H₂ dissociation. By contrast, on Pd₄, one adsorbed sulfur increases, while one co-adsorbed chlorine decreases the adsorption energies compared to the clean cluster. We discuss the implications of such effects in the context of the preparation of noble metals based hydrogenation catalysts of improved thioresistance, needed by the refining industry.

I. INTRODUCTION

As specifications on sulfur and aromatics contents in diesel fuels become ever more severe, the development of more active as well as sulfur tolerant hydrogenation catalysts appears as an increasingly important issue for the refining industry. Halogens incorporated in the solid's formulation, or in the stream of reactants, are known to impart some degree of thioresistance to noble metals (Pt, Pd) based hydrogenation catalysts. Very little is known about the microscopic origin of this effect, although it could provide important guidelines for the preparation of new catalysts. A mechanism involving electrons attraction by halogens bound to the carrier and mediating an electron deficiency of supported metal particles, is usually invoked. However, such a long range effect on electronic structure may appear very unlikely. We have therefore undertaken systematic first-principles simulations aiming at probing the direct effect of adsorbed chlorine on the structural, electronic and adsorptive properties of the Pd (111) surface and Pd₄ clusters, poisoned by sulfur (2), (5), (7).

II. METHODS

The calculations were based on the density functional theory (DFT). For the clusters, we used the Gaussian 94 code (1) under the B3LYP option. Scalar relativistic effects for Pd were incorporated through the use of the LanL2DZ basis set, whereas the standard 6-311(d,p) basis set was chosen for the elements S, Cl, C and H. All geometries were fully relaxed. More details can be found in (2). The calculations on model surfaces were performed using the VASP code (3) using a plane-wave pseudopotential formalism. Exchange and correlation effects were included within the generalized gradient approximation (4) (GGA). We used a supercell geometry consisting of a palladium (or platinum) slab four layers thick with a 3x3 surface cell, and a vacuum gap of thickness equivalent to six layers. Adsorbates and adatoms were introduced on one side of the slab and allowed to fully relax, as well as the first two layers of metal atoms, the remaining two layers being fixed at bulk positions. Full details can be found elsewhere (5).

III. RESULTS AND DISCUSSION

The computed adsorption energies of sulfur and chlorine on palladium substrates are compared in Table 1. The magnitude of these energies correspond to strong chemisorptions. Both on the electron deficient clusters and on the full surfaces, sulfur binds more strongly than chlorine. The nature of these bonds has been demonstrated elsewhere (2), (5) : while the sulfur-palladium bond is essentially covalent, the chlorine-palladium bond has a significant ionic character, both on surfaces and clusters. The adatoms bind more strongly on the surface than on the cluster.

Bulk and surface metal-sulfur bond strengths are compared in Table 2 for Pd and Pt. For the bulk, we use either the cohesive energy per M-S bond as defined in (6), or the standard heat of formation of the isostructural sulfides which also includes the bulk metals cohesive energies. Albeit the surface bonds follow the same tendencies as the bulk bonds, their differences appear much less marked.

The competitive adsorption between sulfur and chlorine is analysed in Table 3: the strong repulsive interaction seen between co-adsorbates sharing two palladium atoms decreases rapidly as the S-Cl distance increases. On Pd₄, S and Cl can even mutually strengthen their adsorption when they share a single Pd atom. On the surface, the destabilization for S and Cl sitting in corner sharing or non adjacent three-fold hollows is quite comparable to that induced by increasing coverage with sulfur alone. Co-adsorption of S and Cl on palladium can therefore be taken as quite likely for systems where externally imposed chemical potentials of chlorine and sulfur are comparable (see (5) for a more detailed discussion).

The molecular chemisorption on ethylene is the first step of its heterogeneous catalytic hydrogenation. The computed adsorption energies of ethylene on our clean model substrates are reported in Table 4. The « top » π configuration is clearly preferred on the Pd₄ cluster, whereas the the di- σ bridging configuration is favoured on both the Pd(111) and Pt(111) surfaces, in accordance with other computational studies and experiment. Platinum binds ethylene a little more weakly than palladium.

As shown in Table 5, sulfur and chlorine co-adsorbed on the palladium surface or the Pd₄ cluster have contrasted effects on ethylene chemisorption. It is slightly enhanced by sulfur, and weakened by chlorine on the cluster. The cooperative effect of S and Cl leads to a significant poisoning of ethylene adsorption, obviously in a non-linear fashion. On the Pd(111) surface, a moderate poisoning is brought about by

0.22 ML sulfur, while chlorine has no effect at the same level of coverage. The mixed ad-layer behaves more like chlorine, which we take as an evidence of effective depoisoning.

We have shown elsewhere (5) the microscopic details of poisoning by sulfur of the dissociative chemisorption of molecular hydrogen on Pd(111), and the depoisoning effect of co-adsorbed chlorine: the latter involves a reduced barrier to dissociation, and restored stability of atomic H bound to the surface with respect to associative desorption. In the mixed ad-layer, the effect of chlorine is again dominant, indicative of another direct depoisoning effect.

IV. CONCLUSIONS

In summary, we have found that although sulfur binds more strongly than chlorine to palladium (or platinum) surface atoms, co-adsorption is likely to occur both on very small clusters and on extended metallic surfaces: in the latter case islands of chlorine may segregate because lateral repulsions between adsorbed sulfur atoms are stronger than between adsorbed chlorine atoms. Co-adsorption of chlorine and sulfur affects the molecular adsorption of ethylene differently on very small palladium clusters and on periodic surfaces, respectively weakening and strengthening the interaction. In both cases the effect is non-linear in the sense it is not the average of the effects of the separate adatoms.

We have demonstrated therefore the likeliness of a direct induction of thioresistance by co-adsorption of an halogen on the palladium surfaces. However, on very small palladium aggregates, chlorine could on the contrary amplify the poisoning by sulfur. For practical purposes, this would imply avoiding too high dispersions of the active metal in the supported catalyst.

Future studies should focus on the diffusion and segregation of adatoms at metal surfaces in presence of activated hydrogen, as well as the determination of energy profiles along reaction paths of hydrogenation reactions, in order to enable evaluations of kinetic data by Monte Carlo simulations (8).

ACKNOWLEDGMENTS

This work was partly performed within the Groupement de Recherche Européen « Dynamique Moléculaire Quantique Appliquée à la Catalyse et à l'Adsorption », supported by Institut Français du Pétrole, Centre National de la Recherche Scientifique, Total, and the University of Vienna.

REFERENCES

- (1) *Gaussian 94, Revision B.3; Gaussian Inc.; Pittsburgh, PA, 1995.*
- (2) Valerio, G.; Toulhoat, H. *J. Phys. Chem.*, **100**, 26, **1996**, 10827.
Valerio, G.; Toulhoat, H. *J. Phys. Chem. A*, **101**, 20, **1997**, 1969.
- (3) Kresse, G.; Hafner, J. *Phys. Rev. B*, **49**, **1994**, 14251; Kresse, G.; Furthmüller, J. *Comput. Mater. Sci.*, **6**, **1995**, 15; Kresse, G.; Furthmüller, J. *Phys. Rev. B*, **54**, **1996**, 11169.
- (4) Perdew, J.; Chevary, J.A.; Vosko, S.H.; Jackson, K.A.; Pederson, M.R.; Singh, D.J.; Fiolhais, C. *Phys. Rev. B*, **46**, **1992**, 6671.
- (5) Gravil, P.; Toulhoat, H. « *Hydrogen, Sulfur and Chlorine coadsorption on Pd(111): A Theoretical Study of Poisoning and Promotion* », Accepted by *Surface Science*, **1999**.
- (6) Toulhoat, H.; Raybaud, P.; Kasztelan, S.; Kresse, G.; Hafner, J. *Catalysis Today*, **50**, **1999**, 629.
- (7) Gravil, P.; Toulhoat, H. « *Ethylene, Sulfur and Chlorine coadsorption on Pd(111): A Theoretical Study of Poisoning and Promotion* », Accepted by *Surface Science*, **1999**.
- (8) Neurock, M.; Hansen, E.W. *Computers chem. Engng.*, **22**, **1998**, S1045.

Table 1. Adsorption energies of sulfur and chlorine on model metallic substrates (kCal.mol⁻¹)

Substrate	Sulfur	Chlorine	Ref.
Pd ₄	-85.3	-56.4	(2)
Pd ₆	-81.4	-65.2	(2)
Pd(111) ($\theta_s=0.33$)	-109.5	-71.1	(5)

Table 2. Comparison of computed bulk and surface metal-sulfur bond strengths (kCal.mol⁻¹)

System	E _{M,S}	ΔH°_f	Ref.
Bulk PdS	45	-16.9	(6)
S @ Pd(111) ($\theta_s=0.33$)	109.5	-	(5)
Bulk PtS	56.3	-19.5	(6)
S @ Pd(111) ($\theta_s=0.33$)	111.1	-	-

Table 3. Changes of the total adsorption energy of S+Cl as a function of S-Cl distance, relative to infinite separation (results from Ref. (5) for Pd(111)).

Substrate	S-Cl distance (nm)	Pd shared	E _{ads} (S+Cl) (kCal.mol ⁻¹)	Change (%)
Pd ₄	(i)	0	-141.7	0
Pd ₄	0.47(ii)	1	-142.9	+5.3
Pd ₄	0.47(iii)	2	-134.3	-5.2
Pd(111)	(iv)	0	-190.7	0
Pd(111)	0.187(v)	2	-16.6	-91.3
Pd(111)	0.323(vi)	1	-174.8	-8.3
Pd(111)	0.485 (vii)	0	-185.6	-2.7

(i): Adsorption of S and Cl on separate clusters, S stabilized in three-fold site (face of the tetrahedron), Cl in bridge site.

(ii): Adsorption of S on a three-fold site and Cl on a bridge site (non adjacent edge) of the same cluster

(iii): Adsorption of S on a three-fold site and Cl on a bridge site (adjacent edge) of the same cluster

(iv): Adsorption of S and Cl in separate cells at the low coverage limit ($\theta_s=0.11$)

(v): Adsorption of S and Cl in two edge-sharing adjacent three-fold hollow sites.

(vi): Adsorption of S and Cl in two corner-sharing opposite three-fold hollow sites.

(vii): Adsorption of S and Cl in two next to next neighbour three-fold hollow sites.

Table 4. Adsorption energies of ethylene on model metallic substrates (kCal.mol⁻¹)

Substrate	E _{ads}	Configuration	Ref.
Pd ₄	-18.5	π	-
Pd ₄	-9.4	di- σ	-
Pd(111)	-14.7	π	-
Pd(111)	-23.5	di- σ	(7)
Pt(111)	-10.6	π	-
Pt(111)	-20.2	di- σ	-

Table 5. Effect of sulfur and chlorine on the adsorption of ethylene on palladium (kCal.mol⁻¹)

Substrate	E _{ads} (C ₂ H ₄)	Configuration	Ref.
Pd ₄	-18.5	π	-
Pd ₄ S	-20.8	π	-
Pd ₄ Cl	-16.1	π	-
Pd ₄ SCl	-7.6	π	-
Pd(111)	-23.5	di- σ	(7)
Pd(111) + 0.22MLS	-19.3	di- σ	(7)
Pd(111) + 0.22MLCl	-23.5	di- σ	(7)
Pd(111) + 0.11MLS + 0.11 ML Cl	-22.3	di- σ	(7)

MOLECULAR MODELING OF GAS OIL HYDRODESULFURIZATION

Gang Hou[†] and Michael T. Klein^{*}

[†]Department of Chemical Engineering
University of Delaware
Newark, DE 19716
hou@che.udel.edu

^{*} Department of Chemical and Biochemical Engineering
Rutgers, The State University of New Jersey
Piscataway, NJ 08854
mtklein@jove.rutgers.edu

ABSTRACT

The hydrodesulfurization (HDS) process chemistry and reaction network have been modeled at the molecular level. The following sulfur compound types have been considered: mercaptans, sulfides, disulfides, thiophenes (T), benzothiophenes (BT), dibenzothiophenes (DBT), and their alkyl and hydrogenated derivatives. The steric and electronic effects of the alkyl side chain of thiophenic compounds (T, BT, and DBT) are taken into account. The dual-site mechanism - σ site for direct desulfurization and τ site for hydrogenation on catalyst surface - is incorporated; the corresponding dual-site LHHW formalism is constructed to describe the complex kinetics. A rigorous molecular model for gas oil HDS is thus developed fast and successfully by aid of the Kinetic Modeler's Toolbox (KMT). The model matches pilot plant data very well and can be used to optimize the HDS process.

KEYWORDS: Hydrodesulfurization (HDS), Molecular Modeling, Kinetic Modeling

INTRODUCTION

Hydrodesulfurization (HDS) has been one of the most important oil refining processes. The process chemistry has been studied extensively over the past two decades [1-3]. However, with more and more stringent environmental regulations, our interests in HDS process have been renewed. Low sulfur specifications caused the refiners to look at the hydrotreating options and thus more rigorous models are desired to better improve the process. In this paper, a practical molecular level modeling of HDS process is introduced and developed, which is part of a much wider effort aiming at automated molecule-based kinetic modeling of gas oil hydroprocessing [4].

MODEL DEVELOPMENT

Classification of Sulfur Compounds

The petroleum feedstock contains the following sulfur compound types: mercaptans, sulfides, disulfides, thiophenes (T), benzothiophenes (BT), dibenzothiophenes (DBT), and their alkyl and hydrogenated derivatives. HDS reactivity depends critically on the molecular size and structure of the sulfur compounds. The mercaptans, sulfides and disulfides have, generally, fast kinetics compared with the thiophenic compounds (T, BT, and DBT as shown in Figure 1). The substituent groups adjacent to the S atom on thiophenic compounds generally retard HDS. While methyl groups distant from the S atom generally increase HDS activity - an effect attributed to increased electron density on the S atom - those adjacent to the S atom decrease reactivity due to steric effect [2].

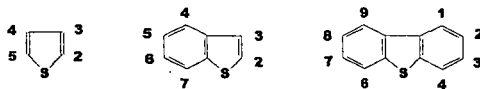


Figure 1. Thiophenes (T), Benzothiophenes (BT), and Dibenzothiophenes (DBT).

Those significant positions on T, BT, and DBT are identified as listed in Table 1. For example, it has been found that 4,6-dimethyldibenzothiophene (4,6-DMDBT) remains intact until the final stages of HDS of a light oil. The substituent groups on the significant and non-significant positions have different steric and electronic effects on HDS reactivities. As shown in Table 1, for example, we need at least two monomethyl, three dimethyl, and three trimethyl-substituted molecular structures to account for this position difference for alkyl-DBTs up to C3.

Table 1: The significant positions of thiophenic compounds.

Sulfur	Significant Position	Non-significant	Factor* (steric+electronic)	Representative Structures
T	2, 5	3, 4	$f_{1,T} \ll f_{2,T}$	2C1, 3C2, 2C3, 1C4
BT	2 (3, 7)	4, 5, 6	$f_{1,BT} \ll f_{2,BT}$	2C1, 2C2, 2C3, 2C4
DBT	4, 6	1, 2, 3, 7, 8, 9	$f_{1,DBT} \ll f_{2,DBT}$	2C1, 3C2, 3C3

* Subscript 1 denotes there is an alkyl chain at a significant position; 2 for non-significant position.

Reaction Pathways and Network

The following reaction pathways shown in Figure 2 are used to describe the HDS chemistry. The mercaptans, sulfides, and disulfides can be easily desulfurized. The T, BT, DBT and their alkyl

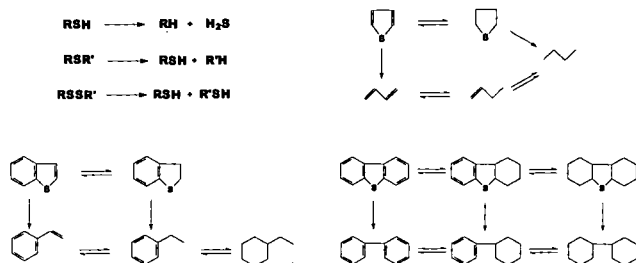


Figure 2. HDS reaction pathways and network.

derivatives can go through either the hydrogenation reaction at the τ site or the direct desulfurization reaction at the σ site on the catalyst surface [3].

Reaction Kinetics

Table 2 shows the rate laws used to model HDS kinetics. The classical dual-site mechanism - σ site for direct desulfurization and τ site for hydrogenation on catalyst surface in HDS process - is utilized to implement the corresponding dual-site LHHW formalism. This rate law is derived from the model compound studies by assuming the rate-determining surface reaction step between adsorbed reactants and two competitively adsorbed hydrogen atoms for both types of reaction [5].

Table 2: HDS rate law.

$$r = \frac{f_{\sigma} k K_{A,\sigma} K_{H_2,\sigma} [A] [H_2]}{(1 + \sum_i K_{i,\sigma} [I] + \sqrt{K_{H_2,\sigma} [H_2]})^n} + \frac{f_{\tau} k_{\tau} K_{A,\tau} K_{H_2,\tau} [A] [H_2] - [B]/K}{(1 + \sum_i K_{i,\tau} [I] + \sqrt{K_{H_2,\tau} [H_2]})^n}$$

Where r is reaction rate, $[I]$ is concentration of component, k is rate constant, K_i is adsorption constant of component, K is equilibrium constant and n is the exponent of inhibition term (3 for HDS).

The two global factors (f_{σ} and f_{τ}) are introduced to account for the total steric and electronic effects of substituents on thiophenic compounds at both σ and τ sites.

RESULTS AND DISCUSSION

A detailed molecular level kinetic model for HDS of light gas oil has been developed using the Kinetic Modeler's Toolbox (KMT) - a software package that automates the kinetic modeling of industrial complex processes [4]. The complete reaction model was built automatically in only 2 CPU seconds and solves very fast in less than 2 CPU seconds on an Intel Pentium II 333Mhz machine.

The current version of the model containing 243 species and 437 reactions was tuned to pilot plant data and the parity plot (Figure 3) shows the model matches the experimental data very well and can do a good job even in very low sulfur levels (<50ppm). The parity guarantees the model follows the right trends of the molecular conversions in the process stream and the developed model can certainly provide the quantitative insights to improve the HDS process.

CONCLUSIONS

The automated molecule-based kinetic modeling strategy was successfully extended to build rigorous HDS model as part of the effort to model gas oil hydroprocessing [4]. To rigorously model the HDS chemistry, it is necessary to incorporate at least all the representative molecular structures with substituents at both significant and non-significant positions. It is also very important to incorporate dual-site mechanism and implement the corresponding LHHW formalism to take into account the inhibitions of various compounds in the process stream (especially the H₂S inhibition at σ sites). The developed HDS Model matches the pilot-plant data very well and can be used to optimize the low sulfur hydrotreating process quantitatively.

REFERENCES

1. Girgis, M.J., and Gates, B.C., *Ind. Eng. Chem. Res.* **30**, 2021 (1991).
2. Topsøe, H., Clausen, B.S., and Massoth, F.E., in "Catalysis Science and Technology" (J.R. Anderson and M. Boudart, eds.), Vol.11. Springer-Verlag, New York, 1996.
3. Whitehurst, D.D., Isoda, T., and Mochida, I., *Advances in Catalysis*, **42**, 345 (1998).
4. Hou, G., Klein, M.T., 2nd International Conference on Refinery Processes Proceedings, AIChE, Houston, TX (1999)
5. Vanrysselberghe V., and Froment, G.F., *Ind. Eng. Chem. Res.* **35**, 3311 (1996).

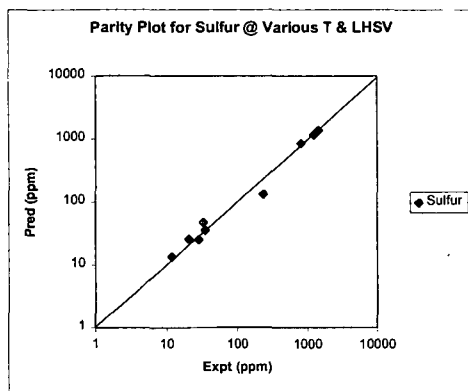


Figure 3. Parity plot of HDS model.

Molecule-Based Modeling of Gasoil Fluid Catalytic Cracking

Ankush Kumar
Department of Chemical Engineering
University of Delaware, Newark, DE 19716

Michael T. Klein
College of Engineering
Rutgers, The State University of New Jersey
Piscataway, New Jersey 08854-8058

INTRODUCTION

Fluid Catalytic Cracking (FCC) is a major refinery process designed to upgrade heavy and less valuable petroleum products to gasoline and lighter products. The feedstock for the FCC process ranges from light gas oils to heavy hydro-treated resids. The complexity of the feedstock, and the associated analytical chemistry and computational obstacles, helped shape early FCC modeling approaches (2,3,7). The traditional need for easily deployed reaction models led to the formulation of simple, lumped kinetic models. Lumped models often fail to capture the complex FCC chemistry and as a result are specific to the feedstock, the catalyst used and the operating conditions. Additionally, lumped models do not give the detailed product distribution required for process design and optimization.

The new paradigm is to track each molecule in the feed and product through the process and to move towards models having fundamental kinetic information. This has led to the modeling of the chemistry at the mechanistic level (5,6). These mechanistic models have a large number of gaseous and surface species and, hence, are very CPU intensive. Thus, on the one hand, the need for a detailed molecular representation and fundamental kinetic information make the use of mechanistic models attractive, but, on the other hand, the large solution time renders them of limited use in practice. This motivates the development of pathways-level models. Pathways-level models are not as large and complex as the mechanistic models because of the exclusion of reactive intermediaries, e.g., surface species. They also offer the advantage of being solved in a reasonable amount of time. They offer the opportunity to incorporate detailed kinetic information by the inclusion of all important observable molecules explicitly, and hence have the predictive capability lacking in the lumped models.

Developing such molecularly explicit models for gasoil fluid catalytic cracking is now possible because of two enabling advances. First, recent developments in analytical chemistry now allow a molecularly explicit stochastic description of gasoils. Second, the explosion in computational power makes possible the necessary bookkeeping to generate and solve reaction networks with a large number ($O(10^3)$) of molecules. The aim of this work is to develop an automated capability for building pathways-level FCC models for heavy hydrocarbons (e.g. gasoils). In the following sections, we will briefly discuss the methodology used for determining a molecular description of the feedstock and then also outline the strategy used for computer-generation of gasoil FCC pathways-level kinetic model.

FEEDSTOCK CHARACTERIZATION

The ability of a reaction model to describe the product distribution depends to a large extent on the initial conditions i.e., the structure and the mole fractions of the molecules in the feedstock. Such detailed characterization for the heavier feedstock, such as gasoils, is seldom available. Even modern analytical techniques reveal only structural attributes (i.e. the number of aromatic rings, number of saturated rings, number of sidechains, etc.) rather than the detailed individual molecular structures. The first challenge, then, is to determine a set of molecules and associated mole fractions characteristic of the feed from routinely available analytical data, such as true boiling point distribution, average molecular weight, elemental analysis, NMR data and GC/MS lumps. This can be done using the *MoleGen* technique (4).

In this technique, molecules are represented in terms of a collection of molecular attribute building blocks (e.g. number of aromatic rings, number of naphthenic rings, number and length of sidechains, etc.). Each attribute is represented by a probability density function. Monte Carlo sampling of the set of probability density functions provides a large ensemble of molecules ($O(10^3)$). The properties of this ensemble of molecules are compared to experimentally obtained analytical data to obtain an optimal set of probability density functions. These optimized probability density functions contain the statistical description of the feedstock and can be easily transformed into a set of molecular structures and their associated mole fractions.

MODEL BUILDING

Pathways models for complex feedstocks, such as gasoils, can have a large number of molecules and their reactions. It can be quite tedious and time-consuming to build such models by hand. This motivates the automation of the model building process.

To automate the process of reaction network building use is made of graph theoretic concepts. In this approach, a molecule is represented by a graph, the atoms being the nodes of the graph and the bonds being the edges of the graph. For all the reactions in FCC, the connectivities of only a few of the atoms in the involved molecules change. This means that a reaction can be represented by the change in the connectivity of only a few anodes in the graph. The connectivity matrices of the reactants are combined into an augmented reactant matrix, which, after permutation gives the reduced matrix for the reactants, containing the connectivities of only those atoms whose connectivity changes in the reaction process. The bond breaking and forming (i.e., the reaction) is then carried out by simple matrix addition operations (1).

The chemistry is represented through the implementation of reaction rules. These rules rely on theoretical and experience-based kinetic approximations and are useful tools in keeping the size of the model realistic without significantly effecting the product distribution. The reaction network is then converted to a set of differential equations using the *OdeGen* parsing code (1). Conceptually, the resulting mathematical model can then be solved with appropriate initial conditions and rate constants. However, during the developmental stage, the rate constants for most of the reactions are usually not known *a priori* and the model has to be solved within an optimization framework to determine the rate constants.

This requires that the number of rate parameters must be kept to a reasonable number to obtain true rate constant information from optimization to the experimental data. Even with the use of reaction rules for the complex FCC chemistry the detailed reaction model can have a large number of reactions and their associated rate constants ($O(10^3)$). Clearly, some organizational or "lumping" scheme that does not sacrifice the basic chemistry is in order. To this end, it is useful to realize that much of the complexity is statistical or combinatorial, and that the large number of reactions and rate parameters in the pathways-level model can be handled by lumping the reactions involving similar mechanistic steps into one reaction family. The kinetics of all the reactions within the same reaction family are described by a common set of parameters. Differences in the reactivity within the same reaction family can be traced to differences in the heat of the reaction.

RESULTS AND MODEL DIAGNOSTICS

These ideas of feedstock characterization and automated model building were applied to gasoil FCC reaction modeling. The analytical data available for gasoil included boiling point distribution, average molecular weight, Clay Gel analysis, MS lumps and average parameters from NMR analysis. These analytical data were used to determine a stochastic molecular representation of the feed using the *MolGen* technique. The feed was described in terms of 222 representative molecules and their mole fractions.

The feed was then grouped into a few compound classes (paraffins, iso-paraffins, naphthenes and aromatics), which, in turn, were allowed to react through a limited

number of reaction families (cracking, isomerization, dehydrogenation, hydrogenation, and aromatization). This allowed the division of all the reactions into a small number of reaction families with associated rate parameters. Table 1 shows the model diagnostics for the final model. The use of reaction family concept allowed the description of all the rate constants for 3293 reactions in terms of about 30 rate parameters.

Feed Molecules	222
Total number of molecules	823
Paraffin Cracking Reactions	574
Paraffin Isomerization Reactions	206
Olefin Cracking Reactions	131
Naphthenic Cracking Reactions	138
Aromatic Cracking Reactions	435
Hydrogenation Reactions	274
Dehydrogenation Reactions	221
Model Generation Time	433s
Model Solution Time	< 1 minute

Table 1. Gasoil Fluid Catalytic Cracking Model Diagnostics

To develop the optimal reaction network and to determine the rate constants the model predictions were constrained to match the pure components as well as gasoil experimental data. As an example of the quality of fit between model and experimental values Figure 1 shows the results for n-heptane cracking.

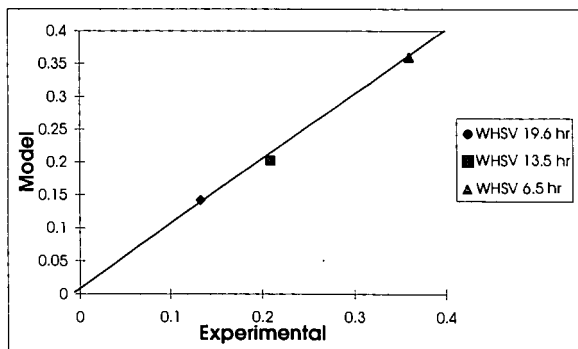


Figure 1a. Parity Plot for Heptane Conversion at different weight hourly space velocity (WHSV).

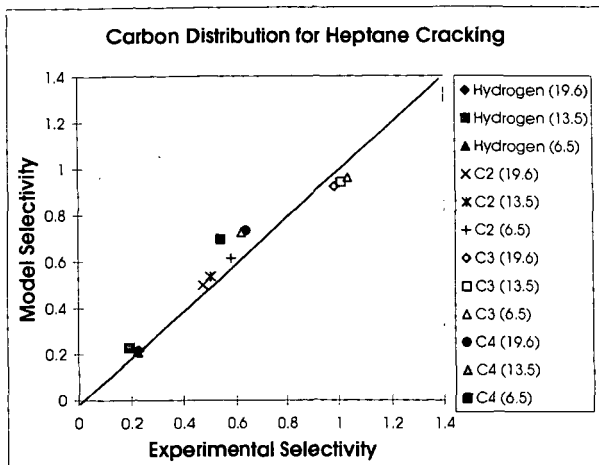


Figure 1b. Parity Plot of Selectivity by Carbon number for n-heptane cracking. Values in brackets are the WHSV.

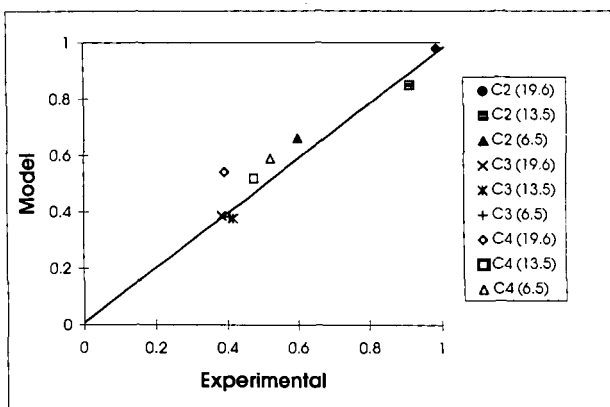


Figure 1c. Parity Plot of Paraffin / Olefin ratio for n-heptane cracking. Values in brackets are the WHSV.

CONCLUSIONS :

1. Graph theory was successfully used to generate a molecularly explicit gas oil FCC model containing 823 species and 3293 reactions.
2. The parity of the predicted results was reasonably good with the experiments. This suggests that the stochastic approach for generation of the feedstock and the reaction family concept for expressing the rate constants are very good tools for predicting the reactivity of a complex mixture.
3. This approach to automated pathways-level model building can be easily extended to other feedstocks and catalyst systems in order to obtain kinetics information.

REFERENCES

1. Broadbelt, L. J., Stark, S. M., Klein, M. T., "Computer Generated Pyrolysis Modeling: On-the-fly Generation of species, Reactions and Rates", *I. & E. C. Res.*, **33**, 790-799 (1994).
2. Jacob, S. M., Gross, B., Volts, S. E., and Weekman, V. W., "A Lumping and Reaction Scheme for Catalytic Cracking", *AIChE J.*, **22**, pp. 701-713 (1976).
3. John, T. M., and Wojciechowski, B. W., "On Identifying the Primary and Secondary Products of the Catalytic Cracking of Neutral Distillates", *J. Catal.*, **37**, pp. 348 (1975).
4. Kumar, A., Campbell, D., Klein, M. T., "Computer Assisted Kinetic Modeling: Interfacing Structure and Reaction Network Builders", *ACS Symposia Preprints*, v **42 (3)**, 662-665, (1997).
5. Watson, B. A., Klein, M. T., and Harding, R. H., "Mechanistic modeling of n-heptane cracking on HZSM-5", *Ind. Eng. Chem. Res.*, **35(5)**, pp. 1506-1516 (1996).
6. Watson, B. A., Klein, M. T., and Harding, R. H., "Catalytic Cracking of Alkylcyclohexanes: Modeling the Reaction Pathways and Mechanisms", *International Journal of Chemical Kinetics*, **29(7)**, pp. 545 (1997).
7. Weekman, V. W., and Nace D. M., "Kinetics of Catalytic Cracking Selectivity in Fixed, Moving, and Fluid Bed Reactors", *AIChE J.*, **16**, pp. 397-404 (1970).

KINETIC SOLVENT EFFECTS ON HYDROXYL HYDROGEN ATOM ABSTRACTIONS

Janusz Luszyk
 Steacie Institute for Molecular Sciences
 National Research Council of Canada
 100 Sussex Drive, Ottawa, Ontario
 Canada K1A 0R6

The rates of radical reactions are commonly assumed to be independent of the solvent. We have demonstrated that this assumption is fully justified for hydrogen atom abstraction from cyclohexane by cumyloxy radicals.¹ However, we have also demonstrated the occurrence of dramatic solvent effects on the rates of H-atom abstraction from phenol and *tert*-butyl hydroperoxide by the same radical.² These very large solvent effects were attributed to hydrogen bond formation between the substrate, XOH, and hydrogen bond accepting (HBA) solvents, S. The magnitude of this kinetic solvent effect (KSE) is therefore determined by the strength of the interaction between XOH, the hydrogen bond donor (HBD), and the HBA solvent. This led us to predict that the magnitude of a KSE (i.e., the rate constant ratio, k^A/k^B , measured in two solvents, A and B) would "depend on the Lewis acidity of XOH, (but would) generally be independent of the nature of the radical which abstracts the hydrogen atom".² That is, for the reaction



the ratio of the measured rate constants in solvents A and B will generally be independent of the structure of Y, i.e., $(k^A_{\text{XOH/Y}})/(k^B_{\text{XOH/Y}}) = \text{constant}$ (for the same XOH).

We have confirmed this prediction using phenol and α -tocopherol (vitamin E) as hydrogen atom donating reactants, XOH, and two Y[•] radicals having grossly different absolute reactivities in hydrogen atom abstraction.³ The highly reactive Y[•] radicals were alkoxyis, cumyloxy (CumO[•]) in the case of phenol and *tert*-butoxy (BO[•]) in the case of α -TOH. A single, relatively unreactive Y[•] radical was chosen, 2,2-diphenyl-1-picrylhydrazyl (DPPH), because of the ease with which its decay kinetics could be monitored in a conventional spectrophotometer via its strong visible absorption.

Dramatic kinetic solvent effects (KSEs) are shown by the kinetic data in Table 1. For example, the rate constants for abstraction of the phenolic hydrogen atom of α -TOH by DPPH[•] and by BO[•] decrease by factors of ~67 and ~60, respectively, on changing the solvent from *n*-pentane to γ -valerolactone. Similarly, the rate constants for hydrogen abstraction from phenol by DPPH[•] and CumO[•] decrease by factors of ~107 and ~136, respectively, on changing the solvent from *n*-octane to ethyl acetate.

These kinetic data in a dramatic fashion confirm our prediction that the magnitude of the KSE on XOH/Y[•] reactions would be essentially independent of the nature of Y[•]. Thus, a plot of $\log(k^S_{\text{TOH/BO}}/M^{-1} s^{-1})$ vs $\log(k^S_{\text{TOH/DPPH}}/M^{-1} s^{-1})$ has most of the points fall very close to the straight line with a slope = 1.0. It is truly astonishing considering that in the same solvent the absolute magnitudes of the two rate constants differ by a factor of over one million. That is, for almost any solvent:

$$k^S_{\text{TOH/BO}}/k^S_{\text{TOH/DPPH}} \approx 1.6 \times 10^6$$

Even more striking are the results with phenol. Once again, the plot of $\log(k^S_{\text{PhOH/CumO}}/M^{-1} s^{-1})$ vs $\log(k^S_{\text{PhOH/DPPH}}/M^{-1} s^{-1})$ has all but one of the points fall very close to the line drawn with a slope = 1.0. In this set of experiments the absolute magnitudes of the two rate constants in the same solvent differ by a factor of 10 000 000 000! That is,

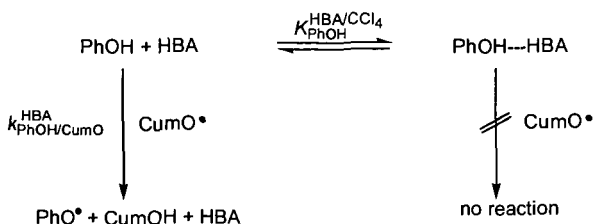
$$k^S_{\text{PhOH/CumO}}/k^S_{\text{PhOH/DPPH}} \approx 1.0 \times 10^{10}$$

Our findings were more recently additionally confirmed with peroxy^{4,5} and carbon-centered⁶ radicals, respectively.

Our studies on kinetic solvent effects (KSE) on free radical reactions have also serendipitously led to a completely new method for measuring equilibrium constants for hydrogen bonding from a variety of XOH to very many hydrogen-bond acceptors

(HBAs) in CCl_4 solvent, $K^{\text{HBA}/\text{CCl}_4}_{\text{XOH}}$. Since this method does not rely on infrared spectroscopy it can also be used to measure $K^{\text{HBA}/\text{CCl}_4}_{\text{XOH}}$ for HBAs containing hydroxylic groups provided only that the hydroxylic hydrogen atom in XOH can be abstracted by free radicals. We demonstrated the validity and simplicity of this new technique using phenol as XOH. Our kinetic measurements yielded $K^{\text{HBA}/\text{CCl}_4}_{\text{PhOH}}$ with HBA's which do not contain OH groups and which serve as a check for our method and $K^{\text{HBA}/\text{CCl}_4}_{\text{PhOH}}$ with HBA's which do contain OH groups, acetic acid, methanol, and *tert*-butyl alcohol.

We suggested a kinetic model² to explain the progressive reduction in the rate of hydrogen atom abstraction from phenol (and *tert*-butyl hydroperoxide) by cumyloxy radicals, CumO^\bullet , as the HBA abilities of the solvents increased. It invoked reactive non-hydrogen bonded XOH and non-reactive hydrogen-bonded XOH, e.g.,



Although we now recognize that this model is oversimplified³ it does yield a very simple and useful kinetic equation, viz.,²

$$k^{\text{CCl}_4}_{\text{PhOH}/\text{CumO}} = k^{\text{HBA}}_{\text{PhOH}/\text{CumO}} (1 + K^{\text{HBA}/\text{CCl}_4}_{\text{PhOH}} [\text{HBA}]) \quad (2)$$

which can be rearranged to

$$\frac{1}{k^{\text{HBA}}_{\text{PhOH}/\text{CumO}}} = \frac{1}{k^{\text{CCl}_4}_{\text{PhOH}/\text{CumO}}} + \frac{K^{\text{HBA}/\text{CCl}_4}_{\text{PhOH}} [\text{HBA}]}{k^{\text{CCl}_4}_{\text{PhOH}/\text{CumO}}} \quad (3)$$

Thus, for *dilute* phenol and HBA in CCl_4 (where their activity coefficients will be unity) a plot of the reciprocal of the rate constant (i.e., $1/k^{\text{HBA}/\text{CCl}_4}_{\text{PhOH}/\text{CumO}}$) measured at 25 °C against $[\text{HBA}]$, the concentration of the HBA in CCl_4 , should yield a straight line with an intercept equal to the reciprocal of the measured rate constant in CCl_4 and with a (slope) / (intercept) ratio equal to $K^{\text{HBA}/\text{CCl}_4}_{\text{PhOH}}$. The kinetically derived equilibrium constants for hydrogen bonding between phenol and HBAs are summarized in Table 2 and are compared therein with the ranges of equilibrium constants which have been obtained by the infrared (IR) method at 25 °C.

CONCLUSIONS

We have demonstrated that for hydroxyl hydrogen atom donors rate constants for hydrogen atom abstractions are strongly solvent dependent and independent of the nature of the abstracting radical species. Thus, provided rate constants have been measured for the reaction of one radical with a hydroxyl substrate in a range of solvents, then a measurement of the rate constant for reaction of the same substrate with some different radical need to be made in only one of these solvents for values in all the other solvents to be predicted accurately.

A simplified kinetic model advanced for hydrogen atom abstraction from hydroxyl hydrogen atom donors provides a new method for measuring equilibrium constants for hydrogen bonding from these donors to any hydrogen bond acceptors including alcohols.

REFERENCES

1. Avila, D. V.; Brown, C. E.; Ingold, K. U.; Luszyk, J. *J. Am. Chem. Soc.* **1993**, *115*, 466-470.
2. Avila, D. V.; Ingold, K. U.; Luszyk, J.; Green, W. H.; Procopio, D. R. *J. Am. Chem. Soc.* **1995**, *117*, 2929-2930.
3. Valgimigli, L.; Banks, J. T.; Ingold, K. U.; Luszyk, J. *J. Am. Chem. Soc.* **1995**, *117*, 9966-9971.
4. Valgimigli, L.; Banks, J. T.; Luszyk, J.; Ingold, K. U. *J. Org. Chem.* **1999**, *64*, 3381-3383.
5. Lucarini, M.; Pedulli, G. F.; Valgimigli, L. *J. Org. Chem.* **1998**, *63*, 4497-4499.
6. Franchi, P.; Lucarini, M.; Pedulli, G. F.; Valgimigli, L.; Lunelli, B. *J. Am. Chem. Soc.* **1999**, *121*, 507-514.

Table 1. Absolute Rate Constants for Abstraction of the Phenolic Hydrogen Atom from α -Tocopherol (TOH) in Various Solvents at 298 ± 2 K

solvent	10^{-8}	10^{-2}	10^{-7}	10^3
	$k_{\text{TOH/BO}}^{\text{S}}$ ($\text{M}^{-1} \text{s}^{-1}$)	$k_{\text{TOH/DPPH}}^{\text{S}}$ ($\text{M}^{-1} \text{s}^{-1}$)	$k_{\text{PhOH/CumO}}^{\text{S}}$ ($\text{M}^{-1} \text{s}^{-1}$)	$k_{\text{PhOH/DPPH}}^{\text{S}}$ ($\text{M}^{-1} \text{s}^{-1}$)
1 <i>n</i> -pentane	99	74		
2 <i>n</i> -octane	60	74	110 ^b	160
3 <i>n</i> -hexadecane	50	73		
4 carbon tetrachloride	42	36	86	93
5 chlorobenzene	36	27	48	59
6 benzene	31	18	28	31
7 anisole	20	14	5.6	7.2
8 acetonitrile	9.4	4.9		
9 acetic acid	7.7	6.2	1.8	3.1
10 methyl acetate	3.0	1.9		
11 ethyl acetate	2.9	1.6 ₅	0.8 ^b	1.5
12 γ -valerolactone	1.6 ₅	1.1		
13 <i>tert</i> -butyl alcohol	1.8	5.7	0.36	2.9

Table 2. Equilibrium Constants for Hydrogen Bond Formation at 25 °C between Phenol and Some Hydrogen Bond Acceptors Measured by the Kinetic Method (Comparison with 25 °C Equilibrium Constants Measured by Infrared Spectroscopy from the Literature)

HBA	[HBA] max (M) ^a	$k_{\text{PhOH}}^{\text{A/CCl}_4}$ (M^{-1})	
		kinetic	infrared (lit)
MeC(O)OH	1.2	1.4	no value
MeCN	0.6	3.5	4.6-6.5
MeC(O)OEt	1.5	6.6	8.8-12.3
MeOH	1.2	11	no value
<i>t</i> -BuOH	0.5	14	44
pyridine	0.3	30	41-53
Me ₂ NCHO	0.17	69	64-76

^aMaximum HBA concentration used to determine the equilibrium constant by the kinetic method.

THERMAL CONVERSIONS OF CONJUGATED CYCLIC POLYENES WITH ENDOCYCLIC *TRANS* CARBON CARBON DOUBLE BONDS

Dieter Hasselmann, Christoph Richter, Martin Hoppe, and Martin Glunz
Faculty of Chemistry, Organic Chemistry, Ruhr-University
Universitätsstrasse 150, D-44780 Bochum, Germany
e-mail: hasselmann@orch.ruhr-uni-bochum.de

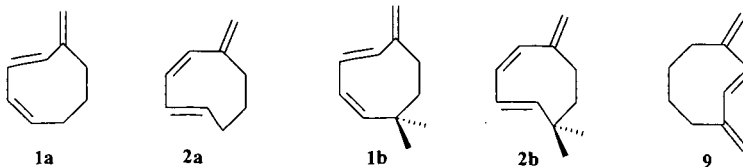
ABSTRACT

The strained monocyclic triene hydrocarbons (1*Z*, 3*E*)-5-methylene-1,3-cyclooctadiene (**1**) and (1*E*, 3*Z*)-5-methylene-1,3-cyclooctadiene (**2**) with endocyclic *trans* carbon carbon double bonds have been found to be key reactive intermediates in the complex thermal rearrangements of the *cis*-bridged bicyclic cyclobutene, 2-methylenebicyclo[4.2.0]oct-7-ene (**3**). Gasphase thermolysis (>160 °C) of **3** leads to three monocyclic trienes, **4**, **5** and **6**, and to two tricyclic alkenes, **7** and **8**. Indirect evidence for the involvement of **1** and **2** in the rearrangements of **3** follows from trapping intermediate **2** with furan and from their thermal generation by the cycloreversions of their independently synthesized *Diels-Alder* adducts with furan, respectively. Independent syntheses of the thermo-labile trienes **1** and **2** and of related hydrocarbons allows to directly investigate their thermal properties. Competing routes for stabilization of **1** - **3** to mono-, bi- and/or tricyclic products and their mechanistic implications are discussed. From experimental enthalpies of activation and molecular mechanics calculations energy profiles are modeled. Torquoselectivity as a function of ring size is discussed for *cis*-3,4-bridged cyclobutenes related to **3**.

I. INTRODUCTION

Thermal reorganizations of organic compounds often turn out to be highly stereoselective or even stereospecific. Frequently these reactions can be classified as concerted. These transformations usually demand only 'low' temperatures at which alternative reaction channels, e.g. those involving radical paths, are not accessible for energetic reasons. On the other side 'high' temperatures are required for reactions involving the thermal generation of radicals by breaking a carbon carbon bond. The cleavage of a simple C-C single bond necessitates an energy of about 80 - 90 kcal/mol, in crack processes of alkanes in many cases this is in accordance with temperatures up to 500 °C. However, temperatures for bond breaking can be lowered considerably by taking recourse to molecular strain and / or electronic stabilization of the carbon radical centers generated. This can be achieved to an extent that competition between concerted and multistep radical reactions has to be taken into account.

In this context monocyclic cyclobutenes easily undergo thermal cycloreversions to acyclic 1,3-butadienes in concerted reactions.¹⁻³ These archetypal electrocyclic reactions stereospecifically follow 'allowed' conrotation.^{1, 2} In simple cases the 'disallowed' disrotatory alternative is found to be energetically disfavored by about 10 kcal/mol.⁴ The profound electronic impact of substituents on the direction of conrotation observed in cyclobutene - butadiene reorganizations has found much attention, recently, from theory⁵ as well as from experiment.⁶⁻⁸ However, the stereochemical course of the cycloreversion of 3,4-bridged cyclobutenes which were structurally constrained proved to be considerably more complex. As a function of ring size of the annulated rings these compounds were found to thermally undergo 'allowed' conrotatory and / or 'forbidden' disrotatory ring openings to give *E/Z*-cyclohexadienes and / or *Z/Z*-stereoisomers.⁹⁻¹¹ The border-line case between both directions of cycloreversion, however, seems to rest with bicyclic cyclobutenes having attached a five or six membered ring.



Of special interest in this respect, therefore, is the thermal behavior of *cis*-3,4-bridged bicyclic cyclobutenes, e.g. 2-methylenebicyclo[4.2.0]oct-7-ene (3). The exocyclic methylene substituent in the 2-position of 3 should exert special effects on the mechanistic course and the energetics of the transformations of this hydrocarbon. Accessibility and thermal stability of the strained monocyclic conjugated triene hydrocarbons (1*Z*, 3*E*)-5-methylene-1,3-cyclooctadiene (1) and (1*E*, 3*Z*)-5-methylene-1,3-cyclooctadiene (2), expected to be central, although labile intermediates in the thermal rearrangements of 3, are of key importance. We now report on independent syntheses of 1 and 2. The thermal properties of these hydrocarbons have been determined as well as those of 3. The results provide insight into the competing pathways of stabilization, as for instance by electrocyclicization, by intramolecular cycloaddition, by direct geometric isomerization via diradicals, and / or by hydrogen migration. Suitably geminal methylated derivatives, 1b and 2b, and *E*-dimethylenecyclooctene 9, significant for the question of a direct geometric stereomutation, have been included in our investigations. Energy profiles for the thermal reorganizations involved are modeled from experimental enthalpies of activation and molecular mechanics calculations. Torquoselectivity⁵ as a function of ring size is discussed for *cis*-3,4-bridged cyclobutene 3 and related compounds.

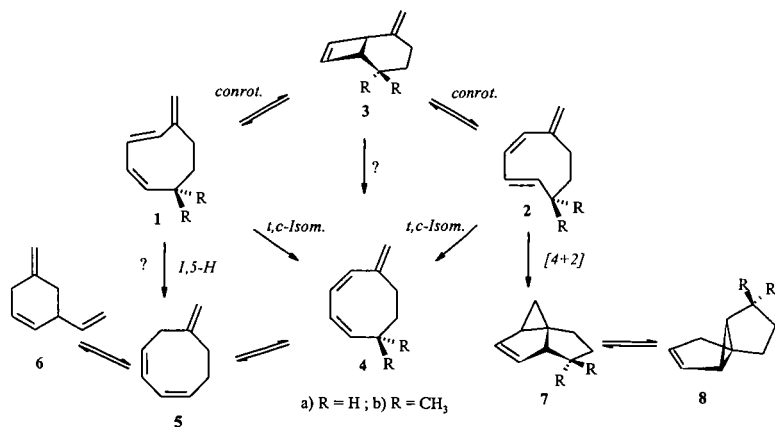
II. PROCEDURE

Thermolyses of 3 have been performed at low pressure (1-5 mbar) in the gasphase in a conditioned 20 l pyrex vessel. The flask was heated in an air-thermostat with a temperature constancy better than 0.1 °C and was connected to a high vacuum line with greaseless stopcocks. Kinetic measurements have been followed gaschromatographically. Rearrangements of the thermally labile hydrocarbons 1, 2 and 9 had to be carried out in solution. Toluene-*d*8 and cyclohexane-*d*12 were used as solvents to follow the reactions quantitatively by ¹H-NMR spectroscopy at 400 MHz.

Experimental details of the synthetic procedures for the relevant compounds will be reported elsewhere.

Molecular mechanics calculations have been performed with the programs MM2ERW¹² and MMEVBH¹³ developed by W. R. Roth¹⁴ and co-workers on the basis of Allinger's¹⁵ MM2 procedure. The MM2ERW¹² forcefield allows one to calculate conjugated π -systems with high accuracy without embarking on quantum-mechanical methods. The MMEVBH procedure has been developed^{13,14} to calculate heats of formation of hydrocarbons, conjugated and non conjugated polyenes as well as those of radicals and diradicals.

Scheme 1. Mechanistic Pathways for the Thermal Reorganizations of C₈H₁₂ Isomers 1 - 3, and Geminal Dimethyl Substituted Derivatives.



III. RESULTS

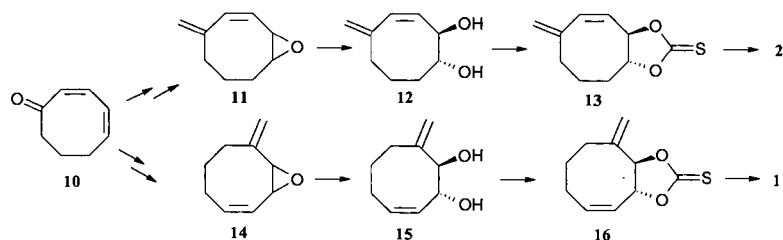
In the temperature range of about 165 to 215 °C gasphase thermolysis of the bridged bicyclic vinylcyclobutene 3 results in the formation of five new isomeric hydrocarbons. These can be grouped into two sets, on the one side into the three monocyclic trienes 4, 5, and 6, and on the

other side into two tricyclic alkenes **7** and **8**, with **4** and **7** constituting the main products.¹⁶ The kinetics of the decrease of **3** follows a first order reaction with $\log A = 13.27 \pm 0.06$ and $E_a = 36.13 \pm 0.12$ kcal/mol. However, not all of the products are primary ones. Under the reaction conditions conjugated triene **4** is in fast equilibrium with its 1,5-hydrogen shift product **5**. From this, secondarily the monocyclic unconjugated **6** is formed. The activation parameters for the mutual conversions $4 \leftrightarrow 5 \leftrightarrow 6$ have been determined independently at lower temperatures by starting with **5**.¹⁷ The tricyclic alkene **7** slowly undergoes a *vinylcyclopropane-cyclopentene* rearrangement to spiroalkene **8**. In view of our experimental findings and earlier results on *cis*-bicyclo[4.2.0]oct-7-ene¹⁸ the mechanistic pathways given in Scheme 1 have to be taken into account.

Central to product formation from **3** are the properties of the strained trienes **1** and **2** which could be formed by allowed conrotatory cycloreversion with inward and outward rotation of the exocyclic methylene substituent. However, these *trans*-cycloalkenes are unstable at the high temperatures necessary to convert **3**. Indirect evidence for the involvement of **1** and **2** is derived from our findings that **2**, but not **1**, can be trapped in the presence of furan as *trans*-[4+2] cycloaddition products and that thermal decomposition ($T > 155$ °C) of the four *Diels-Alder* adducts possible from **1** and **2** with furan, which all have been synthesized independently, results in the same product mixtures as that found from **3**.¹⁶ Mechanistically still unanswered are the questions if the observed *Z,Z*-product **4** is generated from **3** by direct disrotation, by direct cleavage of a double bond $1 \rightarrow 4$ or $2 \rightarrow 4$, respectively, or if a multistep sequence $3 \rightarrow 1 \rightarrow 5 \rightarrow 4$ is followed with a 1,5-hydrogen shift in **1** as the crucial step.

Substituting hydrogen by geminal methyl groups as in **3b** after electrocyclicization should lead to labile triene intermediates **1b** and **2b**. In **1b** stabilization by a concerted 1,5-hydrogen shift would be blocked and recyclization should dominate. Results of gasphase thermolyses at 175 - 220 °C with **3b** as an educt show, indeed, **7b** to be the main product followed by rearrangement to **8b**. The *Z,Z*-triene **4b** is formed only to a minor extent.¹⁹

Scheme 2. Synthetic Routes to Trienes (1*Z*, 3*E*)-5-methylene-1,3-cyclooctadiene (**1**) and (1*E*, 3*Z*)-5-methylene-1,3-cyclooctadiene (**2**).



Independent syntheses of the central intermediates **1** and **2** are accomplished for the first time by following a modified Corey/Winter²¹ protocol as shown in Scheme 2. Using such a sequence for the synthesis of strained trienes seems to be without precedent. Key steps are stereospecific ring openings of the vinyloxiranes **11** and **14** to give *trans*-diols **12** and **15**, respectively, after regioselective formation from dienone **10**, and desulfuration of the *trans*-thionocarbonates **13** and **16** at about room temperature and at low pressures to generate **1** and **2** with high isomeric purity.²⁰ The structures of both isomers have been characterized without doubt by NMR spectroscopy. Additionally, the *E*-configuration of the central carbon carbon double bond in **1** has been secured by formation of the same *Diels-Alder* adducts with furan as those known from an independent route¹⁶ and by X-ray structure analysis of one of the adducts with diphenylisobenzofuran.²⁰ Synthesis of the geminal methylated isomers **1b** and **2b** proved to be more difficult and a modified route using β -hydroxyphosphinioxides as intermediates had to be taken.²² *E*-Dimethylenecyclooctene **9** is obtained by a multistep sequence to the *Z*-isomer followed by sensitized photoisomerization.

Slightly above room temperature triene **1** with a central *trans* double bond starts to cyclorevert to **3** and to isomerize to *Z,Z*-triene **4** in a 2 : 1 ratio, approximately. Not completely conjugated triene **5**, stable at the reaction conditions, is not observed. In toluene-d₈ and followed at temperatures of 30 - 70 °C reaction $1 \rightarrow 3$ shows $\log A/s^{-1} = 13.2 \pm 0.2$ and $E_a = 25.6 \pm 0.3$ kcal/mol. Trienes **2** and **2b** with the *trans* double bond in the end of the conjugated system prove

to be thermally more stable. At 60 -120 °C they predominantly undergo electrocyclization to 3 and 3b with $E_a = 26.7 \pm 0.3$ kcal/mol and $E_a = 26.9 \pm 0.9$ kcal/mol, respectively. The Z,Z-trienes 4 are formed, but to a smaller extent; from 2b traces of 7b are observed. However, thermolyses of 2 and 2b are complicated by some dimerization. At 50 - 95 °C E-cyclooctene 9 isomerizes to the Z-isomer with $E_a = 25.8$ kcal/mol, exclusively.²⁰

Schematic energy profiles of the reactions involved can be modeled by combining our experimentally determined activation parameters with enthalpies of formation calculated by the above forcefield programs for educts, products and the reactive intermediates participating. It is clearly shown that besides dominant electrocyclization in the first two cases the reactive trienes 1, 2 and 9 can be stabilized competitively by direct double bond cleavage to diradical transition structures followed by rotation and recombination to their thermally more stable Z-isomers, even at temperatures close to room temperature. Ring opening in 3 by disrotation and stabilization of *trans*-triene 1 by a 1,5-hydrogen shift does not take place. These findings are discussed with those of our earlier results on thermal rearrangements of hydrocarbons related to 3 which have contracted rings^{23, 24} and those of the relevant literature.

In addition, it is shown that by using substrates 3 stereospecifically substituted at the *exocyclic* methylene carbon the formations of the tricyclic products 7, formally intramolecular *Diels-Alder* reaction products, follow multistep routes via diradical intermediates.^{16, 19} Nevertheless, in some cases product formation with high stereoselectivity has been found.

IV. CONCLUSIONS

Highly strained monocyclic *trans*-trienes (1Z, 3E)-5-methylene-1,3-cyclooctadiene (1) and (1E, 3Z)-5-methylene-1,3-cyclooctadiene (2), obtained by direct syntheses for the first time, are established as key intermediates in the multiple thermal rearrangements of the 3,4-bridged vinylcyclobutene 2-methylenebicyclo[4.2.0]oct-7-ene (3). 1 and 2 stabilize competitively by electrocyclization to 3 and to their less strained Z-isomers 4 by direct double bond cleavage even at temperatures slightly above room temperature. The later also applies to the thermal stabilization of E-dimethylenecyclooctene 9. Ring opening in 3 by disrotation and by 1,5-hydrogen shift in 1 are not important.

Combining experimental enthalpies of activation and the results of forcefield calculations the energy profiles of these hydrocarbon reactions show that diradical transition structures are accessible and are of major importance. These findings are also of relevance to other hydrocarbon systems comprising 3,4-bridged cyclobutene structures.

ACKNOWLEDGMENTS

Financial support of this research by the Deutsche Forschungsgemeinschaft and the Fonds der Chemischen Industrie is gratefully acknowledged. The authors thank H.-J. Loch and A. Schaefer for valuable experimental contributions. We also thank N. Lehmann for skillful experimental assistance.

REFERENCES

- (1) Woodward, R. B.; Hoffmann, R. *The Conservation of Orbital Symmetry*; Academic Press: New York, 1970; *Angew. Chem., Int. Ed. Engl.* **1969**, *8*, 781-932.
- (2) Woodward, R. B.; Hoffmann, R. *J. Am. Chem. Soc.* **1965**, *87*, 395-396.
- (3) Houk, K. N.; Li, Y.; Evanseck, J. D. *Angew. Chem., Int. Ed. Engl.* **1992**, *31*, 682.
- (4) Roth, W. R.; Rekowski, V.; Börner, S.; Quast, M. *Liebigs Ann.* **1996**, 409-430.
- (5) Dolbier, W. R., Jr.; Koroniak, H.; Houk, K. N.; Sheu, C. *Acc. Chem. Res.* **1996**, *29*, 471-477.
- (6) Kirmse, W.; Rondan, N. G.; Houk, K. N. *J. Am. Chem. Soc.* **1984**, *106*, 7989-7991.
- (7) Dolbier, W. R., Jr.; Koroniak, H.; Burton, D. J.; Bailey, A. R.; Shaw, G. S.; Hansen, S. W. *J. Am. Chem. Soc.* **1984**, *106*, 1871-1872.
- (8) Curry, M. J.; Stevens, I. D. R. *J. Chem. Soc., Perkin Trans. 2* **1980**, 1391.
- (9) Branton, G. R.; Frey, H. M.; Skinner, R. F. *Trans. Faraday Soc.* **1966**, *62*, 1546.
- (10) Goldstein, M. J.; Leight, R. S.; Lipton, M. S. *J. Am. Chem. Soc.* **1976**, *98*, 5717-5718.
- (11) Branton, G. R.; Frey, H. M.; Montague, D. C.; Stevens, I. D. R. *Trans. Faraday Soc.* **1966**, *16*, 146-152.
- (12) Roth, W. R.; Adamczak, O.; Breuckmann, R.; Lennartz, H.-W.; Boese, R. *Chem. Ber.* **1991**, *124*, 2499-2521.
- (13) Roth, W. R.; Staemmler, V.; Neumann, M.; Schmuck, C. *Liebigs Ann.* **1995**, 1061-1118.

THE USE OF REACTION INTERMEDIATES TO PROBE SUPERCRITICAL FLUID SOLVENT EFFECTS

John E. Chateauneuf

Department of Chemistry Western Michigan University, Kalamazoo, MI 49008

Joan F. Brennecke

Department of Chemical Engineering, University of Notre Dame, Notre Dame, IN 46556

ABSTRACT

Reactions of free radicals and other reaction intermediates in supercritical fluids (SCFs) have proven to be excellent mechanistic probes of the influence of SCF solvation and SCF solvent effects on a variety of categories of chemical reactions in SCFs. This presentation will focus on mechanistic studies of reaction intermediates and, in particular, free radical reactions in SCFs and their relationship to our overall understanding of reaction chemistry under sub-critical and supercritical conditions. Three categories of reactivity that may be influenced in different fashions by SCF solvation and solvent effects will be described. The categories are: 1) diffusion-controlled reactions; 2) activated processes; and 3) reactions that may be influenced by solvent cage effects. The importance of solute-solute, solute-solvent and solute-cosolute interactions to these categories of reactivity will be addressed.

I. INTRODUCTION

Experimental, (1-9) theoretical (10-13) and simulation (7,14-24) investigations have now clearly documented that the local solvent density of SCFs about a dilute solute may be significantly greater than the bulk density of the fluid. This effect of enhanced solvent-solute interaction is often referred to as local density augmentation or SCF solvent clustering. Spectroscopic techniques and solvatochromic probes (1-9) have been particularly useful in the identification and quantification of local density enhancement about dilute solutes. Solvatochromic shifts and fluorescence intensity ratio measurements in a variety of SCFs have shown significant density dependent deviations in behavior from normal liquid solvents, and from behavior predicted from solution based theory. For example, *Kajimoto et al.* (5) have investigated the charge-transfer (CT) emission of (N,N,-dimethylamino)benzotrile in SC CHF₃. Bathochromic shifts of the CT emission are expected to vary linearly with solvent polarity, according to Onsager reaction field theory. (5) While *Kajimoto* found reasonable agreement with liquid data in high density SCF, large deviations from expected values occurred in the medium and low fluid density regimes. These deviations were attributed to solvent aggregation around the dilute solutes. Similar results have been observed for solvatochromic absorption probes where plots of the solvent polarity parameter, ET, versus density were also found to deviate from *McRae-Bayliss* theory at moderate to sub-critical densities. (4)

The physical and chemical properties of free radicals have also played an instrumental role in understanding local density enhancement about dilute solutes in SCFs. *Randolph* and coworkers (9,19-23) have demonstrated that electron paramagnetic resonance (EPR) spectroscopy of stable nitroxide free radicals may be used as an extremely versatile probe to simultaneously measure reaction kinetics and local solvent density augmentation. The nitrogen hyperfine splitting constants of nitroxides (AN) are known to be sensitive probes of solvent polarity and probe the cybotactic region of the solvent, i.e., probes the immediate volume around the nitroxide that has been

affected by the nitroxide radical. Therefore, AN values may be used to reflect degrees of solvation. The experimental data of Carlier and Randolph (9) for di-tert (9, 19-22) have clearly demonstrated that local density augmentation (solvent-solute clustering) does not generally correlate with kT . This indicates that local density enhancements are short-range effects and not related to long-range fluctuations that are responsible for the maximum in kT , and other phenomenon related to criticality, such as very large negative partial molar volumes of dilute solutes in SCFs. Therefore these results indicated that "supercritical fluid clustering" is not a long-range critical effect, but rather a result of short-range structural effect of solvation. This supports previous interpretations by Kajimoto, et al. in 1988, (5) and Knutson, et al. in 1992. (7) To date, several different methods of investigation of solvent-solute interactions have demonstrated that local density augmentation may be as much as two to three times the bulk solvent density and exhibits a maximum at fluid densities of one third to 0.8 of the critical density.

In addition to solvent-solute interactions in SCFs, it is also known that addition of small quantities (1-5 mol %) of cosolvent greatly enhances solubility of organic solutes in SCFs. This methodology is routinely used to enhance SC extraction and chromatography performances. Spectroscopic studies have indicated that this phenomenon is a result of enhanced solute-cosolvent interactions and may result in local composition enhancements in the cybotactic sphere as large as 8 to 10 times the bulk composition. (1-2, 7-8) Cosolvent enhancements are observed to increase from high to low mixture densities approaching the critical pressure in the compressible region of the SC solvent mixture. However, local compositions significantly greater than the bulk have been observed at temperatures and pressures well removed from the critical temperature. This indicates that changes in the local environment are not direct functions of the proximity of the critical point but, as with local density, are also controlled by short-range solvation interactions. Therefore, a second form of SCF "clustering" exists, local composition enhancement.

II. RESULTS

We have used several different types of reaction intermediates, including free radicals, electronically excited states, carbocations and radical anions to probe the influence of the above mentioned solvation effects on various categories of chemical reactions in supercritical fluids. (25-31) For example, we have examined the solvent density dependence of the non-geminate diffusion-controlled reactions of benzyl free radical and the triplet-triplet annihilation reaction of benzophenone (measured by second order kinetics). (25-26) In both cases these reactions were found to be influenced only by changes in the bulk physical property of change in diffusivity, and not by local solvent density enhancements. We have also found that this is true for diffusion-controlled reactions that are measured by pseudo-first-order kinetics. (27) However, for reaction that contain some activation, i.e., not fully diffusion-controlled, the influence of local composition "cosolvent enhancements" can appear as significantly enhancing absolute rate constants when bulk reactant concentrations are used in the kinetic analysis. (28-31)

III. CONCLUSIONS

Several examples of these types of reactions will be presented in order to demonstrate that factors that drive chemical reactions in supercritical fluids are often predictable and can be better understood when the specific reaction mechanisms under consideration are carefully examined.

ACKNOWLEDGMENTS

The authors would like to acknowledge support from the following agencies, foundations and institutions: the National Science Foundation, the Department of Energy, the Army Research Office, and the Western Michigan University Faculty Research and Creative Activities Support Fund. In addition, acknowledgment is made to the Donors of the Petroleum Research Fund, administered by the American Chemical Society, for partial support of this research.

REFERENCES

1. Yonker, C. R.; Frye, S. L.; Kalkwarf, D. R.; Smith, R. D. *J. Phys. Chem.* **1986**, *90*, 3022.
2. Kim, S.; Johnston, K. P. *AIChE J.* **1987**, *33*, 1603.
3. Kim, S.; Johnston, K. P. *Ind. Eng. Chem. Res.* **1987**, *26*, 1206.
4. Yonker, C. R.; Smith, R. D. *J. Phys. Chem.* **1988**, *92*, 2374.
5. Kajimoto, O.; Futakami, M.; Kobayashi, T.; Yamasaki, K. *J. Phys. Chem.* **1988**, *92*, 1347.
6. (a) Brennecke, J. F.; Tomasko, D. L.; Peshkin, J.; Eckert, C. A. *Ind. Eng. Chem. Res.* **1990**, *29*, 1682. (b) Zhang, J.; Lee, L. L.; Brennecke, J. F. *J. Phys. Chem.* **1995**, *99*, 9268.
7. Knutson, B. L.; Tomasko, D. L.; Eckert, C. A.; Debenedetti, P. G.; Chialvo, A. A. In *Supercritical Fluid Technology*, F. V. Bright and M. E. P. McNally, Eds., ACS Symposium Series 488, American Chemical Society: Washington, DC, **1992**; p. 60.
8. Eckert, C. A.; Knutson, B. L. *Fluid Phase Equil.* **1993**, *83*, 93.
9. Carlier, C.; Randolph, T. W. *AIChE J.* **1993**, *39*, 876.
10. Lee, L. L. *Molecular Thermodynamics of Nonideal Fluids*, Butterworths, Boston, **1988**.
11. Cochran, H. D.; Lee, L. L.; Pfund, D. M. *Proc. Int. Symp. on Supercritical Fluids*, M. Perrut, Ed., Nice, France, **1988**, p. 245.
12. Cochran, H. D.; Lee, L. L. in *Supercritical Fluid Science and Technology*, K. P. Johnston and J. M. L. Penninger, Eds., ACS Symposium Series 406, American Chemical Society: Washington, DC **1989**; p. 27.
13. Cochran, H. D.; Lee, L. L.; Pfund, D. M. in *Fluctuation Theory of Mixtures*, E. Matteoli, Ed., *Adv. in Thermo. Ser.*, Taylor and Francis, **1989**.
14. Petsche, I. B.; Debenedetti, P. G. *J. Chem. Phys.* **1989**, *91*, 7075.
15. Wu, R.-S.; Lee, L. L.; Cochran, H. D. *Ind. Eng. Chem. Res.* **1990**, *29*, 977.
16. McGuigan, D. B.; Monson, P. A. *Fluid Phase Equil.* **1990**, *57*, 227.
17. Chialvo, A. A.; Debenedetti, P. G. *Ind. Eng. Chem. Res.* **1992**, *31*, 1391.
18. Chialvo, A. A. *J. Phys. Chem.* **1993**, *97*, 2740.
19. O'Brien, J. A.; Randolph, T. W.; Carlier, C.; Ganapathy, S. *AIChE J.* **1993**, *39*, 1061.
20. Randolph, T. W.; O'Brien, J. A.; Ganapathy, S. *J. Phys. Chem.* **1994**, *98*, 4173.
21. Ganapathy, S.; O'Brien, J. A.; Randolph, T. W. *AIChE J.* **1995**, *41*, 346.
22. Ganapathy, S.; Randolph, T. W.; Carlier, C.; O'Brien, J. A. *Int. J. Thermophysics* **1996**, *17*, 471.
23. Ganapathy, S.; Carlier, C.; Randolph, T. W.; O'Brien, J. A. *Ind. Eng. Chem. Res.* **1996**, *35*, 19.
24. Liu, Q.; Wan, C.; Zewail, A. H. *J. Phys. Chem.* **1996**, *100*, 18666.
25. Roberts, C. B.; Zhang, J.; Brennecke, J. F.; Chateaufneuf, J. E. *J. Phys. Chem.* **1993**, *97*, 5618.
26. Roberts, C. B.; Zhang, J.; Chateaufneuf, J. E.; Brennecke, J. F. *J. Am. Chem. Soc.*, **1993**, *115*, 9576.
27. Zhang, J.; Roek, D. P.; Chateaufneuf, J. E.; Brennecke, J. F. *J. Am. Chem. Soc.* **1997**, *119*, 9980.

28. Chateauneuf, J. E.; Roberts, C. B.; Brennecke, J. F. in *Supercritical Fluid Technology*, F. V. Bright and M. E. P. McNally, Eds., ACS Symposium Series 488, American Chemical Society: Washington, DC, 1992; p. 106.
29. Roberts, C. B.; Chateauneuf, J. E.; Brennecke, J. F. *J. Am. Chem. Soc.* **1992**, *114*, 8455.
30. Roberts, C. B.; Brennecke, J. F.; Chateauneuf, J. E. *AIChE J.* **1995**, *41*, 1306.
31. Roberts, C. B.; Chateauneuf, J. E.; Brennecke, J. F. *J. Am. Chem. Soc.* **1992**, *114*, 8455.

THE SOLUTION PHASE CHEMISTRY OF ATOMIC HYDROGEN. REACTIONS WITH ORGANIC SUBSTRATES.

Dennis D. Tanner,¹ Pramod Kandanarachchi,^{1,2} Nema! C. Das,¹ and James A. Franz.²

Contribution from the Department of Chemistry, University of Alberta,

Edmonton, Alberta, Canada T6G 2G2¹ and

The Pacific Northwest National Laboratory, Richland, WA 99352 USA.²

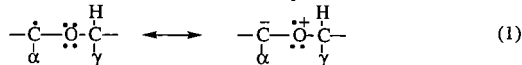
ABSTRACT

The solution-phase reaction of microwave-generated hydrogen atoms with terminal olefins is regioselective. Since addition is to the terminal end of the olefin, the reaction yields a secondary radical which undergoes either reaction with atomic hydrogen, disproportionation, combination, or addition to another olefin. At higher temperatures (23 °C) the olefin undergoes competitive allylic abstraction. The absolute rate constants for the addition of atomic hydrogen to mono- and trisubstituted olefins were determined and the data was used to extract the activation parameters for addition. Using competition kinetics the absolute rate constants for allylic abstraction were also determined. The stabilization of the carbon centered radical by an oxygen substituent was determined by the regioselective addition of a hydrogen atom to the terminal carbon of a vinyl ether or acetate. The same secondary radical can be formed by abstraction of an α -hydrogen from a dialkyl ether. The stereoelectronic enhancement or lack thereof of the rate constants for the reaction responsible for the formation of the radical intermediates will be discussed. The resonance effects due to oxygen were also investigated for addition to the five and six-membered rings of dihydrofuran and dihydropyran and for abstraction of the α -hydrogen from the saturated heterocycles.

I. INTRODUCTION

Recently, we reported a method for obtaining the absolute rate constants for the nonhomogeneous (gas-liquid) reaction of the addition of atomic hydrogen to an olefin.^{3b} The reaction of 1-octene was reported to be very close to diffusion controlled ($k_a^{25^\circ\text{C}} = 4.6 \times 10^9 \text{ M}^{-1} \text{ s}^{-1}$). The same kinetic method can be used to evaluate the stabilizing effect of a carbon centered radical having a geminal oxygen substituent. The addition of hydrogen to a terminal olefin was found to be regioselective, (i.e., only addition to give the most stable secondary, or tertiary radical)^{3a} The same regioselectivity was found for addition to the vinyl ether, a vinyl ester also underwent regioselective addition to give a radical center on carbon containing a geminal oxygen substituent.

The high reactivity and selectivity for a hydrogen atom on carbon α - to an oxygen substituent has been attributed to the resonance stabilization of the radical, eq. 1.⁴



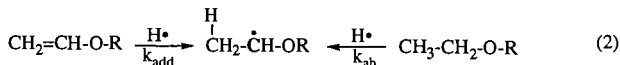
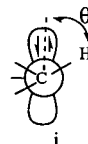
The importance of this resonance form has been substantiated by the observation that the EPR spectra of the radical shows a γ -hydrogen hyperfine coupling constant larger than that of the α -hydrogen (i.e., hyperconjugation).^{5,6}

The effect of this type of resonance stabilization predicts that a large solvent effect will stabilize or destabilize the contribution of a charge separated species. The reactions were carried out in both polar (acetone) and nonpolar (hexane) solvents.

Another approach to the question of reactivity and stability of the carbon radical α to an oxygen atom has been popularly termed stereoelectronic control.⁷

II. RESULTS & DISCUSSION

In order to probe the importance of this type of resonance stabilization the reactivity of an olefin which formed a radical α - to oxygen was looked at as a function of the dihedral angle formed between the reactive hydrogen and the doubly occupied orbitals on the oxygen lone pair, i . The secondary radical formed from addition to a vinyl ether can also be formed by abstraction of hydrogen from the α -position of the saturated ether, see eq. 2.



Using the same kinetic method developed for the reactions of atomic hydrogen with one octene,^{3a-c} after correcting the addition results for abstraction, disproportionation, combination, and addition of the α -radical to another molecule of vinyl ether the algorithm for the absolute rate constant for addition, eq. 3 was used to determine the value of k_a . The results of the addition and abstraction reactions for several ethers are listed in Table 1. An example of the entries used in the algorithm (eq. 3) for one of the determinations (-72 °C, acetone) is given in Table 2. A similar table was constructed for the other solvent.

$$k_a = f^{-1/2} \left[\frac{(\Delta P/\Delta t)_{\text{total}} (k_{\text{diff}}(\Delta P/\Delta t)_{\text{C,D}})^{1/2}}{[\text{olefin}][\Delta P/\Delta t]_{\text{RH}_2}} \right] \quad (3)$$

A plot of $\log(f^{1/2} k_a)$ vs the olefin concentration was used to calculate the value of k_a in both acetone (O) and hexane (●). When [olefin] is equal zero, $f = 1$, and the absolute rate constant for addition was determined, see Fig. 1.

[Fig. 1]

When the reactions were carried out at several temperatures an Arrhenius plot was used to calculate the activation parameters and the absolute rate constants of k_a for the reactions of ether in both solvents, see Fig. 2.

[Fig. 2]

The abstraction rate constant for the abstraction of the α -hydrogen from dibutyl ether was determined from the competition kinetics between the abstraction reaction and addition of $H\cdot$ to 1-octene. Since the value of k_a for 1-octene is known,^{3b} the value for k_{ab} from the ether could be calculated. The competition kinetics was carried out to diminished olefin concentration. Using the experimentally determined activation parameters for the addition and abstraction reactions listed in Table 1 and using the calculated and experimental ΔH_f of the reactants intermediates and products the free energy profile, Fig. 3 was constructed.

Stereoelectronic control for radical reactions has been proposed to have its maximum effect when the dihedral angle, θ , is 30° .^{7b} Model compounds claimed to have this geometry are cyclic ethers, tetrahydrofuran and tetrahydropyran. When $H\cdot$ was allowed to react with tetrahydrofuran or tetrahydropyran, at several temperatures (see Table 1) the abstraction reactions which form the radical at the 2-positions showed rate constants which were slower than the open chain ether. The rate constants determining for the formation of the radical by regioselective addition were the approximately same for the 6-membered ring, and only 5 x faster for the formation of the radical at the 2-position of furan, see Table 1.

The effect of multiple oxygen substitution α - to a radical center was investigated using as models, diethyl acetal and triethyl orthoformate. The relative rate of abstraction by $D\cdot$ of the tertiary hydrogen compared to the secondary hydrogen of the acetal, $CH_3CH(OCH_2CH_3)_2$ was estimated from the 2H -NMR of the reaction mixtures at several temperatures. A plot of the relative rates of deuterium incorporation vs. $1/T$ gave a value of $(k_{3^\circ}/k_{2^\circ}/H = 0.91 \pm 0.12)^{25^\circ C}$, while abstraction of the tertiary radical from the orthoformate, $(C_2H_5-O)_3C-H$ could not be detected although there was considerable $D\cdot$ incorporation from secondary H abstraction.

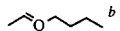
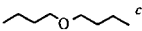
III. CONCLUSIONS

The absolute rate constants for the carbon centered radicals geminally substituted with oxygen can be compared to the value obtained from both addition to 1-octene or allylic abstraction from the terminal olefin.³ Both the addition and abstraction rate constants are within experimental error the same for the olefin and the vinyl ether. Only in the case of 2,3-dihydrofuran is the rate constant for addition more than one power of 10 faster, while abstraction from furan is slower than the open chain ether.

REFERENCES

1. (a) Department of Chemistry, University of Alberta. (b) Postdoctoral Fellow, University of Alberta, 1996.
2. Batelle Pacific Northwest Laboratories.
3. (a) Tanner, D.D.; Zhang, L. *J. Am. Chem. Soc.* **1994**, *116*, 6683. (b) Tanner, D.D.; Zhang, L.; Kandanarachchi, P. *J. Phys. Chem.* **1996**, *100*, 11319. (c) Tanner, D.D.; Zhang, L.; Kandanarachchi, P. *J. Phys. Chem. (A)*, **1997**, *101*, 9327.
4. Elad, D. *The Chemistry of the Ether Linkage*, Interscience Publisher, **1967**, Chapter 8, p. 355.
5. (a) Wertz, J.E.; Bolton, J.R. *Electron Spin Resonance*, Chapman and Hall, New York, **1986**, 112-114. (b) Dobbs, A.J.; Gilbert, B.C.; Norman, R.O.C. *J. Chem. Soc. (A)*, **1971**, 124.
6. Fisher, H. Z. *Naturforsch* **1965**, *20A*:428.
7. (a) Haydag, K.; McKelvey, R.D. *J. Org. Chem.* **1976**, *41*, 2222. (b) Malatesta, V.; Ingold, K.U. *J. Am. Chem. Soc.* **1981**, *103*, 609. (c) Beckwith, A.L.J.; Easton, C.J. *J. Am. Chem. Soc.* **1981**, *103*, 615. (d) Griller, D.; Howard, J.A.; Marriot, P.R.; Scaiano, J.C. *J. Am. Chem. Soc.* **1981**, *103*, 619.

Table 1. The Absolute Rate Constants for Addition and Abstraction Reactions by Atomic Hydrogen

Substrate	Solvent	($k_{rel}^{25^\circ C}$) ^a	$k^{25^\circ C} \times 10^9$ ($M^{-1}s^{-1}$)	$\Delta\Delta E_a$ (Kcal/mol)	ΔE_a (Kcal/mol)	log A
	Acetone	0.38±0.06	1.59	-0.49±0.05	4.8±2.9	13.2±4.2
	Hexane	1.14±0.40	4.79	-0.28±0.05	5.0±2.9	13.8±3.6
	Acetone	0.03±0.02	0.13	0.63±0.5	5.9±3.4	12.9±4.1
	Hexane	0.04±0.08	0.16	-0.1±1.0	5.2±3.9	12.5±4.9
	Acetone	0.20±0.10	0.84	-0.45±0.8	4.8±3.7	12.9±4.4
	Acetone	0.06±0.05	0.25	1.93±1.2	7.2±4.1	14.0±4.9
	Acetone	0.55±0.15	2.31	0.66±0.4	5.96±3.3	14.0±3.9
	Acetone	0.005±0.003	0.02	0.06±0.5	5.4±3.4	11.7±4.1

^a1-Octene was used as reference ($k_{rel} = k/k_{1-octene}$). ^bAddition reactions. ^cAbstraction reactions by atomic deuterium.

Table 2. Absolute Rate Constants ($f^{1/2}k_a$) for the Addition of Deuterium Atoms to Vinyl Butyl Ether at -72 °C in Acetone

[olefin]	$10^4(\Delta p/\Delta t)_{tot}^{bulk}$ ^a	$10^4(\Delta p/\Delta t)_{c,d}$ ^b	$10^7[R^*]$	$10^4(\Delta p/\Delta t)_{RD_2}$ ^c	$10^8[H^*]^c$	$10^{-3}f^{1/2}k_a^d$
mol L ⁻¹	mol L ⁻¹ s ⁻¹	mol L ⁻¹ s ⁻¹	mol L ⁻¹	mol L ⁻¹ s ⁻¹	mol L ⁻¹	M ⁻¹ s ⁻¹
1.12	6.19	5.37	7.84	0.82	11.9	4.09
0.45	7.36	5.60	8.43	1.13	15.2	11.20
0.09	1.90	1.33	3.90	0.34	9.92	30.57
0.045	1.01	0.81	3.05	0.19	6.42	40.83
0.034	0.58	0.19	1.47	0.16	2.69	63.47
0.022	0.52	-	-	-	(2.35)	126.7

^aExperimentally measured as the change in the concentration of vinyl butyl ether with time. ^bThe rate of the formation of combination and disproportionation products (see ref. 3b). ^cThe rate of the formation of radical-deuterium atom combination products (see ref. 3b). ^dCalculated by using eq. 3.

Table 3. Experimental and G2MP2 Enthalpies, 298K

Species	$\Delta H_{f,298}$ Kcal/mol, calcd, G2MP2	$\Delta H_{f,298}$ Kcal/mol, exptl	G2MP2 Enthalpy, 298K, hartrees
H	-	52.1 ^a	-0.497639
C(3P)	-	171.3 ^a	-37.781527
O(3P)	-	59.6 ^a	-74.976317
	-	-53.3 ^a	-
	-	-29.9 ^a	-
	-43.85	-44.0 ^a	-232.004551
	-18.28	-21.47 (Benson ^b)	-230.802457
CH ₃ OCH=CH ₂	-24.67	-24 ±2 ^a	-192.758133
CH ₃ OCH ₂ CH ₃	-52.3	-51.7 ^a	-193.963445
CH ₃ OC•HCH ₃	-9.05	-11.8 (bde 93)	-193.313900
	-0.9	-4.0, -2.9 (92.1 ^c or 93.2 ^d bde)	-231.355426
	-7.65	-12.4 (est., assumes 93 bde) ^e	-270.582035 -270.150798 ^f

^aLias, S.G.; Bartmess, J.E.; Liebman, J.F.; Holmes, J.L.; Levin, R.D.; Mallard, W.G. "Gas Phase Ion and Neutral Thermochemistry" *J. Phys. Chem. Ref. Data* **1988**, *17*, Supple. 1. ^bBenson, S.W. "Thermochemical Kinetics. Methods for the Estimation of Thermochemical Data and Rate Parameters", 2nd Ed. Wiley-Interscience, New York, N.Y. ^cLaarhoven, L.J.J.; Mulder, P. *J. Phys. Chem. B* **1977**, *101*, 73-77. ^dMuedas, C.A.; Ferguson, R.R.; Brown, S.H.; Crabtree, R.H. *J. Am. Chem. Soc.* **1991**, *113*, 2233. ^eThe heat of formation of tetrahydropyran is -53.3 Kcal/mol (ref. a above). Dihydropyran, -29.9. JMP2=FU/6-31G** enthalpy, 298K.

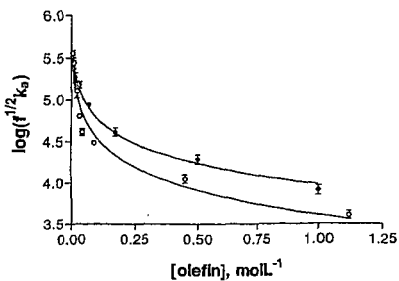


Fig. 1. The variation of the apparent rate constant $\log(f^{1/2}k_a)$ of vinyl butyl ether with the concentration of the olefin in (O) acetone and (●) hexane.

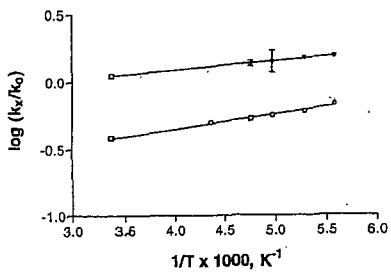


Fig. 2. An Arrhenius plot for the relative rates of addition to vinyl butyl ether in; (O) acetone, and (●) hexane.

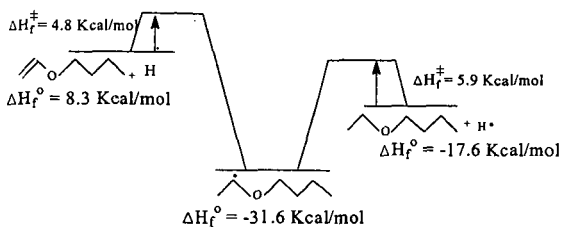


Fig 3. The free energy profile for the formation of methyl butoxy methyl free radical

REACTIONS OF ATOMIC HYDROGEN IN WATER: SOLVENT AND ISOTOPE EFFECTS

David Bartels
Chemistry Division,
Argonne National Laboratory
Argonne, IL 60439

I. INTRODUCTION

It has been known for many years that hydrogen atoms can be easily created and studied in water using radiolytic techniques [1]. The use of CW EPR detection coupled with electron radiolysis proved extremely useful in estimating many reaction rates, and revealed the interesting phenomenon of chemically induced dynamic electron polarization (CIDEP). [2] In recent years, we have made use of pulsed EPR detection to make precision reaction rate measurements which avoid the complications of CIDEP. [3] Activation energies and H/D isotope effects measured in these studies [4-14] will be described below.

An interesting aspect of the hydrogen atom reactions is the effect of hydrophobic solvation. EPR evidence -- an almost gas-phase hyperfine coupling and extremely narrow linewidth -- is quite convincing to show that the H atom is just a minimally perturbed gas phase atom inside a small "bubble". In several systems we have found that the hydrophobic free energy of solvation dominates the solvent effect on reaction rates.

II. PROCEDURE

The basic apparatus used in these measurements is illustrated in figure 1. Pulses of 3 MeV electrons are produced with a van de Graaff accelerator and strike the aqueous sample in an EPR cavity. The de-oxygenated solutions are recirculated through the cell at a high rate to allow signal averaging at 120Hz repetition frequency. In general acidic solutions (pH=2) are used to convert solvated electrons to hydrogen atoms on a nanosecond timescale and increase the signal amplitude. A small amount of methanol (ca. 10^{-2} M) is typically added as well to scavenge hydroxyl radicals. However, a major advantage of this technique is the ability to work in neutral and alkaline solution when necessary.

Some typical data from the experiment is plotted in figure 2. Immediately following the 12-50ns electron pulse, a 25ns x-band microwave pulse is applied to the cavity. After approximately 120ns, the sensitive detection electronics are switched in, and a free induction decay from the hydrogen atom is detected as in figure 2. In general the microwave frequency is set to about 10MHz above or below the Larmor frequency for the H atom low field transition. The effective damping time constant for the free induction decay is given by

$$1/T_2(\text{eff}) = 1/T_2^0 + k_s[S] + \sum_i k_{\text{ex}}^i [R_i] \quad (1)$$

where $1/T_2$ is the natural dephasing rate and $\sum k_{\text{ex}} [R_i]$ is the effect of second order reaction and spin exchange. This latter term is not negligible, but roughly constant over the five microsecond timescale of the experiment. A plot of the dephasing rate vs. scavenger concentration [S] gives the scavenging rate constant k_s as intercept.

III. RESULTS

Table 1 summarizes a large (but not exhaustive) number of hydrogen atom rate constant measurements in terms of Arrhenius activation energies and pre-exponential factors. Some of the greatest surprises were reactions of H with the nitrate [10] and hydrazinium [9] ions and with the per-iodic acid molecule [6], which have quite large activation energies, but enormous pre-exponential factors. These ion reactions involve large solvent (hydrogen bond) reorganization on the way to the transition state, and the large entropy increase dominates the activation free energy. In the case of per-iodic acid, the hydrated H_5IO_6 species must lose two water molecules and rearrange to IO_3^- and hydroxyl radical product. The rearrangements involved in the hydrazinium ion and nitrate ion reactions are not so obvious, and deserve further study.

The hydrophobic nature of the H atom solvation was demonstrated convincingly in the study of its addition to benzene [14]. The activation energy in solution is similar to that in the gas phase, but the rate constant is some forty times faster. Using the assumptions of transition state theory, the solvent effect (ratio of rates in gas phase to those in aqueous phase) can be reduced to an expression involving only the solvation free energies of reactants and transition state. Then, assuming that the transition state solvation free energy is very nearly the same as that of benzene itself or cyclohexadiene (both known from solubility measurements), the rate enhancement in water reduces simply to

$$k_{aq}/k_{gas} = \exp\{(\Delta G_{hyd}(H)/RT)\} = L^{-1} \quad (2)$$

and L is just the Ostwald solubility parameter for the hydrogen atom. The size and polarizability of the H atom are very similar to the H_2 molecule, and using the solubility of H_2 as a model in this equation produces essentially quantitative agreement with the benzene reaction rate data. The reaction is accelerated by the collapse of the hydrophobic solvation sphere of the H atom, resulting in a "hydrophobic attraction" of the H and benzene.

Other comparisons with gas phase reaction rate data are typically limited by the quality of the gas phase data available. In the case of methanol, the activation energy is found to be ca. 6kJ/mole higher in the aqueous phase, and one should expect an order of magnitude slower reaction rate. Instead, the reaction rate is roughly the same as the gas phase by virtue of a larger pre-exponential factor. We have suggested that this larger pre-exponential might represent a "hydrophobic acceleration" effect similar to that found in the benzene case [4,11].

No doubt the strangest reactions investigated in this work are the reactions of H and D with iodide and bromide ions (giving HI- and HBr- product) [15]. At 3×10^8 and $2 \times 10^6 \text{ M}^{-1} \text{ s}^{-1}$ for iodide and bromide respectively, the reactions have substantial free energy barriers, but the activation energies are zero or slightly negative! Measurements in H_2O/D_2O mixtures reveal a small isotope effect favoring D over H reaction. Other measurements have shown that the light Muonium atom (1/9 the mass of hydrogen) reacts about five times slower than H [7]. It is important to recall that our technique measures the rate of H atom dephasing, and so is not sensitive to any back reactions or equilibria which might occur: only the forward rate is measured. We have considered every alternative we can imagine, and conclude that the only barrier possible for these reactions consists of the water of the solvation shells. We postulate that the strongly hydrated small ions repel approach of the hydrophobic H atom. Molecular dynamics simulation of these systems has been initiated to explore the strange activation energy and isotope effects.

VII. CONCLUSIONS

The pulse radiolysis and EPR techniques described here have proven particularly useful for the study of hydrogen atom reactions in water. The hydrophobic hydrogen atom proves to be a unique probe for solvent and isotope effects in aqueous reactions.

ACKNOWLEDGMENTS

The author would like to express his thanks and appreciation for his coworkers in this research, who did most of the work: P. Han, E. Roduner, S. Mezyk, and A. Lossack.

Work at Argonne was supported by the U. S. Department of Energy under Contract No. W-31-109-ENG-38.

REFERENCES

- [1] G.V. Buxton, C.L. Greenstock, W.P. Helman, and A.B. Ross, *J. Phys. Chem. Ref. Dat.*, **17**, 513, (1988).
- [2] R.W. Fessenden and N.C. Verma, *Faraday Discuss. Chem. Soc.*, **63**, 104, (1977).
- [3] P. Han and D.M. Bartels, *Chem. Phys. Lett.*, **159**, 538, (1989).
- [4] Stephen P. Mezyk and David M. Bartels, *J. Phys. Chem.* **98**, 10578 (1994)
- [5] Stephen P. Mezyk and David M. Bartels, *Can. J. Chem.* **72**, 2516 (1994).
- [6] Stephen P. Mezyk, Roy MacFarlane and David M. Bartels, *J. Phys. Chem.* **98**, 12594 (1994)
- [7] David M. Bartels and Emil Roduner, *Chem. Phys.* **203**, 339-349 (1996)
- [8] Stephen P. Mezyk and David M. Bartels, *J. Chem. Soc. Faraday Trans.* **91**, 3127 (1995)

- [9] Stephen P. Mezyk, Miyoko Tateishi, Roy MacFarlane, and David M. Bartels, *J. Chem. Soc. Faraday Trans.* **92**, 2541 (1996).
 [10] S. P. Mezyk and D. M. Bartels, *J. Phys. Chem.*, **A101**, 6233 (1997).
 [11] S. P. Mezyk and D. M. Bartels, *J. Phys. Chem.*, **A101**, 1329, (1997).
 [12] S.P. Mezyk, A. Lossack, and D.M. Bartels, *Can. J. Chem.*, **75**, 1114, (1997).
 [13] A.M. Lossack, E. Roduner, and D.M. Bartels, *J. Phys. Chem.*, **A102**, 7462, (1998).
 [14] E.Roduner and D.M. Bartels, *Ber. Bunsenges. Phys. Chem.*, **96**, 1037, (1992).
 [15] S.P. Mezyk and D.M. Bartels, *J. Phys. Chem.*, **97**, 4101, (1993).

Table 1: Measured Arrhenius Parameters for H atom Reactions in Water

H reaction partner	$\log_{10}(A/M^{-1}s^{-1})$	E_a / (kJ/mole)
benzene:	12.34	19.1
alcohols:		
methanol	11.64	29.4
ethanol	11.53	24.1
ethanol-d ₅	12.03	31.9
2-propanol	11.86	22.0
2-propanol-d ₅	12.00	27.4
aldehydes:		
propionaldehyde	11.77	22.2
butyraldehyde	12.20	23.9
ketones:		
acetone	11.68	30.7
methyl ethyl ketone	11.25	22.3
diethyl ketone	11.30	21.0
methyl isopropyl ketone	10.96	17.2
methyl isobutyl ketone	11.24	21.2
cyclopentanone	11.15	19.7
iodo compounds:		
iodomethane	11.90	10.39
iodoethane	12.20	11.8
1-iodopropane	12.24	12.0
IO ₃ ⁻	11.96	27.46
HIO ₃	12.83	22.35
IO ₄ ⁻	13.30	36.55
H ₅ IO ₆	17.77	53.0
I ⁻	8.48	-1.0
peroxide and hydrazine:		
H ₂ O ₂	11.26	21.1
HO ₂ ⁻	13.65	25.6
D ₂ O ₂ (D atom reaction)	10.37	17.3
N ₂ H ₄	10.69	16.28
N ₂ H ₅ ⁺	16.95	61.38
nitrite and nitrate:		
NO ₂ ⁻	11.94	15.6
HNO ₂	12.36	21.5
NO ₃ ⁻	15.28	48.7

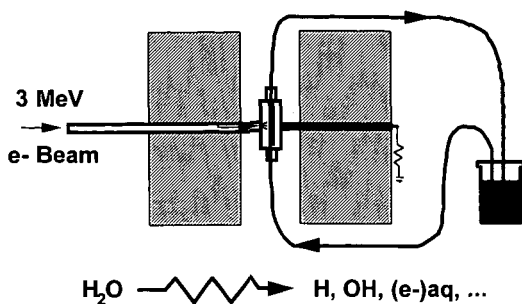


Figure 1. Typical experimental arrangement of the FID attenuation experiment. Temperature controlled aqueous sample is recirculated through a glass cell in the EPR cavity. H atoms are generated by in situ pulse radiolysis with 3 MeV electrons. Scavenger concentrations are changed by successive injections into the flow stream.

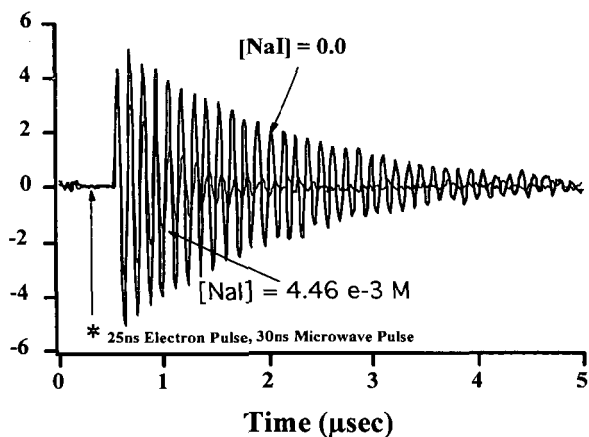


Figure 2. Free induction decay from the H atom low field EPR line. Addition of scavenger (in this example I-) shortens the damping time constant, and provides a pseudo-first order measurement of reaction rate.

THE CONSEQUENCES OF SURFACE CONFINEMENT ON FREE RADICAL CHEMISTRY

A. C. Buchanan, III and Phillip F. Britt

Chemical & Analytical Sciences Division
Oak Ridge National Laboratory
1 Bethel Valley Road
P.O. Box 2008, MS-6197
Oak Ridge, Tennessee 37831-6197

Keywords: Free radicals, pyrolysis, restricted diffusion

ABSTRACT

Mass transport limitations impact the thermochemical processing of fossil and renewable energy resources, which involves the breakdown of cross-linked, macromolecular networks. To investigate the molecular level details of the consequences of molecular confinement on high temperature (275-500°C) free-radical reaction pathways, we have been examining the pyrolysis of model compounds attached to the surface of non-porous silica nanoparticles through a thermally robust Si-O-C_{ary} tether. Pyrolysis of silica-immobilized diphenylalkanes and related ethers have been studied in detail and compared with the corresponding behavior in fluid phases. The diffusional constraints can lead to reduced rates of radical termination on the surface, and enhancement of neophyl-like rearrangements, cyclization-dehydrogenation pathways, and *ipso*-aromatic substitutions. Furthermore, studies of two-component surfaces have revealed the importance of a radical relay mechanism involving rapid serial hydrogen transfer steps resulting from the molecular pre-organization on the low fractal dimension silica surface. Key findings are reviewed in this paper, and the implications of these results for fuel processing are described.

INTRODUCTION

Pyrolysis forms the basis for many current and envisioned technologically important processes for conversion of fossil and renewable resources into volatile fuels or chemicals. Since many of these resources are highly cross-linked, macromolecular organic materials, concerns over mass transport limitations are often well-founded. The effects of mass transport limitations have been documented in the pyrolysis of coal,⁽¹⁾ kerogen,⁽²⁾ cellulose,⁽³⁾ lignin,⁽⁴⁾ biomass,⁽⁵⁾ and polymers.⁽⁶⁾ Predictive models have been developed for pyrolysis of coal, lignin, and cellulose that explicitly include descriptions of mass transport mechanisms.^(1b-4) These mass transport limitations can impact pyrolysis rates, and govern the tar yields and molecular weight distributions.

Our knowledge of the effects of mass transport is primarily on a macro scale, e.g. lumped kinetic parameters and product classes. Pyrolysis studies on complex materials such as coal do not yield direct information about the *individual* chemical processes that control reaction rates, or about the actual molecules that are responsible for formation of particular products. An enhanced understanding of the effects of mass transport limitations on pyrolysis reactions *at a molecular level* has been a goal of our research. Hence, we have been exploring the pyrolysis chemistry of organic molecules that serve as models for constituents in biopolymers and geopolymers. Restricted mass transport conditions have been simulated by confining these molecules to the surface of nonporous silica nanoparticles through a covalent linkage. Many of the manifestations of mass transport limitations on high temperature organic reactions involving free-radical intermediates are now much better understood as a consequence of our extensive studies on these silica-immobilized model compounds. A brief overview of key findings from our studies of hydrocarbon pyrolysis will be presented, and a more detailed review of this work is in press.⁽⁷⁾

PREPARATION OF SILICA-IMMOBILIZED MODEL COMPOUNDS

In selection of a surface-immobilization technique for our investigations of the pyrolysis mechanisms, we were guided by several criteria. Both the support and linkage must be stable at the temperature regime of interest, up to ca. 450-500 °C. The support should have a moderately high surface area with enough accessible active sites for attaching significant quantities of the organic molecules of interest. Any unreacted sites should not be catalytically active, e.g. Brønsted or Lewis acid sites. The position of surface attachment within the organic moiety should be far enough removed from the normal position of thermal reactivity so as not to induce significant substituent effects. For flexibility, the organic functional group used in the attachment should be readily synthesized. Finally, a very important criterion arises from our desire to be able to identify and quantitate all pyrolysis products, both in the gas phase and those that remain attached to the surface

of the support. Namely, although the covalent link should be thermally stable, there must exist a facile chemical method for cleaving products from the surface for analysis. To meet all these requirements, we chose the reaction of substituted phenols with the silanols of a high purity, nonporous fumed silica (Cabosil M-5, 200 m² g⁻¹, ca. 4.5 SiOH nm⁻² or 1.5 mmol SiOH g⁻¹) as shown in Figure 1.⁽⁸⁻¹⁰⁾

Surface coverages can be varied (typical range of 0.06 - 0.6 mmol g⁻¹) by adjusting the initial phenol to surface hydroxyl ratio, and saturated surface coverages are obtained by using excess phenol. Unreacted phenol is removed either by sublimation under vacuum at ca. 270°C or by Soxhlet extraction with a solvent like benzene. The silicon-oxygen-aromatic carbon linkage, Si-O-C_{aryl}, has been found to be thermally robust up to at least 450°C.⁽⁸⁻¹¹⁾ However, the linkage is hydrolytically unstable under aqueous base conditions. This allows us to detach pyrolysis products from the silica surface as the corresponding phenols, as well as any unreacted starting material, for identification and quantitation. This important advantage for our pyrolysis studies also represents a potential limitation for this linkage if reaction studies in aqueous or nucleophilic solvents are of interest. Another limitation of this method is ambiguity in the point of attachment to the surface if a second active functional group (alcohol, thiol, etc.) is present in the molecule. Surfaces can also be prepared with two point attachment of the model compound (Figure 1),⁽¹²⁾ although high efficiencies for di-attachment (80-90%) occur only at rather low surface coverages (ca. 0.1 mmol g⁻¹). We have also found that a variety of two-component surfaces are easily prepared by co-attachment of the molecules to the silica in a single step.^(13,14)

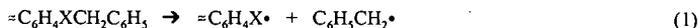
PYROLYSIS STUDIES

The surface-attached diphenylalkanes, =C₆H₄(CH₂)_nC₆H₅ [n=0-4], have been prepared and used as models for aliphatic bridges between aromatic molecules in fossil fuels.^(8,12) The "=" notation is employed as an abbreviation to represent the Si-O-C_{aryl} linkage to the silica surface. In addition, analogs such as =C₆H₄XCH₂C₆H₅ [X = O,⁽¹⁵⁾ S⁽¹⁶⁾], =C₆H₄OCH₂CH₂C₆H₅^(17,18) and =C₆H₄CH₂CH₂OC₆H₅^(17,18) have been recently examined to explore the important effects of heteroatoms. The pyrolysis behavior of surface-immobilized compounds have been thoroughly examined as a function of reaction extent, temperature, surface coverage, and degree of cross linking,^(8,10,12) as well as the presence of a hydrogen atmosphere,^(14,19) a second co-attached molecule of variable structure,^(10,13,14) and a solid-state acid⁽²⁰⁾ or hydrogenation catalyst.⁽¹⁾ The reaction kinetics, mechanisms, and product selectivities have been compared with that of the corresponding molecules in fluid phases. Due to space limitations, only a few of the major findings will be surveyed below with an emphasis on free radical chemistry.

Vacuum pyrolysis reactions were typically performed in sealed T-shaped Pyrex tubes in a temperature controlled (± 1 °C) tube furnace. Volatile products were collected in the side arm trap cooled with liquid nitrogen, while surface-attached products were recovered as the corresponding phenols following basic digestion of the silica. The products were identified and quantitated principally by GC and GC-MS with the use of authentic reference materials and internal calibration standards.

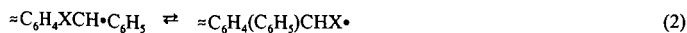
=C₆H₄(CH₂)_nC₆H₅ [n=0,1]. Biphenyl contains only strong bonds that are stable at 400°C. Likewise, we found that the surface-immobilized form, =Ph-Ph, was stable at 400°C for many hours.⁽⁶⁾ This indicates that the silica surface and residual silanol groups did not induce any new reaction pathways. Similarly, surface-immobilized diphenylmethane was also found to be stable at 375-400°C.⁽⁸⁾ This structure would be quite susceptible to acid-catalyzed cracking reactions,⁽²⁰⁾ and their absence is further testament to the inert nature of the fumed silica surface. At higher temperatures (425-450°C), we have recently observed a slow reaction involving a competing cyclization pathway and a previously undetected radical *ipso*-substitution pathway involving =C₆H₄CH•C₆H₅, as shown in Figure 2.⁽²¹⁾ The radical substitution path appears to be promoted by the diffusional constraints, and the selectivity for this path is currently being studied in more detail.

=C₆H₄XCH₂C₆H₅ [X = CH₂, O, S]. These model compounds represent structures containing weak bridges between aromatic rings that cleave at T < 400°C as shown in Eq. 1.



The rate constants and activation parameters measured for X = CH₂⁽⁸⁾ and O⁽¹⁵⁾ at high surface coverages are similar to those reported for fluid-phase analogs, indicating that the unimolecular homolysis steps are not affected by the surface attachment. However, we find that the product distributions are substantially impacted. This is illustrated in Figure 3 for the case of silica-attached 1,2-diphenylethane or bibenzyl. The formation of comparable amounts of surface-attached and gas-phase toluene products demonstrates a general finding that there is enough conformational freedom on the surface to permit oriented hydrogen transfers between surface-bound molecules and surface-bound free radicals. However, restricted diffusion retards the rates of radical termination on the surface through bimolecular coupling of intermediate radicals such as =C₆H₄XCH•C₆H₅. As shown in Figure 3 for the case of bibenzyl, this eliminates the formation of a major product (tetraphenylbutanes) found in fluid phases. As a consequence, new pathways emerge in significant

quantities such as cyclization-dehydrogenation (establishing the phenanthrene skeleton for $X = \text{CH}_2$, but not detected for $X = \text{O}, \text{S}$) and skeletal rearrangements. In particular, neophyl-like rearrangements involving 1,2-phenyl shifts have been found to be important for all cases (Eq. 2).^(8,15,16) The efficiency of the rearrangement path has been found to depend strongly on the



surrounding environment on the surface. Neighboring hydrogen sources are needed to trap the typically less stable rearranged radical. Hence, a low surface coverage of bibenzyl or the presence of neighboring aromatic spacer molecules (such as naphthalene) inhibits this rearrangement path.⁽²²⁾ Conversely, this path is prominent at high bibenzyl surface coverages or in the presence of neighboring molecules that can donate hydrogen (such as diphenylmethane). The resulting hydrogen transfer, radical relay path is important in overcoming some of the effects of diffusional constraints, and has been studied in detail in the pyrolysis of 1,3-diphenylpropane as discussed below. It is important to note that, for bibenzyl, this process is a retrograde pathway that generates a more refractive diphenylmethane linkage. For the benzyl phenyl ether analog, new reactive products (benzophenone and benzhydryl) are generated that were not previously reported in fluid phases. In the benzyl phenyl sulfide case, the rearranged product, $\approx \text{C}_6\text{H}_4(\text{C}_6\text{H}_5)\text{CHSH}$, is particularly unstable and reacts further to form surface-attached diphenylmethane.

Because of the significance of this rearrangement path under restricted mass transport conditions, the pyrolysis of immobilized bibenzyl has been investigated in several different environments. We recently found that a co-attached hydrogen donor, tetralin, is ineffective at retarding the rearrangement path.⁽²²⁾ The impact of hydrogen pressure on this pathway was also studied through pyrolysis of $\approx \text{BB}$ at 400°C in a high pressure reactor in the presence of a nitrogen or deuterium atmosphere (14 MPa).⁽¹⁹⁾ Pyrolysis under D_2 produced the expected higher yields of hydrocracked products such as $\approx \text{C}_6\text{H}_4\text{D}$ and $\text{C}_6\text{H}_4\text{CH}_2\text{CH}_2\text{D}$, as well as lower yields of alkene products, compared with pyrolysis under N_2 or vacuum. However, D_2 pressure was unable to prevent the retrogressive rearrangement pathway (or the cyclization pathway) from occurring under the diffusional constraints. A similar result was also obtained for a different type of silica-immobilized bibenzyl under D_2 , which was prepared by attachment of a carboxylic acid derivative to silica via a $\text{SiO} - \text{Ca}^{2+} - \text{O}_2\text{CPhCH}_2\text{CH}_2\text{Ph}$ ionic linkage.⁽²³⁾

$\approx \text{C}_6\text{H}_4\text{CH}_2\text{CH}_2\text{XC}_6\text{H}_5$ ($X = \text{CH}_2, \text{O}$). 1,3-Diphenylpropane (DPP) has been employed as a model for longer linkages between aromatic clusters in coal that decay at significant rates at 350-400°C by a free radical chain mechanism as shown in Figure 4. Our studies of silica-immobilized DPP showed that this type of linkage also decayed efficiently in this temperature regime under conditions of restricted mass transport, but pyrolysis rates were extremely sensitive to surface coverage and the structure of neighboring molecules on the surface.^(9,12,14) As shown in Table 1, the rate of decomposition of $\approx \text{DPP}$ decreased dramatically with decreases in surface coverage as the rate of the bimolecular hydrogen transfer steps decrease. In particular, hydrogen transfer between two surface bound species (Figure 4, Insert) would be particularly affected by increasing spatial separation on the surface. These effects were amplified when DPP was further restrained by having both ends of the molecule tethered to the surface.⁽¹²⁾ At a surface coverage of 0.1 mmol g^{-1} , the pyrolysis rate decreased by an additional factor of 4-7 for the two $\approx \text{DPP}$ isomers studied, for which about 80% of the molecules were di-attached with the remainder being mono-attached.

The rate of pyrolysis of $\approx \text{DPP}$ at 375°C spanned a remarkably wide range (830-fold), as shown in Table 1, and was very sensitive to the structure of neighboring spacer molecules on the surface. When compared at similar low surface coverages of $\approx \text{DPP}$ (ca. 0.10-0.14 mmol g^{-1}), aromatic spacer molecules such as biphenyl and naphthalene had little effect on the pyrolysis rate. However, spacer molecules containing benzylic C-H bonds, such as dimethylbenzene, diphenylmethane, tetralin, and fluorene, acted as catalysts to accelerate the decomposition of $\approx \text{DPP}$, and the decomposition rates correlated with reported relative rates for hydrogen donation of these molecules to benzylic radicals.^(14,24) This behavior is unique to the diffusional constrained system, since in fluid phases, these molecules behaved like other inert aromatic diluents. This unexpected behavior could be explained by a hydrogen transfer, radical relay mechanism on the surface as illustrated in Figure 5 for the diphenylmethane spacer. Rapid serial hydrogen transfer steps can occur on the surface since the reacting species are pre-organized for reaction in this reduced dimensional reaction space. The involvement of these hydrogen transfer steps for the diphenylmethane spacer were confirmed through isotopic labeling studies with $\approx \text{PhCD}_2\text{Ph}$ as spacer.⁽¹⁴⁾ As shown in Table 1, a full kinetic isotope effect of 2.8 was detected at 375°C for $\approx \text{DPP}$ pyrolysis, and deuterium was incorporated in both the vapor-phase and surface-attached toluene products. The significance of this omnipresent process is that radical centers can migrate by a non-diffusional pathway that overcomes some of the diffusional constraints and promotes the radical chain decomposition pathway. However, as noted earlier, retrogressive reactions for weak cross links as typified by $\approx \text{BB}$ are also limited by hydrogen transfer steps and are promoted by neighboring molecules that can participate in the radical relay mechanism.

Undoubtedly, the efficiency of this pathway also depends on the ability of molecules to become properly aligned for the oriented hydrogen transfer step on the surface, an area that needs

to be studied in more detail. Orientation effects can lead to regiospecificity in hydrogen transfer steps that impact product selectivities. This is illustrated in the pyrolysis of \approx DPP where hydrogen abstraction selectivities (Figure 1) varied modestly with changes in surface coverage, favoring abstraction from the benzylic methylene farthest from the surface at lower surface coverages. More dramatic effects on product selectivities were found during pyrolysis of surface-immobilized 1,4-diphenylbutane where radical chain decomposition products are formed from both benzylic and non-benzylic carbon-centered radicals as described previously.⁽¹⁰⁾ Once again, the presence of neighboring molecules that block or promote hydrogen transfer steps significantly alter product selectivities.

We have also been investigating ether analogs such as silica-attached phenethyl phenyl ether, \approx C₆H₄CH₂CH₂OC₆H₅ (\approx PPE), which are models for important structural elements in lignin.^(17,18) Pyrolysis at 375°C follows a similar course to that observed in fluid phases. Analogous to diphenylpropane, a radical chain pathway is observed that cycles through the benzylic radical, \approx C₆H₄CH•CH₂OC₆H₅, producing phenol and surface-attached styrene products. However, for \approx PPE, a second significant reaction pathway is detected that proceeds through the non-benzylic radical, \approx C₆H₄CH₂CH•OC₆H₅. As in the case of benzyl phenyl ether (see Eq. 2), this radical undergoes an oxygen to carbon phenyl shift resulting (following β -scission and H-abstraction) in the formation of benzaldehyde and surface-attached toluene.⁽¹⁷⁾ This pathway is significant for a number of substituted PPE's, but the selectivity is sensitive to substituent effects in a predictable manner. However, as opposed to fluid phases where dilution of PPE with biphenyl solvent had no effect of the selectivity of the two radical decay paths, the rearrangement path involving the O-C phenyl shift was recently found to be sensitive to the structure of neighboring spacer molecules on the silica surface.⁽¹⁷⁾ Aromatic spacer molecules such as biphenyl appear to hinder the O-C phenyl shift, presumably by steric interference. These spacer effects continue to be investigated.

SUMMARY

Restricted mass transport has been recognized as playing an important role in the pyrolysis of cross-linked, macromolecular systems. A molecular level understanding of the impact of diffusional constraints on pyrolysis mechanisms is crucial to bench marking results from analytical pyrolysis experiments, and could be important in developing more refined predictive models for the pyrolysis of fossil and renewable organic energy resources. Model systems that incorporate diffusional constraints such as polymers and covalently or ionically immobilized compounds can provide some of this needed information. Through our studies of silica-immobilized hydrocarbons, we have obtained comprehensive information on how pyrolysis rates and product distributions can be perturbed by restricted mass transport. In general, the rates of unimolecular homolyses are little perturbed by surface immobilization. However, termination reactions between diffusional constrained radicals are hindered, particularly coupling reactions. This often results in the emergence of competitive radical chain pathways involving unimolecular steps such as skeletal rearrangements and cyclizations. Furthermore, hydrogen transfer processes between diffusional constrained species can be particularly facile, although quite dependent on the distance between, and the orientation of, the participating species. Under optimum hydrogen transfer conditions, rapid serial hydrogen transfers can occur and provide a means for radical sites to be translocated in the matrix without the need for physical diffusion. Such a process promotes radical chain reactions that can produce smaller, more volatile products, as well as retrogressive reactions that produce more refractory products.

ACKNOWLEDGMENTS

This research was sponsored by the Division of Chemical Sciences, Office of Basic Energy Sciences, U.S. Department of Energy, under contract No. DE-AC05-96OR22464 with Oak Ridge National Laboratory, managed by Lockheed Martin Energy Research, Corp.

REFERENCES

1. (a) L. M. Stock, *Acc. Chem. Res.*, 22 (1989) 427; (b) P. R. Solomon, T. H. Fletcher, and R. J. Pugmire, *Fuel*, 72 (1993) 587; (c) M. A. Serio, D. G. Hamblen, J. R. Markham, and P. R. Solomon, *Energy & Fuels*, 1 (1987) 138; (d) P. R. Solomon, D. G. Hamblen, M. A. Serio, Z.-Z. Yu, and S. Charpenay, *Fuel*, 72 (1993) 469; (e) P. Gilot and B. R. Starnore, *Energy & Fuels*, 9 (1995) 126; (f) E. M. Suuberg, in R. H. Schlosberg(Ed.), *Chemistry of Coal Conversion*, Plenum Press, New York, 1985, Chapter 4, p. 67; (g) G. R. Gavalas, *Coal Pyrolysis*, Elsevier, Amsterdam, 1982. (h) W. Wanzl, *Biomass and Bioenergy*, 7 (1994) 131.
2. A. K. Burnham, R. L. Braun, *Org. Geochem.*, 16 (1990) 27.
3. C. D. Blasi, *Biomass and Bioenergy*, 7 (1994) 87.
4. M. A. Serio, S. Charpenay, R. Bassilakis, and P. R. Solomon, *Biomass and Bioenergy*, 7 (1994) 107.
5. Y. Chen, S. Charpenay, A. Jensen, M. A. Serio, and M. A. Wójciewicz, *Prepr. Pap.-Am. Chem.*

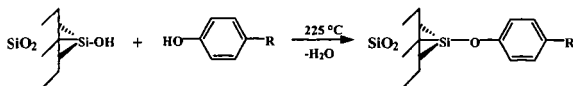
- Soc., Div. Fuel Chem., 42 (1997) 96.
- (a) C. C. Elam, R. J. Evans, and S. Czernik, Prepr. Pap.-Am. Chem. Soc., Div. Fuel Chem., 42 (1997) 993; (b) H. Bar and Z. Aizenshtat, J. Anal. Appl. Pyrolysis, 19 (1991) 265; (c) R. N. Hancox, G. D. Lamb, and R. S. Lehrle, J. Anal. Appl. Pyrolysis, 19 (1991) 333.
 - A. C. Buchanan, III and P. F. Britt, J. Anal. Appl. Pyrolysis, in press.
 - A. C. Buchanan, III, T. D. J. Dunstan, E. C. Douglas, and M. L. Poutsma, J. Am. Chem. Soc., 108 (1986) 7703.
 - A. C. Buchanan, III and C. A. Biggs, J. Org. Chem., 54 (1989) 517.
 - P. F. Britt and A. C. Buchanan, III, J. Org. Chem., 56 (1991) 6132.
 - S. C. Mitchell, C. J. Lafferty, R. Garcia, C. E. Snape, A. C. Buchanan, III, P. F. Britt, and E. Klavetter, Energy & Fuels, 7 (1993) 331.
 - P. F. Britt, A. C. Buchanan, III, E. A. Malcolms, and C. A. Biggs, J. Anal. Appl. Pyrolysis, 25 (1993) 407.
 - A. C. Buchanan, III, P. F. Britt, and C. A. Biggs, Energy & Fuels, 4 (1990) 415.
 - A. C. Buchanan, III, P. F. Britt, K. B. Thomas, and C. A. Biggs, J. Am. Chem. Soc., 118 (1996) 2182.
 - A. C. Buchanan, III, P. F. Britt, J. T. Skeen, J. A. Struss, and C. L. Elam, J. Org. Chem., 63 (1998) 9895.
 - K. Ismail, S. C. Mitchell, S. D. Brown, C. E. Snape, A. C. Buchanan, III, P. F. Britt, D. V. Franco, I. I. Maes, and J. Yperman, Energy & Fuels, 9 (1995) 707.
 - A. C. Buchanan, III and P. F. Britt, Prepr. Pap.-Am. Chem. Soc., Div. Fuel Chem., 44 (1999) 290.
 - P. F. Britt, A. C. Buchanan, III, K. B. Thomas, and S.-K. Lee, J. Anal. Appl. Pyrolysis, 33 (1995) 1.
 - R. D. Guthrie, S. Ramakrishnan, P. F. Britt, A. C. Buchanan, III, and B. H. Davis, Energy & Fuels, 9 (1995) 1097.
 - A. C. Buchanan, III, P. F. Britt, K. B. Thomas, and C. A. Biggs, Energy & Fuels, 7 (1993) 373.
 - A. C. Buchanan, III and P. F. Britt, Prepr. Pap.-Am. Chem. Soc., Div. Fuel Chem., 43 (1998) 630.
 - A. C. Buchanan, III, P. F. Britt, and K. B. Thomas, Energy & Fuels, 12 (1998) 649.
 - S. Ramakrishnan, R. D. Guthrie, P. F. Britt, A. C. Buchanan, III, and B. H. Davis, Prepr. Pap.-Am. Chem. Soc., Div. Fuel Chem., 40 (1995) 555.
 - J. A. Franz, M. S. Alnajjar, R. D. Barrows, D. L. Kasaki, D. M. Camaioni, and N. K. Suleman, J. Org. Chem., 51 (1986) 1446.
 - A. C. Buchanan, III, unpublished results.

Table 1. Pyrolysis of Silica-Immobilized Ph(CH₂)₃Ph at 375°C: Influence of Surface Composition on Pyrolysis Rate

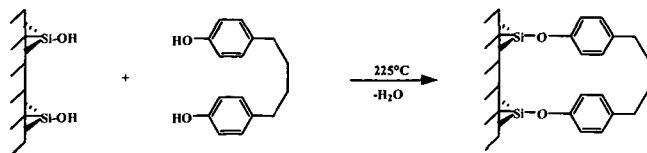
Surface Composition ^a	Coverage (mmol g ⁻¹)	Rate x 10 ⁻⁴ (% s ⁻¹) ^b	Ref.
=DPP	0.59	24	9
	0.14	1.1	9
	0.10	0.72	13
=DPP= (<i>p</i> -, <i>p</i> -)	0.10	0.17	12
=DPP= (<i>m</i> -, <i>p</i> -)	0.09	0.10	12
=DPP / =BP	0.13 / 0.51	2.2	14
=DPP / =NAP	0.12 / 0.44	1.9	14
=DPP / =DMB (3,4-)	0.12 / 0.25	8.5	14
=DPP / =DPM	0.14 / 0.41	37	14
=DPP / =DPM- <i>d</i> ₂	0.12 / 0.35	13	14
=DPP / =TET	0.11 / 0.45	47	25
=DPP / =FL	0.17 / 0.42	83	14

^a Abbreviations for surface-attached species are =DPP (1,3-diphenylpropane, mono-attached), =DPP= (DPP, 80 % di-attached, 20 % mono-attached), =BP (biphenyl), =NAP (naphthalene), =DMB (dimethylbenzene), =DPM (diphenylmethane), =DPM-*d*₂ (PhCD₂Ph), =TET (tetralin), =FL (fluorene). ^b Initial rates for total decomposition of =DPP based on 4-8 thermolyses. Standard deviations (1σ) in reported values are typically ≤ 15%.

Attachment Reaction



Di-attachment



Co-attachment

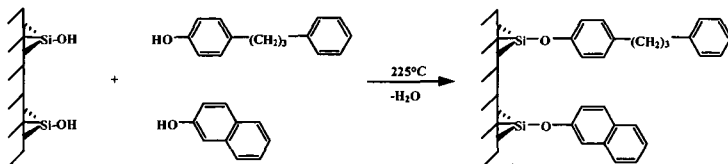


Figure 1. Preparation of silica-immobilized model compounds

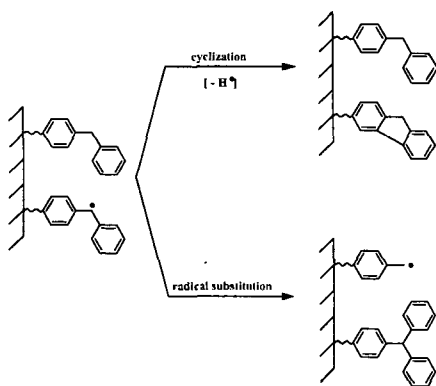
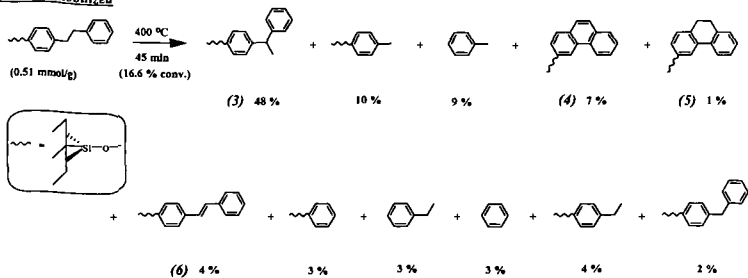


Figure 2. Competing cyclization and radical substitution pathways in pyrolysis of silica-immobilized diphenylmethane.

Silica Immobilized



Liquid Phase

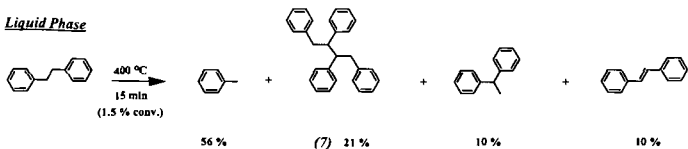
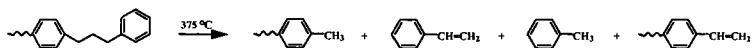


Figure 3. Comparison of pyrolysis products for silica-immobilized and liquid bibenzyl.



Radical Chain Mechanism:

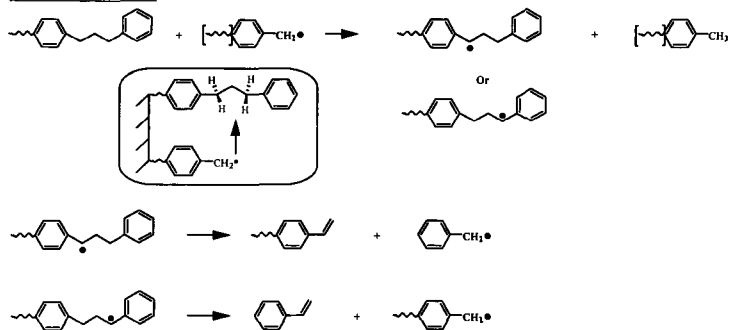


Figure 4. Radical chain propagation steps for the pyrolysis of silica-immobilized 1,3-diphenylpropane. Bracket notation denotes species exists in both gas-phase and surface-attached forms.

Hydrogen Transfer, Radical Relay Mechanism

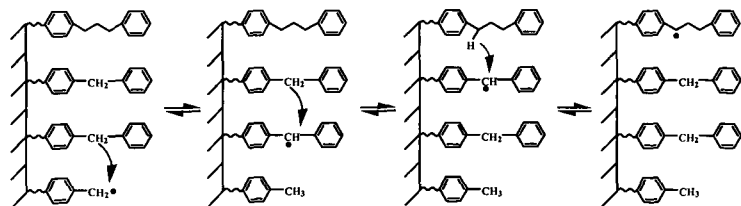


Figure 5. Radical relay mechanism in the pyrolysis of silica-attached 1,3-diphenylpropane.

SELECTIVE OXIDATION OF ALKANES PROMOTED BY COPPER IONS

Donald M. Camaioni, Michael A. Lilga, J. Timothy Bays, John C. Linehan,
Wendy J. Shaw, and Jerome C. Birbaum

Pacific Northwest National Laboratory, Richland, WA, 99352

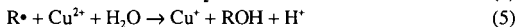
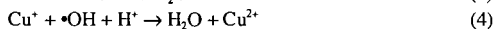
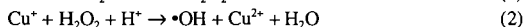
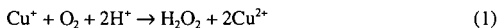
ABSTRACT

A system that uses the Cu(I)/Cu(II) couple and O₂ oxidizes alkanes, including methane, to alkyl ester in trifluoroacetic acid (TFA). Formation of an ester in large part protects the alkyl group from further oxidation, and the esters may then be hydrolyzed to the corresponding alcohol. We show that the system can be adapted to operate electrocatalytically with oxidation of alkane occurring in the cathodic compartment of an electrolysis cell due to the activation of O₂ by electrogenerated Cu(I) ions. The mechanism of the oxidation appears to involve alkyl radicals. Trapping by Cu(II) ions converts the alkyl radicals to the ester product. Alkyl radicals with 2 or more carbons may first convert to olefins which subsequently add TFA to give ester products. The results are compared with oxidation of alkanes in Cu(II)-H₂O₂-TFA.

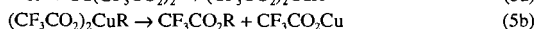
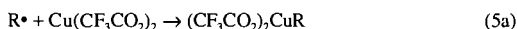
INTRODUCTION

Processes for directly and selectively oxidizing methane to methanol and alkanes to higher alcohols, instead of ketones and acids, could have enormous economic and environmental impacts. A major problem to be overcome is the high reactivity of alcohols toward oxidizing agents, relative to alkanes. Catalytica Advanced Technologies recently reported a significant conceptual advance: methane could be oxidized selectively to methyl sulfate using mercury or platinum catalysts in sulfuric acid.¹ This approach has been extended to other alkanes and ester-forming acids by other groups. Sen has reported extensively on the use of Pd(II) catalysis in TFA.² Also, Vargafik et al. observed Co(II)/Co(III) to be an effective oxidant in TFA.³ Simultaneously, Camaioni and Lilga developed a system based on the Cu(I)/Cu(II) couple and O₂.⁴ In all of these systems, formation of an ester in large part protects the alkyl group from further oxidation, and the esters may then be hydrolyzed to the corresponding alcohol.

The mechanisms of these oxidations are uncertain. The systems developed by Catalytica and by Sen are thought to involve non-radical electrophilic pathways in which metal ion oxidants directly activate the alkane C-H bond. In developing our Cu(I)/Cu(II)-O₂ oxidation system, we assumed free radical mechanisms operate analogous to Fenton-type reactions that operate in aqueous systems (Equations 1-5).

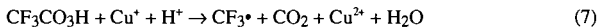
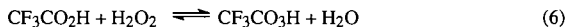


Rates of attack on functionalized substrates by strongly electrophilic radicals such as $\bullet\text{OH}$ and $\text{SO}_4^{\bullet-}$ show a pronounced dependence on the electronic character of the adjacent functional groups (see Table 1). Therefore, a viable system might involve electrophilic radicals abstracting H from alkanes to form organic radicals that subsequently convert to esters on oxidation by transition metal ions. The Cu(I)/Cu(II) couple is well suited for such a system in that O₂ rapidly oxidizes Cu(I) to Cu(II) and generates active oxidizing intermediates (Equation 1) and Cu(II) ions react non-selectively with alkyl radicals to form organocopper(III) intermediates that undergo reductive elimination to give esters or loss of a β -hydrogen to give an alkene (Equations 5a-c). Since TFA adds rapidly to alkenes (Equation 5d), esters are produced in either case.



In this paper, we present a study of alkane oxidation by the Cu(I)/Cu(II)-O₂-TFA system and by the complementary Cu(II)-H₂O₂-TFA system. The latter system was examined because H₂O₂

may be an intermediate in the former system. H_2O_2 reacts with TFA to make trifluoroperacetic acid (TFPA). TFPA oxidizes alkanes at room temperature without need for metal catalysis⁵ and the reactions are reported to occur without generation of alkyl radicals. Primary and methane C-Hs are relatively unreactive. However, Sen observed that addition of Pd(II) accelerated the rate and improved the yield methyl trifluoroacetate from methane.⁶ With respect to our system, reduction of TFPA by Cu(I) may result in decarboxylation (Equations 6 and 7) and initiation of free radical redox reactions.



PROCEDURES

Generally, experiments were performed in TFA solutions that contained the alkanes and other reagents as described below and in the Tables and Figures.

Oxidations promoted by reacting Cu(I) with O_2

In preliminary experiments, oxidations were promoted by reactive dissolution of Cu_2O and Cu metal in TFA solutions containing Cu(II) ions and alkane in contact with air or O_2 gas. Experiments were also performed by adding deoxygenated solutions of Cu(I) trifluoroacetate to solutions of alkane that were stirred under an O_2 atmosphere. See Table 2 for specific conditions and methods. To make the reactions catalytic in Cu ions, oxidations were run in an electrochemical cell that allowed for the generation of known amounts of Cu(I) at known rates without changing the total concentration of copper in the solution. Initial experiments simply used an open beaker with two platinum electrodes and a potentiostat operating in constant current mode. In subsequent experiments, we used a gas-tight, Teflon and glass cell (ca. 100 mL volume). Ports in the top of the cell admitted the electrodes and gas recirculation connections and allowed for gas/liquid sampling. The working electrode was a platinum mesh cylinder. The auxiliary electrode was a platinum mesh flag centered within the working electrode and separated from the working solution by a porous Vycor frit. The solution in the auxiliary electrode chamber was typically 1 M H_2SO_4 . A saturated calomel reference electrode was positioned next to the working electrode via a salt bridge with porous Vycor frit. The salt bridge contained 5 M KO_2CCF_3 . Typically, the cell was operated at a potential of -0.1 V vs. SCE and a current of 50 mA. The cell was connected to a gas recirculation system that consisted of a MasterFlex pump with Teflon pump head and Teflon tubing and 5-L gas ballast that served to minimize changes in gas concentrations during experiments. Initial gas compositions were set with calibrated rotometers and verified by gas chromatography.

Oxidations using H_2O_2 -TFA

Solution experiments were conducted in 5 mL ampoules or in 8 mL screw-top sample vials with Teflon lined caps. Reaction mixtures were made by adding 200 μL of cyclohexane and 39.0 μL of 30% hydrogen peroxide to 2.00 mL of TFA or 2.00 mL of a TFA/Cu(II) stock solution. Anaerobic samples were degassed using three freeze-pump-thaw cycles, and the ampoules flame-sealed. For aerobic samples the head space was purged with oxygen after all components were added. Gas samples were taken using a Hamilton SampleLock™ syringe with a gas sampling needle. Gas analyses were performed by GC-MS and quantified by using an internal argon standard. 300 μL aliquots of each reaction solution were neutralized and the organic components extracted by adding the sample to a test tube containing approximately 0.7 g anhydrous sodium carbonate, 3 mL of dichloromethane and 10.00 μL of a decane in dichloromethane solution that served as an internal standard. After neutralizing the TFA, the dichloromethane layer was dried with magnesium sulfate and analyzed by gas chromatography.

Analyses

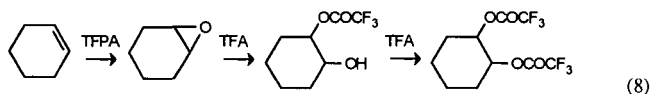
Gas chromatography was performed using an HP 5890 gas chromatograph with a 30-m HP-5MS capillary column (crosslinked 5% phenyl methyl silicone, 0.25 μm film thickness, 0.25 mm column i.d.). Chromatograms were recorded using an HP 5971 mass-selective detector. Gaseous components were quantified by using the mass-selective detector to extract ions unique to each component. All instrument responses were in the linear region of the respective calibration curves, and calibrations were verified periodically. ^1H NMR spectra were recorded at 300 MHz using a Varian VXR-300 spectrometer operating at 7.01 T with a standard 5 mm multinuclear broad band probe. ^1H NMR spectra in TFA were run unlocked, but were referenced

to cyclohexane and matched with spectra of mixtures prepared from authentic samples of cyclohexanol and 1,2-cyclohexanediol in TFA.

RESULTS

Several scoping experiments were performed to learn the potential of Cu promoted oxidations in TFA. Table 2 shows results for oxidations of methane and cyclohexane that were obtained under a variety of conditions. The results show that oxidations could be promoted by addition of Cu(I) solutions, Cu(I) oxides, or Cu(0) metal to solutions of Cu(II) and O₂. Consistent with a report by Vargafitik et al.,^{2a} no conversion was observed with O₂ and just Cu(II). In these experiments, the alkane was present in excess and Cu(I) was the limiting reagent. Therefore, the yields are calculated assuming a stoichiometry of 1 mole of product per 2 moles of Cu(I) ions. Addition of Cu(I) ions as solutions or solid Cu(I) oxides or Cu(0) metal causes the Cu(II) concentrations to increase and eventually precipitate. This situation can be circumvented by performing the oxidations in an electrolytic cell. The oxidations then become catalytic in Cu(I)/Cu(II) ions. The last entry in Table 2 shows a result obtained in a single compartment electrolytic cell. Here, Cu(II) is reduced to Cu(I) at the cathode and presumably water, present in solution, was oxidized at the anode. The 46% yield of cyclohexyl trifluoroacetate is based on the number of electrons discharged through the cell assuming that 2 electrons are required to produce 1 molecule of ester.

In addition to cyclohexyl trifluoroacetate, we observed lesser amounts of secondary oxidation products. Cyclohexanone was present in minor quantities, typically <2% of cyclohexyl trifluoroacetate. Of the possible disubstituted products, the mono and diester of *trans*-1,2-cyclohexanediol were dominant. The high regioselectivity for these secondary products probably is due to oxidation of cyclohexene. Epoxidation by TFPA is facile and subsequent reactions with TFA will give the monoester and diesters (Equation 8).



Electrocatalytic Oxidation of Cyclohexane in the Cu(II)-O₂-TFA System

We performed additional experiments in a divided electrolytic cell so that the cathodically-driven process could be studied, independent of processes occurring at the anode. The cell was closed from the atmosphere so that the gas composition could be controlled and analyzed as the oxidation proceeded. We were particularly interested in learning whether CO₂ was a byproduct. Its production would suggest a mechanism in which TFA is oxidized to CF₃• radicals. In which case, CF₃• or CF₃O₂• may attack alkane C-H bonds (e.g., Equations 9-11).



Figure 1 shows results obtained for cyclohexane oxidation that occurred in the cathodic compartment of the electrolytic cell. Moles of cyclohexyl trifluoroacetate and CO₂ are plotted against the moles of electrons discharged through the cell. CO₂ is a minor product relative to cyclohexyl trifluoroacetate. Therefore, Equations 9, 10 and 11 may contribute in a small way to the oxidation. Perhaps, having 10% water in the system and in situ generation of H₂O₂ favors reaction of Cu(I) with H₂O₂ rather than with CF₃CO₂H. The yield of cyclohexyl trifluoroacetate was found to be strongly dependent on the initial amount of O₂ in contact with the Cu(II) solution. Figure 2 shows the yields of monoester and diester for 3 cases: ~50 mL of air in the cathode compartment, cathode compartment recirculated with a 5-L volume of air, and cathode compartment recirculated with 5 L of O₂. The best yields were obtained with the smallest amount of O₂.

The Cu(II)-H₂O₂-TFA System

Reactions were run under aerobic and anaerobic conditions with and without Cu(II) ions present. Table 3 lists results for reactions run at 25 °C for 24 h. The first and second entries show results obtained with Cu(II) catalysis. The esters of cyclohexanol and *trans*-1,2-cyclohexanediol were the dominant cyclohexane products, and in contrast to the Cu(I)-O₂

system, yields of the diester exceeded yields of monoester. Anaerobic conditions and Cu(II) ions gave the highest yields and largest ratios of diester:monoester. Reactions run without Cu(II) ions gave predominantly monoester and showed little dependence on the presence or absence of O₂ (Table 3). Deno observed even greater preference for monoester using excess H₂O₂ (last entry of Table 3).⁵ NMR spectroscopy (¹H and ¹⁹F) of reaction mixtures showed that Cu(II) ions accelerated the oxidations. The NMR spectra also showed CF₃H was produced in significant quantities when reaction solutions were initially degassed. Gas chromatographic-mass spectral analyses of the gases above the reactions confirmed the identity of CF₃H and provided a measure of the amounts of CF₃H and CO₂ that were produced. The yields of CO₂ reported in Table 3 include dissolved CO₂, whereas yields of CF₃H in Table 3 represent only what was in the gas phase. Considering the solution NMR results, comparable amounts of CF₃H were in solution. The results show that yields of CF₃H were strongly dependent on O₂. Reactions that were run in the presence of O₂ generated little CF₃H, although yields of CO₂ were relatively unaffected when Cu(II) ions were present. Analysis of the results from Cu(II)-catalyzed reactions (Table 3) shows that reaction solutions that were initially degassed gave approximately 1 molecule of CO₂ per molecule of cyclohexane that converted. When O₂ was present initially, the stoichiometry was >1 (compare first and second entries of Table 3 and note that % yield of diester based on H₂O₂ is twice the % yield based on converted cyclohexane). When Cu(II) ions were absent and O₂ was present, the yield of CO₂ was very small. Finally, cyclohexane-d₁₂ was oxidized under anaerobic conditions to determine the fraction of CF₃H produced by Equation 9. In the absence of O₂, the ratio CF₃D/CF₃H was 20/1, both in the presence or absence of Cu(II) ions, showing that CF₃• radicals mainly had abstracted H from cyclohexane.

CONCLUSIONS

These experiments show that Cu ions are effective in promoting selective oxidation of alkanes to alkyl trifluoroacetate esters. Furthermore, it is possible to initiate oxidation in the cathodic compartment of an electrolysis cell making the oxidations catalytic in Cu and enabling continuous operation. The reactions appear to be Fenton-type systems in which oxidations of Cu(I) ion by O₂ and peroxide generate oxidizing species that abstract H to give organic radicals that react with Cu(II) converting to products and propagating a redox chain reaction (e.g., Equations 2-5). In the following discussion we reconcile observations and, in the end, comment on the mechanism of the uncatalyzed H₂O₂ system.

Distribution of Monoester and Diester from Cyclohexane

The distributions of mono and disubstituted products differ markedly for the Cu(I)-O₂-TFA and Cu(II)-H₂O₂-TFA systems. The former favors monoester and the latter favors diester. The former generates H₂O₂ in situ while the latter starts out with H₂O₂. These variations may be accommodated by a free radical redox chain reaction that involves Equations 1-3, 6, 7, 9-11, then 5a, and 5c followed by 5d and 8. Given that Equations 6 and 8 are facile, the different product distributions arise from how introduction of H₂O₂ affects the competing reactions. Presumably, in situ generation of H₂O₂ favors low steady-state concentrations of H₂O₂ such that Equation 6 is slow compared to Equation 2 and Equation 5d (with R(-H) = cyclohexene) is fast compared to Equation 8. Therefore, Equations 6-11 are not important in Cu(I)-O₂ oxidations. However, when starting with H₂O₂ as we do in the Cu(II)-H₂O₂-TFA system, TFA forms (Equation 6) in sufficient amounts such that Equation 8 competes effectively with Equation 5d.

Factors Affecting Yields

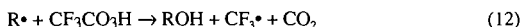
The yields of products have been calculated based on reducing equivalents used in the Cu(I)-O₂ system or H₂O₂ used in the Cu(II)-H₂O₂ system. These yields were generally less than 100% due to reactions that consume reagent without generating alkyl radicals. Equation 4 is an example of such a reaction. Liotta and Hoff observed that solutions of 30% H₂O₂/water in TFA decompose with generation of CF₃H.⁷ Apparently, the decomposition involves radical reactions that serve to initiate alkane oxidations when Cu(II) ions are present or O₂ is absent.

Effects of O₂

O₂ affects the reaction systems in various ways. First of all, it is required when peroxide is not a reagent. Even so, its effect in the electrocatalyzed system is curious in that yields of monoester vary inversely with the amount of available oxygen, i.e., the system is more efficient when starved for oxygen. Other products do not appear with increasing O₂. Therefore, we assume that reduction to water occurs. If so, then it may be that higher concentrations of O₂ allow direct reduction at the cathode and/or greater fractions of Equations 1 and 2 to occur near

the electrode surface where the $\bullet\text{OH}$ is reduced to water much faster than it is scavenged by alkane.

When peroxide is a reagent, the effects of O_2 are complex and not fully understood. In the absence of O_2 , CF_3H and CO_2 were produced in amounts that were comparable to the alkyl esters, and when cyclohexane- d_{12} was used, $\text{CF}_3\text{D}/\text{CF}_3\text{H}$ ratios of >20 were obtained. These observations are consistent with a radical chain decomposition in which propagation steps include: attack on RH by $\text{CF}_3\bullet$; and oxidation of $\text{R}\bullet$ by Cu(II) if present and by $\text{CF}_3\text{CO}_3\text{H}$ if Cu(II) is absent (Equation 12).⁸



When O_2 and Cu(II) ions are present, less CO_2 and little CF_3H were produced. Probably $\text{CF}_3\bullet$ radicals are scavenged by O_2 leaving the less reactive $\text{CF}_3\text{O}_2\bullet$ radical to propagate the reaction (Equation 11). The mechanism in the presence of O_2 and absence of Cu(II) is most uncertain. A dilemma that any radical mechanism must overcome is explaining how cyclohexanol⁸ and then ester are produced without making cyclohexanone and CO_2 . Perhaps, O_2 serves to inhibit the radical chain pathway and allow heterolytic pathways to operate.^{5,8}

ACKNOWLEDGEMENTS

This research was supported by the Advanced Energy Projects program of the U. S. Department of Energy. The Pacific Northwest National Laboratory is a multiprogram national laboratory operated by Battelle Memorial Institute under Contract No. DE-AC06-76RLO 1830.

REFERENCES

1. (a) Periana, R. A.; Evitt, E. R.; Taube, H. "Process for Converting Lower Alkanes to Esters" U.S. Patent No. 5,233,113, Aug. 3, 1993. (b) Periana, R. A.; Taube, D. J.; Evitt, E. R.; Loffler, D. G.; Wentreck, P. R.; Voss, G.; Masuda, T. *Science* **1993**, 259, 340-3. (c) Periana, R. A.; Taube, D. J.; Taube, H.; Evitt, E. R., *Catalytica*, "Catalytic Process for converting Lower Alkanes to Esters, Alcohols, and to Hydrocarbons" U.S. Patent No. 5,306,855, Apr. 26, 1994. (d) Periana, R. A.; Taube, D. J.; Gamble, S.; Taube, H.; Satoh, T.; Fuji, H. *Science* **1998**, 280, 560-4.
2. (a) Hogan, T.; Sen, A. *J. Am. Chem. Soc.* **1998**, 119, 2642-2646. (b) Sen, A. *Acc. Chem. Res.* **1998**, 31, 550-557. (c) Lin, M.; Hogan, T.; Sen, A. *J. Am. Chem. Soc.* **1997**, 119, 6048-6053.
3. (a) Vargaftik, M. N.; Stolarov, I. P.; Moiseev, I. I. *J. Chem. Soc., Chem. Commun.* **1990**, 1049-1050. (b) Gretz, E.; Oliver, T. F.; Sen, A. *J. Am. Chem. Soc.* **1987**, 109, 8109-11.
4. Camaioni, D. M.; Lilga, M. A. U.S. Patent No. 5,585,515, 1996; U.S. Patent No. 5,708,246, 1998; U.S. Patent No. 5,786,505, 1998.
5. Deno, N. C.; Jedziniak, E. J.; Messer, L. A.; Meyer, M. D.; Stroud, S. G.; Tomczesko, E. S. *Tetrahedron* **1977**, 33, 2503-8.
6. (a) Ref. 2a. (b) Sen, A. *Platinum Metals Rev.* **1991**, 35, 126. (c) Kao, L.-C.; Hutson, A. C.; Sen, A. *J. Am. Chem. Soc.* **1991**, 113, 700.
7. Liotta, R.; Hoff, W. S. *J. Org. Chem.* **1980**, 45, 2887-2890.
8. Deno reported cyclohexanol is initially produced (see Ref. 5). Using ^1H NMR, we too observed it to form and esterify in successive steps.

Table 1. Rate Constants^(a) for H-Abstraction from CH₃-X by HO• and SO₄^{-•}

X	HO•	SO ₄ ^{-•}
	<i>k</i> /10 ⁸ M ⁻¹ s ⁻¹	<i>k</i> /10 ⁶ M ⁻¹ s ⁻¹
-OH	9.6	10
-CH ₃ ^(b)	7	2.2
-OCOMe ^(c)	2.2	
-H	0.9	<0.8
-OSO ₃ ⁻	0.5	
-CO ₂ H	0.17	0.014

^(a)From Notre Dame Radiation Laboratory Radiation Chemistry Data Center (<http://www.rcdc.nd.edu/>). ^(b)Total rate constant divided by 2. ^(c)Attack on the acetoxy methyl group is neglected; see value for acetic acid.

Table 2. Yields of Alkyl Ester from Cu(I) Promoted Oxidation in Trifluoroacetic Acid^(a)

Alkane	% ^(b)	Method
Methane	5	Dissolution of Cu ₂ O under 1 atm. of 80/10/10 CH ₄ /O ₂ /N ₂
	9	Addition of CF ₃ CO ₂ Cu solution to 13 atm. 26/1 CH ₄ /O ₂
Cyclohexane ^(c)	17	Addition of CF ₃ CO ₂ Cu to solution stirred in air
	19	Dissolution of solid Cu ₂ O in air
	30	Comproportionation of Cu(0) and Cu(II) in air
	46	Electrolysis of Cu(II) solution in air

^(a)Solutions contained 10 vol% H₂O. ^(b)Based on Cu(I) added assuming 2 moles Cu(I) consumed per mole of ester formed. ^(c)Cyclohexane ~1 M.

Table 3. Oxidation of Cyclohexane in H₂O₂-TFA: Effects of Cu(II) and O₂

Cu(II) M	P _{O₂} Atm	% Yield ^(a)			
		Monoester	Diester	CO ₂	CF ₃ H
0.05	1	7	18	34	0.1
0.05	0	9	52	38	15
0	1	28	10	2	-0.1
0	0	32	10	34	20
0 ^(b)	0.2	66	5	nd ^(c)	nd

^(a)See note (a) in Table 3. ^(b)Deno, et al.,⁵ no Cu ions and [H₂O₂]/[C₆H₁₂] = 1.15.

^(c)not determined.

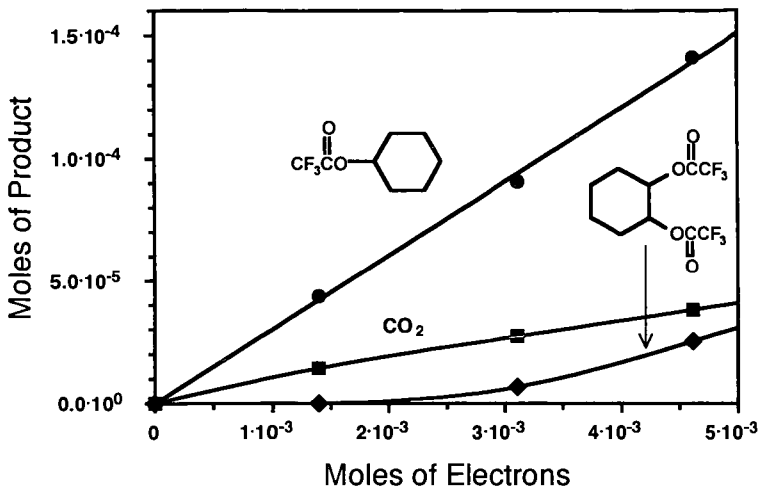


Figure 1. Cu(I)/Cu(II) promoted oxidation of cyclohexane to esters of cyclohexanol (●) and *trans*-1,2-cyclohexanediol (◆) and TFA to CO₂ (■) in the cathodic compartment of a closed, divided electrolysis cell. Conditions: 0.09 M cyclohexane, 0.08 M Cu(II), 10wt% H₂O/TFA, 2.2×10⁻³ moles O₂, E_{applied} = -0.1V vs. SCE.

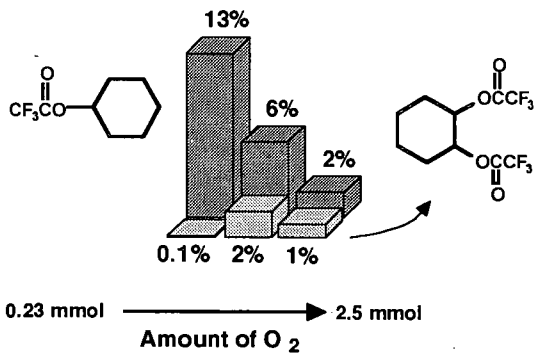


Figure 2. Effect of O₂ contacted with solution on ester yields (% moles product per mole e⁻ discharged). Conditions: 0.09 M cyclohexane, 0.08 M Cu(II), 10wt% H₂O/TFA, 6×10⁻³ moles e⁻ discharged at E_{applied} = -0.1V vs. SCE.

ESTIMATING THE HEATS OF FORMATION OF HYDROCARBON RADICALS BY A SEMIEMPIRICAL CALCULATION

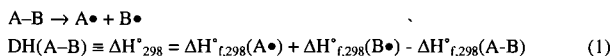
Xiaoliang Ma, and Harold H. Schobert
The Energy Institute, The Pennsylvania State University,
409 Academic Activities Building, University Park, PA 16802

KEYWORDS: hydrocarbon radical, heat of formation, molecular simulation

INTRODUCTION

Hydrocarbon free radicals play a very important role in many thermal-chemistry processes, including combustion, petroleum and coal coking, coal liquefaction and pyrolysis, oil shale retorting, thermal stability of fuels as well as free radical polymerization. To obtain heats of formation (ΔH_f°) of the radicals is very essential for the fundamental understanding of thermal chemistry and mechanism of the free radical process. Many experimental methods have been developed to determine ΔH_f° of free radicals, including halogenation kinetics, polyani relation, chemical activation, equilibrium study, electron-impact measurement, radical buffer, appearance energy, photoacoustic calorimetry, electrochemistry etc.[1-3]. However, the experimental determination of ΔH_f° of free radicals is complicated, difficult and expensive due to the instability of the radicals. In consequence, many approaches have been developed to estimate ΔH_f° of the radicals.

Three principal methods have been developed to estimate ΔH_f° of free radicals. The first method, and also the best characterized, is Benson's group additivity method [4], which estimates the ΔH_f° by summing the contributions of the heats of formation of the various groups, and correcting for various higher order interactions via "correction" terms. The second method is the bond-dissociation-energy (BDE) method that was reviewed in detail by McMillen and Golden in 1982 [5]. BDE is defined as:



According to equation (1), $\Delta H_{f,298}^\circ(A\cdot)$ can be calculated if $DH(A-B)$, $\Delta H_{f,298}^\circ(A-B)$ and $\Delta H_{f,298}^\circ(B\cdot)$ are known. For the estimation of prototypical primary, secondary and tertiary alkyl radicals, McMillen and Golden recommended 98, 95 and 92 kcal/mol for $DH(\text{primary C-H})$, $DH(\text{secondary C-H})$ and $DH(\text{tertiary C-H})$, respectively. For allyl or aryl radicals, a correction term, "resonance stabilization energy" (RSE), was used.

Although both of these empirical estimation methods for hydrocarbon radicals are very common in the chemical literature, the accuracy of the methods is unsatisfactory. Recently, molecular orbital methods have been developed and used to calculate ΔH_f° of compounds, including neutral molecules, ions and radicals. There are two main molecular orbital methods, *ab initio* and semiempirical methods. Of these, the *ab initio* method, having no need for empirically determined parameters, is the more theoretically "pure". However, *ab initio* methods are currently slow, and routine application at any reasonable degree of accuracy to systems of larger molecule and to the calculation of a large number of molecules is still not practical. The semiempirical methods are fast enough for routine application to quite large systems, and to a large number of molecules. With the heats of formation of systems related to those for which the semiempirical methods were parameterized, the accuracy of semiempirical methods is comparable with that of quite large basis set *ab initio* calculations [6].

In 1989, Stewart developed the MNDO-PM3 method for further optimizing parameters of semiempirical methods [7,8]. Stewart calculated the ΔH_f° of 7 hydrocarbon radicals by using this method. The average difference between the calculated and experimental values is 6.24 kcal/mol. In 1996, Camaioni et al. calculated ΔH_f° of 19 hydrocarbon free radicals by the MNDO-PM3 method, and correlated the calculated values with the experimental values [9]. They found that the errors are systematic for families of structurally related radicals.

In this study, we attempt to develop a new method for estimating the ΔH_f° of the prototypical hydrocarbon free radicals. The new estimation method, called PM3-systematic-correlation (PM3-SC) method, is based on both the MNDO-PM3 calculation and correlation between the calculated values and the experimental values from the literature. The errors in Benson's, DBE and MNDO-PM3 and PM3-SC methods are also compared and discussed in detail via statistical analysis.

COMPUTATIONAL METHODS

All quantum chemistry calculations in this study were performed by means of the semiempirical MNDO-PM3 method [7,8], using CAChe MOPAC, version 94. Geometry of the radicals was optimized by using EF method, and the corresponding ΔH_f° of hydrocarbon free radicals were calculated by using doublet multiplicity.

SOURCES OF EXPERIMENTAL DATA

The experimental data are from the available literature. As the experimental data from different sources are somewhat inconsistent with each other, we made the widest possible use of currently common and accepted ones [1-3,5,9-12]. Some of ΔH_f° of alkyl radicals were determined by the empirical BDE method using new BDE parameters reported by Seakins et al. [3] ($DH(\text{primary C-H})=101.05$, $DH(\text{secondary C-H})=98.26$, $DH(\text{tertiary C-H})=96.44$ kcal/mol).

RESULTS AND DISCUSSION

MNDO-PM3-calculated Results and Correlation with Experimental Data

The ΔH_f° values of 46 hydrocarbon free radicals, including primary alkyl, secondary alkyl, tertiary alkyl, alkenyl, aryl and cycloalkyl radicals, were calculated in this study by MNDO-PM3 method. Figure 1 plots the MNDO-PM3-calculated ΔH_f° vs. the experimental ΔH_f° for 46 hydrocarbon free radicals. As a whole, a considerable scatter exists with an R^2 value of 0.9535 and average errors of ± 10.57 kcal/mol. However, after examining the data, it is found that the structurally related radicals exhibit a very good linear correlation, as shown in Figure 1. According to the structural analogy of the radicals and the correlation, we can separate the 46 radicals into 5 groups. The first group consists of 15 primary alkyl radicals, including *n*-alkyl, *i*-alkyl, olefinic and phenylalkyl radicals with the experimental ΔH_f° values from 8 to 56 kcal/mol. A very good linear correlation between the experimental and calculated values was made by the least square fit with an R^2 value of 0.9982, although the calculated values are about 10 kcal/mol lower than the corresponding experimental values. The second group contains the secondary and tertiary radicals with an R^2 value of 0.9986. The MNDO-PM3-calculated values in this group are about 15-16 kcal/mol lower than the corresponding experimental values. The third group contains three cycloalkyl secondary radicals with an R^2 value of 0.9999. Alkenyl and aryl radicals together constitute the fourth group with an R^2 value of 0.9984, except for the 1-naphthylmethyl radical. The 1-naphthylmethyl radical deviates slightly from the regression line. Whether this deviation comes from the MNDO-PM3 calculation or from the experiment is still unclear. The last group consists of three cycloalkenyl radicals with an R^2 value of 0.9998.

The regression lines for alkyl radical groups, including the first, second and third groups, exhibit a similar slope, around 1.0, but with the corresponding intercepts different, being 11.71, 17.79 and 18.61 kcal/mol, respectively. The fourth group (alkenyl and aryl radicals), with intercept of 10.69 kcal/mol, shows the highest slope in all five groups, being 1.26. The group correlation reflects that the errors between MNDO-PM3-calculated and experimental values are systematic and dependent on the families of structurally related radicals. This finding allows one to be able to improve the accuracy of the estimates through scaling the calculated values. The linear regression equation for each group was obtained by a least squares fit. Using these regression parameters to scale the ΔH_f° calculated by the MNDO-PM3 method leads to a very significant reduction of the average error of the estimates, from ± 10.574 to ± 0.453 kcal/mol for the 45 hydrocarbon radicals.

Comparison of Different Estimation Methods Based on Statistical Analysis

In order to compare the errors from different estimation methods, the ΔH_f° values estimated by using Benson's, BDE and MNDO-PM3 methods, respectively, were also calculated. The calculation of ΔH_f° by Benson's method was performed according to reference [4]. The ΔH_f° values estimated by BDE method come from the review by McMillan and Coldren in 1982⁵. Statistical analysis of the errors for each methods was conducted. The experimental values vs. estimated values by Benson, BDE and MNDO-PM3 methods are plotted in Figure 2, 3 and 1, respectively.

With Benson's method, the expectation of errors is -2.901 kcal/mol, indicating the values estimated by this method are lower than the experimental values by about 3 kcal/mol as a whole. These errors can be attributed to that the experimental data used in specifying the group contribution to the ΔH_f° of the radicals in Benson's method are lower. For example, the experimental ΔH_f° values recommended in Benson's method were 26.5, 21.0, 17.6 and 8.4 kcal/mol for ethyl, *n*-propyl, *i*-propyl and *t*-butyl radicals, respectively, while recently, 28.9, 24.0,

21.5 and 12.2 kcal/mol were used instead [3]. The standard derivation of the errors in Benson's method is 1.909 kcal/mol, and thus, is scattered and unsatisfactory as Benson's method considers only the interaction between two linked atoms (short-range effect) and neglects the effect of interval atoms in the molecule (long-range effect).

The ΔH_f° values calculated by BDE method give an expectation of errors of -1.033 kcal/mol. It is still larger although being better than that for Benson's method. However, the standard derivation of the errors in this method is larger, being 2.497 kcal/mol. The errors in this empirical method are probably as the results of both using lower BDE values and using the BDE values derived from simple molecules to different and more complex molecules.

The ΔH_f° values estimated by MNDO-PM3 method exhibit larger errors. The expectation of errors is -8.108 kcal/mol, and the standard derivation is 8.908 kcal/mol, indicating that the ΔH_f° values calculated by the MNDO-PM3 method have to be scaled before use.

In all four methods discussed in this study, the PM3-SC method developed in this study gives the most accurate estimates, as shown in Figure 4. The expectation of errors is -0.001 kcal/mol, and the standard derivation is 0.575 kcal/mol. The statistical analysis indicates that we can use the PM3-SC method to estimate ΔH_f° of hydrocarbon radicals with a standard derivation below 0.60 kcal/mol. In other words, we can be 95 % confident that the difference between the estimated and experimental values is in the interval of ± 1.12 kcal/mol.

CONCLUSIONS

The families of structurally related radicals exhibit a very good linear correlation between the experimental and MNDO-PM3-calculated ΔH_f° values with the R^2 values higher than 0.998. On the basis of the MNDO-PM3 calculations, experimental data and statistical analysis, a new semi-empirical method, the PM3-SC method, has been developed to estimate ΔH_f° of hydrocarbon free radicals. The PM3-SC method can be used to estimate the ΔH_f° for almost all hydrocarbon radicals, including primary-alkyl, secondary-alkyl, tertiary-alkyl, alkylenyl and aryl radicals. The PM3-SC method greatly improves the estimation accuracy and gives an average error of ± 0.453 kcal/mol only for the 46 hydrocarbon radicals, while the Benson's, BDE and MNDO-PM3 methods give the average error of ± 3.18 , ± 2.07 and ± 10.57 kcal/mol, respectively. The statistical analysis shows that with the PM3-SC method the difference between the experimental and estimated values is in the interval of ± 1.12 kcal/mol with 95 % confidence.

ACKNOWLEDGMENTS

This work was supported by the U.S. Department of Energy, Pittsburgh Energy Technology Center, and the Air Force Wright Laboratory/Aero Propulsion and Power Directorate, Wright-Patterson AFB. Funding was provided by the U.S. DOE under Contract DE-FG22-92104.

REFERENCES

1. Lias, S. G.; Bartmess, J. E.; Liebman, J. F.; Holmes, J. L.; Levin, R. D.; Mallard, W. G. *J. Phys. Chem. Ref. Data* **1988**, *17*.
2. Wayne, D. D. M.; Griller, D. *Free Radi. Thermochem.*; Tanner, D. D. Ed.; JAI Press Inc.: London, **1990**; Vol. 1, pp 159-192.
3. Seakins, P.; Pilling, M. J. *J. Phys. Chem.* **1992**, *96*, 9847-9855.
4. Benson, S. W. *Thermochemical Kinetics*; John Wiley & Sons: New York, London, Sydney, Toronto, 1976.
5. McMillen, D. F.; Golden, D. M. *Ann. Rev. Phys. Chem.* **1982**, *33*, 493-522.
6. Dewar, M. J. S.; Storch, D. M. *J. Am. Chem. Soc.* **1985**, *107*, 3898.
7. Stewart, J. J. P. *J. Comp. Chem.* **1989**, *10*, 209-220.
8. Stewart, J. J. P. *J. Comp. Chem.* **1989**, *10*, 221-264.
9. Camaioni, D. M.; Autrey, S. T.; Salinas, T. B.; Franz, J. A. *J. Am. Chem. Soc.* **1996**, *118*, 2013-2022.
10. Tsang, W. *J. Am. Chem. Soc.* **1985**, *107*, 2872-2880.
11. Freund, H. and Olmstead, W. N. *Intern. J. Chem. Kine.* **1989**, *21*, 561-574.
12. Tsang, W. *J. Phys. Chem.* **1986**, *90*, 1152-1155.

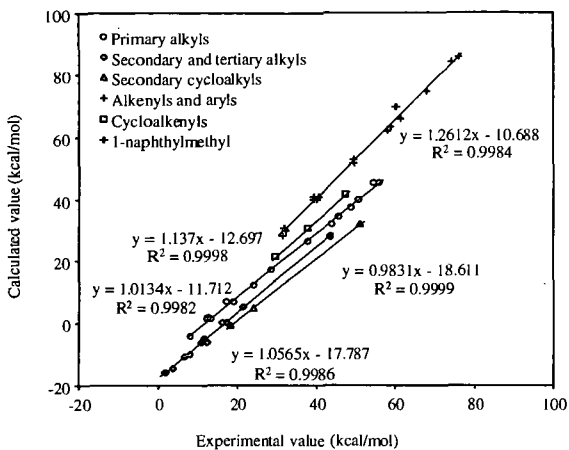


Figure 1 Correlation of MNDO-PM3-calculated ΔH_f° and experimental ΔH_f°

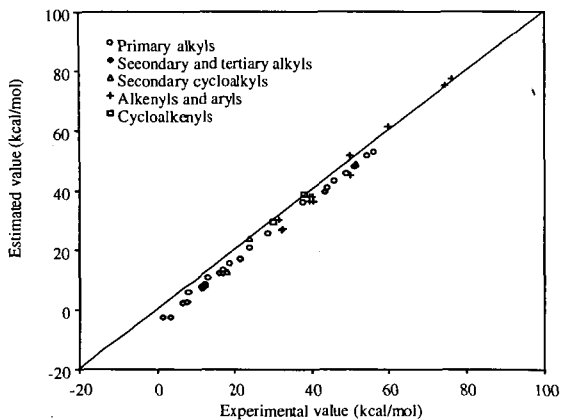


Figure 2 Benson-estimated ΔH_f° vs experimental ΔH_f° for hydrocarbon radicals

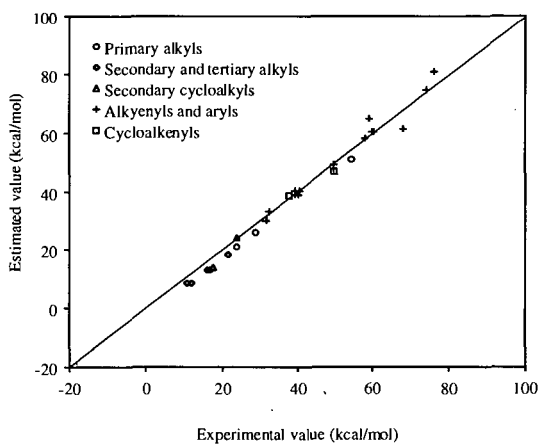


Figure 3 BDE-estimated ΔH°_f vs experimental ΔH°_f for hydrocarbon radicals

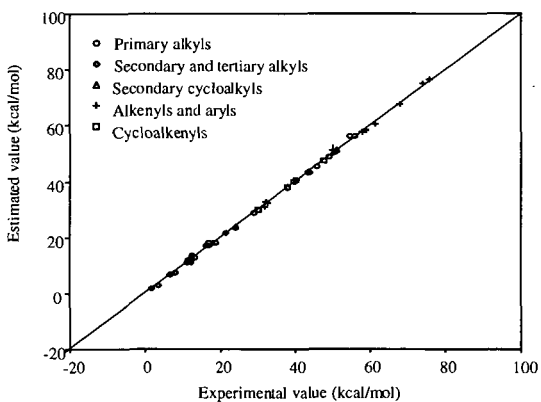


Figure 4 PM3-SC-estimated ΔH°_f vs experimental ΔH°_f for hydrocarbon radicals

ESTIMATING THE ACTIVATION ENERGY FOR HYDROGEN ABSTRACTION REACTIONS BY A SEMIEMPIRICAL CALCULATION

Xiaoliang Ma, and Harold H. Schobert
The Energy Institute, The Pennsylvania State University,
University Park, PA 16802

KEYWORDS: hydrogen abstraction, activation energy, molecular simulation

INTRODUCTION

Free radical processes play very important roles in thermal chemistry in combustion, petroleum and coal coking, coal liquefaction and pyrolysis, oil shale retorting, thermal stability of fuels as well as free radical polymerization. One of the most important elementary reactions in free radical processes is hydrogen abstraction, which involves hydrogen transfer from a hydrogen donor to a hydrogen acceptor (a radical). In a companion paper [1], we have reported our approach to estimating the heats of formation of hydrocarbon radicals. In this paper, we will report our approach to the kinetics of free radical reactions. This work is focused on the estimation of activation energy (E_a) for hydrogen abstraction reactions. To obtain the activation energy of hydrogen abstraction reactions is very essential for the fundamental understanding of hydrogen transfer mechanism, and for the evaluation of hydrogen-donation abilities of hydrogen donors and hydrogen-acceptation ability of radicals. However, experimental methods to determine the activation energy are complicate and difficult, as the radicals are very unstable. Molecular simulation approaches to the hydrogen abstraction reactions have been reported [2-5]. By using the MNDO-PM3 method, Camaioni et al. calculated the heats of formation of the transition states ($\Delta H_f^\circ(\text{TS})$) for 22 hydrogen abstraction reactions [6]. From the correlation of experimental and calculated $\Delta H_f^\circ(\text{TS})$ values, they obtained a linear regression equation:

$$\Delta H_{f,\text{calcd}}^\circ(\text{TS}) = 1.143\Delta H_{f,\text{exptl}}^\circ(\text{TS}) - 8.256 \text{ kcal/mol} \quad (1)$$

In the present study, our objective was to develop a new method for estimating the activation energy (E_a) of the hydrogen abstraction reactions between hydrocarbon radicals and hydrocarbon compounds on the basis of the MNDO-PM3 calculation, experimental data from the literature, transition-state theory and statistical analysis.

COMPUTATIONAL METHODS

All quantum chemistry calculations in this study were performed by using a semiempirical method, MNDO-PM3 method [7,8], in CAChe MOPAC, Version 94. Geometry of the radicals was optimized by using EF method, and the corresponding heats of formation (ΔH_f°) of hydrocarbon free radicals were estimated by the method reported in the other our paper [1]. Geometry of the transition states was located by using the Saddle Calculation method followed by the Minimize Gradient method, and the corresponding $\Delta H_f^\circ(\text{TS})$ was calculated. Calculation of the activation energy is based on the transition-state theory:

$$E_a = \Delta H^\ddagger + (1-\Delta\nu^\ddagger) RT \quad (2)$$

The standard activation enthalpy (ΔH^\ddagger) was calculated by the equation (3):

$$\Delta H^\ddagger = \Delta H_f^\circ(\text{TS}) - \sum \Delta H_f^\circ \text{reactant} \quad (3)$$

For the bimolecular reaction, the $\Delta\nu^\ddagger$ value is -1.

SOURCES OF EXPERIMENTAL DATA

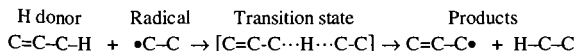
The experimental E_a values are from the available literature. As the data from different sources are somewhat inconsistent, we made the widest possible use of currently common and accepted experimental data. The main sources are from the reference 6 and 9. The experimental values of $\Delta H_f^\circ(\text{TS})$ were calculated by summing the activation enthalpy and ΔH_f° of the reactants:

$$\begin{aligned} \Delta H_{f,\text{exptl}}^\circ(\text{TS}) &= \Delta H^\ddagger + \sum \Delta H_f^\circ \text{reactant} \\ &= E_{a,\text{exptl}} - (1-\Delta\nu^\ddagger) RT + \sum \Delta H_f^\circ \text{reactant} \end{aligned} \quad (4)$$

RESULTS AND DISCUSSION

Hydrogen Abstraction Reaction

A representative hydrogen abstraction reaction of propene and ethyl radical is shown as follows:



In this reaction, ethyl radical (hydrogen acceptor) abstracts a hydrogen atom from propene (hydrogen donor). The corresponding configurations and spin densities for the reactants, transition state and products are shown in Figure 1. The TS structure has linear-centered C-H-C bonds with pyramidal C atoms intermediate between sp^2 and sp^3 with the bond length of 1.307 and 1.322 Å for $C_{\text{propene}}\text{-H}$ and $C_{\text{ethane}}\text{-H}$, respectively. The spin density indicates the location of the free radical (distribution of SOMO). In the TS structure, the radical is relocated on both C_{propene} and C_{ethane} atoms.

Heats of Formation of Transition States ($\Delta H^\ddagger(\text{TS})$)

The heats of formation of the transition states for 37 hydrogen abstraction reactions were calculated by the MNDO-PM3 method. The radicals involved in these reactions include alkyl, allyl and benzyl radicals.

As a whole, a considerable scatter exists, as shown in Figure 2 and 3, and the average error is ± 5.16 kcal/mol for the 37 transition states. However, we observed that the analogous reactions exhibit a very good linear correlation between experimental and calculated values. According to this observation, we can separate the 37 hydrogen abstraction reactions into 6 groups as follows:

Group	Radical	H donor
1	methyl	alkyl-H
2	methyl	alkenyl-H (or aryl-H)
3	ethyl (or propyl)	alkyl-H
4	ethyl (or propyl)	alkenyl-H (or aryl-H)
5	benzyl	alkyl-H or phenylalkyl-H
6	benzyl	partially hydrogenated polyaromatics

The least square fit was made for each group, with the R^2 values of 0.995, 0.999, 0.997, 0.995, 1.000 and 1.000, respectively. The group correlation reflects that the errors between PM3-calculated and experimental values are systematic and dependent on the reaction types. This finding allows one to be able to improve the accuracy of the estimates by scaling the $\Delta H^\ddagger(\text{TS})$ values calculated from MNDO-PM3 method. By using the regression parameters to scale the calculated $\Delta H^\ddagger(\text{TS})$, much accurate estimates are obtained with an average error of ± 0.33 kcal/mol for the 37 hydrogen abstraction reactions. We call this new method as PM3-systematical-correlation method (PM3-SC method).

Activation Energies for Hydrogen Abstraction Reactions

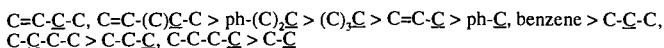
On the basis of the transition-state theory, the activation energies for the 37 hydrogen abstraction reactions have been estimated by the equation (2) using scaled $\Delta H^\ddagger(\text{TS})$ values. The estimated E_a in comparison with the experimental data from the literature are shown in Figure 4 for methyl, ethyl, propyl and benzyl as a hydrogen acceptor, respectively. In order to compare the errors from different estimation methods, the E_a values estimated by MNDO-PM3 method and Camaioni's method (using the linear regression (1) to scale the MNDO-PM3-calculated $\Delta H^\ddagger(\text{TS})$ values) are also shown in Figure 4. Statistical analysis of the errors for each method was conducted.

MNDO-PM3 method has an average error of ± 2.07 kcal/mol with the standard deviation of 2.71 kcal/mol. Camaioni's method shows lower average error than MNDO-PM3 method, being ± 1.69 kcal/mol with the standard deviation of 1.78 kcal/mol. In all three methods, our PM3-SC method gives the highest estimation accuracy with the average error of ± 0.24 kcal/mol and the standard deviation of 0.31 kcal/mol. In other words, with PM3-SC method, we can be 95 % confident that the difference between the estimated and experimental values is in the interval between -0.57 and $+0.63$ kcal/mol.

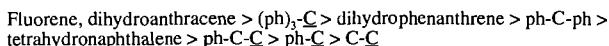
Evaluation of both Hydrogen-donation Ability of Hydrogen Donors and Hydrogen-acceptation Abilities of Radicals

The E_a value for hydrogen abstraction reactions is dependent on both the hydrogen-donation ability of hydrogen donors and the hydrogen-acceptation ability of the radicals. Using the same radical, the hydrogen-donation ability of the hydrogen donors is inversely proportional to the E_a ,

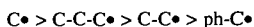
while using the same hydrogen donor, the hydrogen-accepting ability of the radical is inversely proportional to the E_a . Consequently, on the basis of analysis of the estimated E_a values for different hydrogen abstraction reactions, we can quantitatively evaluate both the hydrogen-donation ability of hydrogen donors and the hydrogen-accepting ability of radicals. By comparing the E_a values for hydrogen abstraction reactions with methyl radical as a hydrogen acceptor (the group 1 and 2), we can give the hydrogen-donation abilities of the hydrogen donors in the order as follows:



The underlined C atoms label the position of the donated hydrogen. By comparing the E_a values for hydrogen abstraction reactions with benzyl radical as a hydrogen acceptor (the group 5 and 6), we can give the hydrogen-donation abilities of other hydrogen donors in the order as follows:



On the other hand, by comparing the E_a values for hydrogen abstraction reactions using the same hydrogen donor (e.g. ethan) and different radicals, we can give the hydrogen-accepting abilities of the radicals in the order as follows:



Thus, we can use this method to expect quantitatively both the hydrogen-donation ability of other hydrogen donors and the hydrogen-accepting ability of other radicals.

CONCLUSIONS

After calculating $\Delta H^\ddagger(\text{TS})$ values for the 37 hydrogen abstraction reactions by MNDO-PM3 method and correlating them with the experimental data from the literature, it was found that the analogous reactions exhibit a very good linear correlation between experimental and calculated $\Delta H^\ddagger(\text{TS})$ values with the R^2 values higher than 0.994. On the basis of the MNDO-PM3 calculation, experimental data, transition state theory and statistical analysis, a new semiempirical method, PM3-SC method, has been developed to estimate the E_a for hydrogen abstraction reactions with an average error below ± 0.24 kcal/mol. The 95% confidence limits of the difference between the estimated and experimental E_a values is in the interval between -0.57 and +0.63 kcal/mol. The estimated E_a can be used to evaluate quantitatively the hydrogen-donation ability of hydrogen donors and the hydrogen-accepting ability of radicals.

ACKNOWLEDGMENTS

This work was supported by the U.S. Department of Energy, Pittsburgh Energy Technology Center, and the Air Force Wright Laboratory/Aero Propulsion and Power Directorate, Wright-Patterson AFB. Funding was provided by the U.S. DOE under Contract DE-FG22-921104.

REFERENCES

1. Ma, X. and Schobert, H. H. *Prep. Div. Fuel Chem., ACS* **1999**, in press
2. Yamataka, H., Nagase, S. *J. org. Chem.* **1988**, *53*, 3232-3238.
3. Chen, Y. and Tschuikow-Roux, E. *J. phys. Chem.* **1993**, *97*, 3742-3749.
4. Franz, J. A., Ferris, K. F., Camaioni, D. M. and Autrey, S. T. *Energy Fuels* **1994**, *8*, 1016-1019.
5. Logan, C. F. and Chen, P. *J. Am. Chem. Soc.* **1996**, *118*, 2113-2114.
6. Camaioni, D. M.; Autrey, S. T.; Franz, J. A. *J. Am. Chem. Soc.* **1996**, *118*, 2013-2022.
7. Stewart, J. J. P. *J. Comp. Chem.* **1989**, *10*, 209-220.
8. Stewart, J. J. P. *J. Comp. Chem.* **1989**, *10*, 221-264.
9. Allara, D. L. and Shaw, R. *J. Phys. Chem. Ref. Data* **1980**, *9*, 523

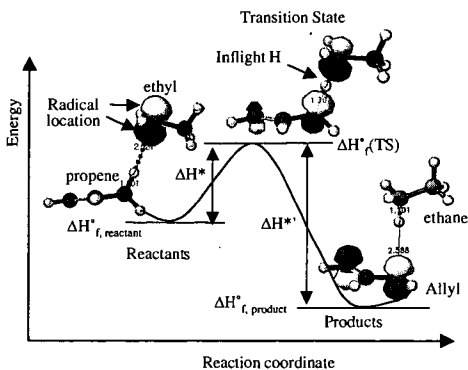


Figure 1 Configurations and spin densities for hydrogen abstraction reaction of propene and ethyl radical

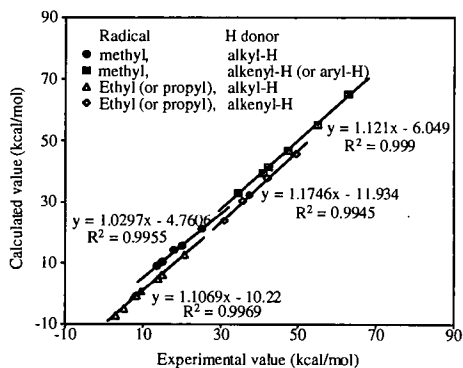


Figure 2 Systematic correlation of experimental and calculated $\Delta H^{\circ}_f(\text{TS})$ for H Abstraction with alkyl radicals as H acceptors

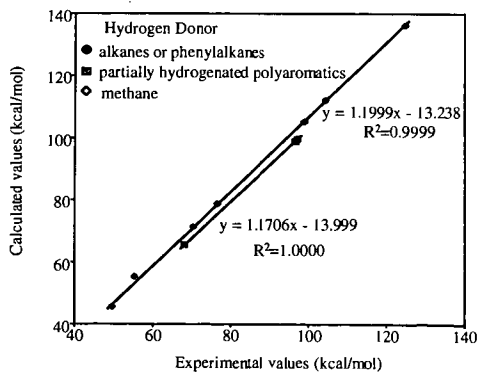


Figure 3 Systematic correlation of experimental and calculated $\Delta H^{\circ}_f(\text{TS})$ for H abstraction with phenyl radical as a H acceptor

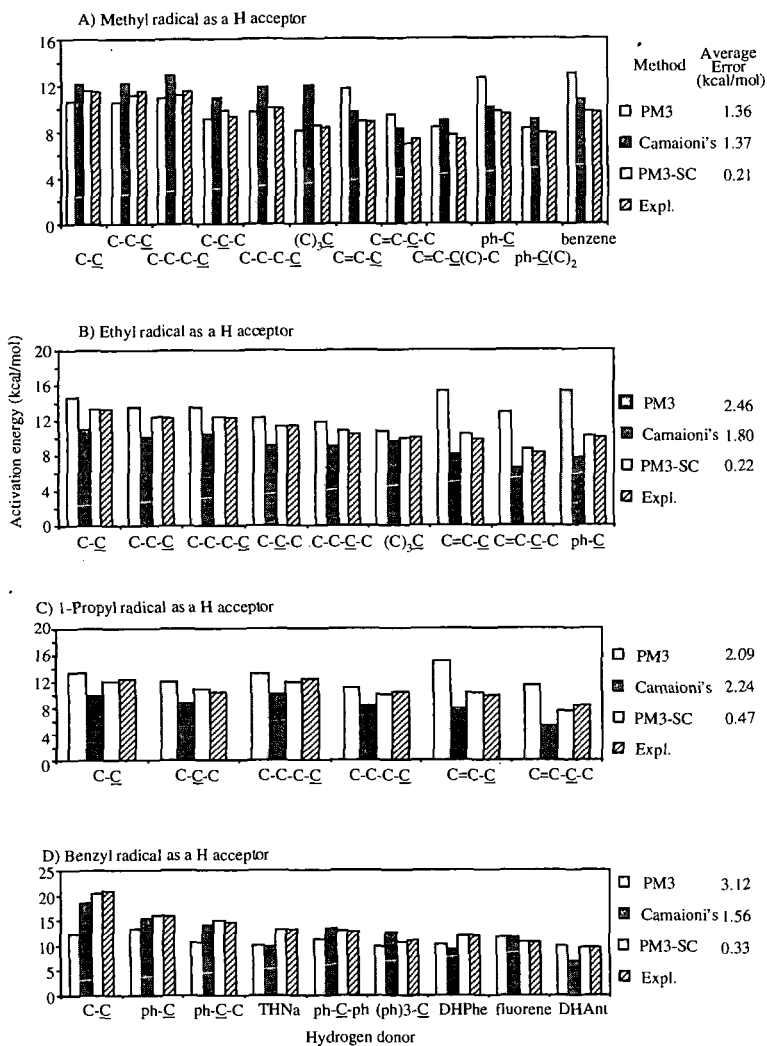


Figure 4 Experimental and estimated activation energies for H abstraction

MECHANISTIC INVESTIGATIONS INTO THE DECARBOXYLATION OF AROMATIC CARBOXYLIC ACIDS

Phillip F Britt,[†] A. C. Buchanan, III,[†] Thomas P. Eskay,[†] and William S. Mungall[‡]

[†]Chemical and Analytical Sciences Division, Oak Ridge National Laboratory,
MS 6197, P. O. Box 2008, Oak Ridge, Tennessee 37831 and

[‡]Department of Chemistry, Hope College, Holland, Michigan 49423

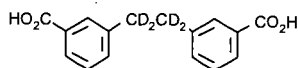
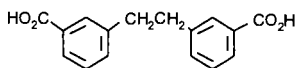
Keywords: Decarboxylation, Pyrolysis Mechanisms, Cross-Linking

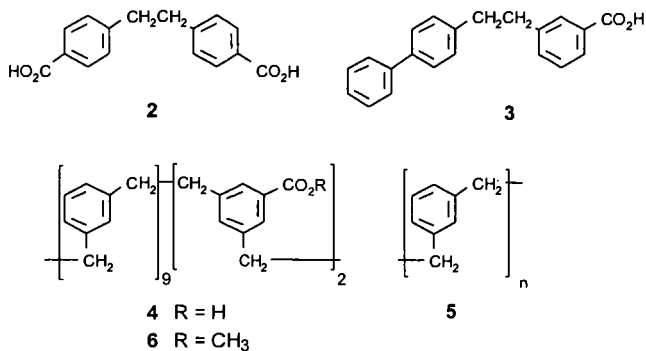
ABSTRACT

It has been proposed that carboxylic acids and carboxylates are major contributors to cross-linking reactions in low-rank coals and inhibit its thermochemical processing. Therefore, the thermolysis of aromatic carboxylic acids was investigated to determine the mechanisms of decarboxylation at temperatures relevant to coal processing, and to determine if decarboxylation leads to cross-linking (i.e., formation of more refractory products). From the thermolysis of simple and polymeric coal model compounds containing aromatic carboxylic acids at 250–425 °C, decarboxylation was found to occur primarily by an acid promoted ionic pathway. Carboxylate salts were found to enhance the decarboxylation rate, which is consistent with the proposed cationic mechanism. Thermolysis of the acid in an aromatic solvent, such as naphthalene, produced a small amount of arylated products (<5 mol%), which constitute a low-temperature cross-link. These arylated products were formed by the rapid decomposition of aromatic anhydrides, which are in equilibrium with the acid. These anhydrides decompose by a free radical induced decomposition pathway to form aryl radicals that can add to aromatic rings to form cross-links or abstract hydrogen. Large amounts of CO were formed in the thermolysis of the anhydrides which is consistent with the induced decomposition pathway. CO was also formed in the thermolysis of the carboxylic acids in aromatic solvents which is consistent with the formation and decomposition of the anhydride. The formation of anhydride linkages and cross-links was found to be very sensitive to the reactions conditions. Hydrogen donor solvents, such as tetralin, and water were found to decrease the formation of arylated products. Similar reaction pathways were also found in the thermolysis of a polymeric model that contained aromatic carboxylic acids. In this case, anhydride formation and decomposition produced an insoluble polymer, while the *O*-methylated polymer and the non-carboxylated polymer produced a soluble thermolysis product.

INTRODUCTION

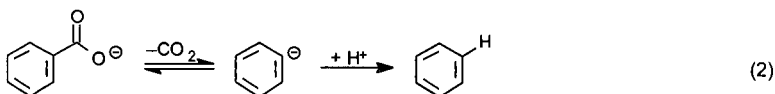
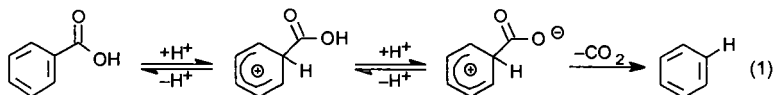
It has been proposed that carboxylic acids and carboxylates, which are prevalent in low-rank coals, are major contributors to retrograde reactions that inhibit efficient thermochemical processing of low-rank coals. In the pyrolysis and liquefaction of low-rank coals, low-temperature ($T < 400$ °C) cross-linking reactions have been correlated with the loss of carboxyl groups and the evolution of CO₂ and H₂O.^{1,2} Solomon et al. has modeled the pyrolytic loss of solvent swelling in coal by including one additional cross-link for every CO₂ evolved,^{2a,c} while Niksa has modeled the evolution rates and yields of oxygen bearing species by including char links when noncondensable gases (CO₂, H₂O, and CO) are expelled.^{2a} Pretreatments such as methylation or demineralization reduce cross-linking and CO₂ evolution in pyrolysis.^{2a,3,4} Exchange of Na⁺, K⁺, Ca⁺⁺, or Ba⁺⁺ into demineralized coals increase cross-linking and CO₂ evolution in pyrolysis and liquefaction.^{2,5} These results suggest that the reaction pathways that lead to decarboxylation may play an important role in the cross-linking of the coal polymer. However, the chemical pathways for decarboxylation of aromatic carboxylic acids are not understood at temperatures relevant to coal processing (300–450 °C).⁶ Therefore, to gain a better understanding of the role of decarboxylation in cross-linking reactions in low-rank coals, we have studied the liquid phase pyrolysis of simple (1–3) and polymeric (4–6) model compounds containing aromatic carboxylic acids from 250–425 °C (see below). These model compounds were chosen because aromatic carboxylic acids are known to exist in low-rank coals,⁷ their decarboxylation pathways can lead to cross-linking (see below), and homolysis of the weak bibenzylic bond provides a constant source of free-radicals that mimics some of the reactive intermediates found during the thermal processing of coal.⁸ Polymeric models were also investigated to study the impact of restricted mass transport on decarboxylation reaction pathways. A brief overview of the findings of these investigations will be presented as well as new data on pyrolysis of carboxylate salts.



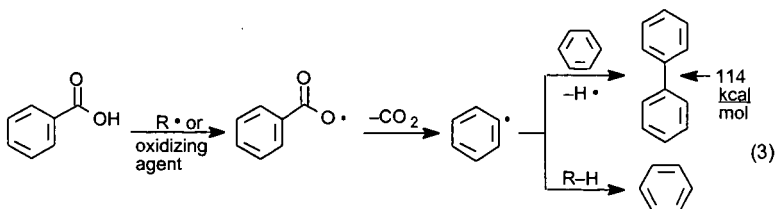


DECARBOXYLATION MECHANISMS

The reaction pathways for decarboxylation of aromatic carboxylic acids are surprisingly complex and dependent on the reaction conditions.⁹ The two major pathways for aromatic decarboxylation reactions are ionic and free radical. In aqueous solution, ionic decarboxylations can be catalyzed by acid or base. Acid-catalyzed decarboxylation reactions are the most common, and the reaction pathways are dependent on acid concentration, ionic strength, and substituents on the aromatic ring.⁹ In dilute acid, *ipso*-protonation of the aromatic ring is the rate-determining step (eq 1), while in highly acidic solutions, the rate determining step is decarboxylation of the aromatic cation. Electron donating substituents accelerate the acid-catalyzed decarboxylation reaction. In the absence of an acid-catalyst, decarboxylation of carboxylate salts or carboxylic acids with strongly electron withdrawing substituents, such as 2,4,6-trinitrobenzoic acid, occur by rate-determining unimolecular elimination of carbon dioxide from the anion (eq 2).



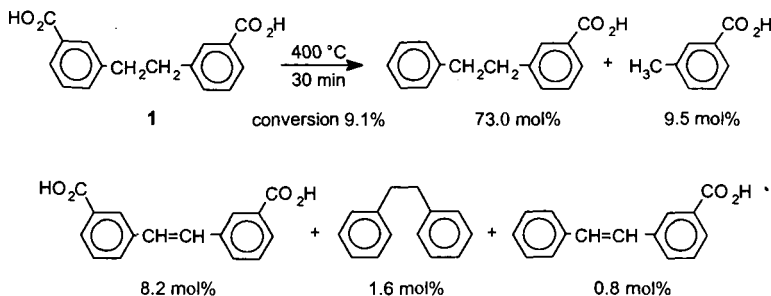
Decarboxylation of aromatic carboxylic acids can also occur by a free-radical pathway. Since free radicals are known to be formed as reactive intermediates in the thermolysis of coal, the free-radical decarboxylation pathway has been viewed as a possible route to cross-linking. Hydrogen abstraction or electron transfer to an acceptor¹⁰ can form the benzoyloxy radical (PhCO₂•) which will rapidly decarboxylate ($\log k \text{ (s}^{-1}\text{)} = 12.6 - 8.6 \text{ kcal mol}^{-1}/2.303RT$)¹¹ to form an aryl radical (eq 3). This highly reactive intermediate can abstract hydrogen or competitively add to an aromatic ring to form biaryls.¹² This aryl-aryl linkage is thermally stable at T = 400°C and would constitute a low-temperature cross-link.



PYROLYSIS OF THE ACID

The liquid phase thermolyses of 1,¹³ 2,¹³ 3,¹⁴ and substituted benzoic acids were conducted between 325-425 °C in sealed, degassed, Pyrex tubes. The reaction mixtures were silylated with *N,O*-bis(trimethylsilyl)trifluoroacetamide (since 1 and 2 were insoluble in most solvents) and quantitated by GC with FID. The products were identified by GC-MS and by comparison to authentic materials. Details of the experimental procedure can be found in references.^{13,14} For

all the compounds studied, decarboxylation was the major product from the thermolyses. Excellent mass balances were obtained in these thermolyses even at high conversion (for 1, 97% mass balance at 67% conversion) indicating that no significant amounts of high molecular weight products were undetected by the GC analysis. A typical product distribution from the thermolysis of 1 at 400 °C for 30 min (9.1% conversion) is shown below. Additional products



detected included 1,1-(3,3'-dicarboxyphenyl)ethane (4.6 mol%), 3-ethylbenzoic acid (1.3 mol%), 1-(3-carboxyphenyl)-1-phenylethane (0.3 mol%), and benzoic acid (0.1 mol%). The average conversion for a set of four 30 min thermolyses at 400 °C was $9 \pm 1\%$, and the average mass balance was $99 \pm 2\%$. At 400 °C, the apparent first-order rate constants for decarboxylation of 1, 2, and 3 at low conversion was $3.7 \pm 0.2 \times 10^{-5}$, $6.6 \pm 0.2 \times 10^{-5}$, and $2.8 \pm 0.7 \times 10^{-5} \text{ s}^{-1}$, respectively. The factor of two difference in the rate constant for decarboxylation of 2 relative to 1 and 3 indicates that the rate of decarboxylation is influenced by the position of the carboxyl group on the aryl ring (see below). The Arrhenius parameters for the apparent first-order rate constant for the decarboxylation of 1 to 1-(3-carboxyphenyl)-2-phenylethane was found to be $\log k (\text{s}^{-1}) = (9.4 \pm 0.4) - (43 \pm 1) \text{ kcal mol}^{-1}/2.303RT$. On the basis of the product distributions, mass balances, and decarboxylation rates, the decarboxylation of 1, 2, and 3 was proposed to proceed by an acid promoted, ionic pathway as shown in eq 1.

To provide additional evidence of the decarboxylation mechanism, the thermolysis of *p*-toluic acid and *p*-toluic acid-*d*₁ (*p*-CH₂C₆H₄CO₂D) were compared at 400 °C.¹⁵ The deuterium isotope effect $k_{\text{H}}/k_{\text{D}}$, determined from the average of four thermolyses on each substrate, was 2.1 ± 0.1 indicating that protonation of the aromatic ring is a rate-determining step (see below). The effect of electron donating substituents on the thermolysis of benzoic acid was also investigated at 400 °C in the liquid phase. As previously found, decarboxylation to the substituted benzene was the major product. A Hammett plot¹⁶ was constructed for the rate of decarboxylation (Figure 1), and a better linear correlation was obtained with σ^+ ($R = 0.999$) than with σ ($R = 0.950$). The slope (ρ) for the plot vs σ^+ was -5.2 indicating that a positive

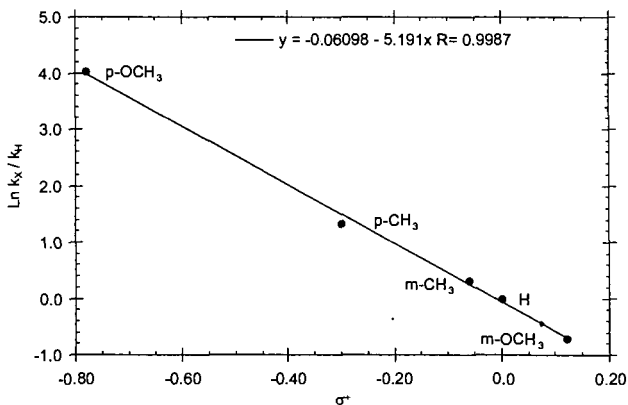
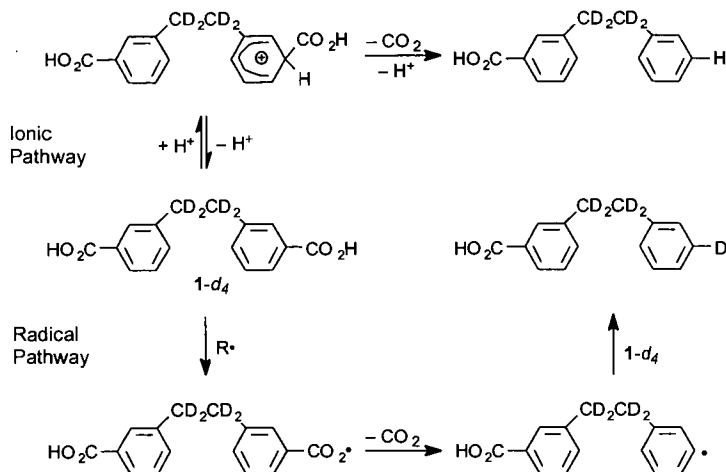


Figure 1. Hammett plot for the liquid phase thermolysis of substituted benzoic acids at 400 °C.

charge develops in the transition state in the decarboxylation, which supports the proposed cationic mechanism for decarboxylation. Since in low-rank coals all the aromatic rings are substituted with electron donating substituents, such as alkyl and oxygen functional groups,¹⁷ it is predicted that acid promoted decarboxylation reactions will be very rapid at 400 °C ($t_{1/2} < 30$ min).

To investigate the possibility that the free-radical pathway may also contribute to the decarboxylation reaction, the thermolysis of 1 containing deuterium in the ethylene bridge (1-*d*₄) was investigated.¹³ If decarboxylation proceeds by the acid-promoted ionic pathway, a *d*₄-monoacid will be produced, while a free-radical pathway would place a deuterium at the 3-position of the aromatic ring (from D abstraction by the aryl radical) to form a *d*₅-monoacid (Scheme 1).¹⁸ The thermolysis of 1-*d*₄ was performed at 325 °C and 400 °C, and the product distribution was similar to that reported for 1. At conversions ranging from 3-9%, GC-MS analysis of the 1-(3-carboxyphenyl)-2-phenylethane product showed no evidence of a *d*₅-species (<5%), based upon the comparison of the observed and calculated M⁺ and (M+1)⁺ peaks for the trimethylsilylated derivative of the *d*₄-monoacid. These data provide convincing evidence that decarboxylation of 1 is occurring predominantly by an ionic pathway in the neat liquid.

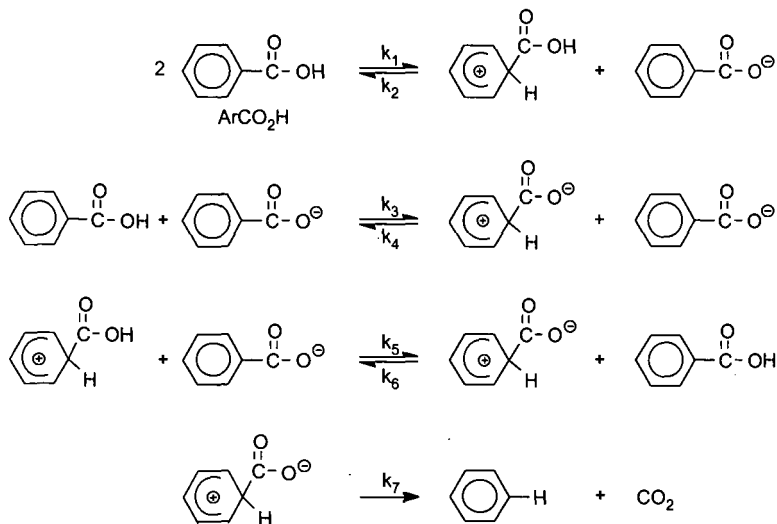


Scheme 1

PYROLYSIS OF CARBOXYLATE SALTS

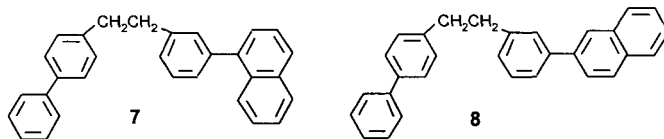
In coal, many of the carboxylic acids exist as carboxylate salts.¹⁹ Exchange of inorganic cations, such as Na⁺, K⁺, Ca⁺⁺, or Ba⁺⁺, into demineralized low-rank coals can significantly decrease liquefaction yields and increase cross-linking.^{2,5} For example, in the liquefaction of Zap lignite (400 °C, 30 min, tetralin, H₂), exchange of potassium cations into an acid demineralized coal decreased liquefaction yields 40% compared to the demineralized coal.^{3,4} Thermolysis of the dipotassium salt of 1 was investigated at 400 °C for 30 min neat, in tetralin, and in naphthalene.²⁰ No thermolysis products were detected and 1 was recovered unreacted (>99 mol%). Calcium benzoate was also found to be relatively stable at 400 °C (0.05% conversion to benzene in 1h). Addition of a small amount of water (1-3 equiv) to the reaction tubes did not significantly alter the conversions. However, if calcium benzoate was added to benzoic acid, the rate of decarboxylation increased. For example, the decarboxylation of benzoic acid increased by a factor of 7.7, 12.3 and 14.8 by the addition of 4.8, 11.1, and 15.1 mol% calcium benzoate, respectively. In the thermolysis of substituted benzoic acids, Manion et al. found that bases, such as pyridine, accelerated the decarboxylation of benzoic acid.¹⁰ It was proposed that decarboxylation occurred by the anionic mechanism (eq 2). However, the cationic mechanism is still consistent with these results (eq 1), and a new mechanistic pathway does not have to be invoked to rationalize these experimental results. In the decarboxylation of 4-aminobenzoic acids in dilute aqueous acid, it was concluded either *ipso*-protonation of the aromatic ring (k₁) or loss of the carboxyl proton (k₂) is wholly or partially rate controlling (Scheme 2).²¹ If the anion decarboxylates, protonation of the aromatic ring is rate controlling (k₃). Thus, if both *ipso*-protonation and proton loss from the carboxylic acid are rate controlling, the rate of decarboxylation would be accelerated for the carboxylate salt. This prediction was confirmed by Kaeding's study on the impact of benzoate salts on the decarboxylation of salicylic acid in benzoic acid at 200-230 °C.²² All the benzoate salts enhanced the decarboxylation rate, although the magnitude varied considerably with the metal. For example, the potassium, sodium, and calcium benzoate accelerated the decomposition of salicylic acid at 212 °C by a factor of 16.1, 10.7 and 6.3, respectively, and the decarboxylation rate was directly proportional to the concentration of the salt. Thus, decarboxylation of carboxylic acids and their salts can be described by the cationic mechanism shown in Scheme 2. In the presence of a weak base, carboxylate salts are formed and a similar series of reactions can be proposed. Moreover,

anilinium and pyridinium ions have been shown to catalyze the decarboxylation of salicylic acid.²³ Thus, a new mechanism does not have to be proposed for the base or salt catalyzed decarboxylation of aromatic carboxylic acids.



ANHYDRIDE FORMATION

The thermolysis of **3** was also studied in a non-hydrogen donor solvent, naphthalene, at 400 °C. In a 10-fold excess of naphthalene, the major products were the same as in the neat thermolysis except for the formation of two new minor products (<3 mol%) **7** and **8**, which constitute cross-linked products. Thermolysis of **1** and **2** in naphthalene also produced naphthylated products, but the yield of these products was ca. three times smaller than that for **3**.



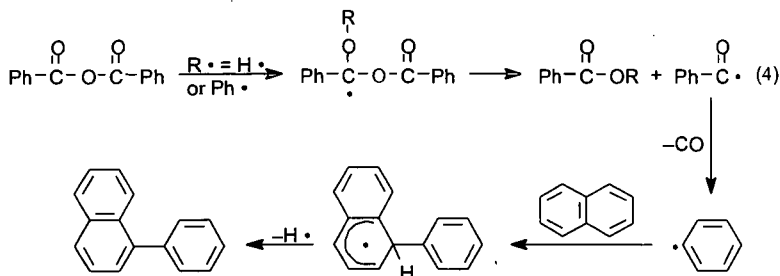
Arylated products were also found when biphenyl was used as the solvent, and 1- and 2-phenylnaphthalene were found in the thermolysis of benzoic acid in naphthalene. The formation of **7** and **8** were reduced by tetralin, a hydrogen donor solvent, indicating that the arylation reaction proceeded by a free radical pathway. The arylated products could also be reduced by small amounts of water (0.5-3 equiv).

The formation of small quantities of arylated products in the aromatic solvents was surprising on the basis of the liquid phase experiments. The yield of arylated products was found to be very sensitive to the reaction conditions and trace amounts of water, and at times, it was very difficult to obtain reproducible data. After the thermolysis of many model compounds had been investigated, it was concluded that the arylated products arise from formation and decomposition of aromatic anhydrides. In the thermolysis of benzoic acid in naphthalene (2.5 equiv) at 400 °C, a small amount of benzoic anhydride (ca. 1.4%) was observed in addition to benzene (1.2%), 1-phenylnaphthalene (0.06%), and 2-phenylnaphthalene (0.06%). When water (0.5 equiv) was added to the mixture of benzoic acid and naphthalene, benzoic anhydride was not observed. In the thermolysis of **3** in naphthalene, a small amount of the anhydride of **3**, (0.4%), was observed by HPLC and by LC-MS (by comparison with an authentic sample). These studies confirmed that anhydrides could be formed under the sealed tube reaction conditions used in this study and that small amounts of water minimize their formation.

Next, the thermolysis of the anhydrides were investigated since there was little literature information on the pyrolysis of aromatic anhydrides at moderate temperatures (<500 °C). It was discovered that the anhydrides decomposed very rapidly under the reaction conditions. The decomposition of benzoic anhydride (7.5% conversion) at 400 °C in naphthalene (10 equiv) was ca. 8 times faster than that for benzoic acid (0.97% conversion) under similar reaction

conditions. The major products from the thermolysis of benzoic anhydride in naphthalene were benzene (29.5 mol%), 1-phenylnaphthalene (40.4 mol%), 2-phenylnaphthalene (26.4 mol%) and phenyl benzoate (6.2 mol%). The anhydride of **3** also decomposed more rapidly than **3** (ca. 22-times faster) at 400 °C in naphthalene. The yield of arylated products was also shown to be sensitive to the nature of the aromatic acceptor (i.e., ease and reversibility of addition) and concentration of hydrogen donors.

The high conversions for the aromatic anhydrides were surprising. The C(=O)-O bond dissociation energy for benzoic anhydride was estimated as 84 kcal mol⁻¹.¹⁴ At 400 °C, C-O homolysis (to form the PhCO• and PhCO₂•) would not occur to any significant extent (<<1%). Therefore, it was proposed that the decomposition of the aromatic anhydride occurred by an induced homolysis reaction (eq 4), which has been observed in the decomposition of benzoyl



peroxide.²⁴ The induced decomposition is an addition-elimination reaction in which radicals add to the anhydride (most likely the C=O bond) and cleave to form a stable product, such as phenyl benzoate, and a new chain carrying radical, i.e., the benzoyl radical. The benzoyl radical will rapidly decarbonylate ($\log k \text{ (s}^{-1}\text{)} = 14.6 - 29.4 \text{ kcal mol}^{-1}/2.303RT$)²⁵ to form the phenyl radical. The phenyl radical can add to an aromatic ring to form an arylated product¹² and produce a hydrogen atom, which can continue the chain reaction.²⁶ The induced decomposition pathway also requires that more CO be formed than CO₂. In the thermolysis of benzoic anhydride and the anhydride of **3**, the ratio of CO:CO₂ was 3:1 and 25:1, respectively. The excess CO is consistent with the induced decomposition pathway and inconsistent with pure homolysis. In the thermolysis of acid **3** in naphthalene (10 equiv), the ratio of CO:CO₂ is 1:4. Thus, in the absence of water, small amounts of the aromatic anhydrides are in equilibrium with the parent carboxylic acid. Under free radical conditions, the anhydride undergoes a rapid free radical induced decomposition reaction, which produces aryl radicals that can lead to cross-linked products. Water and hydrogen donor solvents can reduce the yield of cross-linked products. However, can this sequence of reactions occur in the polymeric network structure of coal? To investigate this possibility, polymeric models of aromatic carboxylic in low-rank coals were prepared and their thermal chemistry investigated.

THERMOLYSIS OF POLYMER MODEL

The polymer model compound **4** was prepared with 2.3 acids per 100 carbons,²⁷ which is similar to the concentration of carboxylic acids in Beulah-Zap coal, 2.2 acids per 100 carbons.¹⁷ Overall, the TGA behavior of **4** is analogous to that reported for low-rank coals in which CO₂ evolution occurs prior to tar evolution and *O*-methylation reduces char yield (i.e., cross-linking).^{2,27} The carboxylated polymer **4**, forms ca. 2.4 times more char upon heating to 800 °C than the non-carboxylated polymer **5**. This indicates that the carboxylic acids are enhancing cross-linking in the polymer. Pyrolysis of **4** at 400 °C in a T-shaped tube, in which the volatile products are removed from the reaction, produced significant amounts of a THF insoluble residue (74 ± 2 wt%) independent of the thermolysis time (15-60 min). However, the thermolysis of **5** and **6** at 400 °C for 60 min produced a THF soluble residue. FTIR and solid-state ¹³C NMR analysis of the THF insoluble residue confirmed the presence of the aromatic anhydride linkage. Thermolysis of **4** in a sealed tube, in which the volatile products were not allowed to escape, produced a THF soluble product and no anhydride was observed by FTIR. Thus, aromatic anhydrides can form low-temperature cross-links that hold the polymer structure together. However, if the anhydride linkages were completely hydrolyzed (confirmed by FTIR), the polymer remained insoluble. It is proposed that the anhydride linkages in the polymer decompose by an induced decomposition reaction to form aryl cross-links as was observed for the simple model compounds. In support of this mechanism, CO evolution is observed in the TG-MS experiments before significant depolymerization of the polymer backbone occurs. Thus, the small amount of cross-linking observed in the simple model compounds is enhanced in the polymer models. However, the extent of anhydride formation and cross-linking is very sensitive to the experimental conditions and the presence of water. Can similar chemistry occur in the thermal processing of low-rank coal? To answer this question, additional characterization

studied are need on low-rank coals to determine if carboxylic acids form anhydrides during pyrolysis.

SUMMARY

The thermolysis of aromatic carboxylic acids was investigated to determine the mechanisms of decarboxylation at temperatures relevant to coal processing, and to determine if decarboxylation leads to cross-linking (i.e., formation of more refractory products). From the thermolysis of simple and polymeric coal model compounds containing aromatic carboxylic acids at 250-425 °C, decarboxylation was found to occur primarily by an acid promoted ionic pathway. Carboxylate salts were found to enhance the decarboxylation rate, which is consistent with the proposed cationic mechanism. Thermolysis of the acid in an aromatic solvent, such as naphthalene, produced a small amount of arylated products (<5 mol%), which constitute a low-temperature cross-link. These arylated products were formed by the rapid decomposition of aromatic anhydrides, which are in equilibrium with the acid. These anhydrides decompose by a free radical induced decomposition pathway to form aryl radicals that can add to aromatic rings to form cross-links or abstract hydrogen. Large amounts of CO were formed in the thermolysis of the anhydrides which is consistent with the induced decomposition pathway. CO was also formed in the thermolysis of the carboxylic acids in aromatic solvents which is consistent with the formation and decomposition of the anhydride. The formation of anhydride linkages and cross-links was found to be very sensitive to the reactions conditions. Hydrogen donor solvents, such as tetralin, and water were found to decrease the formation of arylated products. Similar reaction pathways were also found in the thermolysis of a polymeric model that contained aromatic carboxylic acids. In this case, anhydride formation and decomposition produced an insoluble polymer, while the *O*-methylated polymer and the non-carboxylated polymer produced a soluble thermolysis product.

ACKNOWLEDGMENT

This research was sponsored by the Division of Chemical Sciences, Office of Basic Energy Sciences, U.S. Department of Energy, under contract No. DE-AC05-96OR22464 with Oak Ridge National Laboratory, managed by Lockheed Martin Energy Research, Corp. T.P.E. was supported in part by an appointment to ORNL Postdoctoral Research Associates program administered jointly by Oak Ridge Institute for Science and Education and ORNL.

REFERENCES

- (a) Suuberg, E.M.; Lee, D.; Larsen, J.W. *Fuel* **1985**, *64*, 1668. (b) Suuberg, E.M.; Unger, P.E.; Larsen, J.W. *Energy and Fuels* **1987**, *1*, 305.
- (a) Solomon, P.R.; Serio, M.A.; Despande, G.V.; Kroo, E. *Energy and Fuels* **1990**, *4*, 42. (b) Ibarra, J.V.; Moliner, R.; Gavilan, M.P. *Fuel* **1991**, *70*, 408. (c) Solomon, P.R.; Best, P.E.; Yu, Z.Z.; Despande, G.V. *Prepr. Pap.-Am. Chem. Soc., Div. Fuel Chem.* **1989**, *34(3)*, 895. (d) Niksa, S. *Energy and Fuels* **1996**, *10*, 173.
- Serio, M.A.; Kroo, E.; Charpenay, S.; Solomon, P.R. *Prepr. Pap.-Am. Chem. Soc., Div. Fuel Chem.* **1993**, *38(3)*, 1021.
- Serio, M.A.; Kroo, E.; Teng, H.; Solomon, P.R. *Prepr. Pap.-Am. Chem. Soc., Div. Fuel Chem.* **1993**, *38(2)*, 577.
- Joseph, J. T.; Forria, T. R. *Fuel* **1992**, *71*, 75.
- Benzoic acid has been reported to decarboxylate by a unimolecular reaction (1,2-elimination) in the gas phase at 490 °C. Winter, K.; Barton, D. *Can. J. Chem.* **1970**, *48*, 3797.
- Hagaman, E.W.; Lee, S.K. *Energy and Fuels* **1995**, *9*, 727.
- The thermal chemistry of bibenzyl has been thoroughly studied, so the perturbation of the carboxyl substituent on the known reaction chemistry of bibenzyl can be determined. (a) Miller, R. E.; Stein, S. E. *J. Phys. Chem.* **1981**, *85*, 580. (b) Poutsuma, M. L. *Fuel* **1980**, *59*, 3357. (c) Stein, S. E.; Robaugh, D. A.; Alfieri, A. D.; Miller, R. E. *J. Am. Chem. Soc.* **1982**, *104*, 6567.
- (a) Taylor, R. In *Comprehensive Chemical Kinetics* Bamford, C.H.; Tipper, C.F.H. Eds.; Elsevier Publishing Co; New York, 1972; Vol. 13, pp 303-316. (b) Longridge, J. C.; Long, F. A. *J. Am. Chem. Soc.* **1968**, *90*, 3092.
- (a) Manion, J. A.; McMillen, D. F.; Malhotra, R. *Energy and Fuels* **1996**, *10*, 776. (b) Manion, J. A.; McMillen, D. F.; Malhotra, R. *Prepr. Pap.-Am. Chem. Soc., Div. Fuel Chem.* **1992**, *37(4)*, 1720.
- Chateaufneuf, J.; Luszyk, J.; Ingold, K. U. *J. Am. Chem. Soc.* **1988**, *110*, 2886.
- (a) Fahr, A.; Stein, S.E. *J. Phys. Chem.* **1988**, *92*, 4951. (b) Chen, R.H.; Kafafi, S.A.; Stein, S.E. *J. Am. Chem. Soc.* **1989**, *111*, 1418.
- (a) Eskay, T. P.; Britt, P. F.; Buchanan, III, A. C. *Energy Fuels* **1996**, *10*, 1257. (b) Eskay, T. P.; Britt, P. F.; Buchanan, III, A. C. *Prepr. Pap.-Am. Chem. Soc., Div. Fuel Chem.* **1996**, *41(2)*, 739.

- ¹⁴ (a) Eskay, T. P.; Britt, P. F.; Buchanan, III, A. C. *Energy Fuels* **1997**, *11*, 1278. (b) Eskay, T. P.; Britt, P. F.; Buchanan, III, A. C. *Prepr. Pap.-Am. Chem. Soc., Div Fuel Chem.* **1997**, *42(1)*, 20.
- ¹⁵ Toluic acid-*d*₁ was prepared by the hydrolysis of toulic anhydride with D₂O using the procedure described for preparation of benzoic acid-*d*₁ in: *Organic Syntheses with Isotopes. Part II*; Murray, A., III; Williams, D. L., Eds.; Interscience Publishers: New York, 1958; p 1279.
- ¹⁶ Isaacs, N. *Physical Organic Chemistry*, 2nd ed.; Longman Group: London, 1995; pp 149-187.
- ¹⁷ Jung, B.; Stachel, S. J.; Calkins, W. H. *Prepr. Pap.-Am. Chem. Soc., Div. Fuel Chem.* **1991**, *36(3)*, 869.
- ¹⁸ Abstraction of a deuterium from the ethylene bridge is thermodynamically favored based on benzylic C-H, aryl C-H, and the carboxy O-H bond strengths of 85, 111, and 101 kcal/mol, respectively. (McMillen, D. F.; Golden, D. M. *Annu. Rev. Phys. Chem.* **1982**, *33*, 493.) Furthermore, Fahr and Stein have shown that in the reaction of phenyl radicals with toluene-*d*₁ at 450 °C, >90% of the hydrogen abstraction from toluene occurs at the methyl position rather than from the aromatic ring.¹²
- ¹⁹ Kuznetsov, P. N.; Kuznetsova, L. I.; Bimer, J.; Salbut, P.; Gruber, R.; Brodski, D. *Fuel* **1997**, *76*, 189. For example, the ratio of free carboxylic acids to carboxylate salts is ca. 1:1 for Kansk-Achinsk brown coal.
- ²⁰ Eskay, T. P.; Britt, P. F.; Buchanan, III, A. C. *Prepr. Pap.-Am. Chem. Soc., Div Fuel Chem.* **1996**, *41(2)*, 1084.
- ²¹ Los, J. M.; Rekker, R. F.; Tonsbeek, C. H. T. *Recueil* **1967**, *86*, 622.
- ²² Kaeding, W. W. *J. Org. Chem.* **1964**, *29*, 2556.
- ²³ Willi, A. V. *Trans. Faraday Soc.* **1959**, *55*, 433.
- ²⁴ Koenig, T. In *Free Radicals*; Kochi, J. K., Ed.; John Wiley and Sons: New York, 1973; Vol 1, Chapter 3, p 116-118. Studies on the thermal decomposition of benzoyl peroxide (PhCO₂)₂ found that the rate of decomposition varied considerably from solvent to solvent while radical scavengers reduced the rate. It was determined that a chain reaction occurred in certain solvents in which the phenyl radical, formed from O-O homolysis followed by decarboxylation of the benzoyloxyl radical, could abstract hydrogen from the solvent. The solvent radicals would add to the benzoyl peroxide to form the benzoyloxyl radical and an ester. For example, in diethyl ether, 1-ethoxyethyl benzoate was isolated in 95% yield.
- ²⁵ Solly, R. K.; Benson, S. W. *J. Am. Chem. Soc.* **1971**, *93*, 2127.
- ²⁶ It is not known if a free hydrogen atom is eliminated or whether a radical hydrogen transfer (RHT) reaction occurs. In the thermolysis of aromatic aldehydes in naphthalene at 400 °C,¹⁴ significant quantities of benzyl alcohol were formed (and no significant quantities of other products expected from hydrogen atom chemistry, such as biphenyl, ethyl benzene, or benzene) which implies a RHT pathway.
- ²⁷ (a) Britt, P. F.; Mungall, W. S.; Buchanan, III, A. C. *Energy Fuels* **1998**, *12*, 660. (b) Mungall, W. S.; Britt, P. F.; Buchanan, III, A. C. *Prepr. Pap.-Am. Chem. Soc., Div Fuel Chem.* **1997**, *42(1)*, 26.

PREDICTIONS OF ACTIVITY PATTERNS FOR METHANE REFORMING BASED ON COMBINATORIAL PATHWAY GENERATION AND ENERGETICS

Raúl E. Valdés-Pérez

Computer Science Department, Carnegie Mellon University, Pittsburgh, PA 15213, USA

Ilie Fishtik

Department of Chemical and Biochemical Engineering, The University of Iowa,
Iowa City, IA 52242, USA

Andrew V. Zeigarnik

Laboratory of Chemical Kinetics and Catalysis, Lomonosov Academy of Fine Chemical
Technology, Moscow, 117571 Russia

ABSTRACT

We have applied the method to carbon formation in CO₂ reforming of methane over eight transition metals, starting with a list of 164 elementary steps and published UBI-QEP calculations of their activation energies and using the MECHEM program for combinatorial pathway generation. The predicted coking pattern Fe > Ni > Ru > Rh, Ir, Pd > Cu, Pt is consistent with experimental results from the literature. Current work focuses on deriving an activity pattern for the production of CO+H₂ in methane reforming.

INTRODUCTION

During the past decades, physical chemistry and surface science have provided a basis for understanding catalytic processes at the molecular level.¹ However, the search for active, stable, and selective catalysts for any given chemical process still remains largely empirical and is performed in the face of great uncertainty about most aspects of the process.² For example, ideally the choice of catalysts should rely on knowledge of the reaction mechanism and kinetics and of the physical properties and structure of the catalyst, promoters, and support, among others. However, usually neither the mechanism nor kinetics of elementary steps is known.

Recent advances in computational methods have enabled searching comprehensively for hypothetical reaction pathways³ and bulk calculations of activation energies and enthalpies of candidate elementary steps.⁴ A combination of these techniques holds the promise of increasing the suite of systematic tools that can guide catalyst design.⁵

This article reports an initial attempt to combine combinatorial pathway generation with energetics for the purpose of catalyst design. The method adopts MECHEM^{2,6-8} – a computer aid for mechanism elucidation. To develop the approach, we focused on predicting the relative coking properties of metal single-crystal catalysts for carbon dioxide reforming of methane. This choice is motivated by the availability of published data and by the importance of coking control in the conversion of natural gas to syngas.⁹ The method enables finding a list of “best” coking pathway/catalyst pairs, which are then used to construct a qualitative ranking of metals in their activity toward coking. The advantage of basing a predicted activity pattern on the relative barriers of pathways rather than the relative barriers of presumed rate-determining steps is that it removes the need to postulate rate-determining steps, which ultimately only make sense in the context of a larger pathway.

Our starting data, taken entirely from Ref. 4, consist of 164 elementary steps and their activation energies for eight transition-metal catalysts. The single-crystal catalysts were Cu(111), Ni(111), Pd(111), Pt(111), Rh(111), Ru(001), Ir(111), and Fe(110). Activation energies were calculated by the UBI-QEP method.¹⁰ The accuracy of the calculated activation energies was claimed to be about 2 kcal/mol.⁴

METHODS

Background on Computational Methods. MECHEM^{2,6-8} is an ongoing, multi-year project whose goals are to provide high level assistance for the elucidation or exploration of chemical reaction mechanisms. Technical details can be found in specialized journals.¹¹ The basic approach is to comprehensively search the possible elementary reactions and pathways in a “first principles” spirit. The principle involved is that an elementary step involves a small (user-adjustable) number of changes in the bonding of the reactants. Since in mechanism elucidation the reaction starting materials are known, MECHEM builds elementary steps of the form *known reactants* → X + Y and then solves for all possible structures of the unknowns X and Y by using ad-hoc graph algorithms and assuming, say, at most three or four total changes (cleavage or formation) to the connectivity of all the molecular graphs, including X and Y. One could contrast this “logical” approach to generating elementary steps with an alternative empirical approach that, say, only generates steps that follow specific reaction schemata such as migratory insertion, reductive elimination, radical recombination, dissociative adsorption, and so on. An advantage of the “first principles” or logical approach is that there is an enhanced potential for finding reaction mechanisms that otherwise would escape notice. After X and Y become specific species, the program

considers all possible second steps in a similar way. The "space" of possible pathways is simply the set of possible lists of such elementary steps. The only unchangeable built-in assumption in MECHEM is that all elementary steps have at most two reactants and at most two products.

The program organizes its search in stages of simplicity, by first trying to find mechanisms that involve fewer species and steps. A chemist/user drives the process by supplying assumptions, based on experimental evidence and background knowledge. These assumptions are in the form of constraints whose templates (about 120) are implemented and available for use.

Pathway/catalyst generation. To explore coking pathways in conformity with our source energetics data,⁴ we formulated the starting materials as CH₄(ads) and CO₂(ads) and the sole target product as monoatomic carbon. These species and all intermediates or by-products below are actually surface species, although their notation will not indicate this fact.

We made use of the 82 elementary steps (forward and reverse, totaling 164) and their activation energies over eight single-crystal transition metal catalysts reported by the cited authors. MECHEM was constrained to reject any generated step or species that was not on this list. Thus, there were $8 \times 164 = 1312$ separate activation energies or step/catalyst pairs.

To simplify the task, we excluded any step/catalyst pair whose activation energy exceeded 30 kcal/mol; these would be much less likely to enable good coking pathways. Thus, a new constraint was added to MECHEM that rejects any complete (or partially-constructed) pathway whose steps cannot all take place on one metal and still remain below the energy ceiling. Thus, a sequence whose first step was within the energy ceiling only for metals Fe and Ni, and whose second step was within ceiling only for Pt and Pd, would be discarded because their intersection was empty. The alternative would be to run the program once for each catalyst under consideration; but considering them jointly turns out to be more convenient.

Pathway selection criteria. We chose four measures of the likelihood that a pathway will lead to substantial coking; in all four cases, smaller values are better: (1) the number of pathway species; (2) the number of pathway steps; (3) for a specific metal, the maximum activation energy appearing in the pathway; (4) the maximum possible stoichiometric yield of carbon obtainable through the pathway, expressed as the *cost* in moles of CH₄ and CO₂ required to form 1 mole of surface carbon.

For the task of catalyst ranking, the preference for more concise pathways (having fewer species or steps) is justified as follows. The fewer pathway species, the fewer the opportunities for side reactions that diverge from coking; given N species, there are N^2 formally possible bimolecular and N unimolecular steps. In this article we do not include an explicit measure of the potential for side reactions, but a preference for fewer pathway species can deal somewhat with this issue.

The preference for fewer steps is justified by the uncertainty in the calculated activation energies. The more steps, the greater the chances of an (undetected) inaccuracy that would render bad a seemingly good pathway. If mistakes in the calculated energies occur with probability p and are independent, then the probability of a mistake for a pathway of length L equals $1 - (1 - p)^L$ which approaches unity exponentially with pathway length.

Measures of the pathway energy barrier more elaborate than a simple *maximum* could be used, and we have experimented with several of them, but here we opt for the simplest choice. The use of maximum activation barriers to characterize pathways assumes that the pathway step with the highest barrier is the slowest. The principled choice of slowest steps should be based on knowledge of surface species concentrations and preexponential factors, but these data are not available.

Finally, we need a measure of *how much* coking can be achieved via a given pathway. Lacking data on reaction rates, we will use a heuristic measure of "selectivity" that is based only on the plain pathway: the maximum possible yield of surface carbon that can be obtained by freely varying the pathway stoichiometric numbers, but keeping them non-negative. The problem of finding the maximum possible yield can be formulated as a linear optimization problem and solved with the simplex algorithm.¹² The basic ideas are to require one mole of carbon after a time t_1 , to express the possible concentration changes in terms of the stoichiometries of the individual steps, and then to minimize the "cost" (i.e., the molar amounts) of starting materials at the prior time t_0 . A by-product of the optimization is a stoichiometric number for each pathway step.

However, there is a subtlety in the cost measure. Since some steps are below the energy ceiling of 30 kcal/mol in both directions, we score pathways in two ways: (1) keeping the original forward direction of steps, and (2) augmenting the pathway with all the reversed steps that are within the energy ceiling. In the latter case, the *maximum energy* measure is calculated over the step directions that correspond to the positive stoichiometric numbers as determined by the linear optimization. If a stoichiometric number is zero, we consider the energy only of the forward direction.*

* This tactic is not absolutely correct, since it is possible that a more limited use of backward steps will lead to the most advantageous combination of energy and cost, in the sense of enabling a pathway to survive the comparisons described in the next section. However, given the small sizes of our pathways, we believe that this omission is not important.

Combining measures. We know of no principled way to combine these four measures or objectives into a single optimizable objective. However, since the formulation is equivalent to a multi-objective optimization problem, we can use the standard concept of a Pareto optimum. A Pareto optimum is a solution which is not dominated by any other solution; one solution dominates another if it is better on one of the objectives and is no worse on all the other objectives.

Thus, we will find all the Pareto optima, that is, those pathway/catalyst pairs that are not dominated by any other pair in the sense of minimizing the four objectives of steps, species, energy, and cost. We will iterate this procedure several times: after finding the first set (depth 0) of Pareto-optimal pathway/catalyst pairs, we will delete these solutions and all supersets of any of these pathways that involve the same catalyst and do not improve the score along one of the measures; then we collect the (depth 1) Pareto optima among the remaining pathway/catalyst pairs. By carrying out this procedure several times to a depth of 1 or 2, combined with deleting a metal after its place in the ranking is determined, we will obtain a ranked list of good coking pathway/catalyst pairs, together with its justification in terms of explicit coking pathways.

Generating pathways of increasing complexity. MECHEM's task is to generate all the simplest (fewest species or steps) mechanisms that can form the declared products or intermediates from the starting materials, while respecting any user-specified constraints. (Here, the constraints are that (1) only steps from our list of 164 elementary steps are allowed, and (2) the activation energy of any directed step must be within 30 kcal/mol.) However, we need to generate not just the simplest mechanisms, but all mechanisms over some range of complexity.

One *reject-supersets* approach to this problem was used earlier:⁶ after finding N simplest mechanisms, an artificial constraint is activated which rejects any future mechanism that contains within itself any of the N previous mechanisms. At the next run the program will not stop after finding the same N mechanisms, but instead will search for more complex mechanisms that are guaranteed a degree of novelty with respect to the previous runs. The *reject-supersets* approach has a drawback, though. Consider the schematic pathway $A \rightarrow X + Y$, $2X \rightarrow T$, which has four species, two steps, some maximum activation energy, and a cost in the starting material of A equal to 2. No more complex pathway will be allowed to contain this two-step pathway, so the three-step pathway $A \rightarrow X + Y$, $2X \rightarrow T$, $Y \rightarrow X$ will never be considered, even though its cost would be reduced to 1 from the previous 2. (Of course, the steps are increased and the maximum activation energy could rise.) Thus, it is possible that we could miss a good pathway.

A second approach to the problem of generating more complex pathways is simply to reject any future mechanism that contains exactly S species and R steps, where S and R describe the last batch of pathways found. This *more-complex-pathways* approach avoids the cited drawback of the *reject-supersets* approach, but suffers from a potential combinatorial explosion in the number of pathways.

The entire procedure, while somewhat detailed, has been largely automated and is the same from one reaction to the next.

RESULTS

We generated coking pathways by repeatedly using the *more-complex-pathways* approach until a run generated over one thousand pathways; then we switched to the *reject-supersets* approach. We continued collecting pathways up to a limit of seven species not counting CH_4 , CO_2 , and C . The result was a total of 11678 pathways (all the computations were done in a few hours on a 300 MHz, 64Mb laptop computer).

Each pathway was evaluated according to the four measures *steps*, *species*, *energy*, and *cost* over each of the eight catalysts. As explained above, sometimes a pathway/catalyst pair gave rise to two sets of scores, depending on whether pathway steps were allowed to have positive stoichiometric numbers in the backwards direction. The total ensuing number of pathway/catalyst scores was 99267.

The first three sets of Pareto-minimal pathways are shown below. Each step is annotated with its activation energy, and following the listed metal are the scores: number of extra *species*, number of *steps*, maximum activation *energy* barrier, and the minimum *cost* in moles of starting material that is stoichiometrically obtainable via the pathway.

Depth 0

1. CO_2 -[4.5] \rightarrow O + CO
 2. $2(\text{CO})$ -[0.9] \rightarrow CO_2 + C
- Fe, species = 2, steps = 2, energy = 4.5, cost = 1

Depth 1

1. CO_2 -[6.7] \rightarrow O + CO
 2. $2(\text{CO})$ -[6.4] \rightarrow CO_2 + C
- Ni, species = 2, steps = 2, energy = 6.7, cost = 1

Depth 2

1. CH_4 + CO_2 -[8.1] \rightarrow HCOO + CH_3
2. HCOO -[3.2] \rightarrow OH + CO
3. CO_2 + OH -[3.5] \rightarrow HCOO + O

4. $2(\text{CO}) - [0.9] \rightarrow \text{CO}_2 + \text{C}$
Fe, species = 5, steps = 4, energy = 8.1, cost = 1

1. $\text{CH}_4 + \text{CO}_2 - [8.1] \rightarrow \text{HCOO} + \text{CH}_3$

2. $\text{HCOO} - [3.2] \rightarrow \text{OH} + \text{CO}$

3. $2(\text{CO}) - [0.9] \rightarrow \text{CO}_2 + \text{C}$

Fe, species = 4, steps = 3, energy = 8.1, cost = 3

1. $\text{CO}_2 - [12.7] \rightarrow \text{O} + \text{CO}$

2. $2(\text{CO}) - [3.9] \rightarrow \text{CO}_2 + \text{C}$

Ru, species = 2, steps = 2, energy = 12.7, cost = 1

We judged that Fe is the single best coking metal, because it possesses the best overall solution (at depth 0) and is backed up by two more pathways at depth 2 that, unlike the first solution, make use of interactions between CH_4 and CO_2 . The next step is to delete Fe from further consideration and consider the seven remaining metals.

After Fe, the best catalyst appears to be Ni, which is followed in turn by Ru. After repeated minimizations to some depth, followed by excluding from further consideration the metals which we judged to be the next best, we obtained the results summarized below.

Take all metals

Depth 0: 1 Fe pathway \Rightarrow Depth 1: 1 Ni pathway \Rightarrow Depth 2: 2 Fe and 1 Ru pathways

Conclude: Fe is best. Exclude Fe

Depth 0: 1 Ni pathway \Rightarrow Depth 1: 3 Ru and 1 Rh pathways \Rightarrow Depth 2: 18 pathway/catalyst pairs (5 Ni)

Conclude: Ni is best after Fe. Exclude Fe, Ni

Depth 0: 3 Ru and 1 Rh pathways

Conclude: Ru is best after Fe, Ni. Exclude Fe, Ni, Ru

Depth 0: 23 pathways (9 Ir, 8 Pd, 6 Rh)

Conclude: Ir, Pd, Rh are best after Fe, Ni, Ru. Exclude Fe, Ni, Ru, Ir, Pd, Rh

Depth 0: 10 pathways (8 Pt, 2 Cu)

Conclude: Pt, Cu are the two worst

Our overall ranking of metals based on this detailed analysis of coking pathways is: Fe > Ni > Ru > Rh ~ Ir ~ Pd > Cu ~ Pt. Thus, according to the available elementary steps and activation energies, Fe and Ni favor coke formation the most, and Cu and Pt the least.

DISCUSSION

Comparison of results with literature. Coke deposition on metals from both CH_4 and CO_2 or their mixtures is a very complex process.^{13,14} Catalyst resistance to coking strongly depends on the nature of the support^{15,16} and promoters,^{17,18} which is one reason why direct comparisons of coking for various transition metals have not been carried out. Another reason is that noble metals are expensive and industry prefers to use promoted nickel catalysts instead, which are the focus of most studies. So, there is scarce experimental precedence for comparing our predictions to empirical results.

The only reliable qualitative conclusion about carbon deposition in CO_2 reforming of methane that we are able to discern from numerous experimental investigations is that the noble metals (Pd, Rh, Ru, Ir, and Pt) are generally less susceptible to coke deposition than Fe, Co, and Ni.¹⁹ Our findings are in complete agreement with this pattern, as well as with the data that stability of carbides decreases from iron to nickel, with copper carbide unknown.²⁰

Interestingly, Trimm⁹ discusses an activity pattern Fe > Ni > noble metals for steam reforming that is consonant with our results and with the cited pattern of Arutyunov and Krylov.¹⁹ This consonance supports the Rostrup-Nielsen conjecture that the steps of both mechanisms are similar.²¹

Limitations. We have not considered coke removal, only its formation. The data on activation energies⁴ suggest that the coke-removal rate must be very high: the activation energies for the step $\text{CO}_2 + \text{C} \rightarrow \text{CO} + \text{CO}$ are zero for Cu, Ni, Pd, Pt, Rh, and Ir, 1.1 for Ru, and 6.1 kcal/mol for Fe. The Pareto-minimal pathways show that the highest energy barriers among coke formation steps are usually higher. Thus, the lowest (most competitive) energy barrier of the Pareto-minimal pathway at depth 0 is 4.5 kcal/mol. This suggests that coke formation is competitive with coke removal only on Fe (4.5 vs. 6.1 kcal/mol), whereas coke is removed faster than it is formed on the other metals. This obviously contradicts the common knowledge that on Ni, coke is formed faster than it is removed, which is why promoters are used in Ni-based catalysts. Assuming that relative activation energies are a satisfactory heuristic guide to the relative rates of steps, we conjecture that carbon polymerization on the surface and carbon-metal phase formation are faster processes than coke removal. Thus, the monoatomic carbon formed in our coking pathways is consumed by these fast, undesirable processes. So, the more that a pathway/catalyst pair favors coke formation, the more chances that the catalyst will be poisoned with coke.

We did not consider adsorption/desorption steps, which may slightly affect the result.

We are considering only the formation of monoatomic surface carbon, and not the solubility of carbon in the bulk of the metal. The available information on the solubility of carbon in metals somewhat correlates with our ranking of metals: Fe > Ni > noble metals¹⁹ and Rh > Pd > Ru > Ir > Pt (maximum solubility data)²⁰. Also, the data reported by Hei *et al.*⁴ were calculated at zero coverage and we inherit this limitation. A future step will be to re-calculate all the data at higher coverages and refine current data.

Of course, real catalysts are more complicated, due to nonzero surface coverage effects, formation of various carbon-metal phases, carbon dissolution in the bulk, diffusion processes, transformations of monoatomic carbon into polymeric carbon and vice versa, and so on. However, to the extent that some of these complicating effects can be captured in the formulation of elementary steps and their energetic barriers, our method will be able to accommodate them.

Finally, we also neglected preexponential factors and did not try to simulate the kinetics of any of these pathways. Further step will be to estimate preexponential factor using transition state theory.

CONCLUSIONS

We have proposed the combinatorial generation of pathway/catalyst pairs, screened for conciseness, energetics, and stoichiometry, as a computational method for ranking alternative catalysts with respect to a given target property, here, coking in CO₂ reforming of methane. The input to the method is a list of possible elementary steps and their energetics, and the output is a ranking of catalysts augmented with pathway-oriented justifications for the ranking. Rankings and pathways such as these can complement other approaches to catalyst design, e.g., those whose assumed starting point is a serviceable reaction mechanism.

We also started the work on the future use of this method for the ranking of metals in the main reaction: CO₂ + CH₄ → CO + H₂ and on improving the selectivity and activity criteria. One of these criteria is based on the calculation of the apparent activation energy as a function of the surface coverages for intermediate species. Preliminary results of this work show that Ir, Ru, and Rh are best among eight catalyst considered here. Cu, Pd, and Pt are worse than others. Fe and Ni hold an intermediate position.

Our findings on metal catalyst coking for CO₂ reforming are relevant to steam reforming since the list of steps is largely identical for both processes.²¹

REFERENCES

- (1) Somorjai, G. A.; Zaera, F. *J. Phys. Chem.* **1982**, *86*, 3070.
- (2) Cardenas-Galindo, M.; Aparicio, L. M.; Rudd, D. F.; Dumesic, J. A. In *Computer-Aided Design of Catalysts*; Becker, E.; Pereira, C., Eds.; Marcel Dekker: New York, 1993.
- (3) Zeigarnik, A. V.; Valdes-Perez, R. E.; Temkin, O. N. *Langmuir* **1998**, *14*, 4510.
- (4) Hei, M. J.; Chen, H. B.; Yi, J.; Lin, Y. J.; Lin, Y. Z.; Wei, G.; Liao, D. W. *Surf. Sci.* **1998**, *417*, 82.
- (5) Becker, E.; Pereira, C. In *Computer-Aided Design of Catalysts*; Becker, E.; Pereira, C., Eds.; Marcel Dekker: New York, 1993.
- (6) Zeigarnik, A. V.; Valdes-Perez, R. E.; Temkin, O. N.; Bruk, L. G.; Shalgunov, S. I. *Organometallics* **1997**, *16*, 3114.
- (7) Bruk, L. G.; Gorodskii, S. N.; Zeigarnik, A. V.; Valdes-Perez, R. E.; Temkin, O. N. *J. Mol. Catal. A: Chem.* **1998**, *130*, 29.
- (8) Zeigarnik, A. V.; Valdes-Perez, R. E.; White, B. S. *J. Chem. Educ.*, in press.
- (9) Trimm, D. L. *Design of Industrial Catalysts*; Elsevier: New York, N.Y., 1980.
- (10) Shustorovich, E.; Sellers, H. *Surf. Sci. Rep.* **1998**, *31*, 1.
- (11) (a) Valdes-Perez, R. E. *J. Comput. Chem.* **1992**, *13*, 1079; (b) Valdes-Perez, R. E. *J. Comput. Chem.* **1993**, *14*, 1454; (c) Valdes-Perez, R. E. *J. Comput. Chem.* **1994**, *15*, 1266.
- (12) Valdes-Perez, R. E. *J. Phys. Chem.* **1991**, *95*, 4918.
- (13) Rostrup-Nielsen, J. R. In *Catalysis - Science and Technology*, Vol. 5; Anderson, J.; Boudart, M., Eds.; Springer Verlag: Berlin, 1984.
- (14) Bradford, M. C. J.; Vannice, M. A. *Catal. Rev. - Sci. Eng.* **1999**, *41*, 1.
- (15) Bradford, M. C. J.; Vannice, M. A. *Appl. Catal. A: General* **1996**, *142*, 73.
- (16) Sodesawa, T.; Dobashi, A.; Nozaki, F. *React. Kinet. Catal. Lett.* **1979**, *12*, 107.
- (17) Trimm, D. L. *Catal. Today* **1999**, *49*, 3.
- (18) Haliche, D.; Bourab, R.; Cherifi, O.; Bettahar, M. M. *Catal. Today* **1996**, *29*, 373.
- (19) Arutyunov, V. S.; Krylov, O. V. *Oxidative Conversion of Methane*; Nauka: Moscow, 1998 (in Russian).
- (20) Joyner, R. W.; Darling, G. R.; Pendry, J. B. *Surf. Sci.* **1988**, *205*, 513.
- (21) Rostrup-Nielsen, J. R.; Bak Hansen, J. H. *J. Catal.* **1993**, *144*, 38.
- (22) Savitskii, E. M.; Polykova, V. P.; Gorina, N. B.; Roshan, N. R. *Physical Metallurgy of Platinum Metals*; Moscow: Metallurgiya, 1975 (in Russian).

MAGNETIC IMAGING OF FCC FEEDSTOCKS TO MODEL ASPECTS OF THEIR CRACKING KINETICS AND PRODUCT SLATES

P.S. Virk

Department of Chemical Engineering
M. I. T., Cambridge, MA 02139

KEYWORDS: Magnetic Resonance, Catalytic Cracking, Modelling.

INTRODUCTION

Motivation. This work reports on a system for the Magnetic Imaging of FCC Feedstocks, acronym MIFF, that is being devised to model the fundamental chemical aspects of their cracking kinetics and product slates. It is motivated by the need to engineer, and predict the performance of, fluidized cat crackers using modern catalysts to crack ever heavier feeds at ever increasing reaction severities and gasoline selectivities under ever closer environmental scrutiny. NMR imaging adds a unique dimension to FCC feed characterization because of its intimate relation to molecular topology. Thus acid catalysts can crack virtually all the C-C bonds in hydrocarbons except those either within or adjacent to aromatic rings and NMR can directly detect these uncrackable sp²-hybridized aromatic core carbons and their adjacent sp³ benzylic carbons, providing the asymptotic extent to which a feedstock can be cracked and proffering insights into the structures of the product fragments.

Background. Of the voluminous literature on NMR applied to hydrocarbon mixtures, the present work has most been influenced by the classic papers of Knight (1967), Shoolery and Budde (1976) and Deutsche, Jancke and Zeigan (1976), specific articles by Ladner and Snape ((1978), Gillet et al (1981), Netzel et al (1981), and especially Cookson and Smith (1985, 1987), and the texts by Stothers (1972), Breitmaier and Voelter (1987) and Croasmun and Carlson (1994). Earlier efforts relevant to FCC feeds include Bouquet and Bailleul (1986), who used the methods of Cookson and Smith (1985) to assay carbons by their attached protons; Mauleon et al (1987), who devised a coke factor from carbon aromaticity; and a recent note based on the present work (Kim et al 1998) which applied NMR to enhance conventional and mass spectrometric characterizations.

MIFF SYSTEM

Figure 1 schematically depicts the three facets of the MIFF system, sample preparation, NMR experiments, and data analysis. In sample preparation, internal standards are gravimetrically incorporated into the FCC feedstock oils, typically VGOs and ATBs, to enable precise analysis and interpretation of the NMR experiments. Three internal standards are used, namely, deuteriochloroform CDCl₃, as oil solvent and spectrometer lock; dioxane, C₄H₈O₂, abbr DIOX, to assist in spectral integrations; and tetramethylsilane, Si(CH₃)₄, abbr TMS, as a spectral frequency reference. The primary NMR experiments performed provide quantitative C13 and H1 spectra, the spectral regions and individual resonances observed therein being identified and interpreted by additional 1-D and 2-D procedures that include DEPT, COSY, HETCOR, and HMQC. Spectral data are analysed in two trains, according to either their integral regions, abbr IR, or their canonical groups, abbr CG. In the IR train, the observed spectra are parsed into more or less coarse regions, each comprising chemically similar sorts of atoms. The IR train accounts for 100% of feedstock atoms and provides useful overall parameters, such as the percent of feedstock atoms, either carbon or hydrogen, that are aromatic. In the CG train, certain groups of spectral peaks that arise from atoms belonging to particular molecular moieties are recognized, particularly those in n-alkane straight chains and in 2-, 3-, 4-, 5-, and interior-methyl alkane branched chains. The CG train thus provides high-level quantitative information about certain molecular species; however the sum of identified species is but a fraction of the total, typically amounting to ~ 40% of feedstock atoms. Outputs from the coarse but complete IR train and the fine but fractional CG train are shown in the bottom row of Figure 1. The IR train provides carbon and hydrogen aromaticities, as well as more detailed regional data, and thence hydrogen atom counts, and thermochemical information. The CG train detects n-alkane content and chain length, as well as the contents of a variety of methyl-alkane moieties. Both trains are combined to form a set of NMR groups that characterize the feedstock.

NMR EXPERIMENTS

13-C. Figure 2 shows the 13-C NMR spectrum of a VGO feedstock called V2 in Table 1 (infra). The position of a peak on the x-axis, its resonance frequency or chemical shift, c, in units of ppm relative to TMS, is indicative of C atom type, while peak height on the y-axis, its absorption intensity, i, with arbitrary units, is roughly proportional to the abundance of such C atoms in the sample. Precise carbon atom amounts are obtained from peak integration, these integrals being the five continuously increasing stepped segments in the figure, their c-domains and magnitudes being noted below the abscissa. The major spectral regions observed are:

Region	c (range)	C-atom type
TMS	0.0	methyl carbons in TMS
Cal	10 - 52	aliphatic carbons in feedstock, sp ³ hybridized
DIOX	~67	methylene carbons in DIOX
CDCl ₃	~78 triad	C in CDCl ₃ solvent
Car	112 - 150	aromatic carbons in feedstock, sp ² hybridized

The wide separation between the regions of aliphatic and of aromatic carbons is noteworthy, allowing unambiguous delineation of these two broad categories; the integrals corresponding to these regions provide the carbon aromaticity $Car = 16.8\%$. Further demarcations shown below the spectrum, called Cumulative Integral Regions, sort carbon atoms into categories with the following approximate chemical interpretations: Carqt is aromatic quaternary, which are inherently of two kinds, either fused ring junction or substituted, not distinguished here; Carpi and Carpo are both aromatic protonated, the i and o being subtle distinctions between them; the sum $Car(qt+pi+po) = Car$. Among aliphatic carbons, Calhs is aliphatic highly substituted, Calbr is aliphatic branched (single substitution, such as methyl), Calch is aliphatic chains, mainly CH₂, and Calme is aliphatic methyls, all CH₃. Many additional individual spectral regions can be distinguished in Figure 2, and these have been labelled beside their principal peaks as follows: Regions B, D, H, and G (two tall peaks at $c \sim 30$) respectively contain the carbon atoms C1, C2, C3, and (C4, C25) in linear n-alkane chains. Region C contains mainly methyl groups, pendant on a variety of alkane, cyclo-alkane and aromatic structures. Regions E and F contain carbon atoms in C5- and C6-cyclo-alkane rings, as well as C2 in 2-methyl-alkanes. Regions A, I, J and K contain carbon atoms from branched (iso-) alkanes. Peaks of the n-alkane moiety in regions B, D, H, and G, called a Canonical Group, reveal the present VGO to possess an n-alkane chain content of 17.1 C atoms per 100 C atoms of feedstock, with an average chain length $L = 7.8$, that is, for every set of terminal n-alkane atoms (C1, C2, C3), there are 4.8 interior n-alkane atoms (C4, C25).

1-H. Figure 3 shows the 1-H NMR spectrum of VGO feedstock V2. The x-axis is resonance frequency, or chemical shift, h , in units of ppm relative to TMS, indicative of hydrogen type, while the y-axis is absorption intensity, i , with arbitrary units, approximately proportional to the abundance of such hydrogen atoms in the sample. Accurate hydrogen amounts are obtained from integrals of peak intensities, seen as four continuous stepped lines in the figure, their h-domains and numerical magnitudes noted below the abscissa. The 1-H spectrum has the following regions:

Region(s)	h (range)	H-atom type
TMS	0.0	H in methyls of TMS
Hgam, Hbet, Hbzy	0.4 - 3.2	aliphatic H, attached to sp ³ hybridized C atoms
DIOX	~ 3.65	H in methylenes of DIOX
Har	6.5 - 9.2	aromatic H, attached to sp ² hybridized ring C atoms

The wide separation between the regions of aliphatic and of aromatic hydrogens is noteworthy, permitting their unambiguous delineation, and providing the hydrogen aromaticity $Har = 4.1\%$. The Cumulative Integral Regions, shown below the spectrum, have the following approximate chemical interpretations. The aromatic H region is subdivided into Hart, Hard, and Harm, with sum $Har(t+d+m) = Har$; of these, Harm contains H atoms from all aromatic rings; Hard contains H atoms from ≥ 2 - but not from 1-ring aromatics; and Hart contains H atoms from ≥ 3 - but not from ≤ 2 -ring aromatics. Next, Hbzy are benzylic H atoms, attached to aliphatic C atoms bonded to aromatic rings; Hbzy thus reflects the degree of aromatic ring substitution. Of the two broad benzylic peaks in the spectrum, $\alpha 1$ is mainly H atoms on methyls pendant on mono-aromatic rings, while $\alpha 2$ contains a host of other benzylic hydrogens. Hbet are H atoms attached to aliphatic C atoms bonded to other aliphatic C atoms; region Hbeta, with huge peak $\beta 1$, is primarily H atoms in the methylene CH₂ units of alkyl chains, while Hbetb includes H atoms on CH (methine) and CH₂ (methylene), the peaks $\beta 1$, $\beta 2$ including H atoms on alicyclic rings. Hgam, with large twin peaks γ , are H atoms in aliphatic methyls CH₃.

2-D HETCOR. Figure 4 is a 2-dimensional contour plot showing the islands in an H-C atom correlation spectrum of VGO feedstock V2. The HETCOR experiment, described by Gray (1994), is the equivalent of recording full 1-H spectra, such as shown in Figure 3, at each of a myriad slices of a 13-C spectrum, such as shown in Figure 2. A correlation island at chemical shift coordinates $[c, h]$ represents a carbon of shift c connected to a hydrogen of shift h , with island cross-section (actually, its peak height and volume) crudely related to the abundance of the correlated atoms in the feedstock. In Figure 4, with abscissa (F2 axis) c and ordinate (F1 axis) h , the large lens-shaped island #3 at coordinates $[c, h] = [14.2, 0.89]$ arises from the H and C atoms in the terminal methyl group of an n-alkane chain and is so labelled. Numerous other islands are also visible in the figure, with those that have been chemically identified being labelled in three rows respectively representing methyl CH₃, methylene CH₂, and methine CH carbons. Identified islands belong to the following Canonical Groups: n-alkane (C1, C2, C3, C4, C25), 2-methyl alkane (C1, C2, C3), 3-methyl alkane (C1, Me, C3), 4-methyl alkane (C1, C3), and interior-methyl alkane (Me, Cj(unction)). The present HETCOR spectrum had a dynamic range, that is, the ratio of tallest peak height/noise level, of 615, and the 30 islands in Figure 4 resulted from a contour threshold about 3 times higher than the noise level. Decreasing the threshold to 1.5 times noise resulted in 58 islands, of which 23 could be identified, revealing the additional moieties: 4-methyl alkane (C1, C2, C3, C4), 5-methyl alkane (C2, C4), interior-methyl alkane, including phytyl, (Me, Cj, Cj+1, Cj+2, Cj+3), alkyl-cyclo-C6-alkane (Me, Cr(ing)), and alkyl-benzene (C3).

RESULTS

Table 1 presents data from both conventional and MIFF characterizations of six representative FCC feeds, four VGOs V1 to V4 and two ATBs A1 and A2.

Conventional properties include gravity, Conradson carbon residue, and elemental assays of H, C, S, N, from which H elem, H atoms/100 C atoms, has been calculated.

MIFF data, from top to bottom, show results from the IR and CG trains; for samples run in duplicate, average values and an estimate of their experimental uncertainty are both quoted. Among IR train C13

data, the two rows labelled diox/oil are the ratios of carbon atoms in the dioxane internal standard to those in the oil; the gravimetric row was calculated from sample preparation and elemental assays while the spectral row is independently derived from the regional integrals of the experimental spectra. Agreement between these internal standard ratios is a stringent test of C13 NMR data fidelity. The next row, Car, and then the next seven rows, called CIRs for Cumulative Integral Regions, provide a breakdown of feedstock carbon atom types, as percentages. CIRs are so named because each is the accumulation of Detailed Integral Regions, DIRs, which represent the finest parsing of spectral integrals. The chemical significance of Car and the CIRs was earlier considered in connection with the 13-C NMR spectrum in Figure 2. The last row, H count, H / 100 C, is derived from the DIRs by summing the products of DIR amount times the number of H atoms per C atom of the type contained therein. Data from the IR train H1 are analogous to those from the IR train C13, with two diox/oil rows, gravimetric and spectral, followed by Har and then seven CIRs, whose chemical significance was earlier considered with the 1-H NMR spectrum in Figure 3. Finally, the first row of the CG Train C13 provides the average chain length of n-alkane moieties in the feedstock, Lna in C atoms. The second and third rows of the CG train respectively provides the percentages of C atoms in n-alkane moieties Cna, and in methyl-alkane moieties Cma, the latter comprising 2-, 3-, 4-, 5-, and interior-methyl substituted alkane chains. These are used, along with Car from the IR train, shown again in the fifth row, to form a final set of 4 NMR-derived canonical groups for each feedstock. The group Ccs in the fourth row, comprising cyclic and highly substituted aliphatic C atoms, is a (large) remnant obtained from $Ccs = 100 - Cna - Cma - Car$.

Dioxane/Oil Ratios. Figure 5 compares the internal standard ratios of dioxane to oil D/O,g from the gravimetric sample preparation procedure to those derived from spectral integration D/O,s. Data from C13 and H1 spectra are respectively differentiated by large solid and small hollow symbols in the plot and by suffixes c and h in the legend. Linear regression of these data, shown by the dashed line in the figure, yields:

$$(E1) \quad D/O,s = (0.00 \pm 0.01) + (1.08 \pm 0.06) D/O,g.$$

The present NMR integral measurements are accurate to within 8% absolute, with a precision of $\pm 6\%$ relative to one another. Such quantitative fidelity is a tribute to modern NMR spectrometers, which can evidently excite and detect diverse kinds of C and H atoms in the feedstock over wide frequency ranges on both sides of the C and H atoms in the dioxane internal standard.

MIFF Maps. MIFF data in Table 1 provide an aromaticity map, Car vs Har, and an n-alkane chain map, Cna vs Lna, of relevance to FCC performance as discussed in the next section. The aromaticity map showed $Har \approx 0.3 Car$, from which, using feedstock H content $\approx 172 H/100 C$, there are typically 51 aromatic H atoms/100 aromatic C atoms, that is, 51% of the aromatic carbons are protonated. The other 49% of the aromatic carbons must therefore be quaternary, and from the benzylic H atoms we estimate 19% of these to be substituted, so the remaining 30% are fused, at ring junctions. The n-alkane chain map showed that VGO and ATB feedstocks typically possess $[Cna, Lna] = [17 \pm 3, 9 \pm 1]$, with the highest observed content $Cna = 40$ and the longest $L = 12$.

Carbon Atom Groups. The upper panels of Figure 6 present NMR-derived carbon atom groups as pie charts for feedstocks A1 and V4. Each pie has four slices [Cna, Cma, Ccs, Car], respectively the percentages of n-alkane, methyl-alkane, alicyclic + highly substituted, and aromatic carbon atoms in the feedstock. The variations in pie slices between A1 and V4, the former containing more n-alkanes and possessing the lower aromaticity, anticipate differences between their performances in FCC units. By way of comparison, the lower panels of Figure 6 show mass spec-derived data for each of A1 and V4, using the high-resolution electron impact methods described by Fisher (1986, 1990). Mass spec data are compressed into four groups of decreasing Z-numbers [Wpar, Wcyp, Wmono, Wdih], respectively the weight percentages of paraffins, n- and iso- ($Z = 2$), cyclo-paraffins, mono-, di-, tri- and higher ($0 \geq Z \geq -4$), mono-aromatics ($Z = -6$), and di- and higher-aromatics ($Z \leq -8$). The preceding characterizations differ fundamentally in that NMR distinguishes individual atoms by their bonding environment, without regard for the host molecules they inhabit, whereas mass spectrometry distinguishes whole molecules within homologous series of formula C_nH_{2n+Z} . By joint use of the MIFF and mass spec pies we can ascertain $(Wmono + Wdih - Car)$, the aliphatic carbons associated with the aromatic core carbons, which respectively amount to 16% and 29% for A1 and V4, rather larger than Car itself. The methyl-alkane group Cma of MIFF has no analogue in mass spec data because the latter does not distinguish n- from iso-paraffins, both having the same $Z = 2$. Finally, it is curious that, despite their different chemical origins, the n-Alkane content Cna from MIFF and the paraffin content Wpar from the mass spec are numerically within $\pm 2\%$ of one another for each of A1 and V4, and this rough equality between Cna and Wpar also holds for all the other oils in Table 1.

MODELLING FCC PERFORMANCE

Theoretical Basis. Figure 7 depicts the possible relation of our NMR-derived characterizations of a feedstock to its FCC performance, comprising conversion kinetics and products, using data for oil V4. MIFF groups $[Cna, Cma, Ccs, Car] = [19.7, 8.8, 54.2, 17.4]$ are shown in the uppermost ribbon, with segments proportional to their respective abundances. IR train H1 data were used to slightly elaborate Car and Ccs, with aromatic core C atoms classified by their ring sizes, mono-, di-, and tri-+higher, and the benzylic C atoms pendant upon such rings shown as a (small) subset of Ccs. The kinetics of cracking the MIFF groups under acid-catalysed conditions with carbenium ion intermediates are depicted in the

second ribbon from the top, based on the works of Nace (1969), Venuto & Habib (1979), and Pines (1981). N-alkane chains, comprising mainly secondary carbons, are amenable to acid cracking, but with modest kinetics that are further a function of chain length; methyl-alkanes and most of the alicyclic + substituted group crack rapidly, on account of reactive tertiary carbons within them; the entire aromatic core group and the benzylic portion of the Ccs group are not cracked at all. The third ribbon depicts potential products from complete conversion of the feedstock by acid-catalysed cracking only. Gas + gasoline products arise from n-alkanes, methyl-alkanes, alicyclic + substituted carbons excluding the benzylic di- and tri- segments, and mono-aromatics. Light cycle oil LCO is related to the di-aromatic group and to the benzylic carbons attached to di-aromatics, while decant oil + coke DO+C is associated with tri- and higher aromatics and their benzylic carbons. For the present feedstock V4, MIFF data provide potential product yields of $[GG^*, LCO^*, DO+C^*] = [85.4, 6.7, 7.9] C/100 C$. Actual product yields from FCC of V4 at commercial conditions are shown in the bottom ribbon, being $[Gas, Gasoline, LCO, DO, Coke] = [20.4, 43.7, 19.2, 11.6, 5.1] wt\%$. The actual yield of gas + gasoline = 64.1 is appreciably lower than the asymptotic maximum $GG^* = 85.4$ inferred from MIFF, with the actual yields of LCO and DO+Coke correspondingly higher than the asymptotic LCO^* and $DO+C^*$. These differences reflect both kinetic constraints on conversion as well as the operation of additional catalytic reaction paths, such as hydrogen transfer and polymerization, in parallel with the dominant acid cracking path.

Decant Oil + Coke Yields. As an example of how MIFF parameters might be employed to model the yields of FCC products, Figure 8 is a 3-dimensional plot of observed DO+Coke yields, wt%, on a MIFF aromaticity map of Har, H/100 H vs Car, C/100 C. The data can be seen to ascend from the origin at near lower left roughly along a diagonal toward the far upper right. A projection of the observed relationship on the x-z plane reveals that $DO+C \approx 0.9 Car$, about twice as large as the theoretically expected from the parameter $DO+C^*$ computed in Figure 7.

Overall Cracking Kinetics. The overall kinetics of feedstock conversion in the riser of an FCC unit have been considered by Weekman & Nace (1970) whose model, with Voorhies' (1945) expression for coke deposition on the catalyst, can be used to derive the overall cracking rate constant k_0 from operating conditions and observed conversions. The observed k_0 are then normalized to standard residence time τ and temperature T K to provide an apparent cracking rate constant ko^* characteristic of the feedstock. Figure 9 is a 3-D plot of ko^* on a MIFF n-alkane chain map of Lna, C atoms, vs $Cna, C/100 C$, for four FCC feeds, two each VGOs and ATBs, that possessed roughly the same specific gravities, $SG = 0.903 \pm 0.004$, and carbon aromaticities $Car = 15 \pm 1$. Three of these feeds, with chain lengths $8.6 \leq Lna \leq 10.1$ and n-alkane contents $18 \leq Cna \leq 40$, exhibit $ko^* \approx 0.15$, whereas the fourth, with $Lna = 10.6, Cna = 33$ has an appreciably lower $ko^* = 0.10$. These data imply that feedstock conversion kinetics may be retarded by n-alkane chains longer than a critical $Lna^* \approx 10.3$. More extensive data are needed to verify and define a critical (Lna^*, Cna^*, ko^*) surface for kinetic retardation, though it is interesting that Nace (1969) reported the cracking kinetics of pure n-alkanes to reach a maximum at $Lna = 8$ (hexadecane) and then decline for longer chains.

ACKNOWLEDGEMENTS: This work was initiated and supported by Larry Hallee, late of the Stone & Webster Engineering Corporation, Houston, TX. The author is indebted to Jeanne Owens of the MIT Spectrometry Laboratory, for help with NMR spectra, as well as Mike Silverman and Atulya Saraf of Stone & Webster, for discussions of Mass Spec and FCC.

REFERENCES

- Knight, S.A.: Chem. Ind., 1920-1923 (1967).
 Shooley, J.N.; Budde, W.L.: Anal. Chem., **48**, 1458-1461 (1976).
 Deutsch, K.; Jancke, H.; Zeigan, D.: J. Prakt. Chem. Ind., **318**, 177-184 (1976).
 Ladner, W.R.; Snape, C.E.: Fuel, **57**, 658-662 (1978).
 Gillet, S.; Rubini, P.; Delpuech, J.J.; Escalier, J.C.; Valentin, P.: Fuel, **60**, 221-225 (1981).
 Gillet, S.; Rubini, P.; Delpuech, J.J.; Escalier, J.C.; Valentin, P.: Fuel, **60**, 226-230 (1981).
 Netzel, D.A.; McKay, D.R.; Heppner, R.A.; Guffey, F.D.; Cooke, S.D.; Varie, D.L.; Linn, D.E.: Fuel, **60**, 307-320 (1981).
 Cookson, D.J.; Smith, B.E.: Anal. Chem., **57**, 864-871 (1985).
 Cookson, D.J.; Smith, B.E.: Energy & Fuels, **1**, 111-120 (1987).
 Stothers, J.B.: "Carbon-13 NMR Spectroscopy", Academic Press, New York, NY 1972.
 Breitmaier, E.; Voelter W.: "Carbon-13 NMR Spectroscopy: High-Resolution Methods and Applications", 3rd Ed., VCH Publishers, Weinheim, Germany, 1987, pp73-105.
 Croasmun, W.R.; Carlson, R.M.K.: "Two-Dimensional NMR Spectroscopy: Applications for Chemists and Biochemists", 2nd Ed., VCH Publishers, Weinheim, Germany, 1994.
 Bouquet, M.; Bailleul, A.: Fuel, **65**, 1240-1246 (1986).
 Mauleon, J.L.; Sigaud, J.B.; Biedermann, J.M.; Heinrich, G.: Proc. 12th World Petroleum Congress, Houston TX, [18], 1-7, Wiley, London (1987).
 Kim, H.N.; Verstraete, J.J.; Virk, P.S.; Fafet, A.: Oil & Gas J., **96** (37) 85-88 (1998).
 Gray, G.A., Ch 1, pp 46-49 in Croasmun, W.R.; Carlson, R.M.K.: "Two-Dimensional NMR Spectroscopy: Applications for Chemists and Biochemists", 2nd Ed., VCH Publishers, Weinheim, Germany (1994).
 Fisher, I.P.: Fuel, **65**, 473-479 (1986).

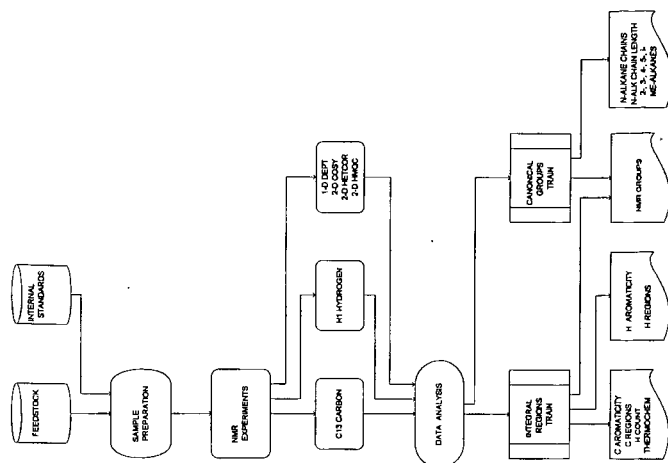
- Fisher, I.P.: Appl. Catalysis, **65**, 189-210 (1990).
 Nace, D.M.: Ind. Eng. Chem., Prod. Res. Dev., **8**, 31 (1969).
 Venuto, P.B.; Habib, E.T.: "Fluid Catalytic Cracking with Zeolite Catalysts", Marcel Dekker, Inc., New York, (1979).
 Pines, H.: pp1-122 in "The Chemistry of Catalytic Hydrocarbon Conversions", Academic Press, New York, (1981).
 Weekman, V.W.; Nace, D.M.: A.I.Ch.E. J., **16**, 397-404 (1970).
 Voorhies, A.: Ind. Eng. Chem., **37**, 318 (1945).

TABLE I. Conventional and MIFF Characterizations of Representative FCC Feedstocks.

Oil		V1	V2	A1	A2	V3	V4
CONV DATA							
API	deg	26.8	24.0	25.5	25.1	20.6	23.4
SG	15.6C	0.894	0.910	0.901	0.903	0.930	0.914
CCR	wt%	-	-	2.62	2.96	0.42	0.27
Elemental Assay							
H	wt%	12.91	12.50	12.94	12.54	12.14	12.47
C		86.63	86.28	86.60	87.08	85.52	86.65
S		0.44	1.03	0.50	0.28	2.22	0.98
N		-	0.19	0.20	-	0.20	0.11
H elem	H/100 C	177.6	172.6	178.0	171.6	169.1	171.5
MIFF DATA							
IR Train C13							
diox/oil	gravimetric	0.116	0.114	0.141 ± 0.000	0.141	0.024 * 0.143	0.094 ± 0.000
diox/oil	spectral	0.113	0.104	0.156 ± 0.000	0.151	0.027 * 0.163	0.104 ± 0.005
Car	C/100 C	12.5	16.8	14.8 ± 0.6	15.8	24.9 ± 0.7	17.4 ± 0.1
CIRs							
Carqt		5.4	7.5	6.6 ± 0.0	7.8	12.6 ± 0.9	8.2 ± 0.6
Carpi		1.8	2.3	1.9 ± 0.0	2.5	3.4 ± 0.1	2.4 ± 0.2
Carpo		5.3	7.0	6.3 ± 0.5	5.5	8.9 ± 0.3	6.8 ± 0.7
Calhs		7.5	7.5	2.9 ± 0.2	4.4	5.1 ± 0.0	6.8 ± 0.9
Calbr		18.9	17.9	13.2 ± 0.2	16.7	15.2 ± 0.5	18.4 ± 0.5
Calch		45.6	42.7	58.3 ± 0.2	51.5	38.7 ± 0.4	43.8 ± 1.2
Calme		15.6	15.1	10.8 ± 0.0	11.6	16.1 ± 0.3	13.7 ± 0.1
H count	H/100 C	182.1	173.6	178.9 ± 0.4	174.3	164.6 ± 1.1	171.7 ± 0.3
IR Train H1							
diox/oil	gravimetric	0.130	0.132	0.159 ± 0.000	0.164	0.028 * 0.169	0.110 ± 0.000
diox/oil	spectral	0.128	0.132	0.165 ± 0.003	0.163	0.029 * 0.197	0.120 ± 0.003
Har	H/100 H	4.3	6.7	3.5 ± 0.2	4.2	7.8 ± 1.0	5.8 ± 0.2
CIRs							
Hart		0.9	1.6	0.6 ± 0.2	0.7	1.5 ± 0.6	1.1 ± 0.2
Hard		1.4	2.2	1.2 ± 0.1	1.0	2.7 ± 0.3	2.0 ± 0.1
Harm		2.1	2.9	1.7 ± 0.0	2.5	3.6 ± 0.1	2.7 ± 0.0
Hbzy		3.4	3.6	3.4 ± 0.3	3.4	7.1 ± 1.3	4.0 ± 0.1
Hbetb		8.5	5.3	7.9 ± 0.6	8.6	9.6 ± 3.3	8.3 ± 0.3
Hbeta		55.1	53.9	64.8 ± 0.1	60.9	48.6 ± 1.1	53.3 ± 0.1
Hgam		28.6	30.5	20.5 ± 0.5	22.9	26.9 ± 2.5	28.7 ± 0.1
CG Train C13							
Lna	atoms	8.1	7.8	10.6 ± 0.0	10.0	8.2 ± 0.0	8.9 ± 0.0
Groups	C/100 C						
Cna	n-Alkane	18.2	17.1	32.6 ± 1.0	28.9	16.4 ± 0.1	19.7 ± 1.4
Cma	Me-Alkane	8.8	7.8	8.1 ± 0.9	11.2	8.2 ± 0.1	8.8 ± 0.1
Ccs	Cyc+Sub	60.6	58.3	44.5 ± 1.3	44.1	50.5 ± 0.9	54.2 ± 1.4
Car	Arom Core	12.5	16.8	14.8 ± 0.6	15.8	24.9 ± 0.7	17.4 ± 0.1
Sum		100.0	100.0	100.0	100.0	100.0	100.0

* Gravimetric dioxane/oil ratios were varied six-fold for samples of oil V3.

MAGNETIC IMAGING OF FCC FEEDSTOCKS



psvirk 99-05-30

Fig. 1. Magnetic Imaging of FCC Feedstocks.

Annotated 13-C NMR Spectrum of a VGO Feedstock

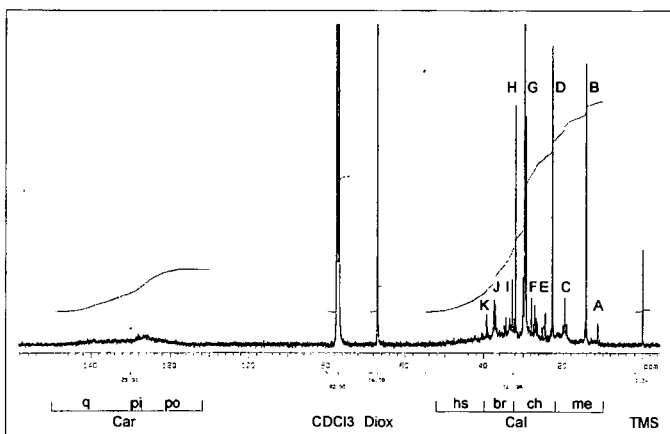


Fig. 2. Annotated 13-C NMR Spectrum of a VGO Feedstock.

psvirk 99-05-30

Annotated 1-H NMR Spectrum of a VGO Feedstock

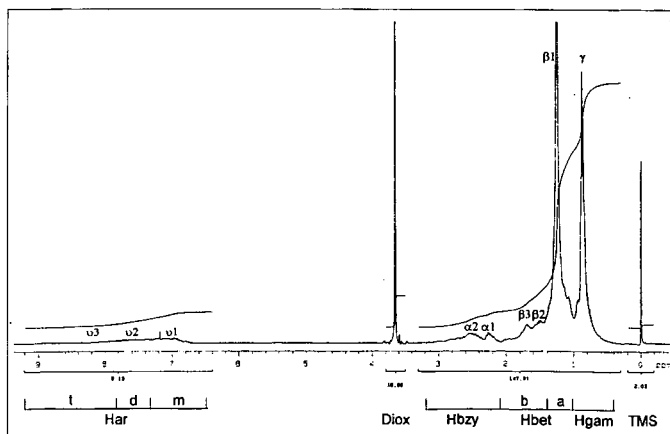


Fig. 3. Annotated 1-H NMR Spectrum of a VGO Feedstock.

psvirk 99-05-30

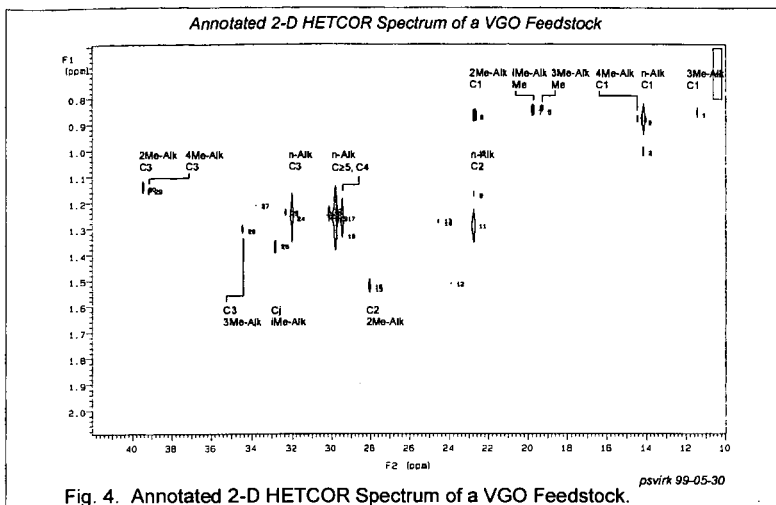


Fig. 4. Annotated 2-D HETCOR Spectrum of a VGO Feedstock.

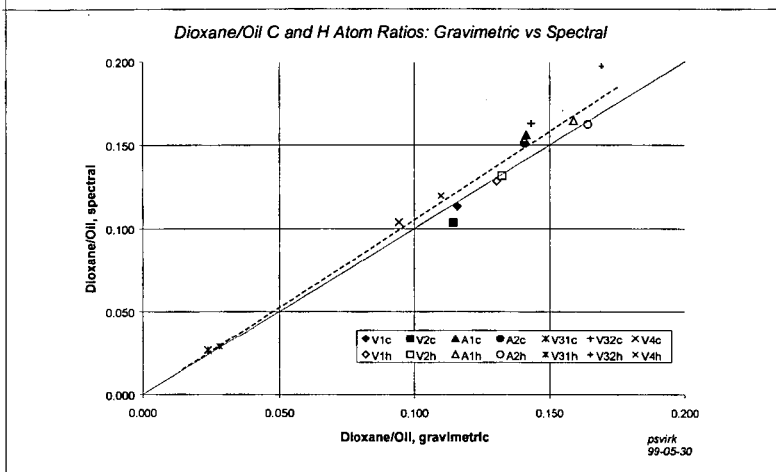


Fig. 5. Dioxane/Oil Ratios of C and H atoms: Gravimetric vs Spectral.

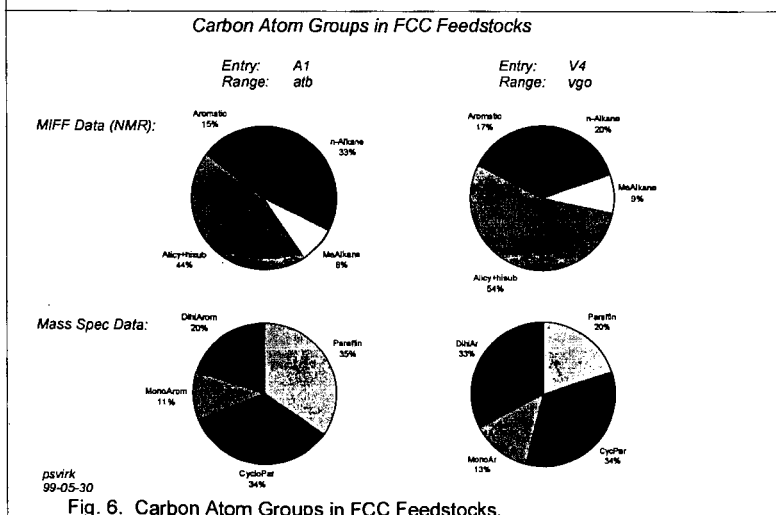
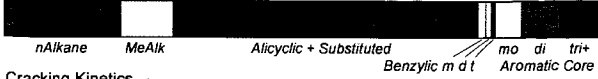


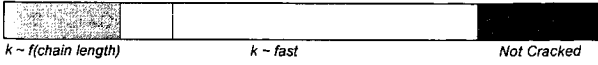
Fig. 6. Carbon Atom Groups in FCC Feedstocks.

Relation of NMR-Derived Feedstock Characterizations to FCC Performance.

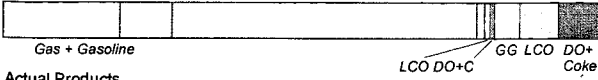
Advanced MIFF Groups



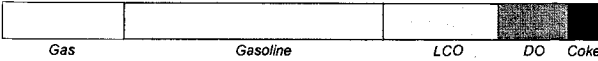
Cracking Kinetics



Potential Products



Actual Products

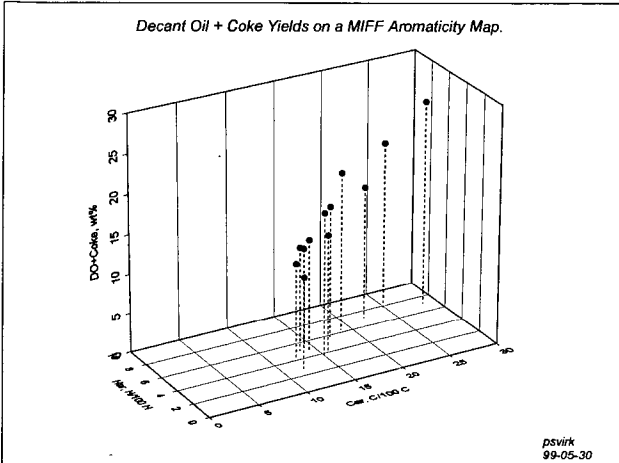


Sample: V4
Range: vgo

psvirk
99-05-30

Fig. 7. Relation of NMR-Derived Feedstock Characterizations to FCC Performance.

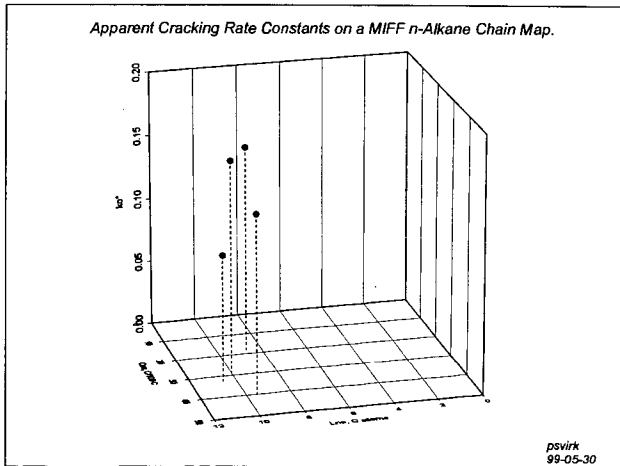
Decant Oil + Coke Yields on a MIFF Aromaticity Map.



psvirk
99-05-30

Fig. 8. Decant Oil + Coke Yields on a MIFF Aromaticity Map.

Apparent Cracking Rate Constants on a MIFF n-Alkane Chain Map.



psvirk
99-05-30

Fig. 9. Apparent Cracking Rate Constants on a MIFF n-Alkane Chain Map.

MODELING OF REACTIVITY OF LEWIS AND BRØNSTED SITES

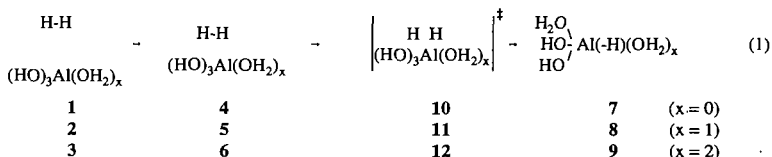
Dan Fărcaşiu

Department of Chemical and Petroleum Engineering, University of Pittsburgh, 1249 Benedum Hall,
Pittsburgh, PA 15261

It is generally considered that the coordinatively unsaturated sites (cus) responsible for the catalytic properties of active aluminum oxide consists of tri- and pentacoordinated aluminum atoms. The remaining possibilities, hexa- and tetraordinated aluminum atoms, are considered coordinatively saturated and, therefore, unreactive. A careful NMR investigation has evidenced, however, only tetra-, penta-, and hexacoordinated aluminum atoms in alumina and in the intracavity material of steamed zeolites. No measurable amount of tricoordinated sites was found.¹ Even if vanishingly small concentrations of tricoordinated aluminum are present, it is difficult to assign all catalytic activity to them. An examination of the relative reactivity of various sites on alumina was, therefore, in order.

The isotope exchange between D₂ and the protons of the solid is a good model reaction for the reactivity of sites on alumina.² Theoretical modeling of the hydrogen chemisorption on alumina was attempted before by both semiempirical³ and ab initio calculations,⁴ at a rather low level of theory. One study considered only tricoordinated sites,^{4a} the other looked at pentacoordinated sites as well and concluded that they were inactive.^{4b} The aluminum sites were modeled by the simple clusters Al(OH)₃ and Al(OH)₅.⁴ It was not clear from the paper^{4b} whether the species considered was the dianion Al(OH)₅²⁻ or a dioxidized, electrically neutral, species of the same formula, but neither of them appears to us to be a good choice.

We considered the reactivity of electrically neutral single clusters, (HO)₃Al(OH₂)_x, containing tri- (1, x = 0), tetra- (2, x = 1), and pentacoordinated (3, x = 2) aluminum atoms. Thus, no unnatural, oxidized species was used. The full reaction profile for dissociative hydrogen chemisorption was studied (Eq. 1).



As the first step, the physisorbed complexes 4 (x = 0), 5 (x = 1) and 6 (x = 2) were examined. Their reaction to form the chemisorbed complexes, 7, 8, and 9, was mapped to determine the transition structures (10, 11, and 12) and the corresponding energies (E_{TS}), which measure the energy barriers for the exchange.

The ab initio calculations were conducted with the program Gaussian 94,⁵ in the manner described previously.⁶ All geometry optimizations were conducted with electron correlation with the MP2 method⁷ or with the DFT-B3LYP⁸ method. The 6-31G*, 6-31-G**, 6-31++G**, 6-311G** and 6-311++G** basis sets were used.

For the tricoordinated aluminum system (x = 0), the geometry of the starting cluster was obtained by the optimization of the species (HO)₃Al(OH₂) (2) and removal of the extra water molecule, on the idea that aluminum oxide surfaces are formed by calcination of hydrated forms. In one approach (A), the angles around the aluminum atom were then frozen as in the hydrated cluster and the other geometrical parameters of the dehydrated cluster were optimized. Alternatively (B), the rigidity of the solid was simulated by freezing the hydrogen atoms in their positions in the hydrated cluster and then optimizing the central part of the cluster (the Al-(O-)₃ group) after the removal of the extra water. The complexes with physisorbed and chemisorbed hydrogen were optimized in the same way. The reactions of tetra- and pentacoordinated aluminum clusters were studied without any constraints on the geometry.

The calculations predicted the hydrogen chemisorption to be endothermic in all cases, the order being $E(x=0) < E(x=1) < E(x=2)$. For $x=0$, the calculation by the approach B gave a much lower endothermicity for the chemisorption than the approach A. The energy barriers for chemisorption were similar, however, for the approaches A and B. Their variation with the coordination number of the aluminum atom was $E_{TS}(x=0) < E_{TS}(x=1) < E_{TS}(x=2)$. Reaction coordinate tracking indicated that chemisorption occurs through the interaction of H_2 with the Al atom, therefore it is a catalysis by a metal ion. A three-center bond involving the aluminum and the two hydrogens is formed, after which one of the hydrogens migrates to an adjacent oxygen atom. the transition state is located along this hydrogen shift. B3LYP calculations give results in reasonable agreement with the MP2 calculations, attesting to the appropriateness of the DFT method for this type of structures.

The calculations indicate tetracoordinated aluminum sites to be catalytically active. As these sites are usually in higher concentration than the pentacoordinated sites and are intrinsically much more active, they should be considered *the* catalytic sites on active alumina.

The second type of acid sites on solid surfaces, the Brønsted sites, are most often characterized by neutralization with a probe base and examination of the product by spectroscopic methods or measurement of the thermal effect of this interaction.⁹ Pyridine (Py) and its derivatives have long been used as probe bases. Comparison of pyridine with 2,6-disubstituted pyridines was proposed to distinguish Lewis from Brønsted sites.¹⁰ The application of the highly crowded homolog, 2,6-di-*tert*-butylpyridine (DTBP) was proposed to distinguish between sites on the outer surface and sites inside cavities or channels.¹¹

It has been pointed out that all types of ionic reactions on solid surfaces must occur through the intermediacy of tight ion pairs.^{9a,12} Thus, the reaction of Py forms $PyH^+ \cdot A^-$ tight ion pairs, where A^- is the anion of the acid site. The direction of adsorption should be the one which maximizes the hydrogen bonding interaction, that is with the $N^+ - H$ perpendicular to the surface (sideways adsorption). A complete analysis of the thermodynamics of protonation in the gas phase and in water solution led to the conclusion that $DTBP^+$ also forms hydrogen bonds at nitrogen.¹³

The line-shape of the NMR signals of protons bonded to nitrogen in pyridinium (PyH^+) and di-*tert*-butylpyridinium ions ($DTBP^+$) in solution indicated a significant difference in their rates of longitudinal relaxation (R_1), the former ion relaxing the slowest. Computer modeling showed that the ratio of relaxation rates is 10-20. A significant difference between the relaxation times ($T_1 = 1/R_1$) for the carbon atoms in β and γ position (4.71 and 4.75 sec for PyH^+ , 0.55 and 0.79 sec for $DTBP^+$) was observed as well. The different positions in the molecule of the N-H group and of those two carbon atoms indicate that the difference in longitudinal relaxation rates originates in a different rate of tumbling in solution, rather than a difference in the electrical field gradient. Calculations of the correlation times for the relaxation of molecules considered as ellipsoid-shape rotors in a medium of given viscosity indicate that the difference in size covers only a part of the difference in tumbling rates (lower τ_c for pyridine). The difference should come from specific interactions with the solvent, most likely in the form of electrical double layers which have to be disturbed during the rotation.

Differences between relaxation times for each individual ion in different acids were also observed. It was established that the differences are not solvent effects, but are brought about by the change in anion. Thus, in the same solvent PyH^+ relaxes slower, that is, tumbles faster, when the anion corresponds to a stronger acid. The reason for this behavior is that in the salt of the weaker acid the ions are ion-paired and the rotation, occurring around an axis perpendicular to the N-H⁺ bond, is hindered by this interaction.

The opposite effect is observed for the $DTBP^+$ cation: the salt of the *weaker* acid, which is present in solution as ion pairs, tumbles faster (relaxes more slowly). This behavior can be rationalized by the anion being situated in the ion pair along the axis around which the molecule rotates to produce the NMR relaxation, that means, at the top of the ring. Therefore, no hydrogen bond $N-H^+ \cdots A^-$ is formed for this cation, a finding which contradicts the assertions of previous authors.¹³

The same orientation should be encountered in chemisorption of DTBP on solid acids, that is with the ring facing the solid surface containing the acid site.

References

- (1) Coster, D.; Blumenfeld, A. L.; Fripiat, J. J. *J. Phys. Chem.* **1994**, *98*, 6201.
- (2) (a) Taylor, H. S.; Diamond, H. *J. Am. Chem. Soc.* **1935**, *57*, 1256. (b) Lee, J. K.; Weller, S. W. *Anal. Chem.* **1958**, *30*, 1057. (c) Hall, W.K.; Leftin, H. P.; Cheselske, F. J.; O'Reilly, D. E. *J. Catal.* **1963**, *2*, 506. (d) Hall, W.K.; Lutinski, F. E. *J. Catal.* **1963**, *2*, 518. (e) Carter, J.; Lucchesi, P.; Corneil, P.; Yates, D. J. C.; Sinfelt, J. H. *J. Phys. Chem.* **1965**, *69*, 3070.
- (3) Zelenovskii, V. M.; Zhidomirov, G. M.; Kazanskii, V. B. *Zh. Fiz. Khim.* **1984**, *58*, 1788.
- (4) (a) Senchenya, I. N.; Kazanskii, V. B. *Kinetika I Kataliz* **1988**, *29*, 1331. (b) Ioka, F.; Sakka, T.; Ogata, Y.; Iwasaki, M. *Can. J. Chem.* **1993**, *71*, 663.
- (5) Frisch, M. J.; Trucks, G. W.; Schlegel, H. B.; Gill, P. M. W.; Johnson, B. G.; Robb, M. A.; Cheeseman, J. R.; Keith, T.; Petersson, G. A.; Montgomery, J. A.; Raghavachari, K.; Al-Laham, M. A.; Zakrzewski, V. G.; Ortiz, J. V.; Foresman, J. B.; Cioslowski, J.; Stefanov, B. B.; Nanayakkara, A.; Challacombe, M.; Peng, C. Y.; Ayala, P. Y.; Chen, W.; Wong, M. W.; Andres, J. L.; Replogle, E. S.; Gomperts, R.; Martin, R. L.; Fox, D. J.; Binkley, J. S.; DeFrees, D. J.; Baker, J.; Stewart, J. P.; Head-Gordon, M.; Gonzalez, C.; Pople, J. A.; *Gaussian 94, Revision D.3*; Gaussian, Inc.: Pittsburgh PA, 1995.
- (6) Fărcașiu, D.; Lukinskas, P. *J. Phys. Chem. A*, **1998**, *102*, 10436.
- (7) (a) Pople, J. *Acc. Chem. Res.* **1970**, *3*, 217. (b) Pople, J. A. *Int. J. Mass Spectrom Ion Phys.* **1976**, *19*, 89. (c) Hehre, W. J.; Radom, L.; Schleyer, P. v. R.; Pople, J. A. *Ab initio Molecular Orbital Theory*; Wiley-Interscience: New York, NY, 1986.
- (8) (a) Hohenberg, P.; Kohn, W. *Phys. Rev.* **1964**, *136*, B864. (b) Kohn, W.; Sham, L. *Phys. Rev.* **1965**, *140*, A1133. (c) Parr, R.G.; Yang, W. *Density Functional Theory of Atoms and Molecules*, Oxford University Press: New York, 1989. (d) Becke, A. D. *J. Chem. Phys.* **1993**, *98*, 5648.
- (9) (a) Fărcașiu, D.; Ghenciu, A. *Progr. NMR Spectroscopy* **1996**, *29*, 129. (b) Cardona-Martinez, N.; Dumesic, J. A. *J. Catal.* **1990**, *125*, 427.
- (10) Murrell, L. L.; Dispenziere, N. C. *J. Catal.* **1989**, *117*, 275.
- (11) (a) Benesi, H. A.; *J. Catal.* **1973**, *28*, 176. (b) Corma, A.; Fornés, V.; Forni, L.; Martinez-Triguero, J.; Moschetti, D. *J. Catal.* **1998**, *179*, 451.
- (12) (a) Fărcașiu, D.; Ghenciu, A.; Li, J. Q. *J. Catal.*, **1996**, *158*, 116. (b) Ghenciu, A.; Fărcașiu, D. *J. Mol. Catal. A*, **1996**, *109*, 273.
- (13) H. P. Hopkins, Jr., D. V. Jahagirdar, P. S. Moulik, D. H. Aue, H. M. Webb, W. R. Davidson and M. D. Pedley, *J. Am. Chem. Soc.*, 1984, *106*, 4341.

SYNERGISTIC EFFECTS OF HYBRID HYDROGEN DONORS TOWARDS STABILIZATION OF PARAFFINIC JET FUELS IN THE PYROLYTIC REGIME

John M. Andrésen, James J. Strohm, Michael M. Coleman and Chunshan Song*
Applied Catalysis in Energy Laboratory, The Energy Institute
The Pennsylvania State University, University Park, PA 16802

KEYWORDS: Pyrolysis, thermal stability, aviation jet fuels.

ABSTRACT

The chemical interactions between n-tetradecane and the hybrid hydrogen donors of benzyl alcohol and 1,2,3,4-tetrahydro-1-naphthol, and benzyl alcohol and tetrahydronaphthalene have been studied. Compared to the use of a single hydrogen donor, the hybrids resulted in synergistic effects towards reducing the pyrolytic degradation of alkanes in jet fuels, resulting in an enhanced suppression of the formation of free radicals.

INTRODUCTION

Future high performance jet fuels are expected to be thermally stable at temperatures up to 900°F¹. Commercially available aviation fuels are high in paraffins, resulting in poor thermal performance due to their tendency to crack under these pyrolytic conditions². Hydrogen donors have been found to stabilize the fuels by terminating the propagation of free radicals from the cracking process^{3, 4}. The pyrolytic cracking of paraffins generates both primary and secondary free radicals, where a certain hydrogen donor may favor the interaction with only one type of free radical. This has been indicated previously, where the effects of hydrogen donors, such as benzyl alcohol (BA) and 1,2,3,4-tetrahydro-1-naphthol (THNol), on the product distribution of pyrolytic stressed tetradecane were studied⁵. Benzyl alcohol was found to reduce the amount of n-alkane cracking products, while THNol greatly reduced the 1-alkene. This was associated with the ability of BA to target primary radicals and, correspondingly, the targeting of THNol towards secondary radicals. Accordingly, this paper focuses on the potential of hybrid hydrogen donor for enhanced pyrolytic stabilization of paraffinic compounds typical for jet fuels. Hybrids of benzyl alcohol with tetrahydronaphthalene and 1,2,3,4-tetrahydronaphth-1-ol have been studied, and their synergistic effect upon tetradecane has been characterized.

EXPERIMENTAL

The compounds used were n-tetradecane (TD, Aldrich 99%), benzyl alcohol (BA, Aldrich 99.8%) tetrahydronaphthalene (THN, Aldrich 99%) and 1,2,3,4-tetrahydro-1-naphthol (THNol, Acros 97%). Stressing of TD alone or in different mixtures with one or two hydrogen donors, were performed for 30 minutes in a fluidized sandbath at 425, 450 and 475°C. A detailed description of the experimental setup and analytical determination of the product distribution using GC and GC/MS, has been reported elsewhere^{2, 5}.

RESULTS AND DISCUSSION

The thermal stability of tetradecane, TD, during the pyrolytic stressing can be expressed on the basis of the amount of TD remaining in the liquid over the amount in the original mixture weighed against the liquid yield of the experiment. This ratio is therefore normalized, and its enhancement when a hydrogen donor is added, compared to that of the TD alone, indicates that the hydrogen donor is indeed improving the thermal stability of the paraffinic compound. Figure 1 shows the remaining TD content over its initial concentration, stressed alone at 425, 450 and 475°C and its mixture with 0.5, 1, 3 and 5 mole% tetrahydronaphthalene (THN). With increasing stressing temperature, there is a dramatic decrease in the TD remaining content with no THN added, from around 85 mole% at 425°C to 27 mole% at 475°C. When THN is added at 425°C, there is a dramatic increase for the first mole% of hydrogen donor added up to 98% and it

stays stable at this level with further increase in the THN content. As the temperature is increased to 450°C, the TD remaining ratio for the TD stressed alone has been reduced to 56%. Again, there is a sharp increase up to 70% after only 0.5 mole% THN, and with further rise in the THN content, this ratio is slowly but steadily increasing to above 80% with 5 mole% THN addition. Increasing the temperature to 475°C, there is again a significant increase for the first half mole% THN added, as for the previous temperatures. A slower but steady rise is observed thereafter up to 5 mole% THN, reaching a TD remaining ratio of close to 50%. Similar behavior for the single addition of BA and THNol with TD has also been found⁵.

The GC traces of the liquid product distribution for TD alone and its mixture with 0.5 mole% THN, stressed at 475°C for 30 minutes, are plotted in Figure 2. As expected, the TD peak is the dominant peak, accounting for a major part of the total peak area. When no THN was added, as is the case for the top trace, a significant part of the total peak area is taken by the products from the thermal cracking of TD. To the left of the TD peak there are typical traces of linear alkanes and alkenes cracking products in the range of C4 to C13. The alkane and alkene with the same carbon number appear in pair, where the alkane is eluted at slightly lower retention times than the alkene, i.e. to the left. When the THN is added, the cracking products are greatly reduced as shown by the reduction in the peak heights and areas of the alkane and alkene derivatives in the bottom trace of Figure 2. The decrease in cracking products obtained by the addition of THN is therefore closely related to the reduced cracking of the TD. Further, the introduction of THN seems to especially reduce the 1-alkene peak in relation to the corresponding alkane peak, when compared to the TD stressed alone. Therefore, the THN seems to particular target the secondary radicals, similar to that found for THNol⁵. Figure 3 shows the ratio of the 1-alkene peak area over that of the corresponding n-alkane for TD alone and with 0.5 mole% THN and BA addition. There is a clear increase in the alkene/alkane ratio for the BA mixture, indicating that BA is indeed targeting the primary radicals. However, for the THN the ratios of the alkene over the alkane peaks are smaller than those observed for the TD alone, indicating that THN targets secondary radicals.

The observed effects on the thermal stabilization of TD by BA, THN and THNol are summarized in Scheme 1. The increased thermal stability of TD when hydrogen donors are added can be linked to the ability of the hydrogen donor to capture radicals formed during the stressing and therefore hinder the cracking. This results in an increased liquid product and enhances the TD remaining ratio, when compared to TD stressed alone. Scheme 1 presents in a simplified manner the role of the different hydrogen donors in the thermal stabilization of TD. A hydrogen is abstracted from the n-tetradecane due to the influence of heat into a secondary radical. The additive can then cap the radical at this stage, preventing the propagation of the reaction and leave the TD intact. THN and THNol have shown good ability to operate on secondary radicals as discussed above. However, if this radical is not stopped, it will undergo a β -scission, yielding a 1-alkene and a primary radical. These primary radicals are targeted by BA⁵. Accordingly, hybrids of BA and THN or BA and THNol should therefore produce synergetic effects at low concentrations towards enhanced thermal stabilization of TD.

Figure 4 compares the TD remaining ratio at 450°C for the TD mixed with a single hydrogen donor, BA, THN or THNol at 1 mole% addition, and that of TD added a hybrid of BA and THN or BA and THNol, at 0.5 mole% each. When added alone, both THN and THNol gave higher thermal stability than that of BA. However, the hybrid of 0.5 mole% BA and 0.5 mole% THN resulted in a clear enhanced thermal stability effect when compared to the 1 mole% single mixtures. This trend is further supported by the studies at 475°C, as shown in Figure 5. For the single hydrogen donor additions at 475°C, the TD remaining ratio increases from 27% for TD alone to around 35% after 1 mole% BA addition, and the use of THN has an even higher impact, where this ratio is around 46% (Figure 5). The hybrid of BA and THN would be expected to be in the range of 35 to 46%, but gave a result of 52% showing a clear synergistic effect between these two hydrogen donors. Correspondingly, the effect from the hybrid of BA and THNol would be expected to be in the range 35 to 39%, but showed an enhancement up to

46%. Although the BA/THN hybrid showed overall higher thermal stability effect at both 450 and 475°C, the synergistic effect from the BA/THNol hybrid was larger when taking into account the effect of the single hydrogen donors. These results are very promising for the development of additives that can work in both the autoxidative regime (150-250°C) and the pyrolytic regime, and further research will study the effect in both these regimes.

CONCLUSIONS

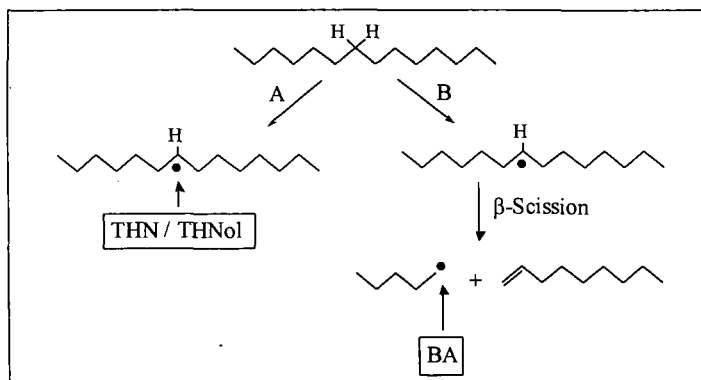
Hybrid hydrogen donors of (i) benzyl alcohol (BA) and tetrahydronaphthalene (THN), and (ii) benzyl alcohol (BA) and 1,2,3,4-tetrahydro-1-naphthol (THNol), have shown a synergistic effect on the thermal stabilization of tetradecane (TD) in the pyrolytic regime. The BA/THN hybrid showed the overall highest ability to stop the thermal decomposition of the paraffinic TD, but the BA/THNol hybrid showed the highest synergistic effect when compared to the BA and THNol alone.

ACKNOWLEDGMENTS

The authors wish to thank the U.S. Air Force Wright Laboratory, the U.S. DOE / Federal Energy Technology Center for their support. We also thank Prof. Harold H. Schobert for his support and helpful discussion.

REFERENCES

- (1) Edwards, T., *Prep. Am. Chem. Soc.- Div. Petro. Chem.*, **1996**, *41(2)*, 481.
- (2) Andrésen, J.M., Strohm, J.J. and Song, C., *Prep. Am. Chem. Soc.- Div. Petro. Chem.*, **1998**, *43(3)*, 412.
- (3) Song, C., Lai, W.-C. and Schobert, H.H., *Ind. Eng. Chem. Res.*, **1994**, *33*, 548.
- (4) Coleman, M.M., Sobkowiak, M., Fearnley, S.P. and Song, C., *Prep. Am. Chem. Soc.- Div. Petro. Chem.*, **1998**, *43(3)*, 353.
- (5) Andrésen, J.M., Strohm, J.J., Coleman, M.M. and Song, C., *Prep. Am. Chem. Soc.- Div. Fuel Chem.*, **1999**, *44(1)*, 194.



Scheme 1. Simplified role of the hydrogen donors, BA, THN and THNol on the thermal stabilization of TD in the pyrolytic regime.

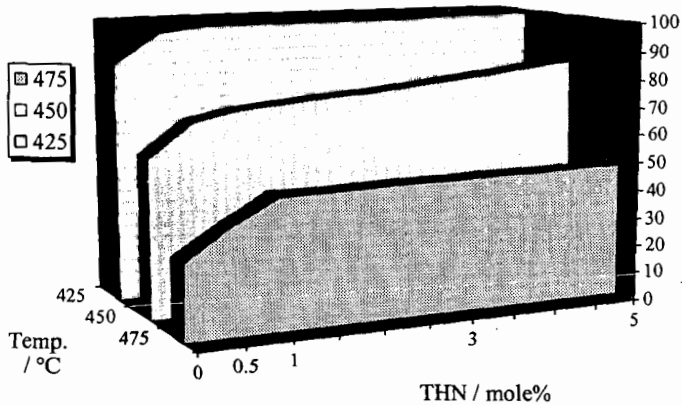


Figure 1. Comparison of remaining TD content over its initial concentration for different mixtures with tetrahydronaphthalene (THN) stressed at 425, 450 and 475°C for 30 minutes.

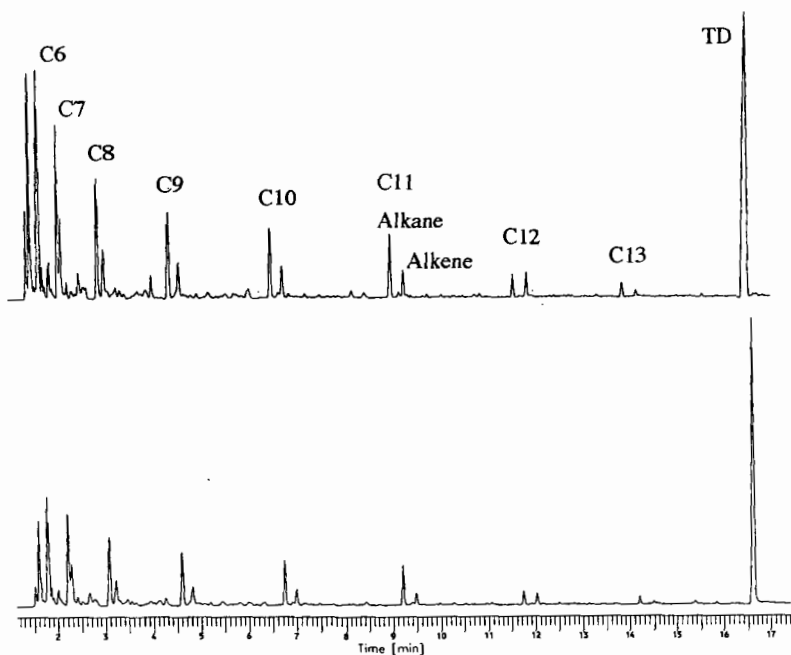


Figure 2. The GC traces of the liquid product distribution for TD alone (top) and its mixture with 0.5 mole% THN (bottom) stressed at 475°C for 30 minutes.

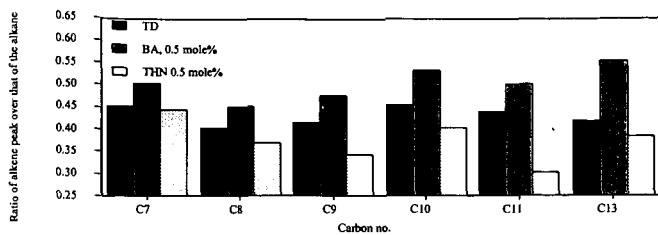


Figure 3. Ratio of the 1-alkene peak area over that of the corresponding alkane for TD alone and with 0.5 mole% THN and 0.5 mole% BA addition stressed at 475°C for 30 minutes.



Figure 4. Comparison of the ratio of TD remaining over that initial for TD mixed with 1 mole% of the single hydrogen donors BA, THN and THNol, individually, and the effect of hybrids at 450°C.

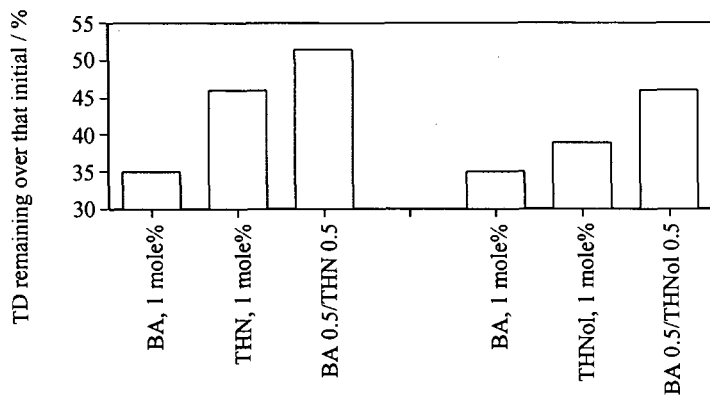


Figure 5. Comparison of the ratio of TD remaining over that initial for TD mixed with 1 mole% of the single hydrogen donors BA, THN and THNol, individually, and the effect of hybrids at 475°C.

ALKYLATED INTERMEDIATE OF CYCLO-ALKANES FOR STABILIZATION OF PARAFFINIC JET FUELS UNDER PYROLYTIC CONDITIONS

John M. Andréseu, James J. Strohm and Chunshan Song*
Applied Catalysis in Energy Laboratory, The Energy Institute
The Pennsylvania State University, University Park, PA 16802

KEYWORDS: Pyrolysis, thermal stability, aviation jet fuels.

ABSTRACT

The thermal stability of linear alkanes, such as tetradecane, in the pyrolytic regime is enhanced by the addition of cyclo-alkanes, in particular decalin. Based on the product distribution from the thermal stressing of their mixtures, decalin was found to target primary radicals, particularly by a sharp reduction in the n-alkane products in relation to that of the 1-alkene. This thermal interaction has been further examined by GC/MS analysis, which revealed the formation of alkylated intermediates of decalin that stabilizes the paraffinic species in the pyrolytic regime.

I. INTRODUCTION

Jet fuels for high Mach applications are required to operate under severe thermal stressing, where exposures up to 900°F are expected¹. Liquids rich in cyclo-alkanes have been found to have superior stability at high temperatures compared to those high in paraffinic content². This has been associated with two factors. Firstly, cyclo-alkanes themselves have higher thermal stability than linear alkanes³. At 450°C after 1 hour, most of a linear alkane such as tetradecane has been pyrolyzed into different products, while trans-decalin mostly remains unconverted. This has been linked to the ability of the trans-decalin to form tertiary radicals after hydrogen abstraction. Further, hydrogen abstraction will transform the decalin into tetralin, which will act as a hydrogen donor⁴ and will strongly enhance the thermal stability of trans-decalin even at low concentrations. On the other hand, as tetradecane experiences hydrogen abstraction forming primary and secondary radicals, this leads to rapid decomposition due to propagation reactions. Secondly, previous studies have shown that decalin improves the thermal stability of tetradecane⁵. Again, this can be based on the buildup of tetralin from the pyrolytic H-abstraction from decalin, where the tetralin will strongly affect the propagation reaction in the mixtures. However, the thermal enhancement effect of decalin has been found at temperatures and concentrations, where the formation of tetralin from decalin can be neglected⁵. Therefore, there must exist additional routes in which the decalin quench the propagation reaction generated from the pyrolytic degradation of tetradecane. Accordingly, this work has studied the reactive intermediates involved during pyrolysis of mixtures with decalin and tetradecane at 450°C, stressed from 12 to 120 minutes. There was a clear thermal stability enhancement with the addition of decalin at all times. The reduction in the thermal cracking of tetradecane was found to derive from the capture of radicals by the decalin, forming alkylated derivatives. By increased thermal stressing, these were further dehydrogenated to form tetralins, which again act as a hydrogen source for stabilization.

II. EXPERIMENTAL

The compounds used were tetradecane (TD, Aldrich 99%) and decalin (DHN, Aldrich 98%, a mixture of 46 mole% cis- and 54 mole% trans-decalin). Stressing of TD alone or in 5 or 30 mole% mixtures with DHN were performed for 12, 30, 60 and 120 minutes in a fluidized sandbath at 450°C as reported elsewhere². The GC-MS was performed on a Hewlett-Packard 5890 Series II GC coupled with a HP 5971A MS detector and a J&W DB-17 column, which was heated from 40 to 290°C with a heating rate of 6°C min⁻¹.

III. RESULTS AND DISCUSSION

Figure 1 shows the remaining TD content over its initial concentration for TD alone and 5 and 30 mole% mixtures with DHN, stressed at 450°C for 30, 60 and 120 minutes. As the TD is stressed, its thermal stability can be expressed on the basis of the amount of TD remaining in the liquid over the amount in the original mixture weighted against the liquid yield of the experiment. This ratio is therefore normalized, and any enhancement in this ratio when DHN is added compared to that

of the TD alone indicates that the DHN is indeed improving the thermal stability of the linear alkane. With increasing stressing time, there is a dramatic decrease in the TD remaining content with no DHN added, from around 56 mole% at 30 minutes to 11 mole% at 120 minutes. When DHN is added there is a significant increase at all stressing times in the TD remaining content. A rapid increase in the thermal stability is achieved with only 5 mole% DHN addition, followed by a slower rise up to 30 mole% DHN mixture. The ratio of the TD remaining content for the 30 mole% DHN mixture over that of TD stressed alone gives an indication of the extent of interaction between the DHN and the TD. The effect of adding 30 mole% DHN is clearly dependent on the stressing time, where the extent of interaction is rising from 17% after 30 min stressing, to 24% at 60 min and is significantly increased to nearly 140 % at 120 min. Clearly, several reaction mechanisms are involved as discussed below.

Figure 2 compares the changes in the C4 to C10 product range from the thermal decomposition of TD with 30 mole% DHN addition at 450°C stressed for 12, 30, 60 and 120 minutes. The n-alkane and 1-alkene peaks appear in pairs, where the n-alkane has a slightly lower retention time than the 1-alkene. After 12 minutes stressing, the concentration of the cracking products is very low (5%), and the amount of 1-alkenes is slightly higher than that of the n-alkanes. At 30 minutes reaction time, the concentration of cracking products has increased to over 30%, and the relative distribution of the 1-alkene is now slightly lower than the n-alkane. As the stressing time is further risen to 60 minutes, the 1-alkene concentration is decreasing due to hydrogenation, alkylation or cyclization reactions⁶. The 1-alkenes are ultimately disappearing after 120 min exposure at 450°C. Compared with the stressing of TD alone at 450°C⁶, the relative concentration of 1-alkenes is higher at all times in the DHN mixture. The 1-alkene/n-alkane relative distributions found after 1 hour for the 30 mole% DHN mixture are comparable to those after only 30 minutes stressing for TD only. This indicates that the DHN is interacting with the thermal decomposition of the 1-alkanes by reducing their probability for hydrogen abstraction and capturing primary radicals, which promotes their alkylation. The ability of the DHN to affect the 1-alkane concentration through suppression of the n-alkanes is further illustrated in Figure 3, where the ratio of the 1-alkene peak area over that of the corresponding n-alkane for TD alone and with 30 mole% DHN addition after 30 minutes reaction time at 450°C is compared. This ratio is around 60% for TD stressed alone and there is a clear increase in the alkene/alkane ratio for the DHN mixture, giving values about 90%. This indicates that DHN indeed is targeting the primary radicals resulting in enhanced thermal stabilization of TD or other paraffinic liquids typical for jet fuels.

The route of preventing the thermal cracking of the linear alkanes by DHN is strongly connected to the ability of the cylo-alkane to become alkylated. Figure 4 compares the GC-MS trace for ethyl-DHN (166 a.m.u.) and dodecyl-DHN (306 a.m.u.) identified in the remaining liquid after stressing the 30 mole% DHN mixture at 450°C for 60 minutes. The main features are deriving from the DHN-ion, giving rise to the mass at 137 and below. The alkylated masses give rise to the parent ions, where the DHN-ion with a mass of 137 combined with either ethyl (mass of 29) or dodecyl (mass of 169) are deriving from the parent ions ethyl-DHN (166) and dodecyl-DHN (306), respectively. Other masses identified are 180, 194, 208, 222, 236, 250, 264, 278 and 292, indicating that alkyl substitution in the whole range C2 to C12 has taken place. However, no evidence of methyl, tridecyl or higher alkyl substitution was found. Neither was any DHN substituted with two alkyls identified. This strengthens the evidence that the thermal stability effect of DHN is initially associated with the capturing of primary alkyl radicals by substitution as illustrated in Scheme 1. The hydrogen abstraction of TD generally leads to a secondary radical. The secondary radical produces a 1-alkene and a primary radical through β -scission. If the primary radical is not captured, it will start a propagation reaction leading to further decomposition of the TD and rapid transformation of the 1-alkenes. The introduction of DHN captures primary radicals in two consecutive steps. First, the primary radical will abstract a hydrogen from the DHN, where the formation of a tertiary radical is favored. Second, the tertiary radical will recombine with a different primary radical. The above scheme will result in two overall effects. Firstly, the thermal decomposition of TD is halted and secondly, the product distribution will favor 1-alkenes. This alkylation process was further confirmed through studies on the stressing products from TD/DHN mixtures after only 30 minutes at 450°C. However, when increasing the stressing time to 120

minutes, the studies on the cracking products show that tetralin is the main product from the thermal decomposition of DHN. This confirms that dehydrogenation of decalin into tetralin is a further stabilizing factor, which becomes increasingly important at longer stressing times.

CONCLUSIONS

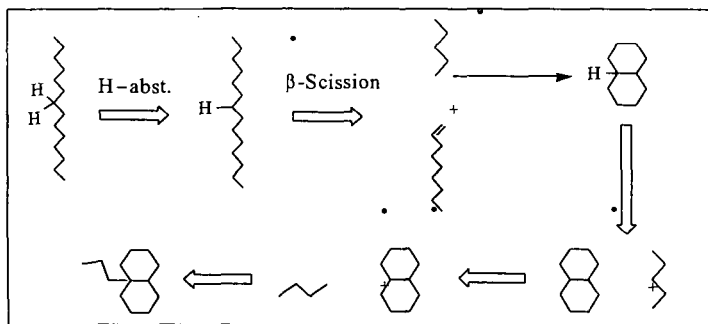
Tetradecane (TD) has been stressed alone and in mixtures with 5 and 30 mole% decalin (DHN) at 450°C, with stressing times ranging from 12 to 120 minutes. A significant increase in the amount of TD remaining was observed at all stressing times upon the addition of DHN. The improved thermal stability of the TD-DHN mixtures was mainly associated with the reduced cracking of the TD due to interactions with the DHN. Enhancements of up to 140% in the ratio of TD remaining over that initial for 30 mole% DHN addition compared to that of TD by itself, were observed. The suppression of the production of linear alkanes was found to derive from the capture of primary radicals by the DHN, forming alkylated derivatives. With increasing stressing times, these were further dehydrogenated to form tetralins, which again act as a hydrogen source for stabilization.

ACKNOWLEDGMENTS

The authors wish to thank the U.S. Air Force Wright Laboratory, the U.S. DOE / Federal Energy Technology Center for their support. We also thank Prof. Harold H. Schobert for his support and helpful discussion.

REFERENCES

- (1) Edwards, T., *Prep. Am. Chem. Soc.-Div. Petro. Chem.*, **1996**, 41(2), 481.
- (2) Andrése, J.M., Strohm, J.J. and Song, C, *Prep. Am. Chem. Soc.-Div. Petro. Chem.*, **1998**, 43(3), 412.
- (3) Song, C. and Lai, W.-C., *Prep. Am. Chem. Soc.-Div. Petro. Chem.*, **1998**, 43(3), 462.
- (4) Andrése, J.M., Strohm, J.J., Coleman, M.M. and Song, C, *Prep. Am. Chem. Soc.-Div. Fuel Chem.*, **1999**, 44(3-4), In press.
- (5) Andrése, J.M., Strohm, J.J. and Song, C, *Prep. Am. Chem. Soc.-Div. Fuel Chem.*, **1999**, 44(1), 199.
- (6) Song, C., Lai, W.-C. and Schobert, H.H., *I&EC Research*, **1994**, 33, 534.



Scheme 1. Simplistic view of the thermal stability effect of DHN associated with the capturing of alkyl radicals by substituting them to their structure.

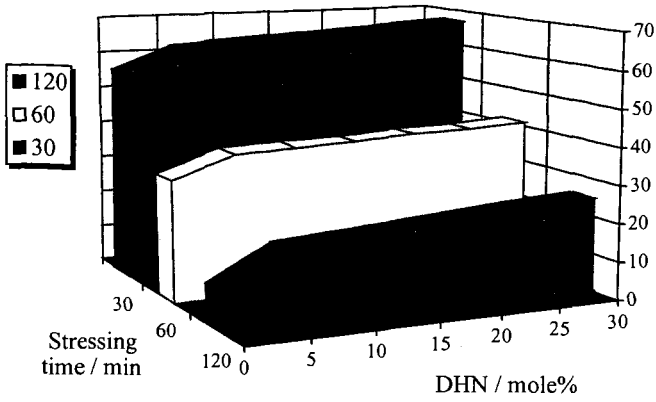


Figure 1. Comparison of remaining TD content over its initial concentration for different mixtures with DHN stressed at 450°C for 30, 60 and 120 minutes.

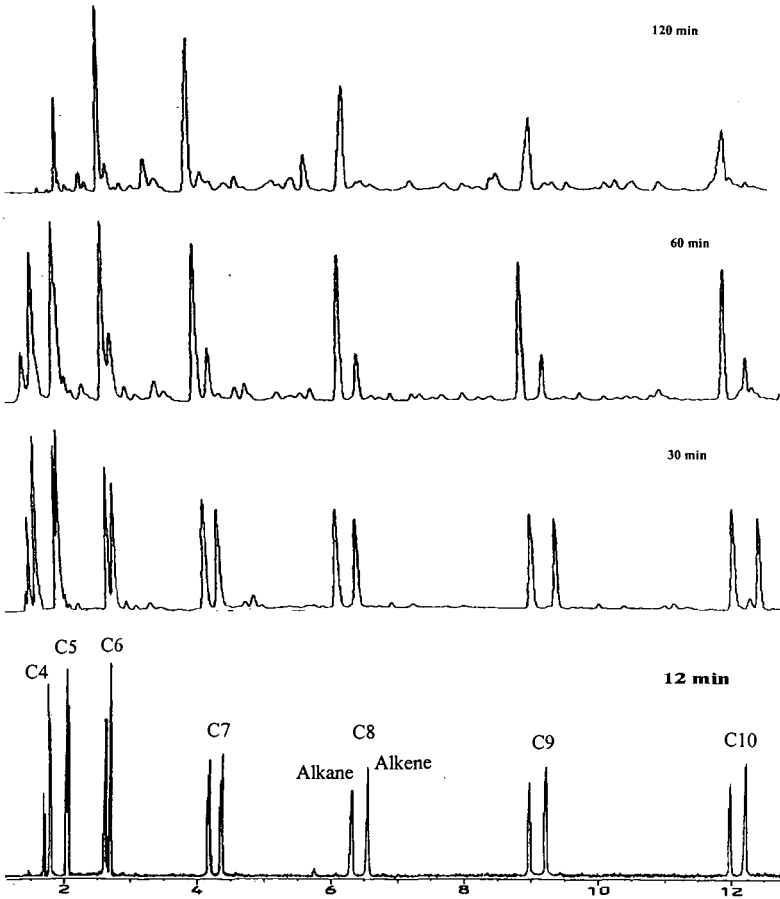


Figure 2. Changes in the TD pyrolysis products C4 to C10 after stressing the mixture of 70 mole% TD with 30 mole% DHN for 12, 30, 60 and 120 minutes at 450°C.

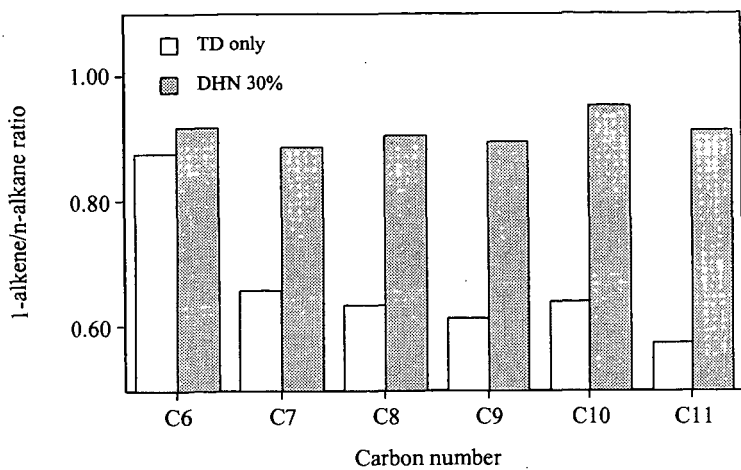


Figure 3. Ratio of the 1-alkene peak area over that of the corresponding alkane for TD alone and with 30 mole% DHN addition at 450°C stressed for 30 minutes.

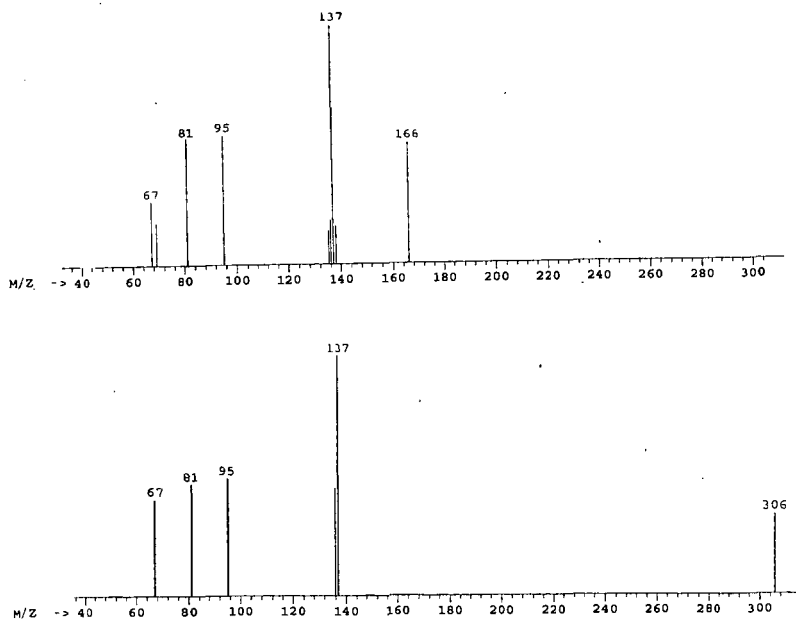


Figure 4. GC-MS traces for ethyl-DHN with parent mass 162 a.m.u. (top) and dodecyl-DHN (306 a.m.u., bottom).